THÈSE

Pour l'obtention du grade de
DOCTEUR DE L'UNIVERSITÉ DE POITIERS
École nationale supérieure d'ingénieurs (Poitiers)
Pôle poitevin de recherche pour l'ingénieur en mécanique, matériaux et énergétique - PPRIMME
(Diplôme National - Arrêté du 7 août 2006)

École doctorale : Sciences et ingénierie en matériaux, mécanique, énergétique et aéronautique - SIMMEA
Secteur de recherche : Mécanique des milieux fluides et acoustique

Présentée par :
André Valdetaro Gomes Cavalieri

Wavepackets as sound-source mechanisms in subsonic jets

Directeur(s) de Thèse :
Yves Gervais, Peter Jordan

Soutenue le 18 juin 2012 devant le jury

Jury :

Président	**Neil D. Sandham**	Professor, University of Southampton, Royaume-Uni
Rapporteur	**Daniel Juvé**	Professeur des Universités, École Centrale de Lyon
Rapporteur	**Tim Colonius**	Professor, Caltech, Pasadena, CA, États-Unis
Membre	**Yves Gervais**	Professeur des Universités, Université de Poitiers
Membre	**Peter Jordan**	Chargé de recherche, Université de Poitiers
Membre	**Joël Delville**	Ingénieur de recherche, Université de Poitiers
Membre	**Jacques Borée**	Professeur des Universités, Université de Poitiers
Membre	**Paulo A. O. Soviero**	Professor, ITA, São José dos Campos, Brésil

THÈSE

Pour l'obtention du grade de

DOCTEUR DE L'UNIVERSITÉ DE POITIERS

ÉCOLE NATIONALE SUPÉRIEURE D'INGÉNIEURS DE POITIERS
(Diplôme National - Arrêté du 7 août 2006)

École Doctorale : Sciences et Ingénierie en Materiaux, Mécanique, Énergétique et Aéronautique

Spécialité : MÉCANIQUE DES MILIEUX FLUIDES ET ACOUSTIQUE

Présentée par

André Valdetaro Gomes Cavalieri

Wavepackets as sound-source mechanisms in subsonic jets

Directeur de thèse : **Yves Gervais**

Co-direction : **Peter Jordan**

Soutenue le 18 juin 2012
Devant la Commission d'Examen

JURY

Neil D. SANDHAM	Professeur, Univ. of Southampton, Royaume-Uni	Président
Tim COLONIUS	Professeur, Caltech, Pasadena, CA, États-Unis	Rapporteur
Daniel JUVÉ	Professeur, École Centrale de Lyon	Rapporteur
Paulo A. O. SOVIERO	Professeur, ITA, São José dos Campos, Brésil	Examinateur
Jacques BORÉE	Professeur, Institut Pprime, Poitiers	Examinateur
Joël DELVILLE	Ingénieur de Recherche, Institut Pprime, Poitiers	Examinateur
Yves GERVAIS	Professeur, Institut Pprime, Poitiers	Examinateur
Peter JORDAN	Chargé de Recherche, Institut Pprime, Poitiers	Examinateur

Remerciements

Bien qu'un travail de thèse soit signé par un seul auteur, le contenu de ce manuscrit reflet la contribution d'un grand nombre de personnes, auxquelles je tiens ici à montrer ma reconnaissance.

Je remercie Tim Colonius et Daniel Juvé d'avoir accepté de rapporter cette thèse et apporter leurs égards vis-à-vis de mon travail. En particulier, pendant les deux dernières années de ce travail j'ai eu la chance de collaborer avec Tim et de beaucoup apprendre avec son immense connaissance et expérience.

Merci également aux deux autres membres externes du jury de la soutenance, Neil Sandham, qui a présidé le jury, et Paulo Soviero, qui a fait un long voyage depuis le Brésil pour pouvoir assister à la soutenance. Je voudrais remercier Jacques Borée pour sa lecture attentive du manuscrit et ses commentaires; et Joël Delville, qui a une contribution scientifique importante à cette thèse, notamment sur la partie expérimentale de la recherche.

J'ai eu le plaisir d'être encadré au long de ces quatre années par Peter Jordan et Yves Gervais, qui m'ont énormément appris sur l'aéroacoustique et la mécanique des fluides. Je remercie Peter pour toutes les longues discussions qui ont façonné ce travail. Son enthousiasme et sa curiosité ont été des moteurs importants pour ma recherche. La rencontre avec Yves au Brésil en 2006 est à l'origine de cette thèse, et son aide a été précieuse pendant la préparation de ce projet, et aussi tout au long de ces années.

En dehors des personnes citées, ce travail a été réalisé en collaboration avec un certain nombre de chercheurs d'autres institutions. Je remercie Mingjun Wei, Jonathan Freund, Gilead Tadmor et Anurag Agarwal, qui ont beaucoup contribué avec ce travail, notamment pendant sa première moitié. La dernière partie de cette thèse a été réalisée en étroite collaboration avec Daniel Rodríguez, que je remercie vivement. Au sein de l'institut Pprime, je remercie

Véronique Fortuné, Damien Biau et Pierre Comte (décedé) pour m'avoir initié aux simulations numériques en mécanique des fluides. Merci à Damien également pour toutes nos discussions sur l'instabilité des jets.

Cette thèse a été financée par le CNPq, Conselho Nacional de Desenvolvimento Científico e Tecnológico. Je remercie également à l'ensemble des professeurs et fonctionnaires de l'ITA, Instituto Tecnológico de Aeronáutica, pour avoir encouragé la réalisation de cette thèse à l'étranger et m'avoir soutenu tout au long de ces quatre années.

Le personnel de l'Institut Pprime m'a apporté un soutien technique indispensable à la réalisation de mon travail. Merci à Alexandre Morel et Jean-Christophe Vergez pour le support informatique, et à Carine Fourment-Cazenave, Patrick Braud et Jean-Marc Mougenot pour leur travail pendant les expériences. Je remercie l'ensemble du personnel de l'atelier et du bureau d'études du CEAT, surtout pour leurs efforts pendant les problèmes (nombreux) survenus au cours de mes expériences.

Le séjour en France a été une expérience formidable, qui doit beaucoup à la bonne ambiance au sein du laboratoire. J'ai eu l'occasion de travailler sur deux sites de l'Institut Pprime, et donc de faire de nombreuses connaissances. Je tiens à remercier l'ensemble des doctorants et post-doctorants que j'ai rencontré au cours de ma thèse pour les bons moments que nous avons partagés: Antoine, Malick, Gaëtan, Afaque, Vincent, Farrukh, Gilles, Alessandro, Sébastien, Guy et Vladimir au CEAT, et Marie, Sébastien, Maud, Aminou, Xavier, Matthieu, Solenn, David, Thomas, Cyril, Ida, Jeoffrey, Thibault et Rémi au Campus.

Je réserve un remerciement à part à Franck, Cyrille, Maxime, Rémy, Guillaume et Stéphane, pour toutes nos longues discussions concernant nos recherches, qui portaient sur des thématiques assez proches. Tous ces échanges ont contribué à la qualité de ce manuscrit. Merci aussi pour votre amitié et pour la bonne ambiance qui s'est tout de suite installé entre nous.

Je remercie à tous les amis de Poitiers, en particulier aux Jomipilos et aux amis du "vendredi soir" Catie, Laurence, Bab et Valérie. Un "obrigado" aux amis venus du Brésil pour nous rencontrer en France: Maria, tia Penha, tio Toninho, Tiago, Ana, Flávio, Adade, Cicléia, Júlia, Wirandé, Fernanda, Carvalhal, Paula, Guguta, Hervan e Fábio Emanuel.

Un grand merci à ma famille, qui a toujours soutenu ma formation et a posé les bases de ce que je suis aujourd'hui, en encourageant ma curiosité et mon goût pour la lecture et les études. Obrigado aos meus pais Edebrande e Márcia, ao meu irmão Davi, e aos "beaux-parents" (a expressão em francês é bem mais bonita, não?) Cássio e Marilda.

Enfin, je remercie mon épouse Aline, à qui je dédie cette thèse. Ce séjour à l'étranger est notre projet commun, et sa réussite doit énormément à son soutien et son amour. Nous avons vécu ensemble toutes les étapes de cette aventure, et maintenant nous nous préparons pour de

nouveaux défis. Je sais qu'avec toi tout sera plus facile et heureux. Eu te amo!

Résumé

On considère les paquets d'ondes hydrodynamiques comme mécanismes de génération de bruit des jets subsoniques.

Cette approche résulte tout d'abord de l'analyse de données numériques - DNS d'une couche de mélange (Wei et Freund 2006) et LES d'un jet à Mach 0,9 (Daviller 2010) - permettant de déterminer les propriétés des sources en termes de compacité, d'intermittence et de structure azimutale. L'identification d'un rayonnement intermittent associé aux modifications des structures cohérentes des écoulements permet de proposer un modèle de paquet d'onde pour représenter ce phénomène dans l'analogie de Lighthill, dont l'enveloppe présente des variations temporelles d'amplitude et d'étendue spatiale. Celles-ci sont tirées de données de vitesse de simulations numériques de jets subsoniques, et un accord de l'ordre de 1,5dB entre le champ acoustique simulé et le modèle confirme sa pertinence.

L'exploration du concept proposé est ensuite poursuivie expérimentalement, avec des mesures de pression acoustique et de vitesse de jets turbulents subsoniques, permettant la décomposition des champs en modes de Fourier azimutaux. On observe l'accord des directivités des modes 0, 1 et 2 du champ acoustique avec le rayonnement d'un paquet d'onde. Les modes 0 et 1 du champ de vitesse correspondent également à des paquets d'onde, modélisés comme des ondes d'instabilité linéaires à partir des équations de stabilité parabolisées. Finalement, des corrélations de l'ordre de 10% entre les modes axisymétriques de vitesse dans le jet et de pression acoustique rayonnée montrent un lien clair entre les paquets d'onde et l'émission acoustique du jet.

Mots clés : aéroacoustique, jets – bruit, bruit aérodynamique, vélocimétrie par images de particules.

Abstract

Hydrodynamic wavepackets are studied as a sound-source mechanism in subsonic jets. We first analyse numerical simulations to discern properties of acoustic sources such as compactness, intermittency and azimuthal structure. The simulations include a DNS of a two-dimensional mixing layer (Wei and Freund 2006) and an LES of a Mach 0.9 jet (Daviller 2010). In both cases we identify intermittent radiation, which is associated with changes in coherent structures in the flows. A wave-packet model that includes temporal changes in amplitude and axial extension is proposed to represent the identified phenomena using Lighthill's analogy. These parameters are obtained from velocity data of two subsonic jet simulations, and an agreement to within 1.5dB between the model and the acoustic field of the simulations confirms its pertinence. The proposed mechanism is then investigated experimentally, with measurements of acoustic pressure and velocity of turbulent subsonic jets, allowing the decomposition of the fields into azimuthal Fourier modes. We find close agreement of the directivities of modes 0, 1 and 2 of the acoustic field with wave-packet radiation. Modes 0 and 1 of the velocity field correspond also to wavepackets, modelled as linear instability waves using parabolised stability equations. Finally, correlations of order of 10% between axisymmetric modes of velocity and far-field pressure show the relationship between wavepackets and sound radiated by the jet.

Keywords : aeroacoustics, jet noise, aerodynamic noise, particle image velocimetry

Contents

List of Figures

Résumé étendu

L'objectif de cette thèse est d'établir une description simplifiée permettant de modéliser la génération de bruit par des jets turbulents subsoniques, en s'appuyant sur les caractéristiques des structures cohérentes présentes dans les écoulements turbulents, qui forment des paquets d'onde hydrodynamiques dans les jets.

Cet objectif est poursuivi ici sur la base de résultats de simulations numériques, du développement de modèles théoriques et d'expériences, dans un effort commun profitant des atouts de chacune des approches et prenant en compte les progrès récents concernant les possibilités de calcul et de mesure des écoulements turbulents et de leur champ acoustique.

Le chapitre I présente une revue bibliographique du bruit de jet, à la fois des points de vue théorique, numérique et expérimental, avec une perspective historique des travaux qui constituent la base de cette thèse.

Des données de simulations numériques sont tout d'abord utilisées comme point de départ pour l'analyse des phénomènes. La possibilité d'étudier des données résolues dans le temps pour toutes les variables de l'écoulement, dans un volume comprenant à la fois le jet et le champ rayonné, est un avantage considérable qu'on a exploité afin de cerner les propriétés fondamentales de l'écoulement vis-à-vis de la génération sonore. On utilise pour cela des simulations des couches de mélange bidimensionnelles (Wei et Freund[203]) et un jet à Mach 0,9 (Daviller[52]).

Les simulations de couche de mélange de Wei et Freund[203] représentent une excellente opportunité pour l'analyse des mécanismes de génération de bruit compte tenu de l'application d'un contrôle optimal, dont l'objectif est la réduction de l'intensité acoustique rayonnée. Dans le chapitre II ces simulations sont examinées en détail afin d'identifier le mécanisme d'action du contrôle permettant de réduire le bruit généré. On observe que cette réduction intervient dans un intervalle de temps limité : la couche de mélange sans contrôle présente un rayonnement intense localisé dans le temps, qui est réduit par l'action du contrôle. L'étude du champ de vitesses de la couche de mélange révèle que le contrôle permet d'éviter l'occurrence d'une interaction entre trois tourbillons, qui, dans le cas sans contrôle, mène au rayonnement intermittent mentionné. L'interaction des trois tourbillons est vue comme une perte, pendant un certain temps, de l'homogénéité axiale de l'écoulement dont il résulte l'émergence d'une longue zone de haute pression entre les tourbillons qui forme une onde acoustique d'amplitude élevée.

Pour la détection systématique de tels événements, on applique une transformée en ondelettes continue aux signaux de pression issus de la simulation de la couche de mélange sans contrôle. Des rayonnements intermittents ont une signature formée de niveaux importants dans la représentation de l'énergie du signal en fonction du temps et de la fréquence, et l'observation de la couche de mélange aux temps correspondant à la génération de ces émissions intermittentes révèle que ces événements résultent également d'interactions entre trois tourbillons.

Dans le chapitre III cette approche est appliquée à la simulation aux grandes échelles d'un jet à Mach 0,9. Les champs acoustique et turbulent sont décrits en modes de Fourier azimutaux ; le bruit rayonné aux angles faibles par rapport à l'axe du jet est dominé par le mode axisymétrique. L'application de la transformée en ondelettes montre des amplitudes élevées des émissions intermittentes, notamment pour le mode 0 aux angles faibles. Des visualisations du champ de pression à l'intérieur du jet montrent une structure de paquet d'onde pour le mode axisymétrique, et l'instant d'émission d'une onde acoustique de forte amplitude est identifié avec la troncature de l'enveloppe du paquet d'onde.

Pour étudier l'effet des modifications temporelles de la structure des paquets d'onde axisymétriques sur le bruit rayonné, on a développé quelques modèles de sources intermittentes dans le chapitre IV, intégrant des variations temporelles de l'enveloppe. L'effet de ces variations est d'abord étudié dans deux problèmes modèles. Dans le premier, une modulation temporelle de l'amplitude maximale est introduite, et dans le deuxième problème la source présente une variation temporelle de son étendue spatiale, deux comportements qui représentent les observations de la simulation de jet subsonique, détaillées dans le chapitre III. Les deux types de variation temporelle de l'enveloppe impliquent une augmentation du rayonnement acoustique, de façon intermittente, ce qui correspond aux analyses des chapitres II et III.

Les deux types de changements temporels de l'enveloppe sont réunis dans un troisième modèle, où la source est représentée par un paquet d'onde dont l'amplitude maximale et l'étendue spatiale varient avec le temps. Pour vérifier la consistance du modèle, on utilise des données du champ de vitesse de la simulation pour en déterminer les paramètres ; le bruit rayonné est calculé en utilisant l'analogie de Lighthill, avec un bon accord avec l'intensité acoustique aux angles faibles donnée par la simulation. La même méthode est appliquée à la simulation numérique directe de Freund[66], avec un accord également proche.

Les modèles de paquet d'onde motivent ensuite l'étude séparée de la contribution de chaque mode azimutal dans les champs turbulent et acoustique. Les modes azimutaux d'ordre bas, et notamment le mode axisymétrique, ont une efficacité acoustique plus importante, comme montré dans l'annexe A du chapitre IV ainsi que dans l'annexe B du chapitre V. En particulier, le format de paquet d'onde du mode 0, donné aux chapitres III et IV, impose une forte directivité des émissions acoustiques vers les angles faibles en raison de l'interférence axiale entres les parties positives et négatives de la source. Cette interférence résulte de l'étendue axiale d'un paquet d'onde, qui est comparable à la longueur d'onde acoustique et empêche l'application d'une hypothèse de compacité.

Les chapitres V et VI sont dédiés à des expériences relatives à l'émission acoustique de jets turbulents subsoniques naturels, et cherchent à mettre en évidence des paquets d'onde comme source de bruit dans ces écoulements. Les couches limites en sortie de la buse sont turbulentes, et les fluctuations turbulentes constituent l'excitation *naturelle* correspondant de façon plus proche aux jets d'applications pratiques. On évite donc l'ambiguïté introduite par le forçage périodique: les jets forcés présentent clairement des structures cohérentes, mais rien n'indique que les jets forcés et naturels ont le même comportement, comme discuté dans la section 1.2.

Les données expérimentales sont étudiées dans le domaine fréquentiel, en opposition aux approches temporelles utilisées dans les chapitres précédents. Ceci est motivé par le manque relatif d'information dans la littérature sur le contenu énergétique des paires (ω, m) relatifs aux champs turbulent et acoustique, où ω la fréquence et m le mode azimutal. Comme l'efficacité acoustique des paquets d'onde est fortement liée à ces deux paramètres, nous avons réalisé des mesures permettant à la fois des décompositions de Fourier en temps et en azimut. En outre, la description des fluctuations en termes de fréquence et nombre d'onde azimutal permet d'utiliser la théorie de la stabilité linéaire comme modèle dynamique des paquets d'onde dans les jets. Les mesures réalisées permettent tout de même l'analyse dans le domaine temporel, comme pour les études de simulations numériques, mais avec des contraintes liées à la quantité de données disponibles. Un exemple d'une telle analyse est l'application de la transformée en ondelettes pour quantifier l'énergie intermittente pour les différents modes azimutaux du champ acoustique. Cette analyse, donnée en l'Annexe, confirme la dominance des émissions axisymétriques et leur forte directivité, tel qu'observé dans la simulation du chapitre III et suggéré par les modèles du chapitre IV.

Les mesures acoustiques détaillées dans le chapitre V montrent que le mode axisymétrique de la pression en champ lointain a la *superdirectivité* caractéristique du rayonnement d'un paquet d'onde (Crow[50]). Cette forte directivité est une indication que le son rayonné aux angles faibles est lié à un paquet d'onde avec une étendue spatiale importante dans la direction axiale. La dépendance de l'intensité du bruit axisymétrique rayonné à $\mathrm{St} = 0.2$ avec le nombre de Mach acoustique du jet est de $M^{9.5}$ pour les angles faibles. Ceci est également cohérent avec le rayonnement d'un paquet d'onde, mais seulement après prise en compte des effets de compressibilité sur le champ de vitesse : l'augmentation du nombre de Mach provoque une *réduction* de l'amplitude du mode axisymétrique des fluctuations de vitesse, un effet prédit par la théorie de la stabilité linéaire.

Les propriétés observées pour le mode axisymétrique du champ acoustique ne sont pas compatibles avec des sources compactes, comme des petites structures turbulentes distribuées dans le jet de façon aléatoire. Ceci renforce l'idée que le bruit aux angles faibles, dominé par le mode axisymétrique, est généré pour la plupart par des paquets d'onde au sein du jet.

Le modèle de Crow est également étendu dans le chapitre V à l'étude des paquets d'onde hélicoïdaux comme sources dans l'analogie de Lighthill. On modélise la structure radiale de ces paquets d'onde avec les modes issus de l'instabilité linéaire de l'écoulement moyen. La directivité obtenue pour les modes azimutaux 1 et 2 dans le champ acoustique est proche des comportements prévus par le modèle.

Dans le chapitre VI, on s'intéresse à la détection des paquets d'ondes pour le mode axisymétrique et le premier mode hélicoïdal dans le champ de vitesse des mêmes jets, avec un accord proche avec des ondes d'instabilité linéaires modélisées par les équations de stabilité parabolisées. Cet accord corrobore l'existence de structures cohérentes, issues d'une instabilité linéaire de l'écoulement moyen de type Kelvin-Helmholtz, dans des jets turbulents à des nombres de Reynolds élevés. Néanmoins, ces structures ne dominent pas le champ de vitesses ; on montre que la dimension caractéristique des structures le plus énergétiques est liée à l'épaisseur locale de quantité de mouvement. Les modes azimutaux 0 et 1 sont tout de même présents dans le champ de vitesse, mais ont des amplitudes plus faibles que les modes plus élevés. Ces basses amplitudes favorisent l'application des modèles linéaires, ce qui explique les bons résultats obtenus avec les équations de stabilité parabolisées. En revanche, en aval du cône potentiel l'accord entre la stabilité linéaire et l'expérience se dégrade, ce qui suggère des effets non linéaires dans cette région.

Le contraste entre les basses amplitudes des modes 0 et 1 dans le champ de vitesse et leur caractère dominant dans le champ acoustique peut s'expliquer par l'efficacité acoustique de chaque mode azimutal, discutée dans les chapitres IV et V. Il y a un effet important d'annulation pour des sources ayant des nombres d'onde azimutaux élevés, ce qui réduit leur efficacité pour la génération sonore.

Des corrélations vitesse-pression sont ensuite utilisées de façon à vérifier cette hypothèse. La corrélation de la pression acoustique en champ lointain avec les paquets d'onde dans l'écoulement, calculée entre les modes axisymétriques de la pression et de la vitesse, est de l'ordre de

10%, valeur plus élevée que de précédents résultats pour les jets subsoniques de la littérature, où des corrélations entre deux points sont calculées en ignorant les contenus azimutaux des champs. Cela montre l'importance des paquets d'onde, et la forte cohérence azimutale qui leur est associée, sur le bruit rayonné, en accord avec la théorie (Michalke[127] ; Michalke & Fuchs[132] ; voir aussi la discussion dans la section 2.1.1).

L'ensemble des résultats présentés dans cette thèse soutient ainsi le concept de paquets d'onde hydrodynamiques, générés par l'instabilité linéaire de Kelvin-Helmholtz de l'écoulement moyen turbulent, comme principales sources de bruit des jets subsoniques pour des faibles angles par rapport à l'axe du jet.

Introduction

Context of the problem

The reduction of aircraft noise is a major challenge currently faced by industry. A 10dB reduction in the radiated sound has been chosen as an objective for 2020 in Europe; this stands for a reduction of an order of magnitude of the acoustic intensity, which requires considerable effort in the reduction of noise from all sources on an aircraft. This objective recently motivated a IUTAM symposium on computational techniques for the prediction of aircraft noise (Astley and Gabard [5]).

Among the sound sources generated by aircraft, the free turbulent jets that exit turbofan engines pose a challenging problem in fluid mechanics. The sound radiated by such jets results from turbulent fluctuations, and hence knowledge of turbulence is required for noise prediction and design for noise reduction. Conceptual difficulties arise thus due to the complexity of jet turbulence. Moreover, in jet aeroacoustics one has to deal with the coupling of the turbulent field with an external irrotational medium; this coupling leads to the notion of *acoustic efficiency*: certain energetic turbulent fluctuations may radiate negligible sound, whereas other low-energy disturbances in the turbulent field may couple more efficiently with the surrounding medium and generate significant radiation.

It is possible, with current computational capabilities, to obtain unsteady solutions of the compressible Navier-Stokes equations for turbulent jets, which include both turbulent and acoustic fields. Such simulations can thus predict the radiated sound by a jet, but with a high computational cost.

On the other hand, the features of a turbulent flow related to sound generation are, in general, not clearly exposed by analysis of a numerical solution, unless it is investigated in some detail. Moreover, a flow simulation by itself does not provide guidelines for reduction of jet noise. A simplified description of the noise-generation mechanisms in turbulent jets is thus valuable, and would allow the proposition of devices acting in the turbulent flow with a view to reducing the radiated sound.

Our objective in the present work is to obtain a simplified description modelling sound generation in turbulent jets. We use simulation, theory and experiment in a unified effort, taking advantage of the relative strengths of each.

In the present work we restrict our analysis to unheated subsonic jets exiting a circular nozzle with a nearly uniform velocity profile. Such a jet is a canonical flow in the literature, with significant past and ongoing research on both turbulent and aeroacoustic properties, and present clear interest for aeronautical applications. Although the exhaust of current aircraft engines comprises a co-axial jet, with a primary heated jet surrounded by a secondary cold stream, single jets can nonetheless be seen as a simpler flow presenting the salient features of co-axial jets, but with a reduced number of flow parameters.

Free jets are also among the first turbulent flows where close analysis revealed the existence of coherent structures forming *hydrodynamic wavepackets*. Analysis of numerical databases led us to investigate wavepackets as a sound-source mechanism. This represents a simplified source description for the radiated sound, in particular for low polar angles θ, measured from the downstream jet axis. Knowledge on sound generation by wavepackets may help to understand the physical mechanisms in noise-reduction devices (see for instance the work of Kœnig [101]), and, more importantly, to propose new methods to reduce the noise generated by turbulent jets.

In what follows we describe the approach chosen for the present work, and the organisation of the present document.

Organisation of the present work

We adopt a strategy using simulation, theory and experiment. The motivation for such can be found in the following quote, taken from the conclusion of the review article of Jordan and Gervais [91]:

> "It seems clear that, despite some formidable obstacles, the future of aeroacoustics is set to be an exciting one, where genuinely new analysis strategies can be made possible by an efficient synergy between theoretical, experimental and numerical disciplines, one which takes good advantage of the impressive recent progress in numerical and experimental tools."

We present in chapter I a background on the advances of theoretical, numerical and experimental approaches, as well as a historical perspective on the works forming the foundation of the present effort.

We then use results of available numerical simulations as a starting point in our analysis. The possibility of studying temporally resolved data for all flow variables, in a spatial volume comprising the jet, is a considerable advantage that we have explored with a view to discerning the salient flow features for sound generation.

For such, we have disposed in this thesis of a number of numerical simulations: the direct numerical simulations (DNS) of optimally-controlled mixing layers of Wei and Freund [203], the large-eddy simulation (LES) of a Mach 0.9 jet of Daviller [52], and the direct numerical simulation of Freund [66]. This analysis is reported in chapters II, III and in a part of chapter IV. It should be stressed that the author was not directly involved in the computation of such simulations, but solely on the extraction of numerical results and subsequent analysis, including the application of post-processing tools.

The analysis of these simulations led us to simplified models for the sound radiated by jets at low polar angles, formulated theoretically using an acoustic analogy in chapter IV. The parameters in the models are then studied to reveal which flow features lead to significant sound radiation. A test of the pertinence of the models is performed using data from simulations: sources constructed using the turbulence field taken from DNS or LES should lead to an acoustic field consistent with the far-field pressure of the simulations.

Confidence on a simplified model allows proposition of experiments where the proposed mechanism is assessed. The last part of the present work deals with measurements of the acoustic and turbulent fields of subsonic jets, described, respectively, in chapters V and VI. Measurements were taken by the author, with the support of the Institut Pprime personnel, in the “Bruit et Vent” anechoic facility at the CEAT, Centre d’Etudes Aérodynamiques et Thermiques in Poitiers.

The focus of the experimental work was on the investigation of a proposed mechanism of sound generation, related to the coherent structures in jets forming wavepackets. The experimental results were studied to discern whether such a mechanism can explain features of the acoustic and turbulent fields. The experiments were studied in the light of theoretical models, either for the sound field resulting from a wavepacket, or for the intrinsic structure of a wavepacket as a linear instability wave, modeled either assuming parallel flow in chapter V or accounting for the jet divergence, using Parabolised Stability Equations (PSE), in chapter VI. The author wrote the program for the parallel flow computations in chapter V, but was not involved in the PSE calculations of chapter VI.

Since most of the results of this thesis were published in the form of journal articles, we have chosen to reproduce these in the present thesis. The journal articles were primarily written by the present author, with inputs from the co-authors of each paper.

We conclude this work with a summary of the main results obtained in the thesis, and with a discussion on some open questions. Finally, we present some perspectives for further work on the subject in order to increase the knowledge on jet noise, but also to devise strategies for reduction of the radiated sound, including active flow control.

Chapter I

Literature review

1 Aerodynamics of subsonic jets

1.1 The mean and fluctuation profiles

The mean velocity profile of a subsonic jet with Reynolds number $\mathrm{Re} = \rho U D/\mu = 5 \cdot 10^5$ is represented in figure I.1.

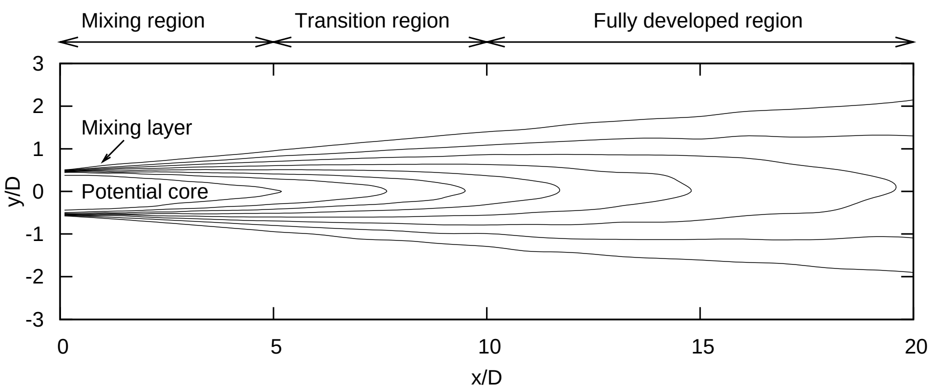

Figure I.1 – Mean velocity contours of a Mach 0.5 jet. Contours are uniformly spaced between $0.1U$ and $0.99U$. Flow goes from left to right. Results from the experiments described in chapter V.

The flow inside the nozzle is characterised by boundary layers whose thickness is small compared to the jet diameter. The resulting mean velocity at the nozzle exit has a "top-hat" profile: in the central zone, the streamwise velocity is constant and equal to the exit velocity U. Close to the jet lipline, in the *mixing layer*, there is a sharp decay of the velocity, that goes to zero at an outer position. This decay in the mixing layer leads to an inflexion point in the mean velocity profile.

The initial mixing region, shown in figure I.1, is characterised by an axisymmetric mixing layer that separates a central zone with uniform flow from the external region, with nearly zero velocities. The central region is called *potential core* since the mean velocity is constant and the fluctuation levels are low. The flow in the potential core can be assumed as irrotational, and thus allows the definition of a velocity potential.

In the outer zone the low velocities can also be assumed as irrotational, but here the predominant phenomenon is the *entrainment* of ambient air by the jet, which is characterised by small, inward radial flow velocities. This zone is referred to as the entrainment region.

If the boundary layer close to the nozzle exit is turbulent, the mixing layer will also be so; otherwise, the mixing layer will be initially laminar, but transition to turbulence will occur downstream. The transition process is initiated by the Kelvin-Helmholtz instability of the inflexional velocity profile (this will be further discussed in section 1.3).

The turbulent mixing layer spreads radially as the flow moves downstream, mostly due to turbulent diffusion of momentum. Between 4 to 6 jet diameters downstream (the precise location changes with the Mach number [108]) the mixing layer reaches the jet centerline and closes the potential core, whose average shape becomes a cone.

Downstream of the end of the potential core, the mean velocity profile takes the shape of a bell, in contrast to the top-hat profile near the nozzle exit. The two shapes of the velocity profile are illustrated in figure I.2(a). For stations downstream of the potential core, the flow is turbulent for all radial positions, and continues to spread radially by turbulent diffusion. This diffusion also causes a reduction of the centerline velocity for downstream positions. This is shown in figures I.1 and I.2(a).

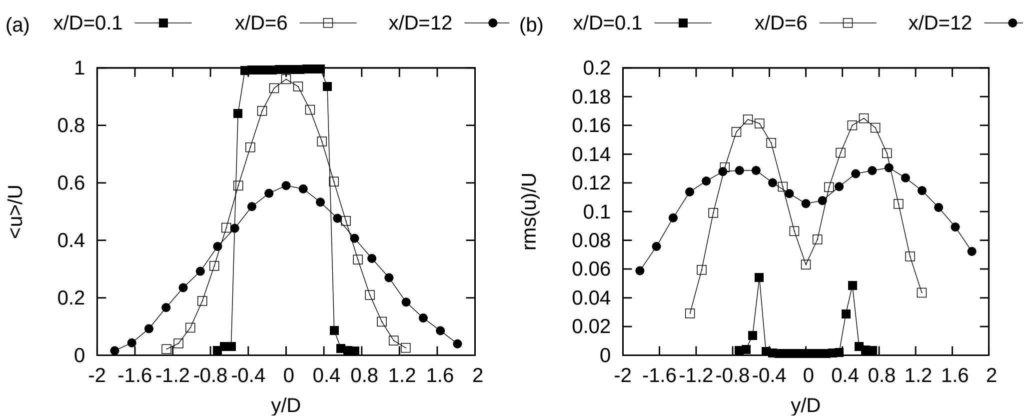

Figure I.2 – Comparison of (a) mean and (b) *rms* profiles for the axial velocity at three axial stations. Results from the experiments described in chapter V.

In the mixing region, the velocity fluctuations are maximal inside the turbulent mixing layer, and are much smaller in the potential core and entrainment regions. This is seen in figure I.2(b). Downstream of the end of the potential core, the fluctuation amplitude still has a maximum close to the jet lipline, but the fluctuations on the centerline become significant. The *rms* profiles tend to become flat for downstream positions as the turbulence evolves.

The mean velocity profiles of the mixing region have the momentum thickness δ_2, given as

$$\delta_2 = \int_0^\infty \frac{\overline{\rho}(r)\overline{u_x}(r)}{\rho_0 U}\left(1 - \frac{\overline{u_x}(r)}{U}\right)\mathrm{d}r \tag{I.1}$$

as a similarity length scale representing the development of the mixing layer. The velocity profiles collapse when plotted as a function of $(y - y_{1/2})/\delta_2$, where $y_{1/2}$ is the position where the jet velocity is $U/2$. An example of the mixing layer similarity is shown in figure I.3(a). Downstream of the potential core there is not such similarity due to the transition of the flow from an annular mixing layer to a developed jet. After $x/D \approx 10$ a new similarity of the velocity profiles can be found, this time using $y_{1/2}$ as a characteristic length of the development of the full turbulent jet. This downstream similarity is illustrated in figure I.3(b), and in this region the jet is considered as *fully developed*. The zone between the mixing and the fully developed regions is labelled as the *transition region*. These three regions are shown schematically in figure I.1.

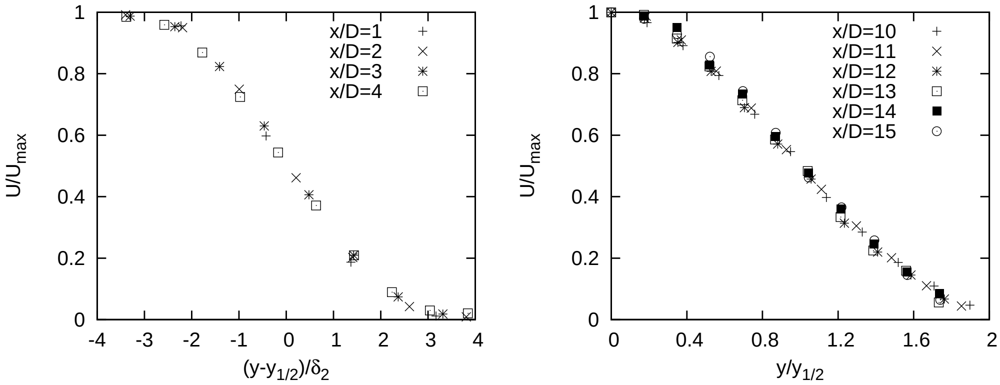

Figure I.3 – Similarity of mean velocity profiles in the (a) mixing layer and (b) developed region. Results from the experiments described in chapter V.

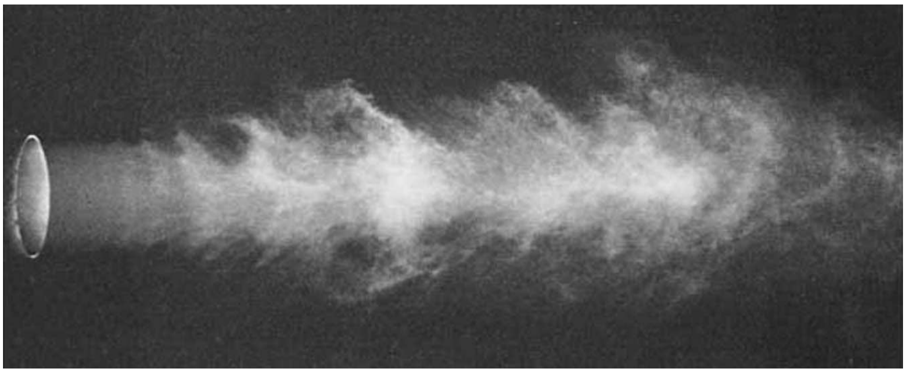

Figure I.4 – Smoke visualisation of a jet with Reynolds number of 6.52×10^4. Taken from Crow and Champagne [51].

1.2 Coherent structures

Early studies on the turbulent fluctuations in free jets were based on a view of turbulent fluctuations as entirely constituted of stochastic eddies, and much of the experimental work was done in order to obtain the correlation lengths that characterise such eddies (see for instance Laurence [110]). This view was to evolve due to the use of measurement techniques other than the standard hot wire.

When pressure fluctuations are measured in the near field of jets, they reveal flow patterns that are more organised. Mollo-Christensen [138] performed pressure measurements in this region. The correlations between microphone signals were significant for microphone spacings greater than a jet diameter, and presented a wave-like shape. The author concluded stating that "it is suggested that turbulence, at least as far as some of the lower order statistical measures are concerned, may be more regular than we think it is, if one only could find a new way of looking at it."

The experiments of Crow and Champagne [51] helped to shed light on the regularity of turbulence conjectured by Mollo-Christensen. Part of the experiments consisted of flow visualisation, with a technique of smoke seeding carefully chosen so as to highlight coherent patterns in jet turbulence, which were already visible in the Schlieren pictures of the first jet diameters of Bradshaw *et al.* [23]. The flow visualisations done in this way revealed a train of coherent 'puffs' scaling with the jet diameter. In successive visualisations these structures were seen to form intermittently, with an average Strouhal number of 0.3 based on the jet diameter D and the exit velocity U. A sample picture from their work is shown in figure I.4.

In order to study in more detail the structures observed in the smoke visualisations, Crow and Champagne added acoustic forcing inside the nozzle in order to impose periodicity in

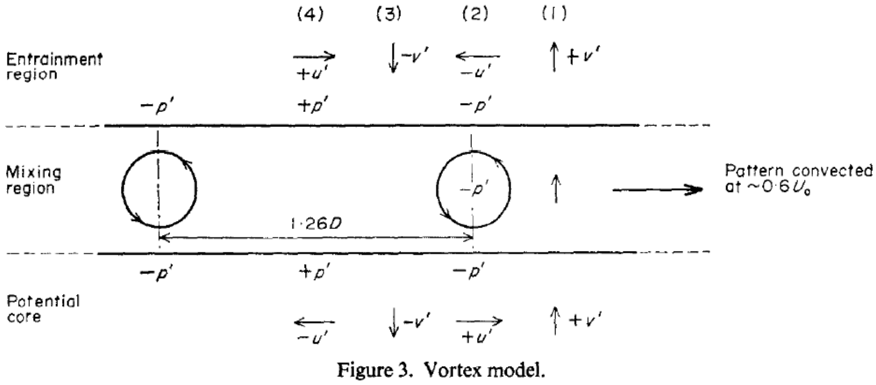

Figure I.5 – Vortex pattern in the mixing layer of jets. Taken from Lau *et al.* [107].

the formation of the puffs. This periodicity allowed measurements with several excitation frequencies and amplitudes, and with a single hot wire it was possible to determine wavelengths and convection speeds due to the phase locking of the flow. As some of the conclusions of the study, we can cite that the excitation Strouhal number that led to the maximum fluctuation amplitude was 0.3, i.e. the same value determined from flow visualisations of the unforced jets; this suggests that the acoustically-forced structures may correspond to actual phenomena in the natural jet. The initial growth of the fluctuation amplitudes behave *linearly* with the forcing amplitude. For the lowest amplitudes, linear behaviour was observed up to $x/D \approx 7$, which is even dowstream of the axial location of saturation of the instability waves. However, the decay measured downstream behaves nonlinearly with the forcing amplitudes. These points will be further discussed in section 1.3.

The work of Lau *et al.* [107] provided a different perspective on the kinematics of coherent structures in natural jets. Based on a hypothesis that axisymmetric ring vortices were present inside the upstream annular mixing layers, following a pattern sketched in figure I.5, the authors made simultaneous pressure-velocity measurements and performed two-point velocity correlations for both sides of the mixing layer. The normalised correlations were significant, and all measurements presented phase relationships corresponding to the proposed vortex pattern.

To determine the extent of the presence of such axisymmetric structures in jets, but also of components with other azimuthal Fourier modes, Michalke and Fuchs [132] evaluated experimentally the azimuthal cross-correlations of both pressure and streamwise velocity in a turbulent low-speed jet; these measurements allow the decomposition of these quantities in azimuthal Fourier modes as a function of frequency. They found that while the energy content for the axisymmetric mode of the axial velocity is low (5% of the overall power spectral density for $\mathrm{St} = 0.45$), for the pressure the axisymmetric mode dominates the fluctuations, and provides 42% of the overall PSD. Hence the low-order azimuthal modes, or, in other words, the azimuthally-coherent structures are more easily detected with pressure measurements. The authors stated that "this may help to explain why large-scale coherent turbulence structures were often overlooked in correlation analyses with hot-wire probes in the mixing region of a jet". For a range of Strouhal numbers between 0.225 and 1, the pressure field was seen to be dominated by azimuthal modes 0, 1, 2 and 3.

Armstrong *et al.* [4] kept the same approach, and made further measurements of the azimuthal coherence for jet Mach numbers ranging from 0.1 to 0.7 in order to evaluate if such azimuthally-coherent structures persist for higher Mach numbers. Results showed the same dominance of low-order azimuthal modes for the whole range of Mach numbers; in fact, the contribution of each azimuthal mode for the total pressure changed little with increasing velocity for Strouhal numbers between 0.175 and 1.8. The authors concluded that the distribution of the overall turbulent pressure between azimuthal modes was only a weak function of the Mach number, and thus coherent structures do persist at higher Mach. However, this overall turbulent pressure does change with Mach number, with a decrease of the normalised energy with increasing Mach.

Moore [142] did flow visualisations of subsonic jets with Mach numbers ranging from 0.3 to 0.9, with and without acoustic forcing. For the visualisations of the unforced jet, pictures were taken with a Schlieren system triggered by peaks in the near-field pressure close to the nozzle exit (about $1D$). Several exposures triggered this way are added to the same image, and the result can be seen as a conditional average of the flow visualisation, the near-field pressure being used as the condition. An azimuthal ring of six microphones was used to discern the azimuthal Fourier modes of coherent structures. Use of different time delays between the near-field peaks and the exposures allows one to trace the axial evolution of coherent structures. Sample visualisations, done for a Mach 0.83 jet, are shown in figure I.6.

Moore noted from the results exemplified in figure I.6 the clear presence of coherent structures for azimuthal modes 0 and 1. Such structures persist in the jet several diameters downstream (at least five jet diameters, according to the author). Moreover, in some visualisations one or two other neighbouring structures are visible, which suggests that the educed coherent structures form a *hydrodynamic wave*, whose phase speed is related to convection velocities of 0.6–0.7 times the jet exit velocity; this can explain the wave-like correlations obtained by Mollo-Christensen [138]. Moore then included acoustic forcing to study the hydrodynamic wave with phase averages. The measurements were compared to results of linear stability theory obtained by Michalke [128], and good agreement was found in the upstream part of the jet. Further

(a) 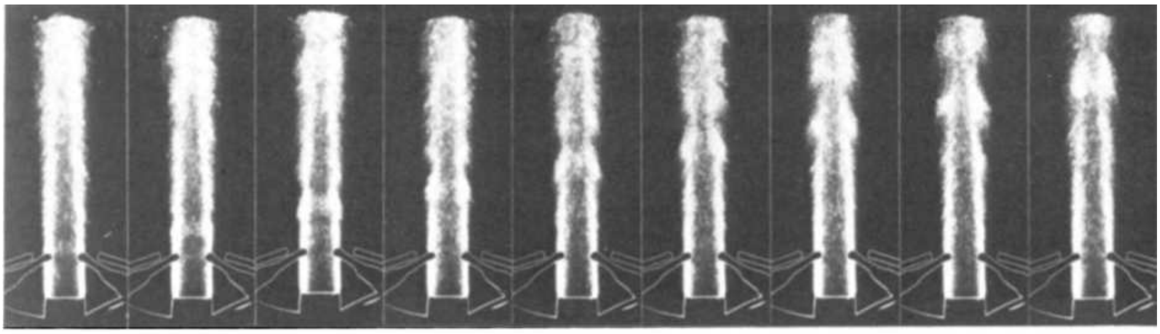

(b) 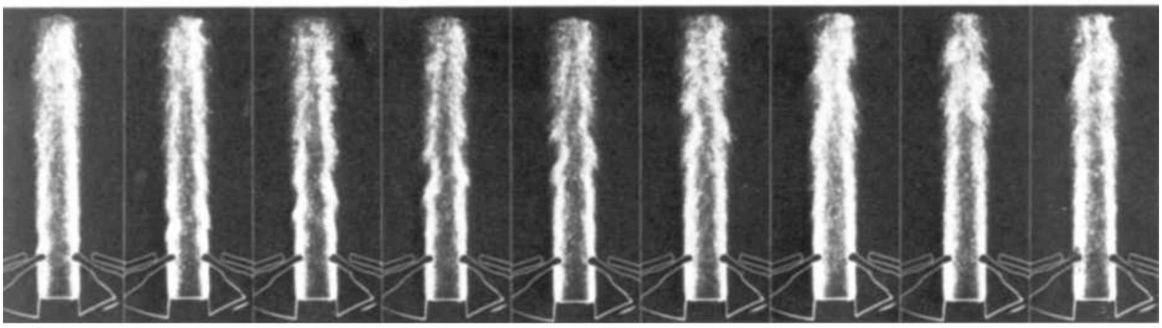

Figure I.6 – Flow visualisations with multiple flash exposures triggered by (a) the axisymmetric mode and (b) azimuthal mode 1 of the near-field pressure close to the nozzle exit of a Mach 0.83 jet. The time delay between trigger and exposures grows from left to right. Taken from Moore [142].

discussion on stability theory is postponed to the next section.

For low forcing amplitudes, the jet response obtained by Moore behaved linearly up to $x/D \approx 7$, in agreement with the results of Crow and Champagne [51]. The linearity of the response of both works is shown in figure I.7. Since the plots have a log scale on the ordinate, a linear response should produce curves with the same shape. We note in figures I.7(a) and (b) that for both experiments linear behaviour is obtained up to 7 diameters downstream for the lowest forcing amplitudes. Crow and Champagne's measurements were done further downstream, and show that even for the lowest forcing nonlinear effects are present for $x/D > 7$. This suggests that linear models are appropriate to model the development of coherent structures, and the linear stability studies, summarised in section VI, are an attempt to do so. However, the evolution of the $\mathrm{St} = 0.3$ curve of the natural jet in Crow and Champagne's experiment (the bottom curve in figure I.7(a) has a shape different from the other curves. Extrapolations of the conclusions about linearity of the forced jets to the natural flow are thus difficult.

Zaman and Hussain [207] and Hussain and Zaman [88, 89] proceeded in the characterisation of the coherent structures in forced jets. For such, phase averages of the flow velocity are

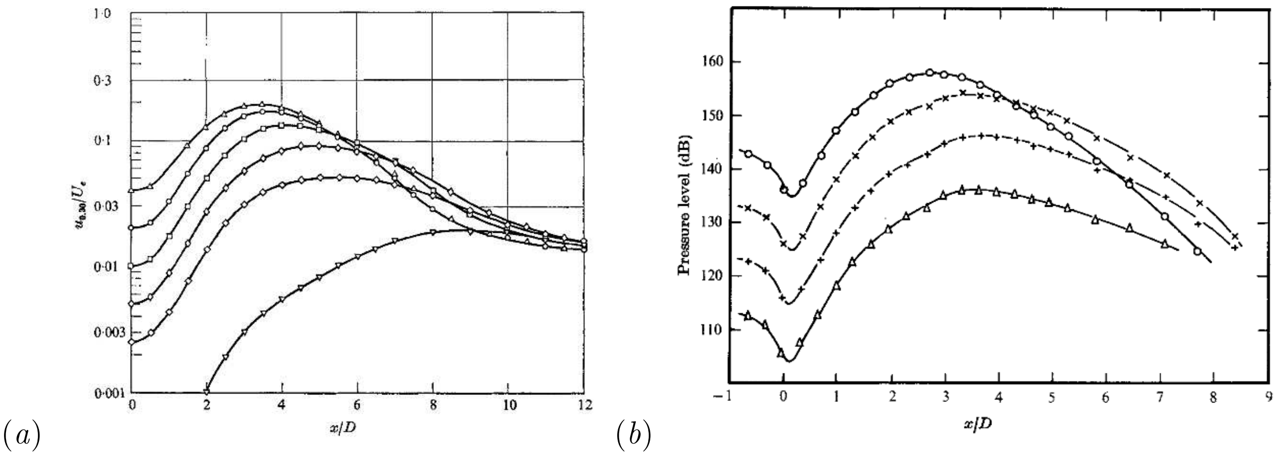

Figure I.7 – Linear and nonlinear behaviour of forced jets in (*a*) Crow and Champagne's [51] and (*b*) Moore's [142] experiment. Forcing Strouhal numbers are 0.3 for Crow and Champagne and ≈ 0.48 for Moore. Lines from bottom to top refer respectively to increasing forcing amplitudes at the nozzle exit. The triangles in Crow and Champagne's experiment refer to the unforced jet.

performed, allowing a triple decomposition of the fluctuations into a mean flow, an organised, periodic motion and an incoherent part corresponding to background turbulence (Hussain and Reynolds [87]). For high forcing Strouhal numbers, vortex pairing was observed in the first jet diameters [88, 207], but was found to be absent when the jet was forced at $\mathrm{St} = 0.3$ [89]. Due to the dominance of this Strouhal number in both unforced and forced jets, structures formed with this frequency were labelled as the 'preferred mode' of the jet. Such structures were seen to remain coherent over an axial extent of several jet diameters, and an axial succession of three coherent structures was obtained by phase averaging. As in Moore's results [142], such structures have the pattern of a hydrodynamic wave.

The artificial excitation imposed in the cited works allows an easier characterisation of coherent structures using phase averages, but the extent of their contribution in a natural flow needs simultaneous measurements at several positions in a jet. A relatively easy way to obtain information on such coherent structures without external forcing is based on pressure measurements in the near field of jets with microphone arrays; the pressure also presents the advantage of highlighting the lower azimuthal modes in the jet, as shown by Michalke and Fuchs [132] and Armstrong *et al.* [4]. Picard and Delville [156] did near-field pressure measurements with a 16-microphone array extending from $1D$ to $5.8D$ of the nozzle exit. The measurements revealed a wave-like structure in the near-field, most of which was found to be represented by the first two POD modes. Velocity measurements were also performed with a hot-wire rake, and pressure-velocity correlations allowed the authors to estimate the conditional average of the whole velocity field, the near-field pressure being used as a condition. This was done using Linear Stochastic Estimation, as proposed by Adrian [1]. Results showed the estimated velocity fields to comprise large-scale vortical structures convecting downstream. The centers of the vortices correspond to the position of minima of pressure, as in the vortex model of Lau*et al.* [107].

Tinney and Jordan [193] did similar measurements of the near pressure field for coaxial jets. The flow from the primary jet was heated, and the resulting configuration is close to a full-scale jet engine. The azimuthal modes in the near field were obtained using a ring of 16 microphones, and the axial structure was explored with a line array of 48 microphones extending up to 9 secondary jet diameters from the nozzle exit. Results showed that most of the near field can be reconstructed from modes 0, 1 and 2 alone, and for $1.08 \leq x/D \leq 6.49$ more than 40% of the near-field energy is given by the axisymmetric mode alone. The near field was shown to have the axial structure of a hydrodynamic wave undergoing spatial amplification, saturation and decay. This supports the idea that coherent structures are not an artifact of low-Reynolds, laboratory jets, and persist for jets with higher Mach and Reynolds numbers reminiscent of flows from jet engines.

1.3 Instability waves

Fundamentals A natural consequence of the aforementioned studies was the modelling of these coherent structures as linear instability waves, especially due to the linear behaviour observed in the first jet diameters [51]. Stability analysis of steady solutions of the Navier-Stokes equations dates back to Lord Rayleigh's work [160], which in itself was motivated by the experiments of Reynolds [164] of pipe flow. These experiments revealed the existence of laminar, regular patterns for lower reference velocities, and of turbulent states for higher velocities, with the appearance of eddies. Rayleigh investigated the instability of the flow in a pipe, neglecting viscous effects in the disturbance equation. Later work included viscosity in an attempt to determine the critical Reynolds number for laminar-turbulent transition, and the field of hydrodynamic stability has greatly developed since. For a review, see for instance the monograph of Criminale *et al.* [49].

The mean flow in the initial section of circular jets is an axisymmetric mixing layer, whose inflexional profile is unstable to infinitesimal wave-like disturbances, a process called *Kelvin-Helmholtz instability*. If we neglect the mixing layer thickness, the flow can be modelled as a vortex sheet; in this case, it is unstable for all disturbance wavenumbers (a derivation of this result is given by Lord Rayleigh [161] or Lamb [106] for the two-dimensional mixing layer, and by Batchelor and Gill [8] for the axisymmetric vortex sheet). For a finite mixing layer momentum thickness, there is a most unstable wavenumber, as shown by Michalke [126].

If the base flow is laminar, it is possible to study its stability by assuming infinitesimal disturbances, which in turn allows linearisation of the Navier-Stokes equations. Moreover, the stability of a given jet velocity profile can be studied assuming, as a first approximation, a *parallel base flow*, which means that the base flow variables are a function solely of the radius, which greatly simplifies the problem at hand. Due to homogeneity in time, azimuth and axial coordinates, and to the linearity of the equations, all flow variables are present in the solutions as a factor $\exp[\mathrm{i}(\omega t - \alpha x - m\phi)]$ times a radial eigenfunction, where the azimuthal mode m is real and frequencies ω and wavenumbers α are, in general, complex.

Two cases of interest are *temporal* instability, where the wavenumber is real, and the imaginary part of the frequency is related to the temporal amplitude growth, and *spatial* instability, with real frequency and imaginary wavenumber describing the spatial growth of fluctuations as they are advected downstream.

To model experiments, the spatial instability seems more appropriate. An initially laminar mixing layer leaving a splitter plate presents small fluctuations of *real* frequencies; such fluctuations may be generated, for instance, by roughness on the wall, vibrations in the experiment, or turbulence in the free stream. If the flow is unstable, some of the frequencies will be amplified as the mixing layer evolves downstream. This will lead to patterns observed in experiments (figure I.8).

If the mixing layer is initially laminar, the exponential spatial growth of the disturbances is often thought of as the initial stage of transition to turbulence. For sufficiently high fluctuation amplitudes, the linearisation of the Navier-Stokes equations using the laminar solution as a base flow becomes invalid, since the disturbances can no longer be approximated as infinitesimal and the quadratic term of the Navier-Stokes equations becomes significant. However, the qualitative similitude between flows at high and low Reynolds number, such as the one in figure I.8, has motivated the use of linearised equations using the *mean turbulent field* as the base flow, and the same instability wave *Ansatz*. Unlike the laminar case, we can no longer think of an isolated wave in a turbulent flow due to the presence of background turbulence. However, one can make an argument, at least qualitatively, based on a scale separation between the instability wave and the turbulent eddies: instability waves scale with a characteristic dimension related to the mean flow, whereas the turbulent eddies will have much lower dimensions, going down to the microscales of viscous dissipation. In this scenario, we can think of two roles for the background turbulence: the first is in establishing the mean turbulent flow, which in turn

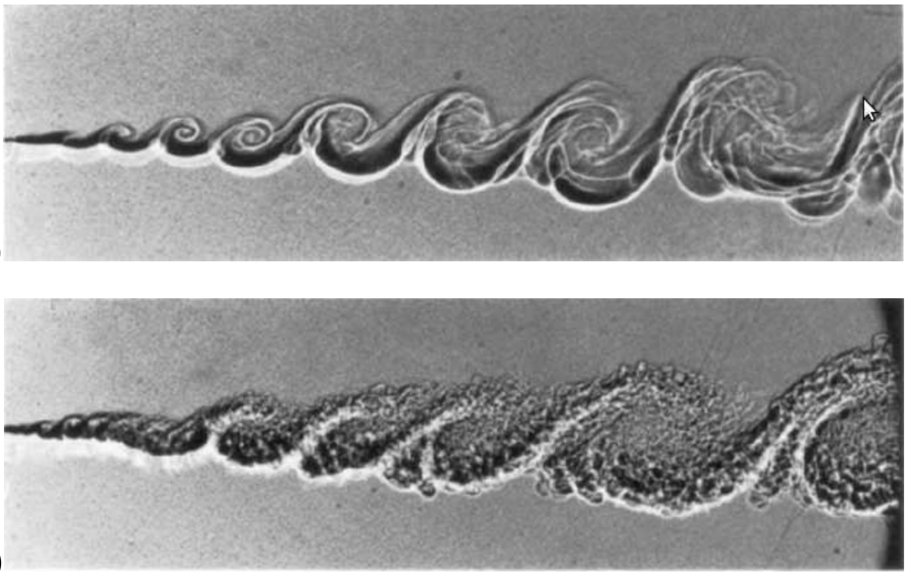

(a)

(b)

Figure I.8 – Schlieren visualisations of two-dimensional mixing layers of helium (upper stream) and nitrogen (lower stream). The Reynolds number of image (b) is four times higher than that of image (a). Taken from Brown and Roshko [27].

dictates the instability-wave properties; secondly, turbulence can provide an eddy viscosity, with a secondary effect which would tend to damp instability waves [51].

The validity of the linearisation of the Navier-Stokes equations for a turbulent flow can only be shown *a posteriori*, based on the eventual agreement with an experiment. This has been the case for a number of works in the literature; an example is the linear behaviour of the evolution of coherent structures over a region extending several jet diameters, as observed by Crow and Champagne [51] and Moore [142], and shown in figure I.7. In what follows, we review some of the calculations of linear instability waves for jets and experiments that confirmed the validity of such approach for turbulent flows. Extensions of the theory including nonlinear interactions are nonetheless discussed.

Results for parallel base flows Batchelor and Gill [8] provided solutions of the temporal instability problem for incompressible jets, whose velocity profile at the nozzle exit was considered as "plug flow", i.e. an axisymmetric vortex sheet. This analysis was extended for compressible jets by Lessen *et al.* [115], who found that increasing Mach number had a stabilising effect, a tendency that was later verified experimentally by Armstrong *et al.* [4]. Crow and Champagne [51] considered that the spatial instability problem was better suited to describe their experiments, since a *real* frequency is imposed in an upstream location by the acoustic forcing. The solutions of both problems were compared to the measurements, and, surprisingly,

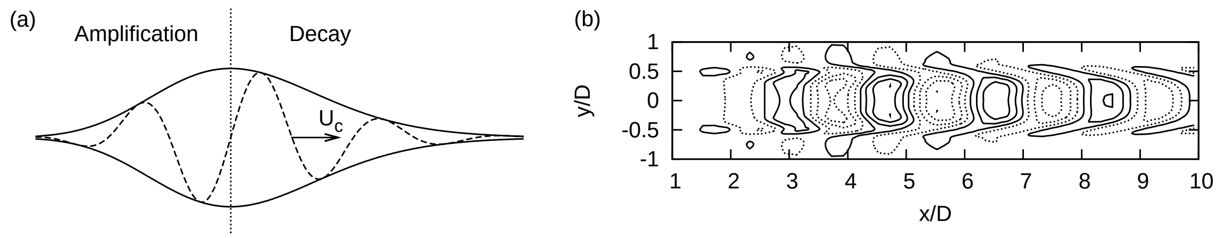

Figure I.9 – (a) One-dimensional representation of a wavepacket with convection speed U_c, and (b) linear stability results (PSE) for the axisymmetric mode of a $M = 0.6$ jet for the axial velocity fluctuations at $St = 0.4$ (full lines for positive contours, dotted lines for negative ones).

the results of temporal instability were closer to the measured convection velocities and growth rates.

The inclusion of a finite shear layer thickness in the analysis by Michalke [128] changed this picture. With a velocity profile close to the one measured two diameters downstream of the nozzle exit by Crow and Champagne, Michalke obtained good agreement of the convection velocities of the spatial instability problem with the measurements of Crow and Champagne. Further results of spatial instability confirmed its pertinence to model coherent structures in forced flows [9, 38, 154]. Moreover, with the progress in measurement techniques it became possible to isolate wave-like fluctuations in the near field of unforced jets, where the pressure is dominated by hydrodynamic fluctuations. These fluctuations were compared with predictions of linear instabity by Suzuki and Colonius [181], and good agreement was found for the axisymmetric and the first two helical modes for Strouhal numbers lower than unity.

Non-parallel and nonlinear effects All the cited works were based on the parallel flow hypothesis. An improvement on the approximations of spatial stability can be done with the assumption of a base flow evolving slowly in the streamwise direction. Solutions involve the method of multiple scales (see Crighton *et al.* [46], chapter 6, for an introduction), as applied by Bouthier [22] for boundary layers. Crighton and Gaster [47] have applied this method for the axisymmetric mode of incompressible jets, and this was followed by an extension for helical modes by Plaschko [157]. Instead of the exponential growth that parallel-flow models predict to extend indefinitely downstream, consideration of the slow divergence of the mean flow causes the amplitude to saturate and decay at downstream positions. The instability wave becomes a *wavepacket*, as sketched in figure I.9(a); a sample result for an instability wave, obtained with linear PSE, is shown in figure I.9(b).

The inclusion of the mean-flow divergence allows a formal determination of the axial envelope of the instability wave in a linear scenario. Two other possibilities to explain the decay of the instability waves were already postulated by Crow an Champagne [51]. The first is that turbulence acts in the coherent structures creating an eddy viscosity that would damp the instabilities, as discussed previously. The second is that for high wave amplitudes nonlinear effects can no longer be neglected. In Crow and Champagne's experiment significant amplitudes were measured at downstream positions for the harmonics ($\mathrm{St} = 0.6$) of the fundamental excitation at Strouhal number of 0.3, which is an indication of nonlinear effects. Another possibility is that two instability waves may interact nonlinearly to form a third wave with a frequency given by the sum or the difference of the first two. This phenomenon was observed in the experiments of Ronneberger and Ackermann [167], which are described in more detail in section 2.2.2.

For aeroacoustic applications, though, instability calculations do not directly provide the radiated sound, since the wavepacket *Ansatz* is not appropriate to describe the acoustic field. To extend the instability-wave solution to the far acoustic field, Tam and Morris [187] and Tam and Burton [184] applied the method of matched asymptotic expansions to obtain the radiated sound by two-dimensional mixing layers. For axisymmetric jets, the same technique was applied by Tam and Burton [185], with good agreement with the pressure field of forced supersonic jets.

The ideas of the method of multiple scales were incorporated in the formulation of the Parabolised Stability Equations (PSE). A review of the method is presented by Herbert [84]. As in previous methods assuming slowly-changing base-flow [22, 47, 157], PSE is based on two length scales: a slow evolution of the mean flow and a fast oscillation related to the wavenumber of the instability wave. This allows the use of a wave-packet *Ansatz* for the solution in a numerical computation. The calculation is simplified numerically by a parabolisation of the equations: the second spatial derivative of the wave-packet amplitude is neglected. This excludes upstream-propagating waves, and a solution can be obtained by marching downstram. An additional advantage of PSE is that it can be extended to the nonlinear range, including thus interactions between instability waves with different frequencies and azimuthal modes.

Linear and nonlinear PSE has been applied for a supersonic jet by Malik and Chang [123], and the results of nonlinear PSE were in good agreement with the evolution of the fluctuations of a low Reynolds number, supersonic jet of Morrison and McLaughlin [145]. A linear PSE model was applied by Gudmundsson and Colonius [80] to the same near-field pressure measurements used by Suzuki and Colonius [181]. In comparison to this last work, where instability waves are modelled using a locally-parallel flow, the authors found significant improvement of the agreement between predictions and experiments of unforced jets. Finally, linear PSE was used to develop a simplified model problem for sound generation of low Reynolds number jets by

Sandham and Salgado [173]. In this work, the authors determined the evolution of a number of linear instability waves, with different values of frequency and azimuthal mode. Subsequently, these waves were used in Lilley's acoustic analogy [118], in the formulation of Goldstein [75]. Pairs of *linear* instability waves of frequencies ω_1 and ω_2 combine to form a *nonlinear* source, whose frequency is given by the difference between ω_1 and ω_2. Instability waves have peak Strouhal number of 0.45, whereas sound radiation peaks at $\mathrm{St} = 0.19$, in agreement with the experiment of Stromberg *et al.* [179].

Convective and absolute instability For an unstable flow, a distinction can be made between *convective* and *absolute* instability. This characterisation for parallel base flows can be made based on the impulse response of the flow, as reviewed by Huerre and Monkewitz [86]. Unstable flows will present disturbances that grow in time and space, at least for one direction $x/t = \text{constant}$. The distinction between absolute and convective instability is related to the temporal growth or decay of disturbances for fixed x: if there is amplification, then the instability is *absolute*; if disturbances decay for fixed x, but grow for some directions $x/t = \text{constant}$, the instability is *convective*.

Unlike the convective instability, where growing disturbances tend to be "carried away" by the flow, in an absolutely unstable flow impulsive disturbances may grow temporally in the upstream direction, providing a resonance to the system that may lead to the domination of the fluctuations by a preferred frequency. While convectively unstable flows are labelled as *amplifiers*, since the evolution of fluctuations is dictated by upstream disturbances, flows with absolute instability are labelled as *oscillators* with a characteristic frequency that does not depend on externally imposed disturbances.

Cold (unheated) jets, such as the ones studied in the present work, are convectively unstable, but sufficiently heated jets may present absolute instabilities. This was shown theoretically by Monkewitz and Sohn [141], and subsequent experiments by Monkewitz *et al.* [140] confirmed the theoretical predictions.

For flows with absolute instabilities, it is appropriate to perform *global* stability calculations. For a jet, this amounts to considering only time and azimuth as homogeneous directions; the flow variables are expanded as two-dimensional eigenfunctions in (x, r) with a $\exp[\mathrm{i}(\omega t - m\phi)]$ dependence, with real m and complex ω. Unstable global modes have negative imaginary parts of ω, and, inversely, for stable modes $\mathrm{Im}(\omega) > 0$. Such calculations are nowadays feasible, but much more numerically intensive than the application of methods based on parallel or slowly-diverging base flows.

A review of applications of global instability is made by Theofilis [190]. Since cold jets are convectively unstable, they present only globally stable modes, but combinations of such decaying modes, which are not orthogonal, may lead to amplitude growth during transients (see discussion by Schmid [176]). An example was recently shown by Nichols and Lele [147], who determined, for a supersonic jet, optimal combinations of global modes for transient growth of the fluctuation energy. Such transient growth causes emission of bursts of acoustic energy to the far field.

2 Aeroacoustics of subsonic jets

2.1 Aeroacoustic theory

2.1.1 Lighthill's acoustic analogy

Mathematical formulation Lighthill's acoustic analogy [116] formulates an aeroacoustic problem by a rearrangement of the continuity

$$\frac{\partial \rho}{\partial t} + \frac{\partial \rho u_i}{\partial x_i} = 0 \tag{I.2}$$

and the Navier-Stokes equations

$$\frac{\partial \rho u_i}{\partial t} + \frac{\partial \rho u_i u_j}{\partial x_j} = -\frac{\partial p_{ij}}{\partial x_j}, \tag{I.3}$$

where p_{ij} stands for the stress tensor of a compressible fluid, in the form of a wave equation. Substitution of the time derivative of eq. (I.2) in the divergence of eq. (I.3) leads to

$$\frac{\partial^2 \rho}{\partial t^2} = \frac{\partial^2 \rho u_i u_j}{\partial x_i \partial x_j} + \frac{\partial p_{ij}}{\partial x_i \partial x_j}, \tag{I.4}$$

and substraction of $c_0^2 \Delta \rho$ leads to an inhomogeneous wave equation

$$\frac{\partial^2 \rho}{\partial t^2} - c_0^2 \Delta \rho = \frac{\partial^2 \rho u_i u_j}{\partial x_i \partial x_j} + \frac{\partial p_{ij}}{\partial x_i \partial x_j} - c_0^2 \Delta \rho, \tag{I.5}$$

which is known as Lighthill's equation. A usual simplification for high-Reynolds number flows is the neglect of the viscous stresses in p_{ij}[1], leading to

$$\frac{\partial^2 \rho}{\partial t^2} - c_0^2 \Delta \rho = \frac{\partial^2 T_{ij}}{\partial x_i \partial x_j}, \tag{I.6}$$

where

$$T_{ij} = \rho u_i u_j + \delta_{ij}(p - c_0^2 \rho) \tag{I.7}$$

is Lighthill's stress tensor neglecting viscous terms.

Note that the c_0 constant in this derivation is, up to this point, arbitrary. If we take it to be the speed of sound in the undisturbed fluid surrounding a turbulent flow, the left-hand side of eq. (I.6) is the appropriate wave equation for a fluid at rest, neglecting viscosity and heat conduction in sound propagation. The right-hand side is non-zero in a turbulent flow. In the acoustic field, where the acoustic disturbances are of order ϵ, we can assume T_{ij} to be zero by noting that $\rho u_i u_j$ is $\mathcal{O}(\epsilon^2)$ and that the isentropic assumption leads to $p = c_0^2 \rho$.

We than take c_0 to be the sound speed outside the turbulent flow and state the problem of eq. (I.6) as an *acoustic analogy*: we consider the problem of sound radiation by sources with intensity $\partial^2 T_{ij}/\partial x_i \partial x_j$ in a medium at rest to be analogous to sound generation by a turbulent flow.

The presence of the double divergence of T_{ij} in the source allows one to identify it with a volume distribution of acoustic *quadrupoles* with axes x_i and x_j, as discussed by Lighthill [116], Crighton [45] or Ffowcs Williams [61]. Just as dipoles are constructed with two monopoles of opposing sign brought together, in a limiting process with constant values of *distance* times *intensity*, quadrupoles are formed by a similar process applied to two dipoles of opposite direction. In this sense, a point quadrupole can be seen as the result of a double cancellation effect, with resulting low acoustic efficiency.

If no solid boundaries are present, the boundary conditions of the acoustic analogy are given by the Sommerfeld radiation condition. Using the Green's function for this problem,

$$G(x,y,t,\tau) = \frac{\delta(t - \tau - \frac{|\mathbf{x}-\mathbf{y}|}{c_0})}{4\pi c_0^2 |\mathbf{x}-\mathbf{y}|}, \tag{I.8}$$

solution of

$$\frac{\partial^2 G}{\partial t^2} - c_0^2 \Delta G = \delta(\mathbf{x}-\mathbf{y})\delta(t-\tau) \tag{I.9}$$

[1] Beside the 1/Re factor in the viscous stresses, they can be shown to give rise to octupole sources, which, for compact sources, are less acoustically-efficient than the remaining quadrupole sources in Lighthill's tensor [45].

subject to the same boundary conditions, the solution for the density can be obtained by convolution of the source terms in the right-hand side of (I.6) with the Green's function, leading to

$$\rho(x,t) - \rho_0 = \frac{1}{4\pi c_0^2} \int_{\mathcal{V}} \frac{1}{|\mathbf{x}-\mathbf{y}|} \left[\frac{\partial^2 T_{ij}}{\partial x_i \partial x_j} \right]_{\tau = t - |\mathbf{x}-\mathbf{y}|/c_0} \mathrm{d}\mathbf{y}. \tag{I.10}$$

Thus, the fluctuations of density can be obtained by a volume integral involving turbulent quantities taken at the retarded time $\tau = t - |\mathbf{x}-\mathbf{y}|/c_0$.

To calculate the sound radiation, though, application of eq. (I.10) without further assumptions would require full knowledge of the turbulent field. This approach is currently possible in computational aeroacoustics (see Wang *et al.* [201] for a review). Another possibility is to develop approximations for the source to obtain, at least qualitatively, some information on the radiated sound. Such approximate models are discussed next.

Source models For most applications, calculation of the radiated sound in the far acoustic field is sufficient. In this region, eq. (I.10) can be rewritten using a relation between spatial and temporal derivatives (see Lighthill [116], or Goldstein [74] for a more detailed derivation), leading to

$$\rho(x,t) - \rho_0 = \frac{1}{4\pi c_0^4} \int_{\mathcal{V}} \frac{(x_i - y_i)(x_j - y_j)}{|\mathbf{x}-\mathbf{y}|^3} \left[\frac{\partial^2 T_{ij}}{\partial \tau^2} \right]_{\tau = t - |\mathbf{x}-\mathbf{y}|/c_0} \mathrm{d}\mathbf{y}. \tag{I.11}$$

To obtain the velocity dependence of the radiated sound, Lighthill proceeded considering that the stress tensor T_{ij} could be approximated by $\rho_0 u_i u_j$ for low Mach number flows, and in this case should be proportional to $\rho_0 U^2$, where ρ_0 and U are reference values for the density and the velocity in the turbulent flow[2]. The influence of the time derivative of T_{ij} is estimated considering that the characteristic time for turbulence is proportional L/U, where L is a reference length. A characteristic frequency is thus proportional to U/L, as in a Strouhal number scaling, and the double time derivative in eq. (I.11) can be roughly estimated as

$$\frac{\partial^2 T_{ij}}{\partial \tau^2} \sim \frac{\rho_0 U^4}{L^2}. \tag{I.12}$$

We can now assume that the volume distribution of T_{ij} is given by a set of uncorrelated turbulent eddies. We consider that each eddy is *acoustically compact*, i.e. its characteristic

[2]This proportionality amounts to assume that changes in Mach number have no effect in the turbulent source, as in an incompressible flow. This was however contradicted by the results of Armstrong*et al.* [4] and Suzuki and Colonius [181]. Lighthill [117] already conjectured that compressibility effects were the reason for the values lower than 8 found for the velocity exponent of acoustic intensity and power. Further discussion on this matter is presented in chapter V.

dimension L is much smaller than the acoustic wavelength λ. This allows the neglect of retarded time differences within a single eddy when applying eq. (I.11), which will amount to the multiplication of the integrand by an eddy volume proportional to L^3. Individual eddies behave thus as point quadrupoles. The density in the farfield due to its sound radiation will thus be proportional to $\rho_0 U^4 L/(c_0^4 x)$.

The far-field pressure is given by $c_0^2(\rho - \rho_0)$, and the acoustic intensity by $p^2/(\rho_0 c_0)$. Therefore, the acoustic intensity was estimated by Lighthill to be of order

$$I \sim \frac{U^8 L^2}{c_0^3 x^2}. \tag{I.13}$$

The radiated power is obtained by a surface integration of the acoustic intensity over a sphere with radius x. The power is thus proportional to $U^8 L^2/c_0^3$. This result became well known as Lighthill's U^8 law. Later experiments (Mollo-Christensen *et al.* [139]) have shown velocity dependences of acoustic intensity close to Lighthill's prediction, albeit slightly higher for small polar angles, and lower for the sideline direction.

The view of turbulence as a group of incoherent eddies was dominant at the time of the formulation of Lighthill's analogy, and one of the first applications of Lighthill's analogy was done by Proudman [159], who considered isotropic turbulence to model the source. Ribner [165] followed a similar approach, but instead of a model of isotropic turbulence he assumed specific forms for the spatial correlations for turbulence and considered the axial symmetry of jets and acoustic compactness to obtain the directivity shape of sound radiation.

Derivations based on compact eddies will not account for coherent structures present in a turbulent jet. If the source is an axially-extended wavepacket, different parts of the fluctuating velocity field will cause interference in sound radiation, and it is important to consider the flow field in Lighthill's analogy as a *volume distribution of quadrupoles*, and not as a superposition of point quadupoles with random phase which are representative of each eddy. In Lighthill's integral the changes in retarded time for different positions become crucial if a source resembles the ones depicted in figure I.9. A first modelling effort of a wave-packet source was done by Mollo-Christensen [138], who proposed a model of a semi-infinite line emitter for jet noise given by a hydrodynamic wave modulated by an envelope function related to the Laguerre polynomials. Such a model reproduced the wave-like correlations measured in the near pressure field of subsonic jets. A sample source proposed by Mollo-Christensen is shown in figure I.10.

Further theoretical work was done by Michalke [127], who considered an expansion of the source in cylindrical coordinates. In this case a Fourier series in the azimuthal angle is a natural expansion, and the linearity of Lighthill's analogy ensures that each azimuthal mode

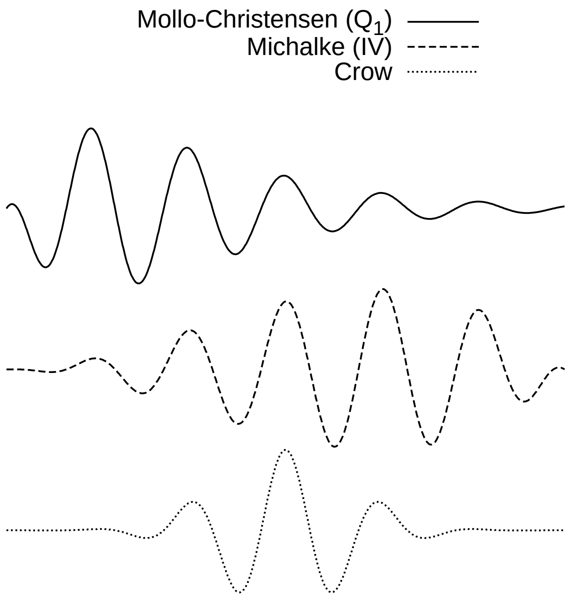

Figure I.10 – Some wave-packet source models for coherent structures in jets

in the source will radiate the same azimuthal mode in the acoustic field. This showed that for sufficiently low frequencies and polar angles[3] the acoustic radiation is dominated by the axisymmetric mode, since the integral solution of Lighthill's equation for the far-field pressure for an azimuthal mode m for the source involves a $J_m(kr'\sin\theta)$ factor, as in eq. (2.25) of the cited work,

$$P_{m\omega}(r,\theta) = \frac{\mathrm{i}^{-m}\mathrm{e}^{\mathrm{i}kr}}{2r}\int_0^L\int_0^R \mathrm{d}x'\mathrm{d}r'\tilde{Q}_{m\omega}(x',r')r'J_m(kr'\sin\theta)\mathrm{e}^{-\mathrm{i}kx'\cos\theta}, \tag{I.14}$$

where P is the pressure, Q is the source in Lighthill's equation, k is the acoustic wavenumber ω/c and J_m is the Bessel function of first kind with order m. The subscripts m and ω refer respectively to the azimuthal mode and the frequency.

The $J_m(kr'\sin\theta)$ factor is due to azimuthal interference in a ring source of radius r'. Recalling the $kr' = 2\pi r'/\lambda$, where λ is the acoustic wavelength, the argument of J_m is proportional to the ratio between the projection of r in the radiation direction and the acoustic wavelength. If this ratio is small, retarded time differences between points in the ring is negligible, and sound radiation from an axisymmetric mode will be much higher than that of the other azimuthal modes, for the $\exp(\mathrm{i}m\phi)$ dependence will lead in this case to *destructive* interference for $m \geq 1$,

[3]More precisely, if the projection of the jet diameter in the radiation direction, $D\sin\theta$, is much smaller than the acoustic wavelength.

and *constructive* interference for $m = 0$. For $kr' \sin\theta = 0$, only the axisymmetric mode radiates, since $J_m(0)$ is equal to 1 for $m = 0$ and is zero for all other m.

This is further illustrated in figure I.11, where we plot in dB the ratio between $J_m(kr' \sin\theta)$ and $J_0(kr' \sin\theta)$ for $r = D/2$ (the jet lipline), assuming the Mach to be 0.9 and the radiation angle to be 30 degrees. For a given Strouhal number, this ratio represents the difference in SPL between the axisymmetric mode and azimuthal mode m, considering that the sources for both modes have the same intensity; it may be thus interpreted as the radiation efficiency for a given mode m if compared to the axisymmetric mode. We see that for low Strouhal numbers there is a sharp decay of this efficiency with increasing m. For instance, for $\mathrm{St} = 0.2$ mode 1 has an SPL 17dB lower than the axisymmetric mode if both modes have the same source intensity. For higher m the efficiency is even lower.

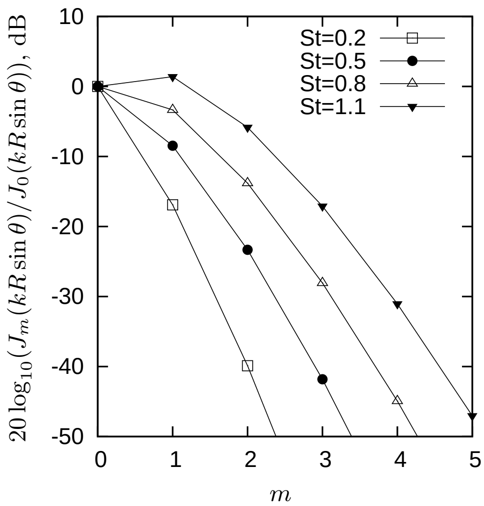

Figure I.11 – Relative efficiencies of azimuthal mode m compared to the axisymmetric case, considering $\theta = 30°$, $M = 0.9$ and $r = D/2$.

This result suggests that for low-frequency radiation at low angles, high azimuthal modes are "cut-off" due to azimuthal interference in the source, and the lower azimuthal modes dominate far-field sound radiation. If there are azimuthally-coherent structures in a jet, with low m, they should in theory be responsible for most of the sound radiation at low frequencies.

Michalke also considered sources in the form of hydrodynamic waves, with amplitude modulation. One such wave-packet source is shown in figure I.10. In this case, eq. (I.14) can be further developed, leading to

$$P_{m\omega}(r,\theta) = \frac{\mathrm{i}^{-m}\mathrm{e}^{\mathrm{i}kr}}{2r} \int_0^L \int_0^R \mathrm{d}x' \mathrm{d}r' \tilde{Q}_{m\omega}(x',r') r' J_m(kr' \sin\theta) \mathrm{e}^{\mathrm{i}\alpha(1-M_c\cos\theta)x'}, \tag{I.15}$$

where α is the wavenumber of the hydrodynamic wave and M_c is the convection Mach number.

Crow [50] (see also Crighton [45]) has also modelled a source in Lighthill's analogy as an axisymmetric wavepacket, with an envelope function given by a Gaussian function $\exp(-x^2/L^2)$. Such a source is sketched in figure I.10. The resulting sound radiation is axisymmetric, and can be calculated analytically. The derivation is shown in Chapter V, leading to a radiated pressure of

$$p(R,\theta,m=0,t) = -\frac{\rho_0 U \tilde{u} M_c^2 (kD)^2 L\sqrt{\pi}\cos^2\theta}{8R} \mathrm{e}^{-\frac{L^2k^2(1-M_c\cos\theta)^2}{4}} \mathrm{e}^{\mathrm{i}\omega\left(t-\frac{R}{c}\right)}, \tag{I.16}$$

where k is the convection wavenumber, M_c is the convection Mach number, R is the distance from the origin, taken to be in the source region, and θ is the polar angle measured from the downstream jet axis.

A significant feature of this result is the exponential dependence of the sound radiation with polar angle, or, more precisely, with $-L^2k^2(1-M_c\cos\theta)^2/4$. This dependence was later labelled as *superdirectivity* by Crighton and Huerre [48]. For subsonic convection, the maximum acoustic intensity is for $\theta=0$, and there is an exponential decay for higher polar angles. This decay is significant for high values of kL and M_c and is related to the sound radiation by a non-compact, wave-like source: the superdirective radiation results from the acoustic interference between positive and negative parts of the source which present phase coherence.

If the convection is supersonic, the maximum radiation is for the Mach angle $\theta = \cos^{-1}(1/M_c)$. Examples of the radiated pressure for subsonic and supersonic wavepackets are shown in figure I.12.

The predictions of Crow's model suggest that to investigate the presence of wave-packet radiation in subsonic jets, the axisymmetric radiation should be measured at low polar angles. Some experiments have addressed this, and are discussed in section 2.2.2.

Ffowcs Williams and Kempton [63] have extended Crow's model in order to include randomness in the convection speed of a wavepacket of frequency ω. This randomness is an attempt to account for the "jitter" observed in the behaviour of coherent structures (see discussion in section 1.2). For low source jitter, the sound radiation is mostly monochromatic at ω. If the randomness is significant, however, there is sound radiation for a wider range of frequencies.

Mankbadi and Liu [125] developed a wave-packet model for the sources in Lighthill's analogy, but, unlike the models proposed by Mollo-Christensen [138], Crow [50] or Ffowcs Williams and Kempton [63], Mankbadi and Liu tried to derive the wave-packet shape from first principles. Based on their previous work [124], the evolution of large-scale structures is determined by conservation in the streamwise direction of the radially-integrated energy. This is done

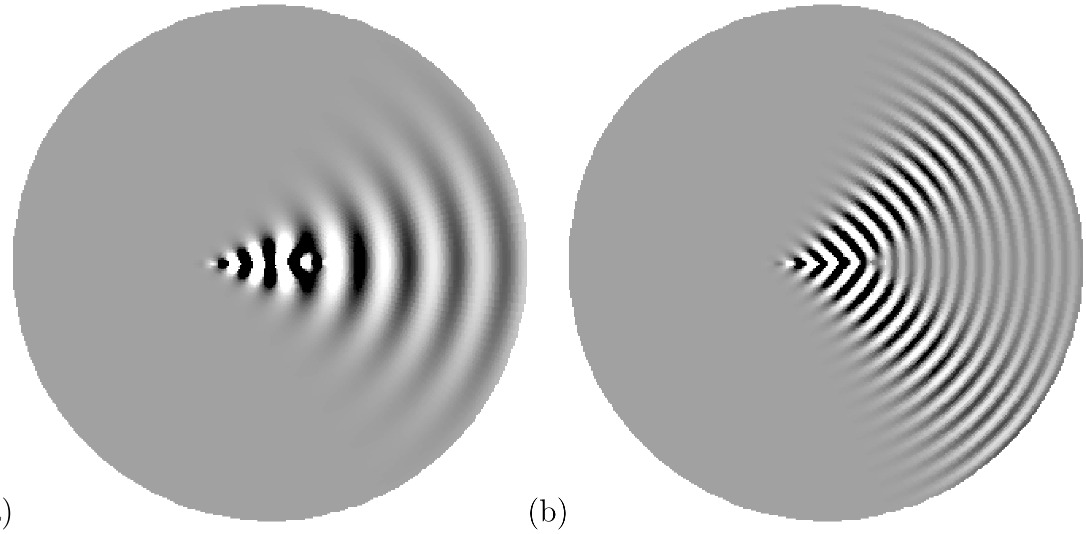

(a) (b)

Figure I.12 – Wave-packet radiation from Crow's source model for (a) $M = 0.9$ and (b) $M = 2.5$. The convection Mach number is supposed as $0.6M$.

after assumptions on the shape of the mean velocity profile, the fine-scale turbulence and the large-scale structures; the latter are obtained by a linear stability calculation. The acoustic radiation from the large-scale structures, which form a wave-packet source, is then calculated individually for each frequency and azimuthal mode using Lighthill's analogy, such as proposed by Michalke [127] or Michalke and Fuchs [132]. Results are presented for azimuthal modes 0 and 1, and reproduce, at least qualitatively, some trends of the experimental far-field pressure of subsonic jets: the sound radiation beams towards low angles, and the peak frequencies for sound radiation were close to the experimental results of Lush [120]. However, the authors made only limited quantitative comparisons, in part due to the lack of measurements of the individual azimuthal modes in the acoustic field.

2.1.2 Inclusion of flow-acoustic effects in acoustic analogies

Phillips [155] proposed a different formulation to deal with sound generation by supersonic flows. He reworked the continuity, Navier-Stokes and energy equations in the form of a convected wave equation, which, in its simplified form (eq. 3.1 in Phillips' paper), is given by

$$\left\{ \frac{D^2}{Dt^2} - \frac{\partial}{\partial x_i} c^2 \frac{\partial}{\partial x_i} \right\} \log\left(\frac{p}{p_0}\right) = \gamma \frac{\partial u_i}{\partial x_j} \frac{\partial u_j}{\partial x_i}, \tag{I.17}$$

where D/Dt is the material derivative, c is the *local* speed of sound, p_0 is the pressure of the undisturbed fluid and γ is the ratio of specific heats. Phillips realised that for high Mach number flows, convection effects in acoustic waves in the moving fluid (inside the jet for the present problem) can no longer be neglected, as well as refraction of sound waves due to the spatial variations of the sound speed. Since the equations of Phillips and Lighthill are both exact, the two formulations include these effects, but whereas convection and refraction are included in the *source* term of Lighthill's analogy, they are explicitely modelled by the *operator* in Phillips' formulation. Therefore, we can think of Phillips' equation as another acoustic analogy, but with an analogous problem of sound propagation in a fluid moving with the average velocity of the real turbulent flow.

Phillips included refraction of sound waves by inhomogeneities of the local speed of sound, but did not account for refraction caused by a mean shear. This effect was previously accounted for by Pridmore-Brown [158], who derived a propagation equation to model sound propagation in ducts with boundary layers; the mean shear is included in a modified wave equation, know as Pridmore-Brown equation, and was seen to redirect acoustic waves towards the duct walls for waves propagating in the flow direction. The neglect of refraction by shear in Phillips' equation was noted by Doak [55] and Lilley [118]; this last author proposed a reformulation of the acoustic analogy in order to obtain the correct Pridmore-Brown operator in the left-hand side, assuming constant mean shear in the streamwise direction (as in parallel-flow assumption in stability theory, discussed in section 1.3). Lilley's equation, neglecting viscous effects and entropy fluctuations, is given by

$$\frac{D}{Dt}\left(\frac{D^2 r}{Dt^2}-\frac{\partial}{\partial x_i}c^2\frac{\partial r}{\partial x_i}\right)+2\frac{\partial u_k}{\partial x_j}\frac{\partial}{\partial x_k}\left(c^2\frac{\partial r}{\partial x_j}\right)=-2\frac{\partial u_j}{\partial x_k}\frac{\partial u_i}{\partial x_j}\frac{\partial u_k}{\partial x_i}, \tag{I.18}$$

where $r=(1/\gamma)\log p$ (see also Goldstein [74] or Colonius *et al.* [41]). The effect of shear in the acoustic waves is apparent in the last term of the left-hand side, which is absent from the operator in Phillips' equation, where it is, in fact, inside the source term.

Phillips' and Lilley's work can be seen as steps to remove flow-acoustic effects from the *source* in Lighthill's equation and include them in the *propagation operator*. A further refinement was proposed by Goldstein [76] as a generalised acoustic analogy. This generalisation permits the selection of an *arbitrary* base flow. The continuity, Navier-Stokes and energy equations are rewritten in an inhomogeneous form, linearised in the disturbance variables. Other acoustic analogies, such as Lilley's, can be obtained as particular cases of the generalised one.

Goldstein's analogy allows the selection of the time-averaged quantities as the base flow, which, compared to the parallel sheared flow assumed in Lilley's equation, is a significant improvement. Hence the flow-acoustic effects caused by the mean flow are modelled by the operator in the generalised acoustic analogy. Moreover, the possibility of choosing an *unsteady* field as a base flow is appealing, since if we could isolate an unsteady part of the flow that did not radiate sound, the formulation of the generalised acoustic analogy using this "silent" base flow would make the analog acoustic problem closest to the actual flow. The question is how to produce such an unsteady, silent flow. Goldstein [76] proposed solutions of incompressible problems as base flows. Later, he proposed a filtering of the flow variables based on the radiating criterion given by the dispersion relation in a medium at rest [77, 78]: the unsteady, silent flow is identified with all the energy in the frequency-wavenumber spectrum that does not lie on the circles given by $\omega = kc$. These ideas were recently pursued by Sinayoko *et al.* [177], who showed that, at least in simplified problems, such separation is possible. Sinayoko *et al.* presented a different formulation of the generalised acoustic analogy, with all radiating variables moved to the operator. This formulation led to calculation of the far-field sound in good agreement with direct numerical simulation. Some questions remain, however, when the $\omega = kc$ filter is applied to isolate an unsteady flow, supposedly silent, to be used in a generalised acoustic analogy, since the said criterion is obtained by an analysis of the source in Lighthill's analogy. Another issue is that isolation of a single wavenumber leads to a filtered field which is unlimited in space, going far beyond the usual assumed boundaries for a turbulent jet.

Increasing sophistication in the formulation of acoustic analogies has the advantage of the inclusion of flow-acoustic interactions in the operator, so that phenomena as refraction are not contained in the equivalent sources. The price paid is a more complex solution. Unlike Lighthill's analogy, for which Green's functions are available in both time and frequency domains (see, for instance, Crighton [45]), allowing a number of properties to be established analytically, in general Green's functions for Lilley or Goldstein's analogies need to be determined numerically. This is done, for instance, by Karabasov *et al.* [96] for Goldstein's analogy. Approximate Green's functions for Lilley's analogy in the high- and low-frequency limits have been derived by Tester and Morfey [189], but in the general case numerical computations of the Green's functions are needed.

One should however keep in mind that the flow-acoustic effects included in the operator are derived assuming low-amplitude acoustic disturbances. In a sheared turbulent flow this assumption is questionable, and in general there is no clear distinction between acoustic, vortical and thermal modes, which are nonlinearly coupled (see discussion by Goldstein [74], chapter 6, or by Kovásznay [105] and Chu and Kovásznay [37]). The analog problem defined by Lilley's or Goldstein's analogies describes *convection and refraction of infinitesimal acoustic disturbances by steady, sheared flows.* Compared to Lighthill's analog problem of sound propagation in a medium at rest, this is clearly closer to the physical phenomena in a turbulent jet; however, this remains an analog acoustic problem which will be different from the actual nonlinear phenomena in a turbulent flow, where, for instance, velocity fluctuation amplitudes are of 10–20% of the reference mean fluid velocity and cannot be considered as purely acoustic.

2.2 Experimental jet-noise studies

2.2.1 General observations of the acoustic field of subsonic jets

One of the first published studies including measurements of the noise of subsonic jets was the work of Mollo-Christensen *et al.* [139]. In this set of experiments significant care was taken in order to reduce parasite sources of sound unrelated to the jet. The authors showed that the overall sound has a single directivity lobe directed downstream. Frequency decomposition of the sound radiation showed that this lobe is composed mostly of low-frequency sound. The high-frequency radiation was seen to have a different directivity pattern; when only Strouhal numbers higher than 2 are considered, the far-field directivity has a peak for a polar angle θ around 45°. As the frequency is lowered, the directivity peak moves progressively to lower polar angles. This leads to different spectral shapes for low and high polar angles.

Lush [120] performed measurements of the noise of subsonic jets, and compared the directivities to predictions of Lighthill's acoustic analogy, assuming that the sources are compact convected quadrupoles, whose basic directivity is modified by a Doppler factor of $(1-M_c\cos\theta)^{-5}$, as shown by Ffowcs Williams [60]. Frequency-dependent directivity plots were obtained from 1/3-octave spectra, and the comparison between the theoretical directivity shapes and the experimental ones was favorable, especially near $\theta = 90°$; however, discrepancies were present for low polar angles for all frequencies considered. Lush also noted that the peak frequency of sound radiation at 90 degrees from the jet axis scales with Strouhal number; however, in his experiments the peak frequency for sound radiation at low polar angles did not change with jet velocity, and was inversely proportional to the jet diameter. A Helmholtz number ($\mathrm{He} = fD/c$) scaling thus applies to the peak frequency at low polar angles. This was also noted by Tanna [188].

The different spectral shapes at low and high polar angles, observed by the cited authors, are illustrated in figure I.13, generated from data from the experiments described in chapter V. We see in the figure the contrast between the sharper spectral peak characteristic of low angles (20 or 30 degrees in figure I.13) with the broader spectra of high polar angles. These shapes, taken from supersonic jet noise data, were fitted with empirical functions by Tam *et al.* [186]; spectra of subsonic jets were also seen to be fitted by these functions by Viswanathan [198]. The empirical shapes were labelled as "large-scale turbulence spectrum" (for low polar angles) and "fine-scale turbulence spectrum" (for high polar angles), implying that two different mechanisms of sound

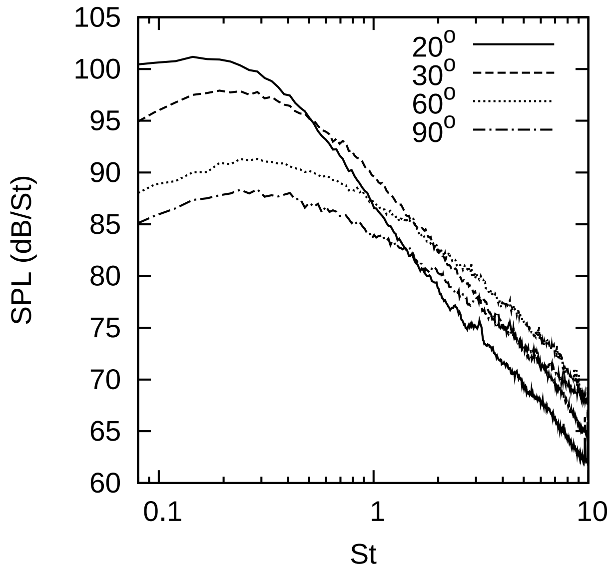

Figure I.13 – Comparison of spectra at $35D$ from the nozzle exit of a Mach 0.6 jet.

radiation are present in jet noise, one dominating each radiation direction. This conjecture, though, is questioned by Kleinman and Freund [100], who note that "such a decomposition is particularly curious since both spectra have a similar spectral peak frequency, which seems inconsistent with the expectation that finer scales should emit higher frequencies". Indeed, the observation of the spectra in figure I.13 shows that there is not a clear separation between the spectral peaks of, say, 20 and 90 degrees.

The downstream directivity of subsonic jets, especially for low Strouhal numbers, as seen in figure I.13, suggests that the low-frequency sound may be related to coherent structures forming a non-compact wavepacket, as discussed in section 2.1.1. We discuss next some experimental investigations on the role of coherent structures in aerodynamic sound generation.

2.2.2 Sound generation by coherent structures

Linear and nonlinear mechanisms of sound radiation by coherent structures The acoustic excitation used to provide a phase locking of the coherent structures in a number of experimental studies (for instance, the works of Crow and Champagne [51] and Hussain and Zaman [89]) leads to some ambiguity when the sound radiation of such flows is studied, since spectra of the radiated sound presents peaks at the excitation frequency, and one usually cannot tell whether such peaks are related to the time-periodic coherent structures or to the propagation and refraction of the acoustic waves used to force the flow.

This ambiguity is illustrated by the work of Moore [142], who tried to discern whether coherent structures, seen to correspond to instability waves, radiate sound in forced jets. The approach consisted of a comparison of the acoustic powers in the far-field and inside the nozzle for the excitation frequency. The result was a *lower* acoustic power in the far field, from which Moore concluded that there was no significant sound radiation by the instability wave. The conclusion was nonetheless disputed by Laufer and Yen [109] and Michalke [130]; this last author affirmed that "this conclusion is, however, questionable, since the sound measured in his experiments consists of contributions from the sound radiated by the excited flow as well as from the exciting sound itself. Hence it can only be concluded that the sound power radiated by the coherent structure is very small compared to that of the exciting sound field."

However, when nonlinear effects are present in the development of instability waves, sound radiation is obtained for frequencies other than the ones involved in the excitation, and can thus be more clearly related to phase-locked coherent structures. Ronneberger and Ackerman [167] forced subsonic jets with pairs of frequencies whose difference was $\Delta \mathrm{St} = 0.2$. This difference frequency was detected in both the near and far pressure fields. The near-field pressure was seen to have a wave-like behaviour, and was identified with an instability wave resulting from the nonlinear interaction of the two primary instability waves forced by the excitation. The radiated sound at the difference frequency was seen to beam at low polar angles, a difference of more than 20dB being found between polar angles $\theta = 30°$ and $70°$. Ronneberger and Ackermann recognised the ambiguity in the analysis of far-field noise for the *direct* excitation of instability waves, and tried also to excite directly the instability wave at $\mathrm{St} = 0.2$ by forcing mechanisms supposed to generate little far-field noise. Their conclusion was that this linear mechanism radiates sound with a directivity shape nearly identical to the nonlinear, difference frequency case; however, the radiated sound by the nonlinear instability wave was more than 20dB higher than the directly forced instability wave. However, care should be taken in the interpretation of this result, since the experimental setup is different from most experimental works with jets, for the nozzle was mounted on a wall of the anechoic chamber.

Laufer and Yen [109] performed measurements of natural and forced jets, but this time the excitation was at a single frequency. The boundary layers at the nozzle exit were also laminar. The peak frequency in the near-field pressure spectra close to the nozzle exit (i.e. in the region of laminar-turbulent transition of the mixing layer) had a Strouhal number based on the momentum thickness of 0.017, which was close to the predicted St for the maximum spatial growth of axisymmetric disturbances according to linear stability theory [128]. At downstream stations, this primary instability wave decayed, and another wave was detected for the subharmonic; this was identified with the pairing of axisymmetric vortex rings. Other subharmonics appear further downstream. For *forced* jets using the same fundamental instability frequency, the same process takes place, but the peaks in the near-field spectra for the fundamental and subharmonics are better defined. For all forced jets, a hydrodynamic wave was detected for the first subharmonic, with amplification, saturation and decay in the axial direction. This envelope was well fitted by a Gaussian function; hence, the measured wave-packet agrees with the source model postulated by Crow [50] (see section 2.1.1). Even more significantly, the radiated sound field at the subharmonic frequency had an exponential dependence of $(1 - M_c \cos\theta)^2$; this *superdirective* radiation (Crighton and Huerre [48]) was predicted by Crow's model.

The results of Laufer and Yen point to a significant role of wavepackets in jet noise; in this case, the wavepackets resulted from a pairing process. However, since the experiments were performed with low-Reynolds, low-Mach jets with laminar boundary layers, questions remained regarding the applicability of these conclusions for jets with high Reynolds and Mach numbers, with turbulent boundary layers. The work of Bridges and Hussain [25] shed some light on the subject. Low Mach number, natural jets with laminar boundary layers at the nozzle exit showed clear peaks in the far-field pressure for both the fundamental and subharmonic frequencies. These peaks were nonetheless absent in far-field spectra of jets with turbulent boundary layers. The authors concluded that the difference between these two cases is that the initially laminar shear layers led to the occurence of clean, phase-locked vortex pairings, while turbulence tends to diffuse the coherent vorticity and prevents such harmonic pairings.

Azimuthal decomposition of the sound field For unforced jets, decomposition of the acoustic field into azimuthal Fourier modes is another way to assess the sound radiation by coherent structures, if one considers a linear scenario where each azimuthal mode in the source corresponds to the same mode in the acoustic field. This is the case for Lighthill's analogy, as observed by Michalke [127] and discussed in section 2.1.1; however, it should be noted that the radiated sound is linear as a function of T_{ij}, but is a nonlinear function of the velocity disturbances, which appear quadratically inside Lighthill's stress tensor. In a linear framework low azimuthal modes in the sound field are an indication of sound radiation by azimuthally-coherent structures in the flow.

Maestrello [121] measured two-point correlations of the far-field over a sphere centered on the nozzle exit. The azimuthal correlations revealed low-angle radiation to be highly coherent. As the polar angle is increased, the azimuthal coherence of the far-field sound decreases. This led Maestrello to postulate that "sound radiated at small angles from the jet axis is probably generated by coherent sources while at large angles (...) the noise sources are most likely incoherent". However, Fuchs and Michel [72] used the correlation data from Maestrello [121, 122] to decompose the far-field pressure at 90 degrees from the jet axis as a function of frequency and azimuthal mode. For lower frequencies (St < 0.4) the far-field sound was seen to be dominated by modes 0, 1 and 2, showing that the coherence of the radiated sound was still significant for large radiation angles.

A more complete evaluation was made by Juvé *et al.* [94], who decomposed the far-field sound into azimuthal modes for polar angles of 30, 60 and 90 degrees to the jet axis. This was done for the overall sound, but also for filtered correlations at Strouhal numbers of 0.15, 0.3 and 0.6. In all cases the radiated sound was dominated by azimuthal modes 0, 1 and 2. For $\theta = 30°$ the axisymmetric mode is dominant, accounting for more than half the energy of the radiated sound. For higher angles, modes 1 and 2 become more important. Mode 2 dominates sound radiation for $\theta = 90°$, and for $\theta = 60°$ modes 1 and 2 have comparable amplitudes in the far field. Filtering for low frequencies did not change significantly this picture. These results are in agreement with the theoretical prediction of Michalke [127] that low-order azimuthal modes are more efficient sound generators, particularly for radiation at low values of the frequency and of the polar angle (see section 2.1.1).

2.2.3 Flow-acoustic correlations

The possibility to simultaneously measure the jet velocity and the far-field pressure is attractive, since correlations between the two quantities can be calculated in a straightforward way, and provide a measure of the contribution of a given position in the flow to the radiated sound, in what was called a *causality* method. This was noted by Lee and Ribner [111], who rewrote Lighthill's analogy to obtain the *autocorrelation* function of the far-field pressure as a volume integral of the *cross-correlation* between the stress tensor T_{ij} and the far-field pressure. The far-field pressure autocorrelation is closely related to the spectra of the radiated sound, since the power spectral density can be obtained by a Fourier transform of the autocorrelation function. Lee and Ribner performed velocity measurements using a hot film to obtain T_{ij} in the radiation direction (which was shown by Proudman [159] to be the only component of Lighthill's stress tensor to radiate to the far-field), and the far-field pressure was measured at $\theta = 40°$. The authors filtered their cross-correlations in narrow frequency bands; as a result, upstream parts of the jet were related to high frequency radiation, and downstream parts were related to lower frequencies.

Later, Juvé *et al.* [95] used a similar approach, but the investigation aimed the evaluation of the instantaneous contribution of a given region to the radiated sound. The time series of the product between the far-field pressure and the second time derivative of the velocity were analysed; such time traces are related to the mentioned instantaneous contribution, and when averaged in time lead to the cross-correlations typical of the causality method. Results showed the contribution of points close to the end of the potential core to be *intermittent*, with periods of intense activity when peaks are observed in the second time derivative of the velocity.

The use of optical measurement techniques prevented contamination in the acoustic field caused by the probe used for velocity measurements. Schaffar [174] applied the causality method using fluctuation measurements taken with a laser Doppler velocimeter. Application of the causality integral led to quantitative agreement with the overall sound and with spectra at low frequencies for sound radiation at low polar angles (20 and 30 degrees to the jet axis). The transition region, downstream of the end of the potential core, was identified as dominant for sound radiation at the cited low angles.

Panda *et al.* [151] used molecular Rayleigh scattering to measure flow velocity and density simultaneously, so that linear, quadratic and cubic terms of $\rho u_i u_j$ could be determined. Correlations of fluctuations downstream the end of the potential core with the far-field sound at 30° to the jet axis were significant for supersonic jets (more than 20% for Mach 1.8), but much lower for subsonic jets, a value around 2% being found for a Mach 0.8 jet.

Hileman [85] did high-speed flow visualisations of a Mach 1.28, perfectly expanded jet, and the resulting images were separated in two groups according to the far-field sound at low polar angles, one related to "noise generation" periods, when intermittent bursts of acoustic energy are detected by a microphone array, and other for periods of "relative quiet"; this is consistent with the observations of Juvé *et al.* [95]. The "noisy" periods were associated with the sudden decay of large scale structures close to the end of the potential core.

2.2.4 Effect of nozzle-exit conditions

The sensitivity of jet noise to the conditions of the nozzle exit is an essential issue. From a practical perspective, if there is such sensitivity, comparisons between noise measurements from different facilities becomes a difficult task, since the precise nozzle conditions need to be reproduced in each experiment. On the other hand, knowledge of the sensitivity of jet noise to the upstream conditions is required in the search for silent nozzles, and would greatly help in the design of noise-reduction controllers, passive or active.

A basic difference regarding sound generation is present if the boundary layer at the nozzle exit is laminar or turbulent; this was studied by Bridges and Hussain [25], who showed that significant differences in spectra are observed for jets with laminar or turbulent boundary layers. However, it is not clear if significant sensitivity to the upstream conditions should be observed among jets with turbulent boundary layers. This topic currently motivates research and debate in the aeroacoustics community.

Viswanathan [198] compared his jet-noise measurements to those of Ahuja [2] and Tanna [188], and found out there was in general agreement between the datasets for low frequencies. However, discrepancies are present for higher frequencies, Ahuja's results being around 5dB higher, and Tanna's measurements 2–3dB higher than Viswanathan's results. This last author concluded that the found differences were due to contamination in the preceding experiments in the form of "rig noise". However, Viswanathan and Clark [200]'s measurements showed 3dB differences between spectra at medium and high frequencies for two studied nozzles, which contradicts the rig noise hypothesis to explain the differences between facilities: this 3dB difference was measured in the same facility, the only difference being the internal contour of the nozzle. Zaman [206] confirmed this trend in another facility by reproducing the two nozzles leading to noise differences in the work of Viswanathan and Clark. Consistently, the "ASME" nozzle, which has an abrupt contraction followed by a small straight section, produced 2–3dB more high-frequency noise than a conical nozzle. Other factors, such as thickness of the nozzle lip and free-stream turbulence, did not seem to change the radiated sound.

Harper-Bourne [82] recently made a compilation of results for facilities with low contraction ratio upstream of the nozzle exit (QinetiQ, Boeing, NASA SHJAR) and others with higher contraction ration (measurements of Lush [120] at ISVR, Tanna [188] at Lockheed, and Olsen *et al.* [150] at NASA Lewis). When scaled to the same distance from the nozzle, the first three low-contraction experiments yielded quite close spectra at 90° from the jet axis. However, the three high-contraction facilities led to more high-frequency noise if compared to the first three. Harper-Bourne attributed this to the differences in the contraction ratio between the experiments.

Recent numerical studies have also addressed this issue [19], and significant effect of the upstream conditions in the radiated sound was found for jets with laminar and transitional boundary layers. Further discussion is postponed to section 2.3

2.3 Contributions of computational aeroacoustics

Direct numerical simulation (hereafter DNS) of turbulent flows has increased the possibilities of study of aeroacoustic phenomena. A numerical solution of a compressible flow includes also the radiated sound, which is therefore directly computed without the application of an acoustic analogy. For this reason, compressible DNS can be seen as a predictive tool for aeroacoustics; however, its computational cost is high. In addition, DNS solutions allow one to probe the simulated flow in ways not possible in experiments, since all flow variables are available simultaneously on a volume. This has motivated the use of DNS of compressible flows as a useful research tool for aeroacoustics. An extensive review of such applications, as well as of the challenges involved on the numerical simulation of sound generation by compressible flows, was made by Colonius and Lele [40].

An early example of direct computation of a compressible shear flow and its radiated sound is the work of Colonius *et al.* [41], who simulated a two-dimensional mixing layer. The sound generation in this case was seen to be related to periodic vortex pairings. The axisymmetric form of the Navier-Stokes equations was used by Mitchell *et al.* [134] to simulate an axisymmetric jet, which, as in Colonius *et al.*'s mixing layer, presented vortex pairings responsible for most of the sound generation.

Finally, with increasing computer power, it became possible to simulate three-dimensional, compressible flows. Freund *et al.* [70] did a calculation of a Mach 1.92 jet, and subsequently a subsonic jet at Mach 0.9 and Reynolds number 3600 [66]. This last DNS could be validated using the experimental results of Stromberg *et al.* [179], and good agreement was found for the mean velocity field and for the radiated sound.

Direct numerical simulations should have sufficiently fine meshes so as to model the smallest scales in a flow, which are related to viscous dissipation. This requirement makes DNS prohibitively expensive at high Reynolds numbers, and limits possible validation of DNS of high-Mach flows, whose experimental counterpart would have a quite high Reynolds number if air in standard conditions were employed; for instance, the experiment of Stromberg *et al.* [179] was done in a low-pressure anechoic chamber (the pressure in the test chamber was kept at 0.018atm), with a jet diameter of 7.9mm, to obtain a Reynolds number of 3600 for a Mach 0.9 jet. An alternative developed to circumvent this difficulty is large eddy simulation (hereafter LES). In an LES, the mesh is chosen so as to discretise the energy-containing part of the wavenumber spectrum (i.e. the larger eddies). The smaller eddies are accounted for by subgrid models. Early examples of LES of compressible subsonic jets and their radiated sound are the work of Bogey *et al.* [20] and of Bodony and Lele [13]; in these works, the Reynolds number is around $6-8\cdot10^4$, which is significantly higher than what was possible with DNS [66]. A review of LES with aeroacoustic applications for jets is presented by Bodony and Lele [14].

DNS and LES solutions have provided material for original investigations of the physical phenomena in aeroacoustics. Some examples are listed below.

Application of acoustic analogies The availability of all flow variables as functions of space and time provides an ideal situation to test and study acoustic analogies, and most of the first studies with numerical solutions of the Navier-Stokes equations presented an application of a given analogy. Colonius *et al.* [41] used Lilley's analogy applied to a two-dimensional mixing layer and Mitchell *et al.* [134] applied Lighthill's analogy for an axisymmetric jet. For three dimensional jets, Lighthill's analogy was applied by Colonius and Freund [39] to a supersonic jet, and by Freund [66, 67]to a Mach 0.9 jet. In all these cases, the result of the acoustic analogy was in close agreement to the radiated sound calculated directly from the simulations, which was expected in view of the exact rearrangements of the flow equations done in the formulation of acoustic analogies.

In the work of Colonius *et al.* [41] a simplified wave-packet shape was fitted using the full source. The sound radiation of this model agreed with the acoustic field of the DNS, which presented a superdirective behaviour. This shows the importance of including source non-compactness in a model of sound radiation by coherent structures, in agreement with the experimental findings of Laufer and Yen [109].

The works of Freund [67] and of Bodony and Lele [15] decomposed Lighthill's stress tensor prior to the solution of the acoustic analogy; their results using the full tensor were nearly identical to the sound obtained by propagation using Kirchhoff surfaces, but when individual terms of the stress tensor are taken, their contribution can be higher than the overall sound. The authors attributed this effect to non-negligible negative correlations between the source consituents (especially between the $\rho u_i u_j$ and the $(p - c^2\rho)\delta_{ij}$ terms), which, albeit appearing separately in Lighthill's analogy, may be related to a single physical phenomenon. This trend was also found by Cabana *et al.* [29], who proposed a new decomposition of the Lighthill's stress tensor into 10 terms; in most of the cases, individual contributions of the terms were much higher than the overall sound, but cancellations between terms led to an overall result that corresponded to the DNS.

Another issue investigated with the help of numerical simulations is the relative robustness of different acoustic analogies, which was studied by Samanta *et al.* [170]. Using a DNS of a two-dimensional mixing layer, the authors calculated the sound radiation using acoustic analogies with a base flow with uniform velocity, which is equivalent to Lighthill's formulation in a convected medium; with a parallel sheared flow, consistent with Lilley's analogy; and with a diverging mean flow in Goldstein's analogy. The sources were decomposed using POD modes. When the full sources are used in the computations, all analogies lead to good agreement with the far-field sound from the DNS. Artificial errors in the sources are then introduced by neglect of some POD modes. Some disturbances lead to the same errors in the far-field results, but a particular change in the source (division of the first POD coefficient by two) caused significant error in Lighthill's formulation, while errors were less severe in the other formulations.[4]

Simplified model problems Instead of setting up a problem to represent a laboratory flow, in numerical simulations one has the freedom to stipulate idealised problems that do not correpond to a practical experiment. The problems so idealised may then be designed so as to expose in a numerical simulation the effects of some flow parameters, hard to change experimentally.

An example of such idealised problems is the temporal mixing layer, which is formed by two streams of same velocity but with opposing sense. Such mixing layers will present vortex roll-up and pairing, but the average convection velocity of the structures is zero, which simplifies considerably the computations (for instance, periodic boundary conditions can be applied in the streamwise direction). DNS of temporal mixing layers was used by Fortuné *et al.* [65] to explore the effects of temperature in both two- and three-dimensional flows. Kleinman and Freund [100] used three-dimensional temporal mixing layers to study the Reynolds number effect on sound radiation. Four mixing layers with different Reynolds numbers and otherwise equal parameters are simulated; in this case, a higher Reynolds number indicates that smaller-scale turbulent structures are present in the flow. Far-field spectra peak for low wavenumbers (low frequencies when temporal spectra are calculated), and the far-field radiation was seen to be independent of Re for these low wavenumbers. This suggests that the large scale turbulent structures are mainly responsible for sound radiation in these flows. The smaller eddies present in high Re mostly alter the far-field spectral shape for higher wavenumbers or frequencies.

Investigation of the effect of flow conditions at nozzle exit In an experimental setting, there are limited possibilities for changing the boundary layer state close to the nozzle exit to investigate the effect of nozzle conditions on the radiated sound, discussed in section 2.2.4. A simple case is when a laminar boundary layer is made transitional or turbulent by the presence of a trip upstream. However, modification of other parameters, such as the boundary layer thickness or the turbulence level, would require changes of the upstream geometry. Although these approaches are feasible, in a numerical simulation one has much more freedom to specify the conditions at the nozzle exit. This has been exploited by Bogey and Bailly [16], who studied the effect of inflow conditions on the jet development and on the acoustic field by changing the upstream forcing in large eddy simulations. Results showed significant effects of the upstream conditions for both the mean flow, the fluctuating velocities and the acoustic field; a particularly significant case involved suppression of the low-order azimuthal modes in the forcing, which

[4] Further discussion on this result is presented on chapter IV.

led to a lengthening of the potential core and a reduction of approximately 2dB of the acoustic radiation.

Greater numerical capabilities today allow the simulation of the flow inside the nozzle, with more accurate resolution, at least for laminar and transitional boundary layers. Bogey and Bailly [19] carried out LES of jets with varying thickness of initially laminar boundary layers, and showed that the initial thickness had a significant impact on vortex roll-up and pairing in the upstream part of the mixing layer, on the velocity fluctuations on the jet centerline and on the radiated sound field.

Optimal control Using numerical simulations it is possible to define an optimal control problem, the typical one for aeroacoustics aiming a reduction of the radiated sound. In such formulations, an objective functional is defined, and a control is specified. A standard numerical simulation without control will provide the initial value of the functional; then, adjoint simulations are usually employed so as to determine the sensitivity of the functional to changes of the control, and an iterative process is set up to determine the optimal control. Application of this method to aeroacoustics is summarised by Freund [68]. As the optimal control is obtained, one has two numerical solutions: an uncontrolled, noisy flow and its controlled, quiet counterpart. This allows comparison of the numerical solutions to evaluate what in the controlled case reduced the radiated sound.

Wei and Freund [203] applied optimal control for a DNS of a two-dimensional, compressible mixing layer. Controls consisted of mass sources, streamwise and transverse body forces and internal energy sources, and were applied at the upstream part of the mixing layer. Although changes of the mixing layer dynamics were slight, reductions of far-field sound of up to 6dB were obtained after application of optimal control. This database was further analysed in the present work, in chapter II.

Since each iteration to obtain the optimal control demands both a direct and an adjoint simulation, the procedure is numerically expensive. For three-dimensional flows, use of large eddy simulations is currently mandatory. The adjoint optimisation was recently applied to supersonic, perfectly expanded jets by Kim *et al.* [99].

Study of linearity and nonlinearity of instability waves In a numerical calculation, the nonlinear effects in turbulence and in sound generation can be easily studied by comparison of a Navier-Stokes solution with an equivalent solution, obtained from the linearised equations. An example is the work of Mohseni *et al.* [136], who compared linear and nonlinear simulations of a Mach 1.92 jet with Reynolds number 2000. The linear computation is performed using the mean flow of the (nonlinear) DNS. There was qualitative agreement between linear and nonlinear simulations: the peak frequency and the directivity shape for the first helical mode were close, but the SPL values differed significantly. The near-field pressure, representative of the large-scale structures, was also compared. The authors found good agreement between linear and nonlinear computations for the peak frequency of the instability for the first helical mode. Two frequencies close to the peak also presented good agreement, but for other values there are significant differences between the evolution of instability waves in the linear and nonlinear computations, which indicates that nonlinear effects were significant.

DNS was used together with PSE by Cheung and Lele [36] to study linear and nonlinear effects on the development of two-dimensional mixing layers and on the radiated sound. The base flow used for linear and nonlinear PSE was the laminar solution. Subsonic mixing layers show the roll-up of vortices that subsequently undergo pairing. The exponential growth of the beginning of the roll-up phase in the DNS was well predicted by both linear and nonlinear PSE, showing, as expected, that nonlinear effects can be neglected in the first stage of transition, when the disturbance amplitudes are small. However, only nonlinear PSE was able to model vortex pairing. Nonetheless, when a mean-flow correction is included in the linear PSE (which amounts to linearising the equations using the mean flow instead of the laminar solution), a better approximation of the pairing dynamics is found. The acoustic field is obtained using the PSE solution in Lilley's analogy [118] in Goldstein's [75] formulation, and sources from nonlinear PSE. Good agreement is found between the acoustic analogy results and the far-field pressure from the DNS.

More recently, Suponitsky *et al.* [180] have proposed a somewhat different framework to study linear and nonlinear mechanisms of sound radiation in subsonic jets, motivated by previous evidence of sound radiation from nonlinear interaction of instability waves in the numerical computation of Sandham *et al.* [171]. Suponitsky *et al.*'s work perform direct numerical simulations of jets with different forcing amplitudes at the inflow boundary. The mean velocity field is kept constant by application of appropriately chosen steady body forces, which allows comparisons of low- and high-amplitude forcings with the same base flow. When the forcing amplitude is low, linear mechanisms prevail, while high amplitudes lead to significant nonlinear effects. Results show a higher acoustic efficiency of the nonlinear mechanism, which leads to a quadratic increase of the radiated sound with increasing forcing amplitude. This is in agreement with the experimental work of Ronneberger and Ackermann [167], described in section 2.2.2.

3 Overview of the research on subsonic jet noise

We list here some general observations from the literature review presented in the preceding sections.

- While the initial picture of turbulence was of eddies without any particular organisation, several subsequent experimental observations of coherent structures, and wave-like sources, were made in the flow field;

- For natural jets, these coherent structures present an intermittent behaviour, which leads to difficulties in experimental assessment of their presence and of their effect on the radiated sound. Flow visualisation and conditional averages confirm nonetheless that jets with high Reynolds and Mach numbers, with practical interest for aeronautical applications, comprise hydrodynamic waves with significant axial extent. This is confirmed by measurements of the near-field pressure, which tends to highlight azimuthally-coherent structures;

- Theoretically, the presence of hydrodynamic waves with significant axial and azimuthal coherence significantly modifies the sound radiation. The axial coherence leads to an interference pattern between neighbouring structures, and to highly directive sound radiation towars low polar angles; and when low-order azimuthal modes are present in a flow, their acoustic efficiency is much higher than that of incoherent turbulence, particularly for low frequencies and polar angles, when analysis is done using an acoustic analogy;

- Despite the experimental evidence of azimuthally-coherent structures in jets, relatively few measurements of the azimuthal modes of velocity and of far-field pressure of jets are available in the literature;

- Coherent strucutures are modelled as instability waves, with success. There is nonetheless an ongoing debate on the importance of nonlinear effects on the development of instability waves, and on the radiated sound field.

We will address these isssues in the studies presented in the next chapters. In Chapter II we study direct numerical simulations of two-dimensional mixing layers, and find that intermittent behaviour of vortical structures and changes in an interference pattern are significant for sound radiation.

A similar study was performed using a large eddy simulation of a jet in Chapter III, with similar conclusions. This led us to model intermittent effects on wavepackets. Such models are described in Chapter IV.

All these studies using numerical simulations indicate that sound radiation at low polar angles can be modelled using axially-extended wavepackets. Chapter V is an evaluation of wave-packet radiation in subsonic jet experiments for azimuthal modes 0, 1 and 2. The agreement of the radiated sound with models of wave-packet radiation confirms the conclusions of Chapters III and IV.

Finally, in Chapter VI we study wavepackets in the velocity field of the jets studied in Chapter V by time-resolved measurements of the azimuthal modes in the velocity field. Measurements are compared to models of instability waves, and we present a discussion on the extent of linear and nonlinear effects in the development of wavepackets.

Chapter II

A study of noise-controlled mixing layers

As a starting point for the present work, we study the numerical computations of two-dimensional, subsonic mixing layers by Wei and Freund [203]. In the computations, optimal control is applied in the upstream part of the mixing layer with a view to reducing the radiated sound. The comparison of the uncontrolled flow with the controlled, silent mixing layers provides a good oportunity to study noise generation mechanisms in shear flows.

In what follows we present a reproduction of the journal article "Intermittent sound generation and its control in a free-shear flow" [35], published in Physics of Fluids, 22(11):115113, 2010.

PHYSICS OF FLUIDS **22**, 115113 (2010)

Intermittent sound generation and its control in a free-shear flow

André V. G. Cavalieri,[1,a)] Peter Jordan,[1,b)] Yves Gervais,[1,c)] Mingjun Wei,[2,d)] and Jonathan B. Freund[3,e)]
[1]*Département Fluides, Thermique, Combustion, Institut Pprime, CNRS-Université de Poitiers-ENSMA, UPR 3346, 43 Route de l'Aérodrome, Poitiers Cedex F86036, France*
[2]*Mechanical and Aerospace Engineering, New Mexico State University, P.O. Box 30001/Dept. 3450, Las Cruces, New Mexico 88003-8001, USA*
[3]*Mechanical Science & Engineering and Aerospace Engineering, University of Illinois at Urbana-Champaign, Urbana, Illinois 61801, USA*

(Received 24 June 2010; accepted 22 October 2010; published online 29 November 2010)

Comparisons are made between direct numerical simulations (DNS) of uncontrolled and optimally noise-controlled two-dimensional mixing layers in order to identify the physical mechanism responsible for the noise reduction. The analysis is carried out in the time domain to identify events that are significant in sound generation and which are acted upon by the control. Results show that a triple vortex interaction in the uncontrolled mixing layer radiates high-amplitude pressure waves to the far acoustic field; the elimination of this triple merging accounts for 70% of the noise reduction accomplished by a body force control applied normal to the shear layer. The effect of this control is shown to comprise vertical acceleration of vortical structures; the acceleration, whose action on the structures is convected across the control volume, leads to changes in their relative convection velocities and a consequent regularization of their evolution, which prevents the triple merger. Analysis of a longer time series for the DNS of the uncontrolled mixing layer using a wavelet transform identifies several similar intermittent, noisy events. The sound production mechanism associated with such noisy events can be understood in terms of cancellation disruption in a noncompact source region, such as described by a retarded-potential formalism. This shows that acoustic analogies formulated from the perspective of quadrupole acoustic sources are, in principle, useful for the modeling of such events. However, this study also illustrates the extent to which time-averaged statistical analysis of sound producing flows can mask the most important source activity, suggesting that intermittency should be explicitly modeled in sound prediction methodologies. © *2010 American Institute of Physics*. [doi:10.1063/1.3517297]

I. INTRODUCTION

Although research in aeroacoustics has made considerable progress since the pioneering work of Lighthill,[1] a clear mechanistic description of how free-shear flow turbulence generates sound remains elusive, and it is thus difficult to propose technical solutions that might reduce the sound power radiated by propulsive jets. In this context, direct numerical simulation (hereafter DNS) constitutes a valuable tool for studying the physics of the noise production. Although this kind of simulation is currently limited to flows with low Reynolds numbers, it facilitates a study of the fundamental vortex dynamics observed in turbulent flows; for a review of these and other applications, see Colonius *et al.*[2] and Wang *et al.*[3]

The work of Wei and Freund[4] provides a valuable opportunity for studying sound production mechanisms, and, in particular, for understanding what can be done to an unsteady vortical flow in order to make it significantly quieter. A two-dimensional, spatially evolving mixing layer was simulated, and by means of an adjoint-based formulation a series of optimally controlled flows were produced and compared with the uncontrolled baseline flow. Reductions in sound intensity of up to 6 dB in the far acoustic field were achieved; however, the differences between the controlled and uncontrolled flows were found to be subtle, with slight differences between the statistics of the various flows despite the one-order-of-magnitude reduction in radiated acoustic power. An analysis based on a proper orthogonal decomposition (POD), where these modes served a surrogates for Fourier modes in this streamwise inhomogeneous flow, showed that there was an underlying organization of the large structures due to the control, which was consistent with increased uniformity of their streamwise advection.

It is clear that such low Reynolds number, two-dimensional flow does not represent fully the turbulence dynamics of, for example, a three-dimensional high speed jet; hence, the extrapolation of the conclusions to other flows should be done with care. Nonetheless, in this simplified case important progress can be made with the understanding of the slight differences between a noisy, uncontrolled flow with quiet, controlled counterparts.

Some subsequent work addressed the differences be-

[a)]Electronic mail: andre.cavalieri@univ-poitiers.fr. Also at Instituto Tecnológico de Aeronáutica, Praça Marechal Eduardo Gomes, 50, Vila das Acácias, CEP 12228-900, São José dos Campos, Brazil.
[b)]Electronic mail: peter.jordan@univ-poitiers.fr.
[c)]Electronic mail: yves.gervais@univ-poitiers.fr.
[d)]Electronic mail: mjwei@nmsu.edu.
[e)]Electronic mail: jbfreund@illinois.edu.

1070-6631/2010/22(11)/115113/14/$30.00

tween the noisy and quiet mixing layers from other perspectives: Eschricht *et al.*[5] showed that there are differences in the wavenumber-frequency spectra of the hydrodynamic pressure fields of the uncontrolled and controlled flows, with less energy being found in the radiating sector of the controlled flow spectrum. In that same effort it was shown that two-point, two-time causality correlations between acoustic pressure and the Lighthill source term were affected by the control: the controlled flow showed more effective source cancellation and was thus a less efficient source of sound.

While these analyses provide a statistical perspective on the differences between the noisy and quiet mixing layers, the precise changes in the flow remained unclear. These approaches, being based on time-averaged statistics, masked the importance of local space-time events. They preclude the evaluation of intermittent events in the flow and the extent to which these may be important in the production of sound. Such intermittency has been found to be important in previous experimental and numerical jet noise studies. High levels of intermittency are also observed in the turbulence toward the end of the potential core in jets. Juvé *et al.*[6] used causality correlations in a Mach 0.9 jet to evaluate the instantaneous contribution of the source at the end of the potential core to the sound intensity at an angle of 30° to the downstream jet axis. The time traces of this contribution consisted of intermittent bursts interspersed by periods with near-zero values.

Hileman *et al.*[7] performed a similar study on an ideally expanded Mach 1.28 jet. The acoustic pressure at 30° had periods of relative quiet interspersed with large amplitude events. A continuous wavelet transform was used to estimate the frequency of the large amplitude peaks and the footprint of the relative quiet periods and of the high-pressure peaks could be detected in the resulting scalograms. The intense events in the acoustic field were used to select corresponding images from flow visualizations, and a subsequent POD analysis of these noise-producing events defined a characteristic loud flow signature, which corresponded to the intermittent intrusion of turbulent structures into the potential core.

The same techniques of Hileman *et al.*[7] were applied by Kastner *et al.*[8] to the Mach 0.9 jet DNS of Freund;[9] similar intermittent bursts were detected in the acoustic field, and the loud turbulent field was shown to have a truncated wavepacket structure, consistent with the conclusions of the experimental Mach 1.28 jet. Similar results have been reported by Bogey and Bailly[10] using a large eddy simulation of a Mach 0.9 jet. At the end of the potential core, intermittent vorticity bursts were observed, and these were correlated with positive pressure peaks in the far field at 40° from the downstream axis.

In this paper, we analyze data from the uncontrolled and controlled mixing layers of Wei and Freund[4] to identify loud intermittent events, particularly those that are suppressed by the control. In Sec. II we briefly describe the numerical simulations. Analysis of the acoustic field in Sec. III A shows that most of the acoustic energy for the uncontrolled flow is associated with a single event. In Secs. III B and III C we examine the vortex dynamics of both the controlled and uncontrolled flows and identify the essential difference between these. This specifically identified the loud flow event. A triple vortex merger leaves behind it an extended region of nearly irrotational flow; this local event momentarily disrupts the axial source cancellation mechanism and a strong pressure wave is emitted. In the controlled flow, the triple merger is prevented, and the source interference persists with much the same efficiency for the entire duration of the simulation.

We cannot of course claim that the triple vortex merger is the dominant mechanism of sound production in practical high-Reynolds-number free-shear flows; indeed it appears unlikely that even vortex pairing occurs or is important for noise generation in such flows, as discussed by Hussain and Zaman[11] and Bridges and Hussain.[12] On the other hand, the observation that the event constitutes an intermittent change in a basic vortex pattern, leading to a rupture of the space-time homogeneity of the hydrodynamic pressure signature and an associated high energy acoustic pressure burst, is a feature shared with the cited jet noise studies.[6–8,10] Furthermore, recent models (see Cavalieri *et al.*)[13,14] reproduce the intermittent behavior of coherent structures in a jet, and, based on an acoustic analogy with retarded-potential solutions, can lead to good predictions of the radiated sound by a turbulent jet.

In Sec. III D, the dynamics of the actuation is studied; we show that the action of the control involves a vertical displacement of vortical structures in the controlled flow, with which there is an associated change in their respective convection velocities and, consequently, their mutual interactions; the triple vortex merger is thus prevented. This indicates how actuation with a transverse force can regularize a given vortex pattern in order to suppress intermittency and thus reduce the radiated noise.

Finally, in Sec. IV, we use a continuous wavelet transform to analyze the acoustic pressure data taken from a longer time simulation of the uncontrolled mixing layer to objectively identify noisy events. Events of the same character as those identified by comparing the controlled and uncontrolled flows are found. These events share a noise signature, with time-scales in the wavelet domain between $60\delta_\omega/\Delta U$ and $200\delta_\omega/\Delta U$, and their behavior is intermittent, since four such events are identified in a time series of $6500\delta_\omega/\Delta U$ without observable periodicity.

II. THE TWO-DIMENSIONAL MIXING LAYER

The flow in this work is the same presented by Wei and Freund;[4] we will therefore only briefly describe it. A two-dimensional mixing layer was computed by direct numerical solution of the compressible, viscous flow equations. The Reynolds number was $\rho_\infty \Delta U \delta_\omega/\mu = 500$, with ρ_∞ as the ambient density of both uniform streams, ΔU as the velocity difference between the streams, δ_ω as the inflow vorticity thickness, and μ as the constant viscosity. The Mach numbers for the free streams were 0.9 and 0.2, and the Prandtl number was 0.7. The physical domain extended from $x=0$ to $x=100\delta_\omega$ and between $y=\pm 80\delta_\omega$.

The mixing layer was excited with eight frequencies f_i,

$$f_i = \frac{f_0}{4}(i + \alpha^{(i)}), \qquad (1)$$

where f_0 is the estimated frequency for the most unstable mode according to linear stability theory, and $\alpha^{(i)}$ are random numbers between -0.5 and 0.5. To reduce the direct effect of the excitation in the radiated sound, the frequencies in Eq. (1) were excited with a solenoidal body force, which is relatively ineffective. This body force is applied upstream of the physical calculation domain. On account of this excitation, the mixing layer presents complex dynamics, without any observable periodicity. Although the Reynolds number is low, some aspects of noise generation by turbulence are expected to be represented.

The control, which was applied in a small square region covering $\delta_\omega < x < 7\delta_\omega$ and $-3\delta_\omega < y < 3\delta_\omega$ near the inflow, was modeled by a source term in the flow equations. Four different controls were applied: a mass source, x- and y-direction body forces, and an internal-energy source. These controls were chosen to be as general as possible: each space-time point of the discrete representation of the control forcing was treated as an independent control variable. We focused our analysis on the flow controlled by application of body forces in the y-direction, but the other controlled flows were also studied.

An optimal control algorithm was implemented. This involved an iterative process in which the adjoint of the perturbed and linearized flow equations was solved numerically to provide the sensitivity of the sound to changes in the control function $\phi(\mathbf{x},t)$. The objective functional to be minimized was

$$\mathcal{J}(\phi) = \int_{t_0}^{t_1}\int_{x_0}^{x_1} [p(\phi(\mathbf{x},t),\mathbf{x},t) - \bar{p}_o(\mathbf{x})]^2 \mathrm{d}\mathbf{x}\mathrm{d}t, \qquad (2)$$

where p is the local pressure and $\bar{p}_o$ is the time-averaged local pressure for the uncontrolled flow. The spatial integration was performed in the region of uniform Mach 0.2 flow, along $y = -70\delta_\omega$, between $x_0 = 0$ and $x_1 = 100\delta_\omega$, and the temporal integration had as limits the start and end times of the control period.

Wei and Freund[4] showed that the controlled flows had noise reductions in the far field for all radiation angles; these reductions were up to 6 dB. The controlled mixing layers presented sound pressure spectra with reductions for the lower frequencies, which contained most of the sound energy; however, the controlled flows radiate more noise for the higher frequencies.

For a harmonically excited mixing layer, with excitation at frequencies f_0, $2f_0$, and six subharmonics of f_0, Wei and Freund[4] obtained results similar to those obtained by Colonius *et al.*,[15] with periodic vortex pairings at fixed locations. For this flow, Wei and Freund showed that their optimal control methodology does not produce any significant sound reduction. This suggests that the harmonically excited mixing layer, with its orderly structure, is near a lower limit for noise generation in a free-shear flow.

The control spectra were also analyzed in that paper and it was seen that the control was broadbanded, with significant energy content at frequencies other than the f_i excitation. The control spectrum also did not match the far field sound spectrum, indicating that the control worked via a nonlinear mechanism in the flow. Further details can be found in Wei[16] and Wei and Freund.[4]

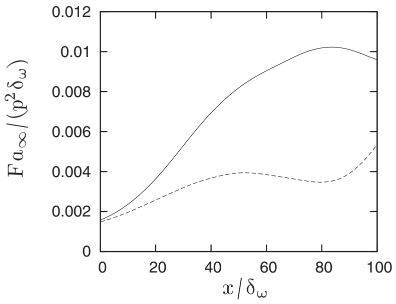

FIG. 1. Sound intensity at the target line for the (——) uncontrolled and (- - -) controlled mixing layers.

III. FLOW CHANGES BETWEEN THE UNCONTROLLED AND CONTROLLED FLOWS

A. Pressure data at the target line

Wei and Freund[4] found that despite the significant differences in the radiated noise between the uncontrolled and controlled flows, the changes in the flow are slight. In order to identify and understand the differences between the mixing layers, we first evaluate how the radiated pressure field is changed by control. Since the control objective is the noise reduction on a horizontal target line located at $y = -70\delta_\omega$ on the $M = 0.2$ side of the mixing layer, we use this line to identify the space-time intervals where the sound reduction is most effective. We define

$$F(x) = \int_{t_0}^{t_1} [p(\phi(\mathbf{x},t),\mathbf{x},t) - \bar{p}_o(\mathbf{x})]^2 \mathrm{d}t \qquad (3)$$

for both the uncontrolled and controlled flows. This allows a spatially localized assessment of the noise reduction; integration of $F(x)$ along the target line for a given control, ϕ, leads to the objective functional $\mathcal{J}$. Figure 1 shows $F(x)$ for the uncontrolled and y-direction body force controlled mixing layers. We see that although there is a noise reduction all along the target line, the control application is especially effective toward the downstream end of the flow domain.

Figure 2 shows pressure signals for three points on the target line: one upstream point, one centered, and one downstream. By means of these figures the temporal locality of the sound reduction can be assessed: a significant portion of the sound reduction at the downstream point occurs over a limited time interval.

Considering the point $(80\delta_\omega, -70\delta_\omega)$, we note that there is no noise reduction for the beginning of the simulation $(ta_\infty/\delta_\omega < 100)$. As explained by Wei and Freund,[4] the noise at the target line is not controllable before a finite propagation period of the control effects. The most remarkable reduction in Fig. 2 happens between $ta_\infty/\delta_\omega = 300$ and $ta_\infty/\delta_\omega = 420$. In this interval the uncontrolled flow presents a large

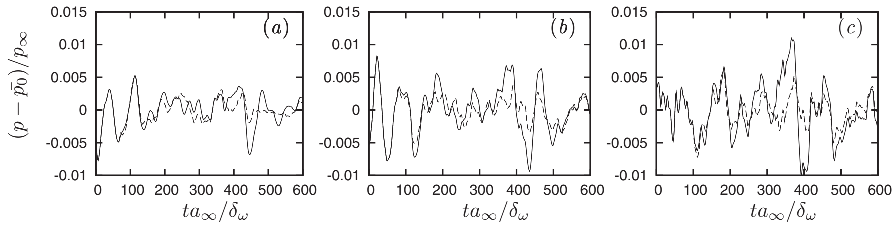

FIG. 2. Pressure for the (——) uncontrolled and (- - - -) controlled mixing layers in the points (a) $x/\delta_\omega=20$, (b) $x/\delta_\omega=50$, and (c) $x/\delta_\omega=80$ of the target line.

positive pressure peak, followed by a negative peak of similar level; the controlled flow presents much smaller amplitude pressure waves during the same period. We thus see that most of the sound reduction is achieved by eliminating this one large peak. In fact, 70% of the reduction of the function F at this point happens during the period $300 < ta_\infty/\delta_\omega < 420$. This suggests that the noise reduction is due to the elimination of a single event in the flow.

B. Flow dynamics for the uncontrolled and controlled flows

Figure 3 shows visualizations of the pressure and vorticity fields for the uncontrolled mixing layer at six different times, and in Fig. 4 visualizations for the controlled case are shown at the same times. The time $ta_\infty/\delta_\omega=367.9$ [Figs. 3(d) and 4(d)] corresponds to the arrival of the large positive pressure peak at the point $(80\delta_\omega, -70\delta_\omega)$ for the uncontrolled mixing layer, as shown in Fig. 2. In Fig. 3(d) this can be seen as a group of positive contours. For the controlled mixing layer, we also see positive contours in Fig. 4(d) around the point $(80\delta_\omega, -70\delta_\omega)$, but with a much smaller amplitude.

The time $ta_\infty/\delta_\omega=312.5$ [Figs. 3(a) and 4(a)] was chosen by calculating the propagation time of a wave in a uniform flow at $M=0.2$ between the points $(80\delta_\omega, -20\delta_\omega)$ and $(80\delta_\omega, -70\delta_\omega)$. For the uncontrolled mixing layer, we can see in Fig. 3(a) that there is high-pressure around the point $(80\delta_\omega, -20\delta_\omega)$, close to the zero-vorticity region lying between the pair of vortices at $x=60\delta_\omega$ and a zone of vorticity that has just crossed the downstream boundary of the computational domain. By following in succession Figs. 3(b) and 3(c) we see how this high-pressure propagates to the $(80\delta_\omega, -70\delta_\omega)$ point on the target line. We see also that there is propagation of a similar high-pressure wave to the $M=0.9$ side of the mixing layer. A similar propagation occurs in the controlled mixing layer, but with a much smaller amplitude, as seen in Figs. 4(a)–4(d). The clearest difference in the vortex dynamics between this flow and the uncontrolled mixing layer is the presence of a vortical region near $x=90\delta_\omega$ for the controlled mixing layer at $ta_\infty/\delta_\omega=312.5$. This last vortex is not visible in Fig. 3(a).

The negative pressure peak for the uncontrolled mixing layer at the point $(80\delta_\omega, -70\delta_\omega)$, shown in Fig. 2, corresponds to the time $ta_\infty/\delta_\omega=396.5$ shown in Fig. 3(f). As was done for the positive pressure wave, we calculate the propagation time of this wave to estimate its origin, and the resulting time is $ta_\infty/\delta_\omega=341.0$, shown in Fig. 3(b). We can see in the uncontrolled mixing layer that a vortical structure enters the long quasi-irrotational, high-pressure region of flow. As

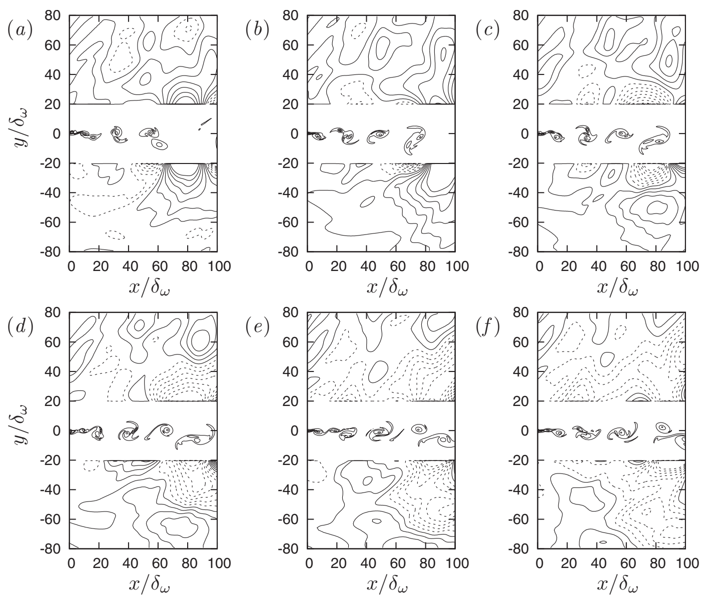

FIG. 3. Uncontrolled mixing layer at times ta_∞/δ_ω =(a) 312.5, (b) 341.0, (c) 354.5, (d) 367.9, (e) 383.0, and (f) 396.5. Center: vorticity modulus, contours from 0.07 to $1.4\Delta U/\delta_\omega$. Outer regions: pressure, contours from -0.02 to $0.02p_\infty$. Negative contours are dashed.

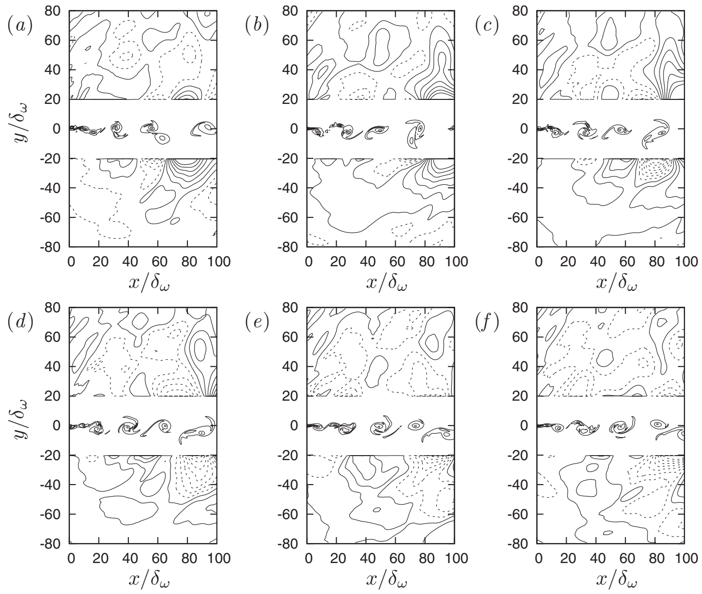

FIG. 4. Controlled mixing layer. Center: vorticity modulus. Outer regions: pressure. Same contours and times of Fig. 3.

this vortex is convected to the end of the computational domain [Figs. 3(c)–3(f)], we see the formation of a low-pressure wave, which propagates to the far field and arrives at $(80\delta_\omega, -70\delta_\omega)$ with a high amplitude. The same times for the controlled mixing layer [Figs. 4(c)–4(f)] show the propagation of a negative pressure wave to $(80\delta_\omega, -70\delta_\omega)$, but with reduced amplitude.

Although the vorticity contours of the mixing layers at $ta_\infty/\delta_\omega=341.0$ (the time where the low pressure wave originates) are similar, for the uncontrolled flow we see a pocket of vorticity enter an extended region of nearly irrotational flow; for the controlled mixing layer, the passage of a similar concentration of vorticity occurs, but the distances between successive vortical regions are more uniform. If we consider the generation of sound-waves from a free-shear flow to be the result of incomplete interference between regions of positive and negative stress, or pressure, as retarded-potential type solutions for the radiated pressure would have us believe, then we see that the occurrence of an intermittent event can significantly disrupt the interference. During this period, the mutual cancellations, which occur between neighboring vortices, are unbalanced, making possible the generation of a large amplitude sound wave. This assertion is consistent with the conclusions drawn by Wei and Freund[4] and Eschricht *et al.*,[5] but we have here identified the actual flow event driving it and so we are in a position to propose a local explanation for the sound production mechanism and its control, free from the cloudiness of averaging.

C. Intermittency in the uncontrolled mixing layer

The difference in the evolution of the vorticity of the uncontrolled and controlled mixing layers is due to a triple vortex interaction that occurs in the uncontrolled flow. Figure 5(a) shows the temporal evolution of this event up to $ta_\infty/\delta_\omega=312.5$, which is shown in Fig. 3(a). We see that this triple merger, which happens only once in the simulation of the uncontrolled mixing layer, leads to the extended irrotational region in Fig. 3(a). A large vortical structure is created by this interaction. The two smaller vortices rotate at high speed around the larger structure, causing the agglomeration to enter the downstream absorbing buffer zone earlier than their controlled counterparts, shown in Fig. 5(b). The controller modifies the flow dynamics such that the triple merger is eliminated. This reduces the extent and level of the high-pressure irrotational region and, as we have seen, the amplitude of the propagated sound wave.

In order to verify that the occurrence of this extended high-pressure region is indeed an intermittent event, we show, in Fig. 6, visualizations of the vorticity field for all other times where a vortex is observed at $x=60\delta_\omega$. We see

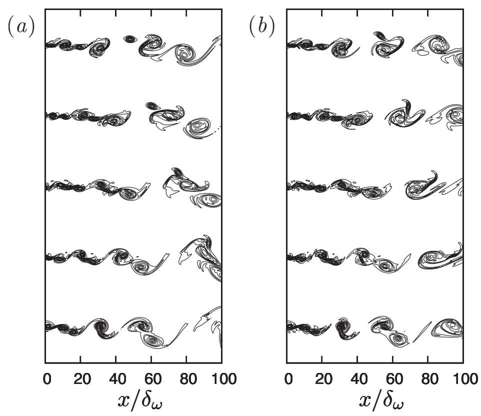

FIG. 5. Instantaneous vorticity modulus for the (a) uncontrolled and (b) controlled mixing layers at times $ta_\infty/\delta_\omega=245.3$, 262.1, 278.9, 295.7, and 312.5, from top to bottom. Contours range from $0.014\Delta U/\delta_\omega$ to $0.7\Delta U/\delta_\omega$.

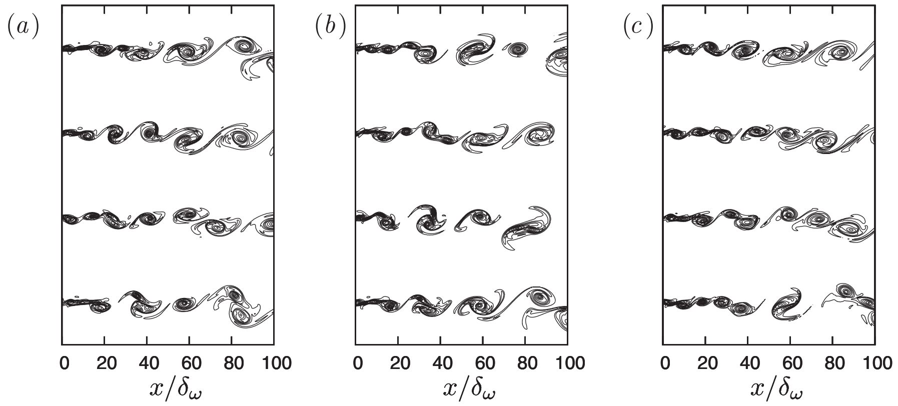

FIG. 6. Instantaneous vorticity for the uncontrolled mixing layer at times ta_∞/δ_ω=(a) 13.4, 58.8, 87.4, and 117.6; (b) 151.2, 206.6, 357.8, and 399.8; and (c) 445.2, 482.2, 505.7, and 544.3. Contour levels range from $0.014\Delta U/\delta_\omega$ to $0.7\Delta U/\delta_\omega$.

that for each image there is at least one other vortex in the domain between $x=60\delta_\omega$ and $x=100\delta_\omega$; there is never an irrotational region as long as that shown in Fig. 3(a). Again, these mechanistic interpretations are consistent with the conclusions drawn by Wei and Freund,[4] who showed, by means of a POD analysis, that the controlled flow approaches a pure advective behavior. The first POD eigenfunctions of the controlled flows are coupled in pairs of similar energy and their representation in the phase plane has circular traces. These are characteristics of flows with pure convection of structures, with a form such as $\cos(\omega t - kx)$, whose POD representation is $\cos \omega t \cos kx + \sin \omega t \sin kx$, with consequent circles in the phase plane. This is not the case for the uncontrolled flow. We see here that the elimination of the vortex merger constitutes a change that is synonymous with a harmonization of the mixing layer, which approaches, for the controlled flow, the intrinsically quiet pattern of pure subsonic advection. In the controlled mixing layer, the vortex pattern becomes more uniform as the triple merging is changed into vortex dynamics that are closer to what happens in the other times of the simulation. We see that the downstream part of the controlled mixing layer shown in Fig. 4(a) is much closer to the vortex configurations of Fig. 6 than the uncontrolled mixing layer at the same time, shown in Fig. 3(a).

This change in the vortex pattern at the end of the mixing layer can also be seen by evaluation of

$$\xi(x,t) = \int_{-\infty}^{\infty} \omega(x,y,t)\mathrm{d}y, \tag{4}$$

which is the radially integrated instantaneous vorticity at x. This integrated vorticity is shown in Fig. 7 for two positions of the mixing layer.

In Fig. 7(b) we see that the temporal pattern of integrated vorticity at $x/\delta_\omega=80$, representing the downstream end of the mixing layer, becomes more regular for the controlled flow. The strengths of the vortices are more homogeneous, as is the temporal spacing between the vorticity peaks. This is particularly the case between $ta_\infty/\delta_\omega=200$ and $ta_\infty/\delta_\omega=350$, which corresponds to the interval over which the triple interaction takes place. On the other hand Fig. 7(a) shows that only slight changes are observed at $x/\delta_\omega=20$. The control is thus effected via small changes in the flow in the upstream region, becoming more noticeable as the vortices are convected and interact. The pairing processes are modified by the action of control and these approach the behavior observed for a mixing layer with harmonic excitation, which is an intrinsically quiet flow.

So far we have only shown results for the y-direction body force actuation. But similar results are observed for the other types of control implemented by Wei and Freund.[4] In all cases the triple vortex interaction is eliminated, and with it the extended region of high-pressure. Figure 8 shows, for

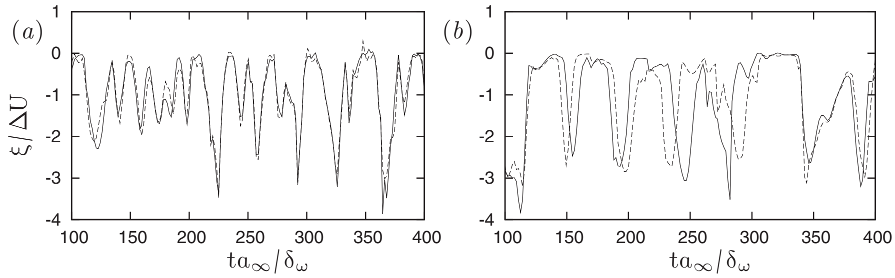

FIG. 7. Integrated vorticity at (a) $x/\delta_\omega=20$ and (b) $x/\delta_\omega=80$: (——) uncontrolled and (- - - -) controlled flow.

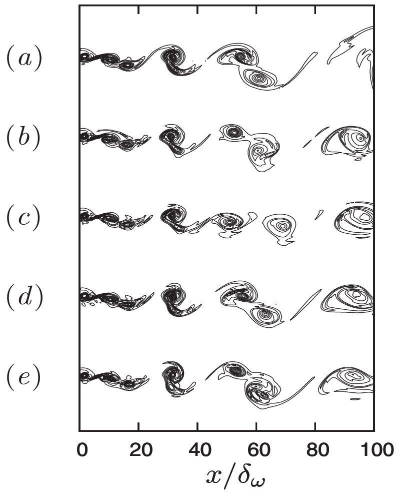

FIG. 8. Vorticity contours at $ta_\infty/\delta_\omega = 312.5$ for the flows with (a) no control, (b) mass source control, (c) x-direction body force control, (d) y-direction body-force control, and (e) internal-energy source control. Same contours of Fig. 6.

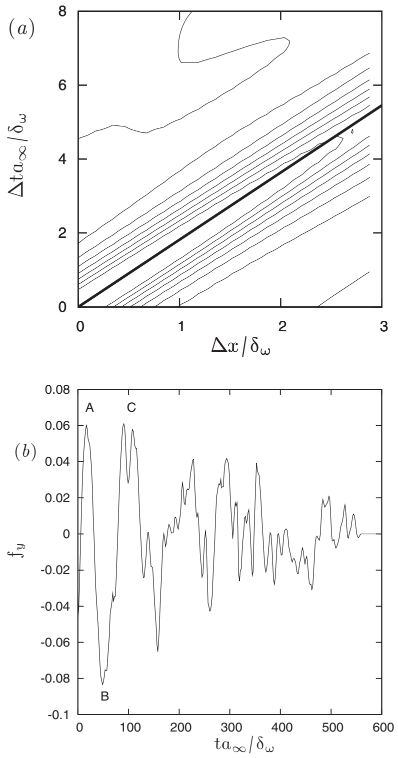

FIG. 9. (a) Space-time correlation at $y=0$ for the optimal y-direction body force control; thin lines show normalized correlation levels from 0.1 to 0.8, and the thick line corresponds to the convection Mach number 0.55. (b) Integrated y-direction body force control.

each of the control cases, the vorticity field at $ta_\infty/\delta_\omega = 312.5$, which corresponds to the long high-pressure region for the uncontrolled mixing layer [Fig. 8(a)]. Although there are slight differences between the vortex patterns, all of them present a smaller zero-vorticity region than the one shown for the uncontrolled flow in Fig. 3(a). The extent of this region is much closer to that shown in Fig. 6. Thus, all of the control formulations prevent the formation of the extended high-pressure zone, which is the essential difference between the controlled and uncontrolled flows.

D. Optimal control dynamics for the *y*-direction body force

Having identified the change in the mixing layer responsible for the noise reduction, we now want to understand the control mechanism, by which the suppression of the triple vortex pairing was achieved. This is of practical interest, as it can suggest how a physical actuator might be conceived for, say, the initial mixing layer of a jet.

We can readily see that the y-direction body force control "follows" the vortical structures in so far as the forces are correlated according to the convection speed, as seen in Fig. 9(a). This characteristic, which was also identified by Wei,[16] is an indication that the control acts on the vortices in a coherent manner as they advect through the control region $\mathcal{C}$.

To estimate the net effect of the control ϕ with distributed y-direction body forces per unit volume, which in the y-momentum equation corresponds to

$$\frac{D(\rho v)}{Dt} = -\frac{\partial p}{\partial y} + \phi - \frac{1}{\mathrm{Re}}\left(\frac{4}{3}\frac{\partial^2 v}{\partial y^2} + \frac{\partial^2 v}{\partial x^2} + \frac{1}{3}\frac{\partial^2 u}{\partial x\,\partial y}\right), \qquad (5)$$

we integrate it over the control region $\mathcal{C}$,

$$f_y(t) = \int\int_{\mathcal{C}} \phi(\mathbf{x},t)\mathrm{d}\mathbf{x}. \qquad (6)$$

Figure 9(b) shows the net y-direction force during the simulation of the controlled mixing layer. We label the distinct peaks of the total force toward the beginning of simulations A, B, and C for later reference.

We see in Fig. 10 the vortical structures that pass through the $\mathcal{C}$ region at times corresponding to the peaks indicated in Fig. 9(b), as well as a representation of the applied control. The vortices are labeled according to the corresponding peaks in Fig. 9(b); since there are two C peaks, two C vortical structures are shown. Each peak in the net force corresponds to a relatively uniform distribution of ϕ over the control region, either in the positive (A and first C peak) or in the negative (B) y-direction. On the other hand, for the second C vortex in Fig. 10(d) we see that the force field is less uniform than those applied to the other structures [Figs. 10(a)–10(c)]; however, even in that case most of the distributed force acts in the same direction, and, as will be shown later, the observed global control effect for the second C vortex is similar to that identified for the other structures.

We can therefore interpret the y-direction body force control for the marked peaks as an approximately uniform

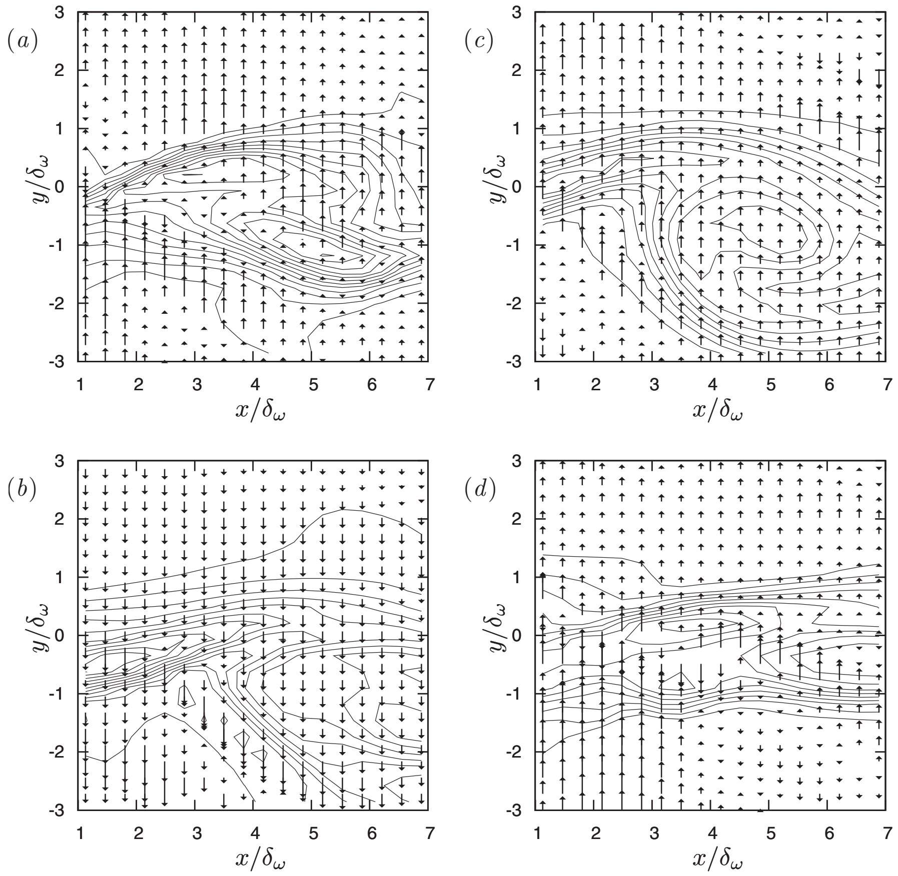

FIG. 10. Vorticity contours at the control region $\mathcal{C}$, and applied control (arrows), at (a), $ta_\infty/\delta_\omega=16.8$ (A vortex); (b), $ta_\infty/\delta_\omega=47.0$ (B vortex); (c), $ta_\infty/\delta_\omega=90.7$ and (d), $ta_\infty/\delta_\omega=107.5$ (C vortices).

force distribution that follows the convection of the vortices through the control region. The effect is a predominantly vertical acceleration of the structures, without any significant changes in the vorticity.

We confirm this conclusion with the observation of Fig. 11, where we follow the convection of the A vortex in the uncontrolled and controlled mixing layers. The effect of the positive forces applied to the A vortex [Fig. 10(a)] can be seen in its downstream evolution. For the controlled flow, there is a positive vertical displacement of the vortex in the controlled flow [Figs. 11(f)–11(h)] compared to the uncontrolled mixing layer [Figs. 11(b)–11(d)]; this is especially visible in Fig. 11(h). Although the body force is only applied upstream, the continued displacement of the vortex is pre-

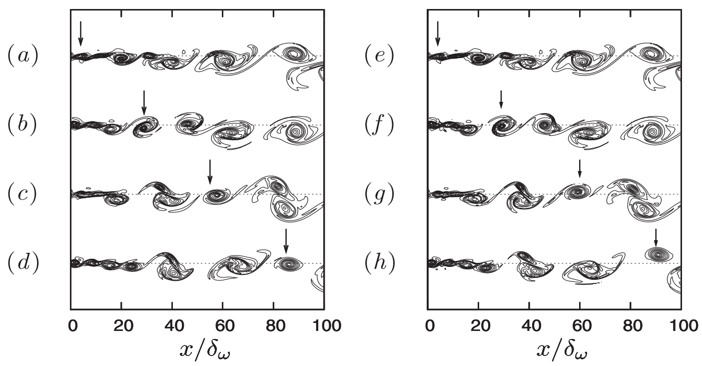

FIG. 11. Vorticity contours for: (a) and (e), $ta_\infty/\delta_\omega=16.8$; (b) and (f), $ta_\infty/\delta_\omega=67.2$; (c) and (g), $ta_\infty/\delta_\omega=117.6$; and (d) and (h), $ta_\infty/\delta_\omega=168.0$. Contours (a)–(d) refer to the uncontrolled mixing layer and (e)–(h) to the y-direction body force control. Arrows follow the convection of the A vortex. Same contours of Fig. 6.

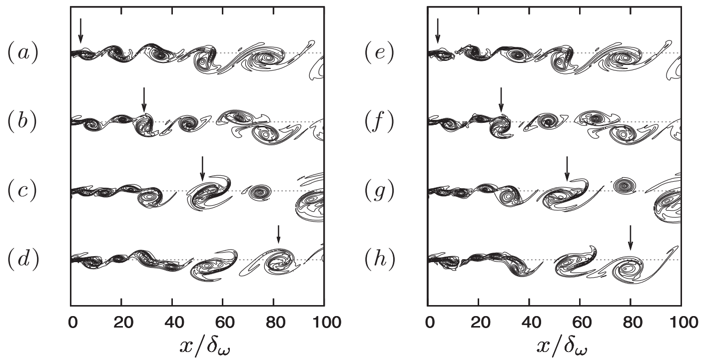

FIG. 12. Vorticity contours for: (a) and (e), $ta_\infty/\delta_\omega=47.0$; (b) and (f), $ta_\infty/\delta_\omega=97.4$; (c) and (g), $ta_\infty/\delta_\omega=147.8$; and (d) and (h), $ta_\infty/\delta_\omega=198.2$. Contours (a)–(d) refer to the uncontrolled mixing layer and (e)–(h) to the y-direction body force control. Arrows follow the convection of the B vortex. Same contours of Fig. 6.

sumably due to the intrinsic instability of the mixing layer: a small disturbance in the position of an upstream structure can be amplified downstream by its interaction with the neighboring vortices.

Furthermore, since the Mach numbers of the upper and lower streams are, respectively, 0.9 and 0.2, an upward displacement of a structure leads to a higher convection velocity. This effect is also observed in Fig. 11, where the displaced vortex in the controlled mixing layer arrives earlier at the downstream end of the physical domain.

Having understood how a vertical force changes the dynamics of the A vortex, we can proceed to evaluate how the control suppresses the triple vortex merger. This is done by the B and C peaks in the y-direction body force, shown in Fig. 9(b).

Figure 12 shows the evolution of the B vortex. Since the B feature in Fig. 9(b) is negative, we see for the controlled mixing layer [Figs. 12(e)–12(h)] a negative vertical displacement of the B vortex, compared to the uncontrolled flow [Figs. 12(a)–12(d)]. As the B vortex comes into the lower stream, its convection speed decreases.

The action of the C peaks in the body force can be followed in Fig. 13. The C peaks in Fig. 9(b) are applied when two close vortices pass in the control region $\mathcal{C}$. These two vortices are marked with full arrows in Figs. 13(a) and 13(d) for the uncontrolled and controlled flows, respectively. The B vortex is also marked in Fig. 13 with dashed arrows. The two C vortices pair just after leaving the $\mathcal{C}$ region. This C structure is directed upward, as a consequence of the positive forces applied in the controlled mixing layer; so, its convection speed is increased.

A clear distinction can then be made between the uncontrolled and controlled flows: in the controlled mixing layer, the faster C vortex approaches the slower B vortex, initiating a pairing process [Fig. 13(g)]; on the other hand, the C vortex in the uncontrolled mixing layer interacts with the upstream vortical structures, leading to the triple vortex interaction analyzed in Sec. III C [Figs. 13(c) and 13(d)]; note that the last time in Fig. 13, $ta_\infty/\delta_\omega=258.7$, shows the beginning of the triple pairing process seen in Fig. 5(a). We thus have two vortex pairings for the controlled mixing layer, instead of the acoustically efficient vortex-tripling.

To summarize, the main effect of the y-direction body force control can be understood as a series of displacements of the vortical structures, with subsequent changes in their convection velocities that lead to a more regular pattern. This conclusion is of practical interest for aeroacoustic noise control: bursts of acoustic energy may be suppressed by an actuation capable of eliminating the intermittent dynamics of flows, and for a sheared flow, such as the initial mixing layer of a jet, this can be accomplished with an appropriate transverse force.

Similar studies of the other controlled mixing layers reveal that the vortex dynamics in all the controlled cases are similar to what is observed for the y-direction body force control. Indeed, we see in Fig. 14 that for all the cases the A

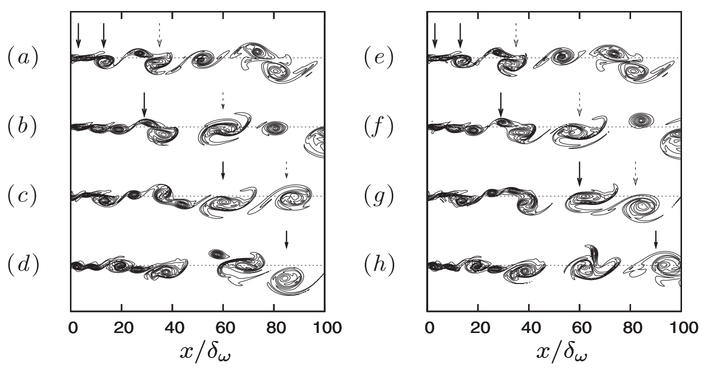

FIG. 13. Vorticity contours for: (a) and (e), $ta_\infty/\delta_\omega=107.5$; (b) and (f), $ta_\infty/\delta_\omega=157.9$; (c) and (g), $ta_\infty/\delta_\omega=208.3$; and (d) and (h), $ta_\infty/\delta_\omega=258.7$. Contours (a)–(d) refer to the uncontrolled mixing layer and (e)–(h) to the y-direction body force control. Full arrows follow the convection of the C vortices and dashed arrows follow the B vortex. Same contours of Fig. 6.

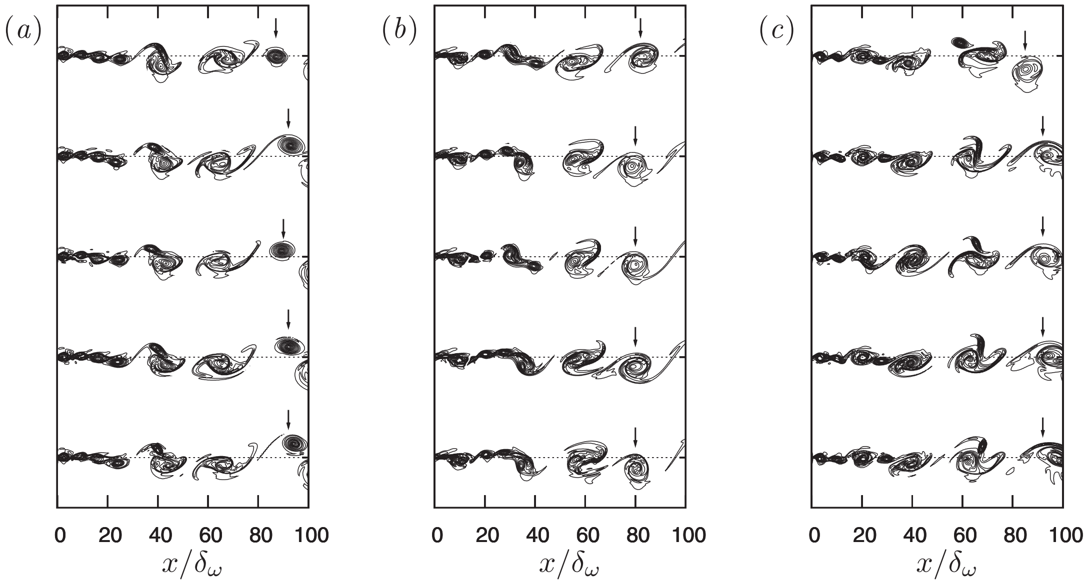

FIG. 14. Vorticity contours for: (a) $ta_\infty/\delta_\omega=168.0$, with the A vortex highlighted, (b) $ta_\infty/\delta_\omega=198.2$, with the B vortex highlighted, and (c) $ta_\infty/\delta_\omega=258.7$, with the C vortex highlighted. Contours from the top downward refer, respectively, to the uncontrolled mixing layer, the mass source control, the x- and the y-direction body force controls, and the internal-energy control. Same contours of Fig. 6.

vortex is displaced upward, the B vortex downward, and the C vortices upward. These vertical displacements likewise lead to higher or lower convection speeds depending on the side of the mixing layer into which the structures are displaced. However, the y-momentum control is the most intuitive; the dynamics of the other controls defies such a simple mechanistic explanation.

IV. DETECTION OF INTERMITTENT RADIATION

To make the analysis more quantitative, we analyzed the pressure signal at the same point $(80\delta_\omega,-70\delta_\omega)$ by means of a continuous wavelet transform. The pseudospectra computed this way are localized in both time and time-scale.

Farge[17] provides a complete review of these methods. The continuous wavelet transform is

$$\tilde{p}(s,t)=\int_{-\infty}^{\infty} p(\tau)\psi(s,t-\tau)\mathrm{d}\tau, \tag{7}$$

where s is the time-scale of the wavelet function. We used Paul's wavelet, defined for $s=1$ with an order m as

$$\psi(1,t)=\frac{2^m i^m m!}{\sqrt{\pi(2m)!}}[1-i(t)]^{-(m+1)}. \tag{8}$$

This is a complex-valued wavelet function; for $m=4$ its real and imaginary parts are shown in Fig. 15. The choice of this wavelet function with $m=4$ is due in particular to its imaginary part, which approximates the shape of the noisy signature of the uncontrolled mixing layer seen in Fig. 2(c), but with a negative sign. We thus expect that similar signatures will have a continuous wavelet transform with high energy content in a small scale range and in a reduced interval of the simulation. The other scales are obtained by dilatation of the so-called mother wavelet, with a normalization by $\sqrt{s}$ in order to maintain unit energy,

$$\psi(s,t-\tau)=\frac{1}{\sqrt{s}}\psi\left(1,\frac{t-\tau}{s}\right). \tag{9}$$

A longer DNS simulation of the uncontrolled flow was used (ten times that of Wei and Freund).[4] The same code was used for the simulation, with an identical grid and the same simulation parameters. The results are obviously identical over the time interval considered in that paper.

The continuous wavelet transform was applied to the pressure signal at the point $(80\delta_\omega,-70\delta_\omega)$ of this long simulation, the same point used in the analysis in Sec. III A [see Fig. 2(c)]. The resulting scalogram is shown in Fig. 16. In Fig. 16(a), which corresponds to the original simulation up to $ta_\infty/\delta_\omega=626.6$, there is a clear peak identified at $ta_\infty/\delta_\omega \simeq 380$, which corresponds to that analyzed in Sec. III A. The data are continued to longer times in Fig. 16(b). Here, we see

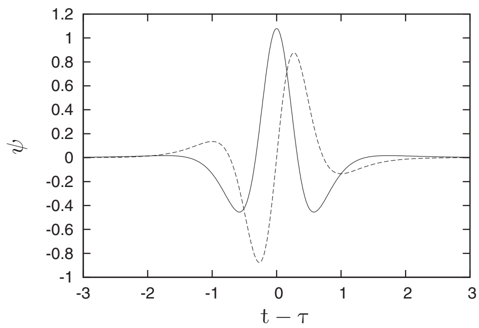

FIG. 15. Paul's wavelet: (——) real and (- - - -) imaginary parts.

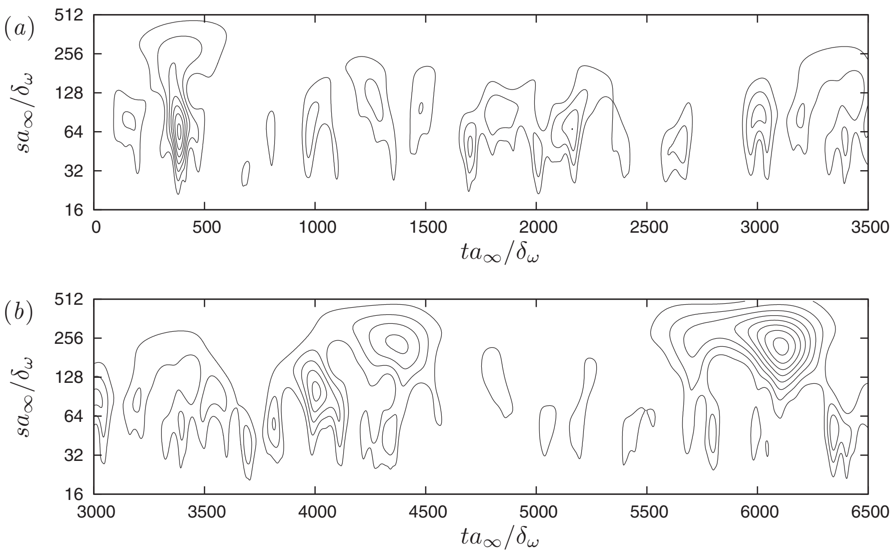

FIG. 16. Wavelet spectrum for the (a) first and (b) second parts of the simulation. Levels are uniformly distributed between 0 and $0.03(p_\infty\delta_\omega/a_\infty)^2$ in steps of $0.003\ (p_\infty\delta_\omega/a_\infty)^2$.

that in the continued longer simulation there are similar peaks concentrated around $ta_\infty/\delta_\omega \simeq 4000$, $ta_\infty/\delta_\omega \simeq 4400$, and $ta_\infty/\delta_\omega \simeq 6100$. We note that the results of Fig. 16 are similar to the experimental wavelet spectrum shown by Hileman *et al.*,[7] which showed periods of relative quiet interspersed with noise generation events.

To isolate the events that correspond to the peaks in the scalogram, we performed a filtering operation based on a threshold α,

$$\tilde{p}_f(s,t) = \begin{cases} \tilde{p}(s,t) & \text{if } |\tilde{p}(s,t)|^2 > \alpha \\ 0 & \text{if } |\tilde{p}(s,t)|^2 < \alpha. \end{cases} \quad (10)$$

The filtered pressure in the wavelet basis is then transformed back to the time domain by means of an inverse continuous wavelet transform. For the inverse transform we used the expression presented by Farge,[17] which gives

$$p_f(t) = \frac{1}{C_\delta}\int_{0^+}^{\infty} \frac{\tilde{p}_f(s,t)}{s^{3/2}} \mathrm{d}s, \quad (11)$$

where C_δ is obtained by the Fourier transform of the mother wavelet $\hat{\psi}(1,\omega)$,

$$C_\delta = \frac{1}{\sqrt{2\pi}}\int_{0^+}^{\infty} \frac{\hat{\psi}(1,\omega)}{\omega}\mathrm{d}\omega. \quad (12)$$

The numerical application of the continuous wavelet transform was performed for a total of 120 time-scales, defined as

$$s_j = 2^{[(j-1)\Delta s]}s_0, \quad (13)$$

where s_0 is the first scale. We chose s_0 to be twice the data-writing period in the simulation and Δs as $s_0/100$. The scale distribution of Eq. (13) allowed us to use the numerical formulation of Torrence and Compo.[18] Application with $\alpha=0$ recovered the original time series with a relative error of 2.2% with the chosen set of scales.

We chose as a filter $\alpha = 0.009(p_\infty\delta_\omega/a_\infty)^2$, since above this value only the high energy concentrations shown in Fig. 16, analogous to that found at the beginning of the simulation, are thus retained. The results of this filtering operation applied to the beginning of the simulation are presented in Fig. 17. We see that the filtered pressure is zero in all but a reduced interval, where the vortex merger signature analyzed in Sec. III A is captured. For the remainder of the simulation, the reconstructed pressure signal is mostly zero, but at the intervals where there are energy concentrations in both time and time-scale we see clear peaks for the pressure. We see in Fig. 18(a) that the filtered pressure around $ta_\infty/\delta_\omega = 4000$ has a pattern similar to that observed in Fig. 17, and which was related to the triple vortex interaction in Sec. III C. In Figs. 18(b)–18(e) we see vorticity contours at the center of the mixing layer at times prior to the arrival of the mentioned

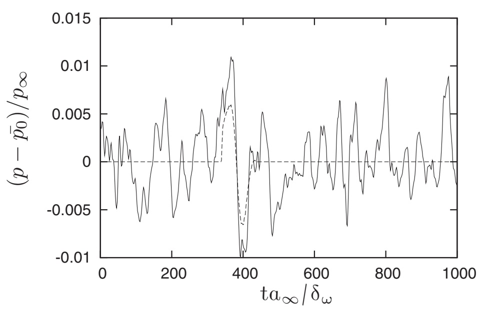

FIG. 17. Wavelet filtering at $(80\delta_\omega, -70\delta_\omega)$: (——) original and (- - -) filtered pressures.

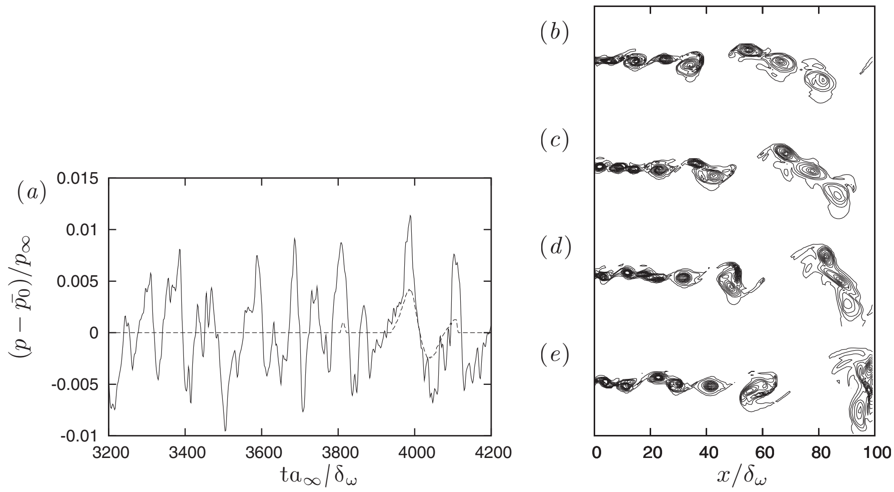

FIG. 18. (a) Wavelet filtering, (——) original and (- - -) filtered pressures. [(b)–(e)] Vorticity contours at $ta_\infty/\delta_\omega=3899.3$, $ta_\infty/\delta_\omega=3916.1$, $ta_\infty/\delta_\omega=3932.9$, and $ta_\infty/\delta_\omega=3949.7$. Contours range from $0.014\Delta U/\delta_\omega$ to $0.7\Delta U/\delta_\omega$.

pressure peaks. There is a triple vortex merger similar to that shown in Fig. 5(a).

Figures 19 and 20 show results for the other intervals of the simulation, when there are nonzero values for the filtered pressure. We see again in Figs. 19(a) and 20(a) a similar pressure signature as that of Figs. 17 and 18(a); and the corresponding vorticity contours, shown in Figs. 19(b)–19(e) and 20(b)–20(e), show triple vortex mergers to occur in each case, just prior to the arrival of the high-amplitude pressure wave at the considered point.

Although the reconstructed pressure signal is equal to zero for all the simulation time but the four events shown in Figs. 17, 18(a), 19(a), and 20(a), the filtered pressure has a rms value equal to 23.6% of the value for the original pressure time series. Thus, although the analyzed events are rare in the dynamics of the mixing layer, they are responsible for a significant portion of the sound power radiated by the flow, and they seem to have been the most easily suppressed by the optimal control.

We can conjecture that an optimal control applied to the extended simulation would again tend to eliminate these noisy events. In order to get a sense of the acoustic benefit which might be obtained, we compare in Fig. 21 pressure spectra for the original time series with spectra computed after the subtraction of the bursts of Figs. 17, 18(a), 19(a), and 20(a). We see that the suppressed events correspond to energy in a frequency band around $f=0.16f_0$. As shown by Wei and Freund, this corresponds to the loud peak in the acoustic field that is reduced by the optimal control.

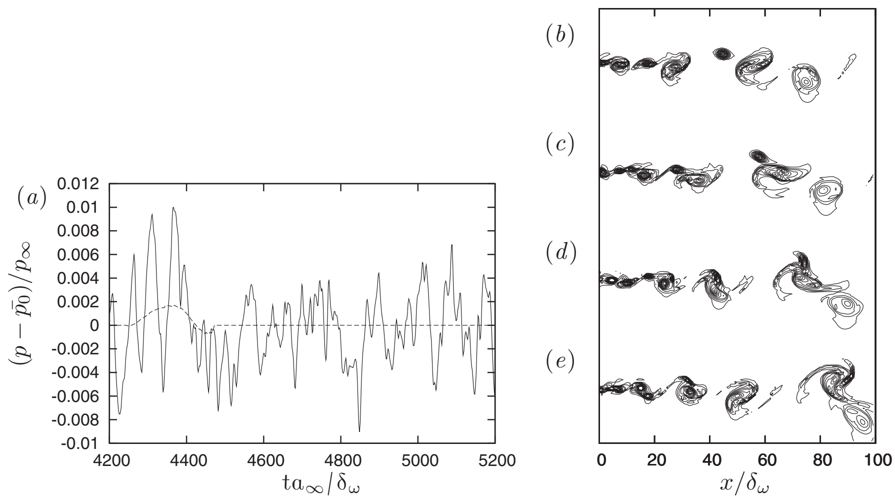

FIG. 19. (a) Wavelet filtering, (——) original and (- - -) filtered pressures. [(b)–(e)] Vorticity contours at $ta_\infty/\delta_\omega=4275.6$, $ta_\infty/\delta_\omega=4292.4$, $ta_\infty/\delta_\omega=4309.2$, and $ta_\infty/\delta_\omega=4326.0$. Same contours as Fig. 18.

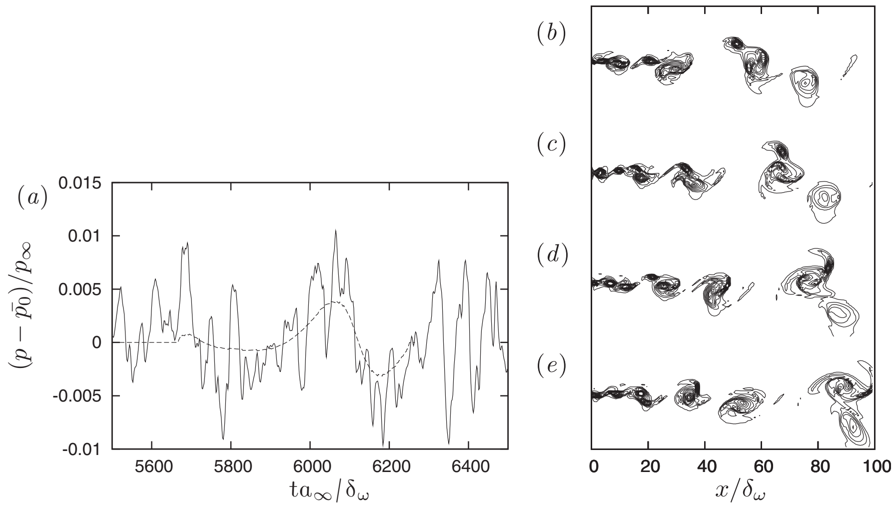

FIG. 20. (a) Wavelet filtering, (——) original and (- - -) filtered pressures. [(b)–(e)] Vorticity contours at $ta_\infty/\delta_\omega=5980.8$, $ta_\infty/\delta_\omega=5997.6$, $ta_\infty/\delta_\omega=6014.4$, and $ta_\infty/\delta_\omega=6031.2$. Same contours as Fig. 18.

V. CONCLUSION

An analysis was carried out to identify and understand the differences between the uncontrolled and controlled mixing layers of Wei and Freund.[4] The analysis of the pressure in the acoustic field showed that the noise reductions are especially significant in the downstream points of the target line, and 70% of the sound reduction in this region is achieved by the suppression of a high-amplitude pressure wave, comprising a compression followed by an expansion. A triple vortex interaction, which occurs only once in the simulation, is shown to lead to these peaks in sound pressure. Control was seen to comprise transverse vortex displacements, which, together with the consequent changes in convection velocity, modify the mutual interactions between neighboring structures in a way that prevents the triple vortex merger in the controlled mixing layer.

Wavelet transform analysis of a longer DNS calculation confirmed that loud events were associated with triple vortex mergers. These are intermittent events in the vortex dynamics of the mixing layer, but their contribution to the overall sound is considerable.

This study demonstrates (confirming the results of previous findings) that such intermittency constitutes a major element in the production of sound by free-shear flows. It should thus be explicitly included in modeling strategies. In many statistical noise prediction schemes such intermittent events are *not* explicitly included, and indeed they are often explicitly excluded by certain modeling assumptions. It is possible that this may explain the poor robustness of nearly all current sound prediction schemes. These are mostly based on second-order turbulence statistics, which, as we have seen, can entirely miss the most important sound producing events: the uncontrolled and controlled mixing layers present almost identical second-order statistics.

In interpreting our results, it should be clear that the plane mixing layer is a model flow that has been studied to determine the fundamental mechanisms of noise production.[15] However, the model problems of Cavalieri *et al.*,[13] with the incorporation of intermittency effects for the large scale structures of a free three-dimensional jet, have shown quantitatively how intermittent changes in a basic flow structure can generate bursts of noise in the far acoustic field of a turbulent jet. This intermittency does not need to be via a triple vortex merger as in the model flow studied in the present paper. Any significant disruption of the cancellation between the successive structures might lead to peaks in the acoustic field.

In terms of the details of the mechanism by which the propagative wave is set up, our study shows that this can be explained in terms of the kind of multipole interference that retarded-potential type solutions imply. This supports the idea that the acoustic analogy models are conceptually correct, though predictive modeling in a manner that incorporates intermittency effects is challenging. These points are the subject of ongoing modeling work.[13]

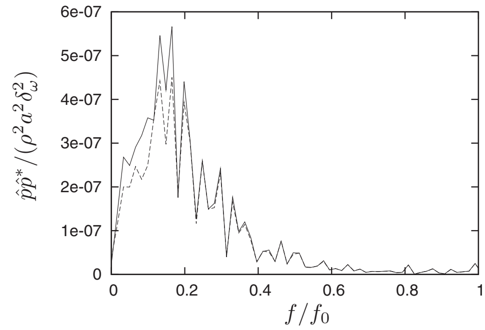

FIG. 21. Pressure spectra at $(80\delta_\omega,-70\delta_\omega)$: (——) original and (- - - -) suppression of bursts.

ACKNOWLEDGMENTS

The present work was supported by CNPq, National Council of Scientific and Technological Development-Brazil. J.B.F. and M.W. acknowledge support from AFOSR for the original mixing layer control simulations. J.B.F. acknowledges support from NASA for this work.

[1]M. J. Lighthill, "On sound generated aerodynamically. I. General theory," Proc. R. Soc. London, Ser. A **211**, 564 (1952).
[2]T. Colonius and S. K. Lele, "Computational aeroacoustics: Progress on nonlinear problems of sound generation," Prog. Aerosp. Sci. **40**, 345 (2004).
[3]M. Wang, J. B. Freund, and S. K. Lele, "Computational prediction of flow-generated sound," Annu. Rev. Fluid Mech. **38**, 483 (2006).
[4]M. Wei and J. B. Freund, "A noise-controlled free shear flow," J. Fluid Mech. **546**, 123 (2006).
[5]D. Eschricht, P. Jordan, M. Wei, J. B. Freund, and F. Thiele, "Analysis of noise-controlled shear-layers," in Proceedings of the 13th AIAA/CEAS Aeroacoustics Conference (28th AIAA Aeroacoustics Conference), American Institute of Aeronautics and Astronautics, 1801 Alexander Bell Drive, Suite 500, Reston, VA 20191-4344, 2007, Vol. 211, pp. 564–587.
[6]D. Juvé, M. Sunyach, and G. Comte-Bellot, "Intermittency of the noise emission in subsonic cold jets," J. Sound Vib. **71**, 319 (1980).
[7]J. I. Hileman, B. S. Thurow, E. J. Caraballo, and M. Samimy, "Large-scale structure evolution and sound emission in high-speed jets: Real-time visualization with simultaneous acoustic measurements," J. Fluid Mech. **544**, 277 (2005).
[8]J. Kastner, M. Samimy, J. Hileman, and J. B. Freund, "Comparison of noise mechanisms in high and low Reynolds number high-speed jets," AIAA J. **44**, 2251 (2006).
[9]J. B. Freund, "Noise sources in a low-Reynolds-number turbulent jet at Mach 0.9," J. Fluid Mech. **438**, 277 (2001).
[10]C. Bogey and C. Bailly, "An analysis of the correlations between the turbulent flow and the sound pressure fields of subsonic jets," J. Fluid Mech. **583**, 71 (2007).
[11]A. K. M. F. Hussain and K. B. M. Q. Zaman, "The 'preferred mode' of the axisymmetric jet," J. Fluid Mech. **110**, 39 (1981).
[12]J. E. Bridges and A. K. M. F. Hussain, "Roles of initial condition and vortex pairing in jet noise," J. Sound Vib. **117**, 289 (1987).
[13]A. V. G. Cavalieri, P. Jordan, A. Agarwal, and Y. Gervais, "Jittering wave-packet models for subsonic jet noise," Proceedings of the 16th AIAA/CEAS Aeroacoustic Conference and Exhibit, Stockholm, Sweden, 2010, AIAA Paper No. 2010-3957.
[14]A. V. G. Cavalieri, G. Daviller, P. Comte, P. Jordan, G. Tadmor, and Y. Gervais, "Using LES to explore sound-source mechanisms in jets," Procedia Engineering **6**, 104 (2010).
[15]T. Colonius, S. K. Lele, and P. Moin, "Sound generation in a mixing layer," J. Fluid Mech. **330**, 375 (1997).
[16]M. Wei, "Jet noise control by adjoint-based optimization," Ph.D. thesis, Department of Theoretical and Applied Mechanics, University of Illinois at Urbana-Champaign, Urbana, Illinois, 2004.
[17]M. Farge, "Wavelet transforms and their applications to turbulence," Annu. Rev. Fluid Mech. **24**, 395 (1992).
[18]C. Torrence and G. P. Compo, "A practical guide to wavelet analysis," Bull. Am. Meteorol. Soc. **79**, 61 (1998).

Chapter III

Intermittent sound generation in a subsonic jet

The study of two-dimensional mixing layers, presented in the previous chapter, showed that optimal control acts via an intermittent change in the structure of the mixing layer, suppressing the interaction of three vortices which led to a pressure burst in the acoustic field of the uncontrolled flow. We also detected similar bursts in a longer simulation of the uncontrolled mixing layer using a continuous wavelet transform.

In this chapter, we study a large eddy simulation of a Mach 0.9 jet in order to ascertain if a similar mechanism is present in such a flow. The three-dimensional behaviour of the flow is treated by a decomposition of both velocity and pressure into azimuthal Fourier modes. As for the mixing layer, we apply the continous wavelet transform to identify acoustic bursts, and observation of the flow field at times corresponding to the generation of bursts allows the identification of noisy events. Both the decomposition of the field in azimuthal modes and the identification of intermittent acoustic radiation are related to previous works in the literature, described in detail in section 2.2.2.

We present in this chapter a reproduction of the journal article "Using large eddy simulation to explore sound-source mechanisms in jets" [31], published in Journal of Sound and Vibration, 330(17):4098-4113, 2011.

Journal of Sound and Vibration 330 (2011) 4098–4113

Contents lists available at ScienceDirect

Journal of Sound and Vibration

journal homepage: www.elsevier.com/locate/jsvi

Using large eddy simulation to explore sound-source mechanisms in jets ☆

André V.G. Cavalieri [a,b,*], Guillaume Daviller [a], Pierre Comte [a], Peter Jordan [a], Gilead Tadmor [c], Yves Gervais [a]

[a] *Institut P', CNRS - Université de Poitiers - ENSMA, UPR 3346, Département Fluides, Thermique, Combustion, CEAT, 43 Route de l'Aérodrome, F86036 Poitiers Cedex, France*

[b] *Instituto Tecnológico de Aeronáutica, Praça Marechal Eduardo Gomes, 50, Vila das Acácias, CEP 12228-900 São José dos Campos, Brazil*

[c] *Department of Electrical and Computer Engineering, Northeastern University, 360 Huntington Avenue, Boston, MA 02115-5000, USA*

A R T I C L E I N F O

Article history:
Accepted 8 April 2011
Handling Editor: J. Astley
Available online 4 May 2011

A B S T R A C T

This paper presents an analysis of data generated by means of large eddy simulation for a single-stream, isothermal Mach 0.9 jet. The acoustic field is decomposed into Fourier modes in the azimuthal direction, and filtered by means of a continuous wavelet transform in the temporal direction. This allows the identification of temporally localised, high-amplitude events in the radiated sound field for each of the azimuthal modes. Once these events have been localised, the flow field is analysed so as to determine their cause. Results show high-amplitude, intermittent sound radiation for azimuthal modes 0 and 1. The mode-0 radiation, which dominates low-angle emission, is found to result from the temporal modulation of a basic axisymmetric wave-packet structure within the flow. Similar intermittent activity, observed, again within the flow, for azimuthal mode 1 suggests a link between the modes 0 and 1 dynamics. Both the amplitude and spatial extent of the axisymmetric wave-packet are modulated, and the strongest axisymmetric propagative disturbances are found to radiate from the downstream end of the wave-packet at moments when the wave envelope becomes truncated. The observed behaviour is modelled using a line-source wave-packet *ansatz* which includes parameters that account for the said modulation. Inclusion of these parameters, which allow the wave-packet to "jitter" in a manner similar to that observed, leads to good quantitative agreement (accurate to within 1.5 dB), at low emission angles, with the acoustic field of the LES. This result is in contrast with results obtained using a time-averaged wave-packet (one which does not jitter), for which a 12 dB error is observed. This result shows that the said modulations are the salient source feature for the low-angle sound emission of the jet considered. Analysis of a longer time series shows the occurrence of several similar high-amplitude bursts in the axisymmetric mode of the acoustic pressure, and a calculation of the radiated sound for this longer time-series, again using the wave-packet *ansatz*, once again leads to good agreement with the LES (now accurate to within 1 dB).

☆ This article is an expanded, peer-reviewed version of an article previously published in Procedia Engineering, 6C, 2010, pp. 104–113.

* Corresponding author at: Institut P', CNRS - Université de Poitiers - ENSMA, UPR 3346, Département Fluides, Thermique, Combustion, CEAT, 43 Route de l'Aérodrome, F86036 Poitiers Cedex, France. Tel.: +33 5 49453820; fax: +33 5 49453663.

E-mail address: andre.cavalieri@univ-poitiers.fr (A.V.G. Cavalieri).

0022-460X/$ - see front matter © 2011 Elsevier Ltd. All rights reserved.
doi:10.1016/j.jsv.2011.04.018

1. Introduction

A number of experimental studies [1–3] have shown that jet noise, especially for low emission angles, is composed of intermittent high-energy bursts. More recently, analysis [4] of the optimally controlled mixing layers of Wei and Freund [5] has revealed that the main change in the controlled flow amounted to the removal of a spatiotemporally localised event, comprising a triple vortex merger, which was particularly efficient in the production of a propagative disturbance. The sound production mechanism associated with this event can be understood in the context of the retarded-potential integrals by which classical acoustic problems can be understood, and which underpin all acoustic analogies. However, on account of the localised nature of the "loud" event, it could not be identified through a consideration of the second- or fourth-order statistics, which have a tendency to "smear" the local information, thus producing a misleading picture regarding the structure of the source and sound fields. This shows how such statistics may be ill-suited for an efficient description of this kind of intermittent source activity. From this, one can infer that modelling based on such statistics will also be poorly adapted; and this may explain why acoustic analogy modelling approaches struggle to provide reliable sound prediction when they are based on such statistics.

An interesting question which one can ask is: If the essential local flow characteristics associated with sound production are clearly identified, can simplified prediction methodologies be made more robust? Analysis of the Wei and Freund databases by three of the authors led to the development of some simple source models [6], by means of which we have begun to address this question; these models are equipped with the parameters, the study of which the numerical data suggests is most important for sound production.

The present paper constitutes our next step in this work. We here study a subsonic jet, which we compute by means of large eddy simulation (hereafter LES). This kind of simulation allows the calculation of flows with Reynolds numbers that would be prohibitively costly for a direct numerical simulation. Although the jet is initially laminar and the computation did not include the nozzle geometry, the present LES is able to reproduce experimental data of turbulent jets, and some validation results are presented in the Appendix. However, our model jet does not reproduce all features of the turbulence and acoustic fields of experimental jets, comprising, as do other calculations of the same kind, a low-pass filtered solution. We expect nonetheless that the present computation correctly reproduces the behaviour of the locally largest structures in the sound producing region of the flow; the fact that good agreement with experimental data is obtained in the peak regions of the spectrum attests to this.

In the present work we endeavour to use this numerical data to identify the salient features of the flow structure where sound production is concerned, and we do so by means of an analysis methodology similar to that applied to the optimally controlled two-dimensional mixing-layer data [4]. We decompose the radiated pressure field into azimuthal Fourier modes, and then analyse the temporal structure associated with each of the modes by means of the wavelet transform (this proved particularly useful in the study of both the low Reynolds number two-dimensional numerical data [4] and high Reynolds number experimental data [7]). In this way we filter the pressure field so as to isolate the temporally localised high-amplitude events. Having identified these we then study the flow data, again aided by Fourier azimuthal decomposition and wavelet transforms, in order to discern the flow organisation which led to the high-amplitude emission.

Results show how strong axisymmetric radiation can be explained by the time-varying modulation of the amplitude and axial extent of an axisymmetric wave-packet in the region upstream of the end of the potential core. The said modulation appears to be associated with the transition from dominance by axisymmetric structure to dominance by higher order azimuthal structure, and the time-scale of the axisymmetric modulation is found to be close to that of the first helical mode. We construct a simple wave-packet line-source model which mimics this behaviour, and we show how the inclusion of space–time "jitter" in the model leads to a quantitative estimate which is within 1.5 dB of the LES computation at low angles.

2. Flow simulation

The numerical algorithm used for the large eddy simulation is the same as that described in [8]. The conservative Navier–Stokes equations are solved by a density-weighted standard Favre-filtered compressible LES formalism, with the macro-temperature closure described in [9], and the filtered structure-function subgrid-scale turbulence model proposed by [10]. Spatial derivatives are computed with a fourth-order-accurate finite scheme [11] for both the inviscid and viscous portion of the flux [12]. A second-order predictor–corrector scheme is used to advance the solution in time. In addition, block decomposition and MPI parallelisation are implemented. The three-dimensional Navier–Stokes characteristic non-reflective boundary conditions (3D-NSCBC), developed by Lodato et al. [13] are applied at the boundaries of the computational domain to account for convective fluxes and pressure gradients across the boundary plane. In order to simulate anechoic boundary conditions, the mesh was stretched and a dissipative term is added to the equations, in the sponge zone, following [14].

2.1. Numerical details

The computations were performed on an IBM *power*6 machine at "IDRIS" using 64 processors. The computational domain comprises 19 million grid points: 400 points in the streamwise direction, and 218 points in both the y and z

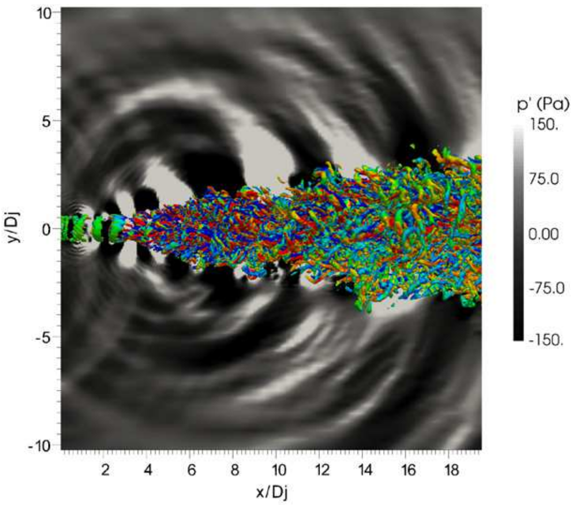

Fig. 1. Snapshot of the $M=0.9$ jet: centre, isosurfaces of positive $Q=0.05(U/D)^2$; outer regions, radiated pressure field.

directions. The extension of the computational domain is $40D\times30D\times30D$ (where D is the jet diameter). The sponge region is from $x=20D$ to $40D$ in the streamwise direction, and from $\pm10D$ to $\pm15D$ in the transverse y and z directions. The minimum grid spacing in the y and z directions is $\Delta_0=r_0/25$ and $\Delta_{x\min}=3\Delta_0$ in the streamwise direction. The axial mesh spacing is constant up to $x=20D$, and then stretched at a rate of 2 percent to match $\Delta_{x\max}=\Delta_{y\max}=\Delta_{z\max}=0.8D$ at the end of the computational domain.

The computations spanned 360 000 time steps ($\Delta t=2.2\times10^{-7}$ s) which corresponds to a total run time of 180 h.

2.2. Flow parameters

The simulation parameters correspond to those of Bogey and Bailly [15]: $M=0.9$ and Reynolds number $\mathrm{Re}=4\times10^5$, with $T_j/T_\infty=1$. The inflow axial velocity profile is given by a hyperbolic tangent profile as [16]

$$u(r)=U_\infty+\frac{(U-U_\infty)}{2}\left[1-\tanh\left[b\left(\frac{r}{r_0}-\frac{r_0}{r}\right)\right]\right], \tag{1}$$

where $b=r_0/(4\delta_\theta)$ and the momentum thickness of the shear layer is $\delta_\theta=0.05r_0$. The initial mean temperature is calculated with the Crocco–Busemann relation and the mean initial pressure is constant. Transition to turbulence is caused by means of solenoidal disturbances, introduced near the inflow boundary, which take the form of a vortex ring, as per Bogey and Bailly [17]. The forcing parameters correspond to those of the "LESmode" simulation of Bogey and Bailly [18].

Fig. 1 shows instantaneous isosurfaces of the Q-criterion, coloured by the streamwise vorticity, in addition to the radiated pressure field. Mean and turbulent flow quantities, integral length scales, radiated OASPL and acoustic spectra have been validated against numerical and experimental data; some validation results are presented in the Appendix.

3. Analysis of sound-source mechanisms

Motivated by the results of Cavalieri et al. [4] we choose in this work to study the LES data using azimuthal Fourier decomposition and temporal wavelet transforms. The latter proved to be well suited to the identification of the aforesaid space–time localised source activity.

3.1. Azimuthal structure of sound field

Throughout the present paper, the jet data is analysed by means of a Fourier series for the azimuthal angle ϕ, measured with respect to the x_3-axis; the x_2-axis corresponds to $\phi=\pi/2$. For the pressure, for instance, we have

$$p(x,r,\phi,t)=p_{A0}(x,r,t)+\sum_{m=1}^{\infty}[p_{Am}(x,r,t)\cos(m\phi)+p_{Bm}(x,r,t)\sin(m\phi)], \tag{2}$$

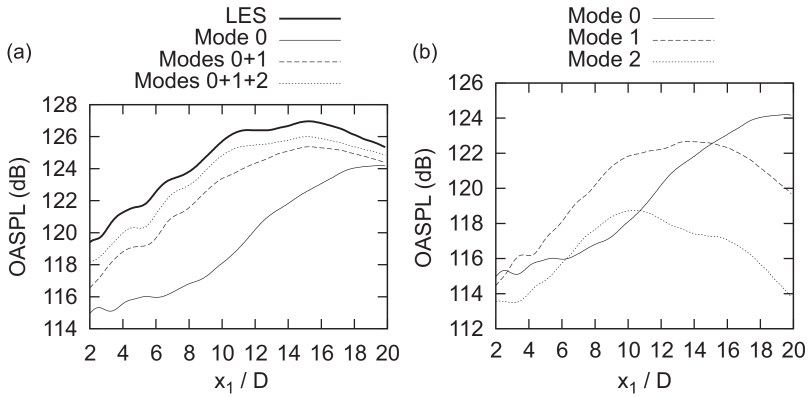

Fig. 2. Azimuthal structure of sound field: (a) modal contributions to overall level; (b) modal directivities.

where the coefficients in the series are given by

$$p_{A0}(x,r,t) = \frac{1}{2\pi}\int_{-\pi}^{\pi} p(x,r,\phi,t)\,\mathrm{d}\phi, \tag{3}$$

$$p_{Am}(x,r,t) = \frac{1}{\pi}\int_{-\pi}^{\pi} p(x,r,\phi,t)\cos(m\theta)\,\mathrm{d}\phi, \tag{4}$$

$$p_{Bm}(x,r,t) = \frac{1}{\pi}\int_{-\pi}^{\pi} p(x,r,\phi,t)\sin(m\theta)\,\mathrm{d}\phi. \tag{5}$$

The Fourier series is expressed in terms of real coefficients; this is preferred as it gives the component of each azimuthal mode m aligned with x_3 (A_m coefficients) and x_2 (B_m coefficients). The coefficients of an equivalent complex-valued Fourier series can nonetheless be obtained as

$$C_0 = A_0, \tag{6}$$

$$C_m = \frac{A_m + \mathrm{i}B_m}{2}, \tag{7}$$

$$C_{-m} = \frac{A_m - \mathrm{i}B_m}{2}. \tag{8}$$

Pressure data on a cylindrical surface at $r=9D$ from the jet axis is decomposed in a Fourier series in ϕ. Fig. 2(a) shows that modes 0, 1 and 2 are sufficient to represent the acoustic field with less than 2 dB difference for all points.

The directivity of the various modes are shown in Fig. 2(b): downstream radiation is dominated by the axisymmetric mode, whereas in sideline directions modes 1 and 2 dominate.

3.2. *Wavelet analysis of the sound field: intermittency*

The continuous wavelet transform

$$\tilde{p}(x,s,t) = \int_{-\infty}^{\infty} p(x,\tau)\psi(s,t-\tau)\,\mathrm{d}\tau \tag{9}$$

is used to analyse the temporal structure of the sound field at each point on the line-array and for each of the azimuthal modes. $\psi(s,t-\tau)$ is a family of wavelet functions, obtained by translation and dilatation of a mother wavelet function $\psi(1,t)$. We use the Paul wavelet with $m=4$:

$$\psi(1,t-\tau) = \frac{2^m i^m m!}{\sqrt{\pi(2m)!}}[1-\mathrm{i}(t-\tau)]^{-(m+1)}. \tag{10}$$

The motivation for using this complex valued wavelet is that it does a better job of producing a coherent signature in the scalogram over an integral scale which can be associated with single "events". This capability is due to the fact that both zero crossings and cusp-like peaks associated with high-amplitude events in the pressure signal are captured and lumped together such that they sign as a single event in the scalogram (see Kœnig et al. [7] for a comprehensive evaluation of the behaviour of different kinds of wavelet).

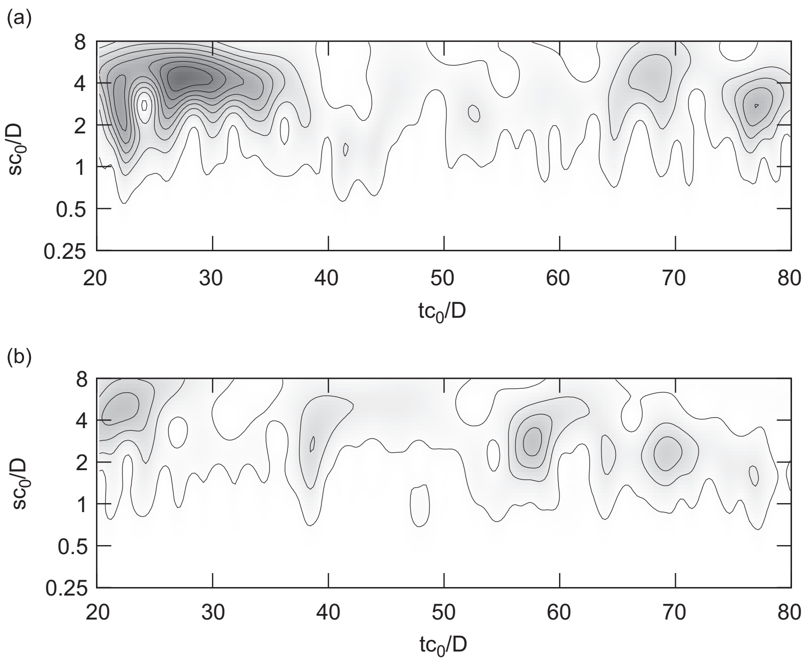

Fig. 3. Scalograms of the acoustic pressure at (a) $\theta = 30^\circ$ and (b) $\theta = 70^\circ$. Contours uniformly distributed between $10^{-5}\sigma^2$ and $5.1\times10^{-4}\sigma^2$ in intervals of $5\times10^{-5}\sigma^2$. Dark regions correspond to high values.

3.2.1. Axisymmetric mode

Two scalograms of the pressure signature of the axisymmetric mode are shown in Fig. 3. The x positions correspond to emission angles of 30° and 70°. Some temporally localised energy concentrations can be seen, and these are especially strong for the pressure at 30°. We will be interested in studying the flow behaviour which is responsible for these high-amplitude events.

In order to isolate these bursts, we apply a filter in wavelet space so as to retain only the high-energy peaks. We define a threshold α and decimate the wavelet coefficient ensemble so as to produce a filtered pressure field:

$$\tilde{p}_f(x,s,t) = \begin{cases} \tilde{p}(x,s,t) & \text{if } |\tilde{p}(x,s,t)|^2 > \alpha\sigma^2, \\ 0 & \text{if } |\tilde{p}(x,s,t)|^2 < \alpha\sigma^2, \end{cases} \tag{11}$$

where σ^2 is the mean square value of the pressure in the time domain. The accuracy of the wavelet transform has been checked with the application of a direct wavelet transform to the LES signals followed by an inverse transform without filtering, which results in the reconstruction of the original time series with a typical relative error of 0.5 percent using 80 scales spanning the frequency content of the jet.

The wavelet transform is here being used simply as an event identifier. Inspection of Fig. 3(a) clearly shows how the transform identifies a high-amplitude event at $tc_0/D \approx 28$. A threshold value of $\alpha = 0.00015$ is used to filter and thereby enhance such signatures (the same value is used throughout the paper), and as such it constitutes a means by which a space–time labelling of such events can be effected; this labelling procedure is relatively insensitive to the precise value of α which is chosen. For a more quantitative analysis of filtered signals this threshold would of course be required to become a parameter of the study; such a parametric study has been performed by Kœnig et al. [7].

A peak in the scalogram may be due to two things: if a signal has intermittent bursts, there will be an energy concentration in the time direction of the scalogram; if a signal comprises a pure tone, there will be a concentration in the scale direction. If both conditions are verified, we have high concentrations in a limited region in both s and t. In this case, this is due to a high correlation of the original signal with a particular scale during a limited time interval. Physically, this corresponds to the presence in the temporal time series of a high-amplitude acoustic wave-packet, whose shape is well described by the wavelet function; such a signature can be interpreted as either an isolated energy burst or as a modulation, comprising an amplitude increase, of a given wave. Both possibilities will give an energy concentration both in time and in frequency, leading to a burst in the scalogram. Based on this we loosely refer to as "bursts" or "events" the energy concentrations in the scalograms which are retained in the filtered signals. Whether these signatures correspond to bursting events or modulated waves is, to a certain degree, peripheral with regard to our objective, which is to analyse and understand the events in the flow which underpin these modulations or "bursts".

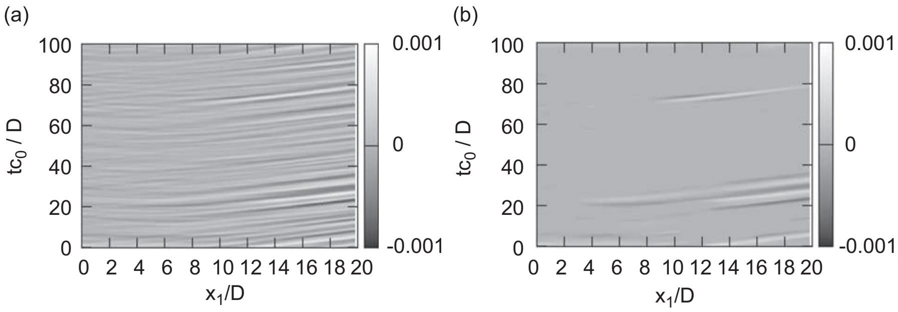

Fig. 4. Pressure at the acoustic field (azimuthal mode 0): (a) original and (b) filtered.

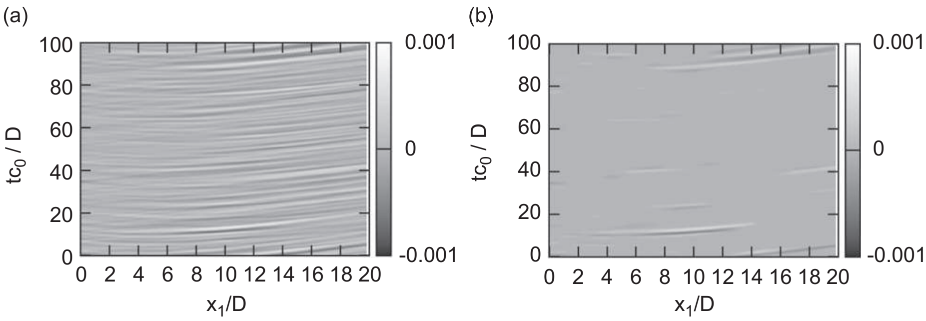

Fig. 5. Pressure at the acoustic field (azimuthal mode 1): (a) original and (b) filtered.

The filtered pressure in the time domain is obtained by application of the inverse wavelet transform:

$$p_{\mathrm{f}}(x,t) = \frac{1}{C_\delta}\int_{0^+}^{\infty} \frac{\tilde{p}_{\mathrm{f}}(x,s,t)}{s^{3/2}}\,\mathrm{d}s. \tag{12}$$

This operation is performed independently for each position x. The original and filtered pressures with $\alpha = 0.00015$ are shown in Fig. 4. This threshold value was used for all of the filtering operations reported in this paper.

Both the unfiltered and filtered pressure signatures show similar phase velocity, indicating that the main sound radiation originates somewhere between 5 and 7 diameters downstream of the exit plane, i.e. just downstream of the end of the potential core; however, it is worth noting that refraction of sound waves by the mean-flow will deform wavefronts such that this "origin" appears further downstream than it actually is. As both filtered and unfiltered fields manifest the same phase speed, we can infer that the turbulent structures in the vicinity of the end of the potential core have a somewhat regular character interspersed with localised high-energy events. These results are consistent with the literature [1–3].

3.2.2. Azimuthal mode 1

The same filtering procedure was carried out for the other azimuthal modes. Fig. 5 shows the original and the filtered pressures for mode 1. The results are similar to those obtained for mode 0, but the intermittent bursts are present at higher emission angles; this is coherent with the directivity of this mode, presented in Fig. 2(b). Analysis of the phase velocity again situates the source in the vicinity of the end of the potential core.

3.2.3. Azimuthal mode 2

Fig. 6 shows similar results for azimuthal mode 2. The bursts are still present, however with lower intensity and a lower degree of spatial correlation.

3.3. Wavelet analysis of the flow field

The same filtering operation is now applied within the confines of the turbulent field. On the jet centreline, the transverse velocity components, v and w, show intermittent peaks downstream of the potential core which are similar to those detected in the acoustic field. Fig. 7 shows the results for the wavelet filter applied to the v velocity component; to examine the relationship between the intermittency on the centreline and the bursts in the acoustic field, we show, in Figs. 7(a) and (b), the filtered v velocity in a retarded-time reference frame (Fig. 8).

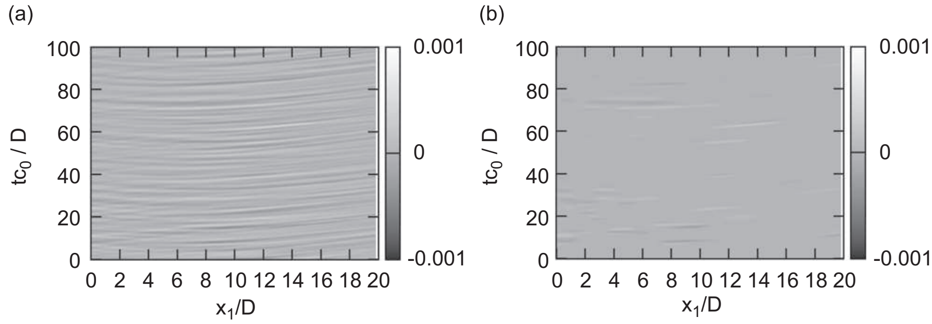

Fig. 6. Pressure at the acoustic field (azimuthal mode 2): (a) original and (b) filtered.

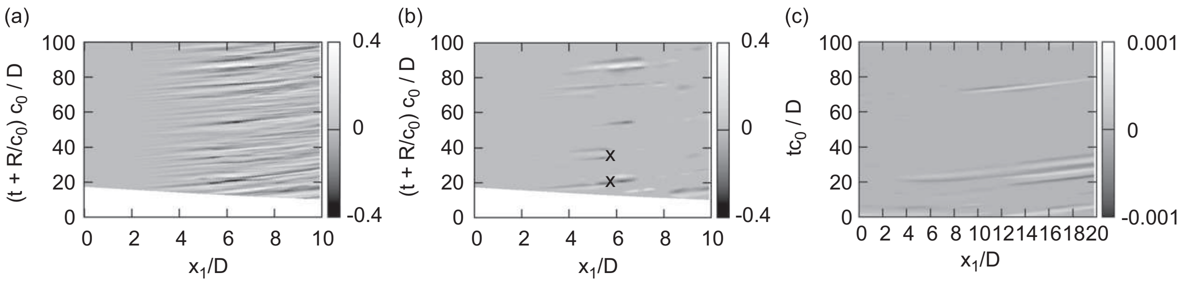

Fig. 7. v velocity component on the jet centreline: (a) original and (b) filtered; and (c) filtered pressure in the acoustic field (azimuthal mode 0).

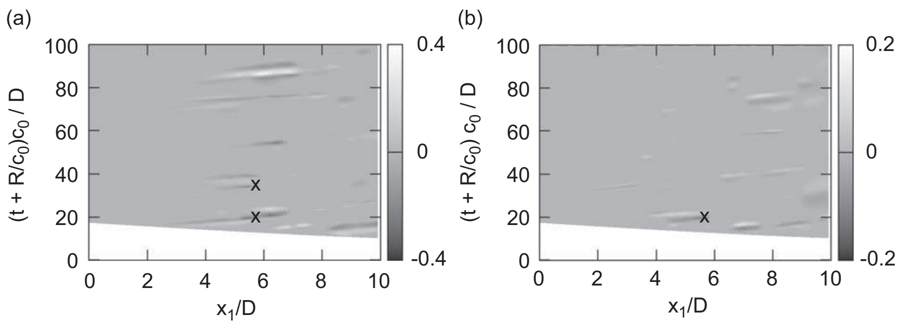

Fig. 8. (a) Filtered v velocity component at the jet centreline and (b) filtered azimuthal velocity (mode 1) at the jet lipline.

Two filtered events in the acoustic field can be observed for mode 0 ($19 < tc_0/D < 35; 70 < tc_0/D < 80$), shown in Fig. 7(c). One of these ($19 < tc_0/D < 35$) correlates well with the flow events identified around $x=6D$, shown in Fig. 7(b) (marked with an $\times$). A second strong signature in the flow field at $(t+R/c_0)c_0/D = 85$ does not correlate with the filtered structure of the axisymmetric mode; however, as shown in Fig. 5(a), we see that it corresponds to an intermittent event in the filtered mode 1 signature.

We performed the same filtering with an azimuthal decomposition of the velocity field at $r=D/2$. Comparison of the filtered v velocity component on the jet centreline with the filtered mode 1 (A_1 coefficient) of the azimuthal velocity component on the lipline shows that the first intermittent burst retained by the filtering is similar for the two variables. As the A_1 component of mode 1 is related to $\cos\phi$, the direction of the mode 1 fluctuation of the azimuthal velocity corresponds to the v Cartesian velocity component of our coordinate system, as shown schematically in Fig. 9(b). We infer that the intermittent event near the end of the potential core, which correlates with the bursts in the acoustic field, are high-amplitude transverse oscillations of the jet at that axial station: a transverse motion associated with azimuthal mode 1.

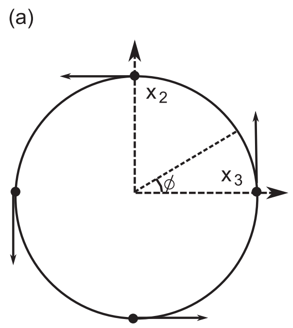

Fig. 9. Direction of velocity vectors of the azimuthal component of velocity for (a) axisymmetric and (b) first helical mode.

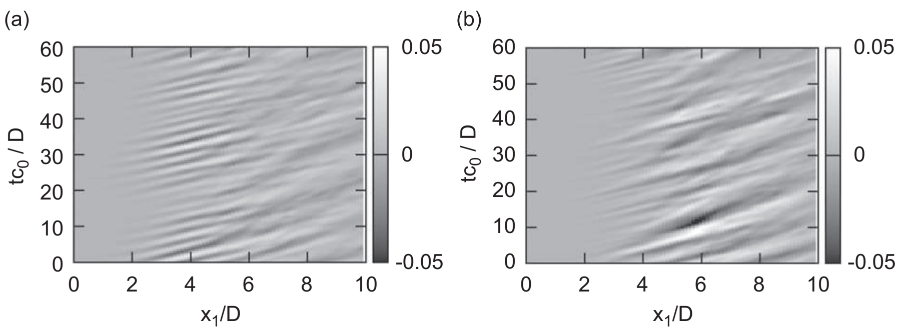

Fig. 10. Pressure at the near field: (a) azimuthal mode 0 and (b) azimuthal mode 1 (B_1 coefficient).

3.4. A model for the axisymmetric pressure burst

Further evidence of the high-amplitude, temporally localised, mode 1 activity in the jet is manifest when we apply the azimuthal decomposition to the near pressure field (which comprises the hydrodynamic footprint of coherent turbulent structures [19]); this is shown in Figs. 10(a) and (b) for a cylindrical surface with $r/D=1$.

The space–time signature of the first two azimuthal modes of the near-field pressure are plotted. The axisymmetric mode shows a clear wave-packet structure, with oscillations whose time-scale is nearly constant, and whose amplitude undergoes modulation in both space and time. This kind of modulation is similar to that modelled by Lele [20] and Cavalieri et al. [6]. For azimuthal mode 1 such an organised wave-packet structure is not so clear. Focusing on the first 10 non-dimensional time units we see how the spatial amplitude modulation of the axisymmetric mode undergoes a sudden reduction in axial extent (this occurs at $tc_0/D=7$). At approximately the same time there is a high-amplitude event seen in azimuthal mode 1, in the vicinity of $x/D=6$; this event corresponds to the peak detected in the transverse velocity (Fig. 7).

The axial variations of azimuthal mode 0 at three times leading up to the abrupt attenuation are shown in Fig. 11. We see how the signatures can be divided into a smooth wave-packet zone (envelopes indicated by the thick lines), and a more disturbed downstream zone. At $tc_0/D=2$ the smooth wave-packet zone extends to $x/D=6$, whereas at $tc_0/D=8$ the wave-packet form has been truncated to $x/D=5$, and the instantaneous amplitude envelope has a steep slope.

In Fig. 12 we get a better sense of the global fluid motion over the duration of this sound-producing event. The cross-section is taken in a plane which is aligned with the direction (identified from the real and imaginary parts of the mode 1) of the helicoidal motion of the flow. Prior to the times shown in Fig. 12 the flow organisation does not present such marked axisymmetry. This implies low levels in the axisymmetric component of the hydrodynamic pressure field. Fig. 12(a) shows the flow organisation (as discerned by its hydrodynamic pressure footprint) when there is a strong increase in the axisymmetric component, but the inclination of the structures just downstream of the axisymmetric wave-packet means that it is abruptly truncated. It is at approximately this moment that the first axisymmetric, negative pressure pulse, identified in Fig. 4 and shown in Fig. 12(a) with a red arc, begins to propagate. A snapshot of the pressure field of the simulation in a plane transverse to the jet at $x/D=7$ is shown in Fig. 13, showing that the generated negative pressure burst is indeed predominantly axisymmetric.

At $tc_0/D=9.514$ the organised axisymmetric wave-packet observed at $tc_0/D=8.576$ has convected downstream, and has maintained its axisymmetry: we now have a strong axisymmetric pressure wave-packet, but with an extended envelope. The evolution to $tc_0/D=12.596$ comprises a second, abrupt, truncation of the axisymmetric wave-packet, again associated with the tilting of these structures in the vicinity of the end of the potential core. The second axisymmetric,

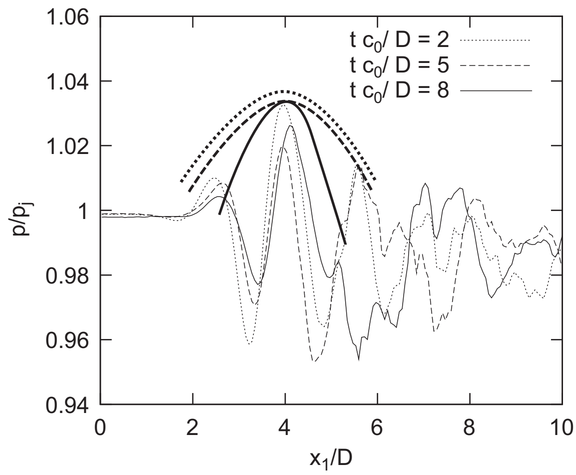

Fig. 11. Azimuthal mode 0 for the near field pressure at three different times.

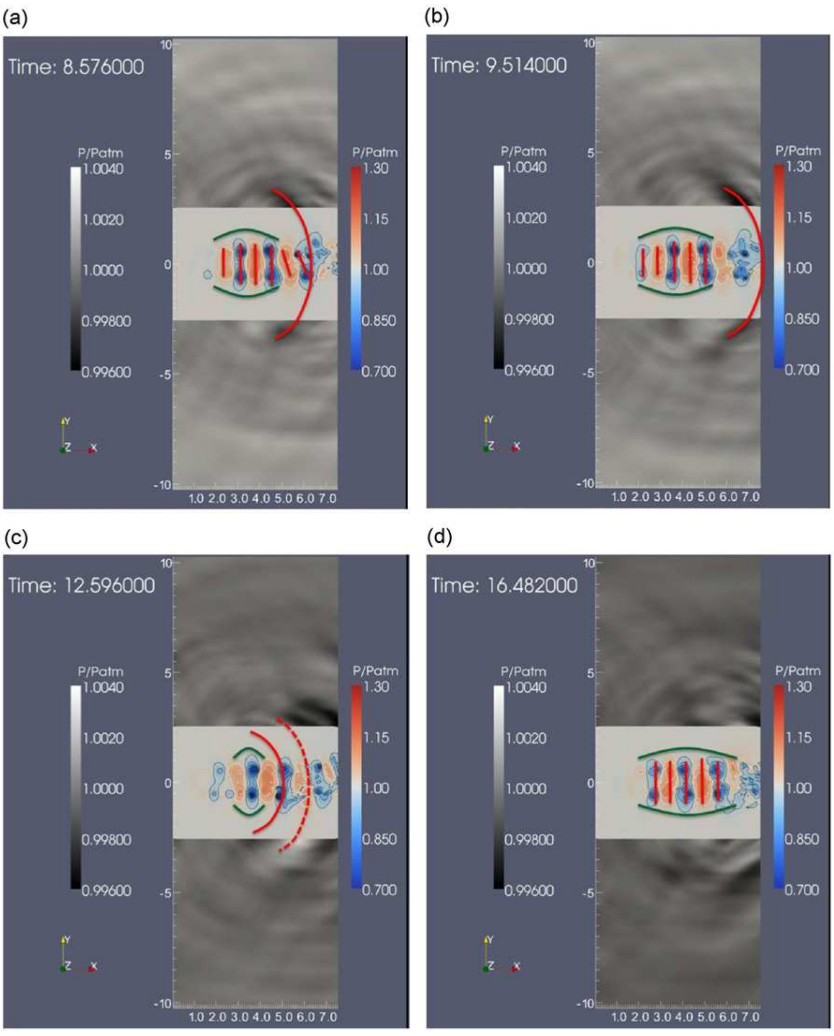

Fig. 12. Pressure at the x_1–x_2 plane of the jet for (a) $tc_0/D = 8.576$, (b) $tc_0/D = 9.514$, (c) $tc_0/D = 12.596$ and (d) $tc_0/D = 16.482$. (For interpretation of the references to color in this figure legend, the reader is referred to the web version of this article.)

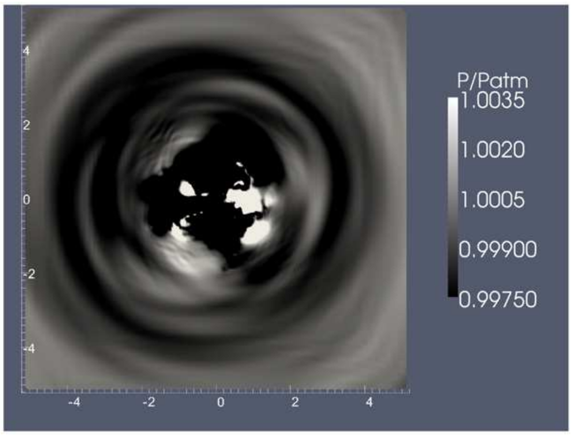

Fig. 13. Pressure field at $x/D=7$ and $tc_0/D=10.5$.

negative pressure pulse is released at approximately this time. Following this a new extension of the wave-packet envelope is observed for $tc_0/D=16.482$.

These observations indicate that the flow drifts in and out of axially coherent axisymmetry. The axisymmetric component of the flow thus experiences spatiotemporal fluctuations in both the amplitude and the axial extension of its envelope. This temporal modulation has a time-scale which is lower than the period of the axisymmetric mode, which corresponds to $\mathrm{St}\approx 0.4$. The temporal modulation of the axisymmetric mode occurs at times when high amplitudes are detected for azimuthal mode 1; this suggests that these events may be related. The possibility that these different azimuthal modes of the flow may be dynamically coupled is currently being explored in a separate study and is beyond the scope of the present paper. Where present investigation is concerned, the salient flow feature with regard to temporally localised high-amplitude sound radiation is the modulation of the axisymmetric wave-packet, and we will focus on this aspect of the flow in what follows.

It is worth mentioning that such behaviour has been both observed and modelled in a number of studies. The truncation [21,22] and temporal modulation [23,20,6] of wave-packets have been studied and shown to lead to an increased sound radiation efficiency. The latter papers both show that at high Mach number the effect of temporal modulation can be important.

Such observations are in agreement with a number of other experimental and numerical studies. Kastner et al. [24], for example, show, for a lower Reynolds number jet computed by DNS, that intermittent bursts radiated to low polar angles are associated with the breakdown of an instability wave near the end of the potential core of a Mach 0.9 jet. Hileman et al. [3] show, in an experimental study of a perfectly expanded Mach 1.28 jet, that intermittent noise generating events at 30° to the jet axis are related to the large-scale entrainment of ambient fluid by coherent structures toward the centre of the jet, and to a consequent shortening of the potential core. Such behaviour may arise on account of the radial displacement of vortex rings which will draw ambient fluid inwards toward the potential core region of the flow, and lead to the truncation of the axisymmetric wave-packet. Our observations are similar to those of Kastner et al.; however, we would like to obtain a more quantitative verification, and we do so in what follows by means of a simplified source model, fitted with the LES velocity data, and whose sound field we then compare with the LES.

4. Quantitative evaluation of the wave-packet radiation

The analysis of the previous section is based on a wave-packet model for the source. In order to determine if this hypothesis is consistent with both the turbulent and the acoustic fields of the present jet, we have fitted an averaged axisymmetric wave-packet to the jet data to check if with this very simplified model we are able to get radiation levels close to those of the LES.

We use a modified version of Crow's model [21,22], which is based on a convected wave for the axial velocity, with spatial modulation given by a Gaussian function. This model, proposed by Cavalieri et al. [6], adds temporal changes of modulation: the frequency and wavenumber of the convected wave remain constant, but the parameters of the Gaussian envelope change in time. The source term is concentrated on a line, and has only the T_{11} component of Lighthill's stress tensor:

$$T_{11}(\mathbf{y},\tau)=2\rho_0 U\tilde{u}(\tau)\frac{\pi D^2}{4}\delta(y_2)\delta(y_3)\mathrm{e}^{\mathrm{i}(\omega\tau-ky_1)}\mathrm{e}^{-(y_1-y_c)^2/L^2(\tau)}, \tag{13}$$

where the wavenumber k for the convected wave is given by $\omega/(M_c c_0)$, M_c being the Mach number of the convected wave.

While the Lighthill source term is known to contain flow–acoustic interaction effects [25], the source *ansatz* we propose is characterised by a convection velocity of $M_c \approx 0.5$ and is concentrated on a line; we thus consider that the model problem we pose essentially describes sound production by subsonically convected hydrodynamic disturbances, rather than sound refraction effects by the radial gradients of the mean flow.

Solving Lighthill's equation for the pressure,

$$p(\mathbf{x},t) = \frac{1}{4\pi}\iiiint \frac{\partial^2 T_{ij}}{\partial y_i \partial y_j}(\mathbf{y},\tau)\frac{\delta\left(t-\tau-\dfrac{|\mathbf{x}-\mathbf{y}|}{c_0}\right)}{|\mathbf{x}-\mathbf{y}|}\,\mathrm{d}\tau\,\mathrm{d}\mathbf{y} \tag{14}$$

with a far-field assumption, and considering that the amplitude $\tilde{u}$ and the width L change slowly if evaluated at retarded-time differences along the wave-packet, leads to an analytical expression for the radiation of the wave-packet [6]:

$$p(\mathbf{x},t) = -\frac{\rho_0 U \tilde{u}\left(t-\dfrac{|\mathbf{x}|}{c_0}\right) M_c^2 (kD)^2 L\left(t-\dfrac{|\mathbf{x}|}{c_0}\right)\sqrt{\pi}\cos^2\theta}{8|\mathbf{x}|}\,\mathrm{e}^{-L^2(t-|\mathbf{x}|/c_0)k^2(1-M_c\cos\theta)^2/4}\,\mathrm{e}^{\mathrm{i}\omega(t-|\mathbf{x}|/c_0)}. \tag{15}$$

By replacing $\tilde{u}$ and L with their time-averaged values the above expression gives the sound pressure radiated by a wave-packet with no such modulation. We will compare the two in order to assess the impact of the wave-packet "jitter".

Eq. (15) shows that the temporally localised truncation of the wave-packet structure, observed in Section 3.4, can lead to high-amplitude radiation to the far field: a reduction in L will result in a significant increase of the first exponential term.

We use data taken from a cylindrical surface with $r = D/2$ to furnish our model. Streamwise velocity data for the axisymmetric mode is used to obtain the parameters of the wave-packet. We proceed as follows:

- The frequency ω is chosen as the peak frequency for the axial velocity at $x_1 = 3.5D$, i.e. the position of saturation of the wave-packet, as seen in Fig. 10(a). For the present jet, this corresponds to a Strouhal number of 0.4.[1]
- The convection Mach number M_c is taken as the lipline value (0.543M); to determine it we use the peak in a frequency-wavenumber spectrum for the axisymmetric component of the streamwise velocity.
- The envelope length $L(\tau)$ and the amplitude $\tilde{u}(\tau)$ are obtained by Gaussian fits to the axisymmetric component of the axial velocity on the jet lipline at each time. In order to do this, we first filter the velocity field, retaining only a range of frequencies from St = 0.3 to 0.5. We then use two approaches to determine an instantaneous wave-packet envelope: we do either a Hilbert transform in time, which is known to give the modulation of a harmonic oscillation if this modulation is bandwidth limited [26], or we use a short-time Fourier series, similar to that described by Tadmor et al. [27]: the temporal dependence of velocity at a position x is considered a harmonic oscillation of frequency ω, but with an amplitude that changes slowly in time:

$$u(x_1,t) = A(x_1,t)\cos(\omega t) + B(x_1,t)\sin(\omega t). \tag{16}$$

The coefficients A and B are obtained with a short-time Fourier series:

$$A(x_1,t) = \frac{2}{T}\int_{t-T/2}^{t+T/2} u(x_1,\tau)\cos(\omega\tau)\,\mathrm{d}\tau, \tag{17}$$

$$B(x_1,t) = \frac{2}{T}\int_{t-T/2}^{t+T/2} u(x_1,\tau)\sin(\omega\tau)\,\mathrm{d}\tau \tag{18}$$

and the instantaneous amplitude of the oscillations is given as $\sqrt{A(x_1,t)^2 + B(x_1,t)^2}$. The moving window width T is taken as the period of oscillation in ω. We then calculate instantaneous lengths and amplitudes using the Gaussian fits for each instantaneous envelope. Some sample fits for the Hilbert transform envelope are shown in Fig. 14.

We compare, in Fig. 15, the results of this model with the SPL of the azimuthal mode 0 of the LES, taking a frequency range from St = 0.3 to 0.5. Two calculations are performed, one for an "average wave-packet", whose amplitude $\tilde{u}$ and width L are constant and equal to the ensemble-average values of the fitted Gaussians, and another for the "instantaneous wave-packet", where $\tilde{u}$ and L change in time according to the instantaneous fits of both the Hilbert transform of the data and of Eq. (16). We show, for the instantaneous wave-packet, two different calculations: an analytical one, which is the direct application of Eq. (15), and a numerical calculation of the integral of Eq. (14), without the far-field assumption, since the domain boundary for the LES is not in the geometrical far acoustic field. The differences between the analytical and numerical calculations are small.

Although highly simplified, the proposed model of a "jittering" wave-packet leads to results which are within 1.5 dB of the LES for low axial angles. This agreement indicates that the proposed *ansatz* for the source comprises the salient

[1] This Strouhal number, together with the jet Mach number 0.9, justify the use of a source concentrated on a line: since D/λ is equal to St M, for the present numerical values the jet diameter is approximately one-third of the wavelength, and we can consider a compact source in the transversal direction; more details can be found in Cavalieri et al. [6]. The non-compactness in the axial direction is nonetheless retained in the calculations.

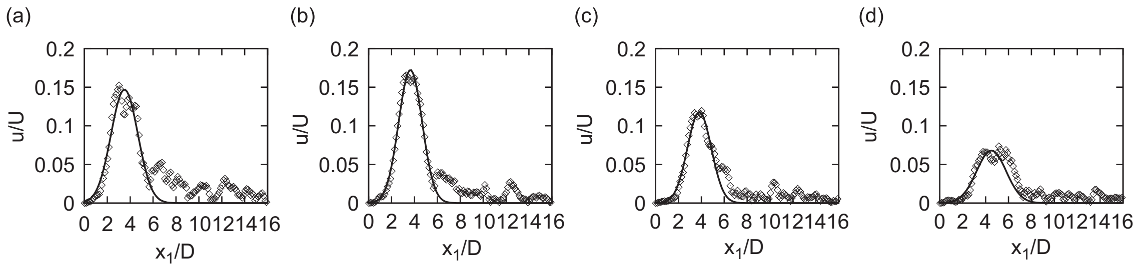

Fig. 14. Hilbert transform of the filtered streamwise velocity (symbols) and instantaneous Gaussian fits (full lines) at $tc_0/D=$ (a) 3.2, (b) 6.4, (c) 9.6 and (d) 12.8.

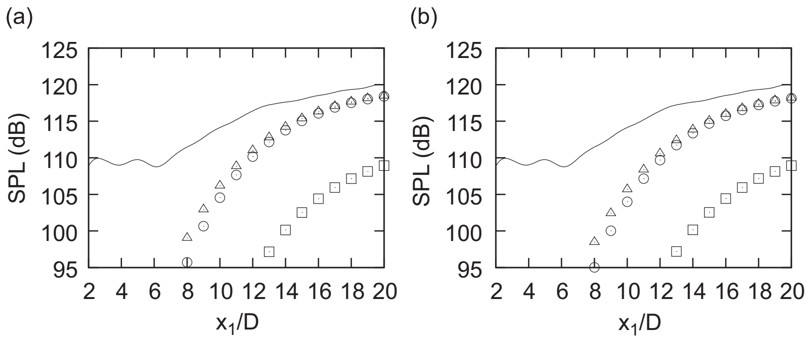

Fig. 15. Mode-0 sound pressure level for the LES (full lines) and model results (squares: average wave-packet; circles: instantaneous wave-packet, analytical; triangles: instantaneous wave-packet, numerical) with envelopes from (a) Hilbert transform and (b) Eq. (16).

features for low-angle sound production. Note that the SPL values of Fig. 15 are close to the OASPL values for mode 0 for low axial angles (Fig. 2), since the analysed frequency range of $0.3 \leq \mathrm{St} \leq 0.5$ contains the peak levels at low axial angles for this jet, and thus dominates the overall level.

The "average wave-packet" results are not so good, and this reflects the sensitivity of the sound radiation to temporal changes in the wave-packet envelope, again showing these to comprise important source parameters. This can be seen in the dependence of acoustic pressure on the envelope width $L(\tau)$, which is inside an exponential function in Eq. (15). The radiation is thus nonlinear with respect to the envelope width, and the average value of $L(\tau)$ does not give an average amplitude in the acoustic field.

5. Evaluation of intermittent bursts in a longer time series

The analysis in Section 3.2 was performed using a short time series of the simulation, corresponding to the flow events analysed earlier. In order to both confirm that similar events occur repeatedly, and to then further test the ability of the wave-packet *ansatz* to quantitatively capture the sound radiation, we consider a longer time series of $450D/c_0$. This time series is comparable with those frequently reported in the archival literature for LES [28–30].

We again apply the wavelet transform, as described in Section 3.2, to the azimuthal mode 0 of the acoustic pressure at $\theta = 30^{\circ}$ to the jet axis. The results are shown in Fig. 16, where we identify eight energy bursts, labelled A–H, in the acoustic field.

The application of the filter described in Section 3.2 to the axisymmetric mode of the acoustic pressure leads once more to a decimation of the sound field, as only the said energy concentrations of the scalogram are retained. The results are presented in Fig. 17. We notice that the A–H bursts of Fig. 16, which are also marked in Fig. 17(b), appear at low axial angles.

We have applied the same fitting procedure of Section 4 for the axisymmetric mode of the streamwise velocity component, and used the wave-packet parameters so obtained to calculate the radiated sound. The result (not shown) is very similar to that obtained for the shorter time-series, but with an improved agreement (1 dB discrepancy with the LES) at low axial angles. We thus confirm the pertinence of the analysis performed using the short time-series.

6. Conclusion

An analysis of data from a large eddy simulation is presented where temporal wavelet transforms are used, following a Fourier azimuthal decomposition, to filter each of the azimuthal modes of the sound field radiated by a subsonic jet.

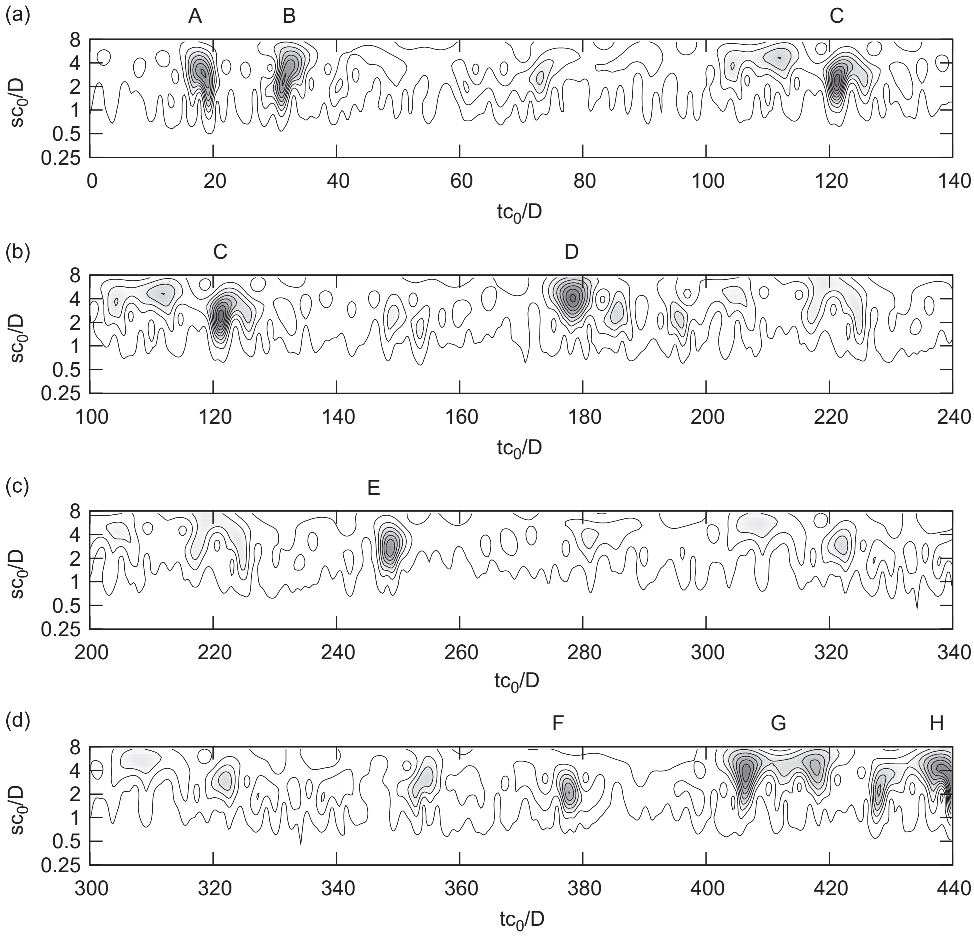

Fig. 16. Scalograms of the acoustic pressure at $\theta = 30^\circ$ for the long time series. Subfigures (a)–(d) refer to successive simulation intervals. Contours uniformly distributed between $10^{-5}\sigma^2$ and $5.1 \times 10^{-4}\sigma^2$ in intervals of $5 \times 10^{-5}\sigma^2$. Dark regions correspond to high values. Labels A–H mark identified acoustic energy bursts.

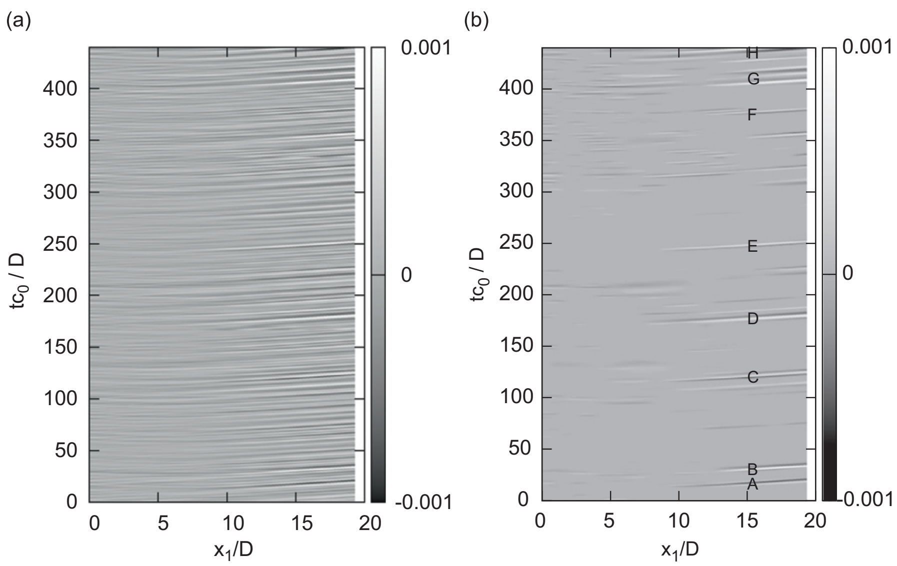

Fig. 17. Pressure at the acoustic field (azimuthal mode 0) at $r = 9D$ for the long time series: (a) original and (b) filtered.

The filtered fields are then studied with respect to the flow, which is also filtered using a wavelet decomposition. The results show the wavelet decomposition to be a useful tool for post-processing of data from such simulations, in so far as they can successfully isolate spatiotemporally localised events which are important for the production of sound, and which tend to be missed by more standard second-order analysis techniques.

The analysis reported in this paper shows how high-amplitude axisymmetric signatures observed in the acoustic field at low emission angles can be associated with the spatiotemporal modulation of the amplitude and axial extent of axisymmetric wave-packets in the flow. This modulation appears to be related to higher order modal activity at the end of the potential core. Quantitative agreement between the sound radiation computed by the LES and that computed using a wave-packet model which comprises space–time "jitter" such as observed in the data reinforces the proposed arguments. Wave-packet jitter is thus shown to comprise a salient source features where low-angle sound radiation is concerned.

Acknowledgements

This work was performed using HPC resources from GENCI- [CCRT/CINES/IDRIS] (Grant 2010- [x2010020912]). The present work is supported by CNPq, National Council of Scientific and Technological Development – Brazil.

Appendix A. Validation of the large eddy simulation

We present in this appendix some results of the validation of the LES used in the analysis of this paper. Fig. A1 presents the mean streamwise velocity, taken at the jet axis, compared to the experimental results of Jordan et al. [31] and Bridges [32]. The cited experiments present differences regarding the potential core length: Jordan et al. [31] present a potential core extending up to $x=7D$, and for Bridges [32] it extends up to $x=8D$. Both values are higher than the ones predicted by the empiric law derived for isothermal jets by Lau et al. [33] ($5.1D$ and $5.26D$, respectively), possibly due to differences in

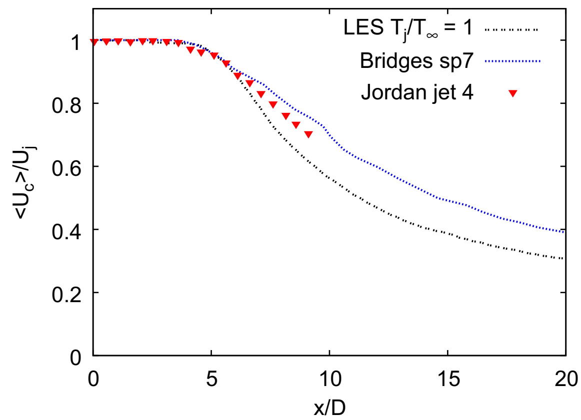

Fig. A1. Mean streamwise velocity along the jet axis.

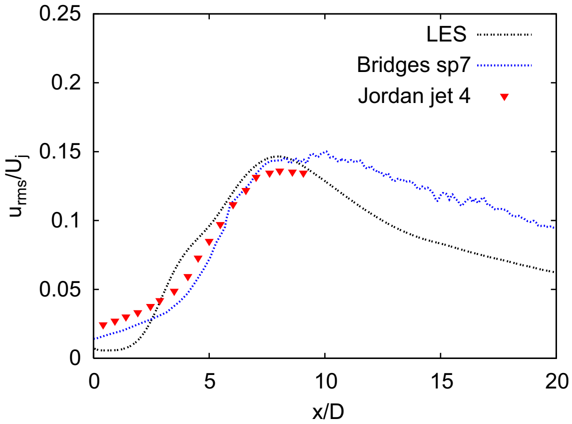

Fig. A2. RMS values of the streamwise velocity component.

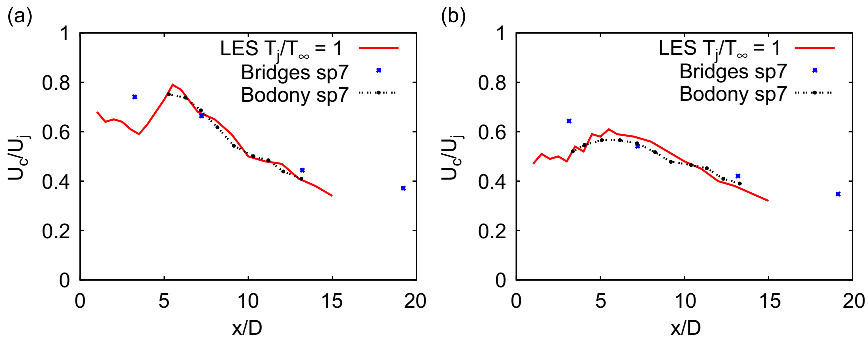

Fig. A3. Convection speed at (a) the jet centreline and (b) lipline.

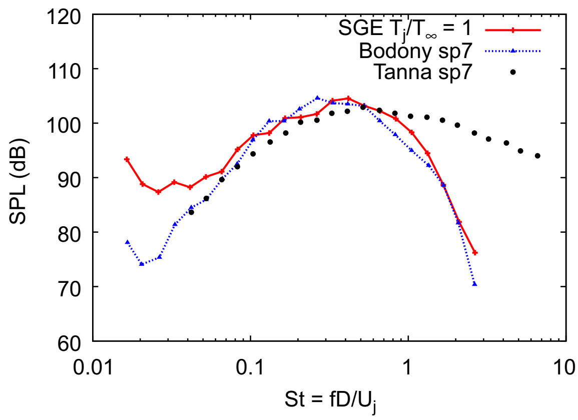

Fig. A4. 1/3-Octave spectra at 72D from the jet exit for $\theta = 45^\circ$.

the nozzle geometry and in the boundary layer conditions at the nozzle exit. To compare the different jets, we corrected all results hereafter in order to match Lau et al.'s law; this was done with an upstream or downstream shift of the origin of the coordinate system. As this correction is done, the profiles of mean streamwise velocity at the jet centreline present good agreement, as seen in Fig. A1.

In Fig. A2 we see comparisons of the rms values of the velocity with the results of Jordan et al. [31] and Bridges [32]. We note that for both components the initial conditions are not matched; thus the inflow excitation does not reproduce exactly the boundary layers in the nozzle of the experiments, which is expected since the present LES does not include the nozzle geometry. However, for the downstream points, and especially for the peak values, the rms values of the present calculation are close to the experimental ones.

Fig. A3 presents comparisons of the convection velocity, which is compared to both the experiment of Bridges [32] and to the LES of Bodony [29] at the jet axis (Fig. A3(a)) and the lipline (Fig. A3(b)). Close agreement is verified for both positions.

In Fig. A4 we see spectra in the far acoustic field for a point at 72D from the jet exit and at $\theta = 45^\circ$ from the jet downstream axis, compared to the experimental results of Tanna [34] and to the LES of Bodony [29] (Bodony and Lele [35]). We note that the present calculation agrees with the experimental results for Strouhal numbers ranging from 0.07 to 1. On the other hand, for lower frequencies the present calculation overestimates the sound. Since the experimental spectrum peak is well calculated by the present method, the present large eddy simulation is a model that represents sufficiently well the large-scale structures and its radiated sound for the Mach 0.9 jet. This spectrum peak is the focus of all the analysis in the present paper.

The spectra for both LES decrease in an abrupt manner for high frequencies if compared to the experimental data. This is due to the limitations in spatial discretisation of the domain of the LES, requiring the use of subgrid modelling.

References

[1] D. Juvé, M. Sunyach, G. Comte-Bellot, Intermittency of the noise emission in subsonic cold jets, *Journal of Sound and Vibration* 71 (1980) 319–332.

[2] G. Guj, M. Carley, R. Camussi, A. Ragni, Acoustic identification of coherent structures in a turbulent jet, *Journal of Sound and Vibration* 259 (5) (2003) 1037–1065.

[3] J.I. Hileman, B.S. Thurow, E.J. Caraballo, M. Samimy, Large-scale structure evolution and sound emission in high-speed jets: real-time visualization with simultaneous acoustic measurements, *Journal of Fluid Mechanics* 544 (2005) 277–307.
[4] A.V.G. Cavalieri, P. Jordan, Y. Gervais, M. Wei, J.B. Freund, Intermittent sound generation and its control in a free-shear flow, *Physics of Fluids* 22 (11) (2010) 115113.
[5] M. Wei, J.B. Freund, A noise-controlled free shear flow, *Journal of Fluid Mechanics* 546 (2006) 123–152.
[6] A.V.G. Cavalieri, P. Jordan, A. Agarwal, Y. Gervais, Jittering wave-packet models for subsonic jet noise, *AIAA Paper 2010-3957, 16th AIAA/CEAS Aeroacoustic Conference and Exhibit*, Stockholm, Sweden, 2010.
[7] M. Kœnig, A.V.G. Cavalieri, P. Jordan, J. Delville, Y. Gervais, D. Papamoschou, M. Samimy, S.K. Lele, Farfield pre-filtering for enhanced source-imaging in jets, *16th AIAA/CEAS Aeroacoustic Conference and Exhibit*, Stockholm, Sweden, 2010.
[8] G. Daviller, P. Jordan, P. Comte, Toward source analysis of turbulent coaxial jets in large-eddy simulation, *19 ème Congrès Francais de Mécanique*, Marseille, France, 2009.
[9] M. Lesieur, P. Comte, Favre filtering and macro-temperature in large-eddy simulations of compressible turbulence, *Comptes Rendus de l'Académie des Sciences* 329 (IIb) (2001) 363–368.
[10] F. Ducros, P. Comte, M. Lesieur, Large-eddy simulation of transition to turbulence in a boundary layer developing spatially over a flat plate, *Journal of Fluid Mechanics* 326 (1996) 1–36.
[11] D. Gottlieb, E. Turkel, Dissipative two-four method for time dependent problems, *Mathematics of Computation* 30 (136) (1976) 703–723.
[12] M. Hayder, E. Turkel, High-order accurate solutions of viscous problem, *AIAA Paper 93-3074*, 1993.
[13] G. Lodato, P. Domingo, L. Vervisch, Three-dimensional boundary conditions for direct and large-eddy simulation of compressible viscous flows, *Journal of Computational Physics* 227 (10) (2008) 5105–5143.
[14] T. Colonius, S.K. Lele, P. Moin, Boundary conditions for direct computation of aerodynamic sound generation, *AIAA Journal* 31 (1993) 1574–1582.
[15] C. Bogey, C. Bailly, Computation of high Reynolds number jet and its radiated noise using large eddy simulation based on explicit filtering, *Computers & Fluids* 35 (2006) 1344–1358.
[16] J.B. Freund, Noise sources in a low-Reynolds-number turbulent jet at Mach 0.9, *Journal of Fluid Mechanics* 438 (2001) 277–305.
[17] C. Bogey, C. Bailly, D. Juvé, Noise investigation of a high subsonic, moderate Reynolds number jet using a compressible LES, *Theoretical and Computational Fluid Dynamics* 16 (4) (2003) 273–297.
[18] C. Bogey, C. Bailly, Effect of inflow conditions and forcing on subsonic jet flows and noise, *AIAA Journal* 43 (5) (2005) 1000–1007.
[19] C.E. Tinney, P. Jordan, The near pressure field of co-axial subsonic jets, *Journal of Fluid Mechanics* 611 (2008) 175–204.
[20] S.K. Lele, Phased array models of shock-cell noise sources, *11th AIAA/CEAS Aeroacoustics Conference (26th Aeroacoustics Conference)*, 2005, pp. 1–20.
[21] S.C. Crow, Acoustic gain of a turbulent jet, *American Physical Society Meeting, Paper IE*, vol. 6, University of Colorado, Boulder, 1972.
[22] D.G. Crighton, Basic principles of aerodynamic noise generation, *Progress in Aerospace Sciences* 16 (1) (1975) 31–96.
[23] N.D. Sandham, C.L. Morfey, Z.W. Hu, Sound radiation from exponentially growing and decaying surface waves, *Journal of Sound and Vibration* 294 (1–2) (2006) 355–361.
[24] J. Kastner, M. Samimy, J. Hileman, J.B. Freund, Comparison of noise mechanisms in high and low Reynolds number high-speed jets, *AIAA Journal* 44 (10) (2006) 2251.
[25] M.J. Lighthill, On sound generated aerodynamically. I. General theory, *Proceedings of the Royal Society of London. Series A, Mathematical and Physical Sciences* (1952) 564–587.
[26] J. Bendat, A. Piersol, *Random Data: Analysis and Measurement Procedures*, Wiley-Interscience, 1986.
[27] G. Tadmor, D. Bissex, B. Noack, M. Morzynski, T. Colonius, K. Taira, Temporal-harmonic specific POD mode extraction, *4th AIAA Flow Control Conference*, Seattle, Washington, 2008.
[28] C. Bogey, C. Bailly, D. Juvé, Noise investigation of a high subsonic, moderate Reynolds number jet using a compressible large eddy simulation, *Theoretical and Computational Fluid Dynamics* 16 (4) (2003) 273–297.
[29] D.J. Bodony, Aeroacoustic Prediction of Turbulent Free Shear Flows, PhD Thesis, Stanford University, 2004.
[30] N. Andersson, L. Eriksson, L. Davidson, Investigation of an isothermal Mach 0.75 jet and its radiated sound using large-eddy simulation and Kirchhoff surface integration, *International Journal of Heat and Fluid Flow* 26 (3) (2005) 393–410.
[31] P. Jordan, Y. Gervais, J.-C. Valière, H. Foulon, Final result from single point measurement, Project Deliverable D3.4, JEAN-EU 5th framework program G4RD-CT2000-00313, Laboratoire d'Études Aérodynamiques, 2002.
[32] J. Bridges, Effect of heat on space-time correlations in jet, *12th AIAA Aeroacoustics Conference*, AIAA 2006-2534, 2006.
[33] J.C. Lau, P.J. Morris, M.J. Fisher, Measurements in subsonic and supersonic free jets using a laser velocimeter, *Journal of Fluid Mechanics* 93 (1979) 1–27.
[34] H. Tanna, An experimental study of jet noise, Part I: turbulent mixing noise; Part II: shock associated noise, *Journal of Sound and Vibration* 50 (1977) 405–444.
[35] D.J. Bodony, S.K. Lele, On using large-eddy simulation for the prediction of noise from cold and heated turbulent jets, *Physics of Fluids* 17 (2005) 085103.

Chapter IV

Intermittent wave-packet source models and radiated sound

The observations made using the simulations in chapters II and III, as well those of previous works in the literature, showed that bursts of acoustic radiation may be caused by intermittent changes in the pattern of convecting coherent structures.

This motivated the inclusion of jitter in a wave-packet source model in order to assess the effect of intermittent changes in the interference pattern created by neighbouring structures, and to verify if such changes can explain the bursts observed in the flow simulations presented in the previous chapters.

In what follows we present a reproduction of the journal article "Jittering wave-packet models for subsonic jet noise" [33], published in Journal of Sound and Vibration, 330(18-19):4474-4492, 2011.

Journal of Sound and Vibration 330 (2011) 4474–4492

Contents lists available at ScienceDirect

Journal of Sound and Vibration

journal homepage: www.elsevier.com/locate/jsvi

Jittering wave-packet models for subsonic jet noise

André V.G. Cavalieri [a,b,*], Peter Jordan [a], Anurag Agarwal [c,1], Yves Gervais [a]

[a] Département Fluides, Thermique, Combustion, Institut Pprime, CNRS – Université de Poitiers – ENSMA, UPR 3346, 43 route de l'Aérodrome, 86036 Poitiers, France
[b] Instituto Tecnológico de Aeronáutica, Praça Mal. Eduardo Gomes, 50, Vila das Acácias, 12228-900 São José dos Campos–SP, Brazil
[c] Institute of Sound and Vibration Research, University of Southampton, University Road, Southampton SO17 1BJ, UK

ARTICLE INFO

Article history:
Received 25 August 2010
Received in revised form
1 April 2011
Accepted 4 April 2011
Handling Editor: D. Juve
Available online 6 May 2011

ABSTRACT

Three simplified wave-packet models of the coherent structures in subsonic jets are presented. The models comprise convected wave-packets with time-dependent amplitudes and spatial extents. The dependence of the radiated sound on the temporal variations of the amplitude and spatial extent of the modulations are studied separately in the first two model problems, being considered together in the third. Analytical expressions for the radiated sound pressure are obtained for the first and third models.

Results show that temporally localised changes in the wave-packet can lead to radiation patterns which are directional and which comprise high-amplitude bursts; such intermittency is observed in subsonic jets at the end of the potential core, and so the models may help explain the higher noise levels and intermittent character of the sound radiated to low emission angles for subsonic jets. By means of an efficiency metric, relating the radiated acoustic power to the fluctuation energy of the source, we show that the source becomes more powerful as its temporal localisation is increased. This result extends that of Sandham et al. (Journal of Sound and Vibration 294(1) (2006) 355–361) who found similar behaviour for an infinitely extended wavy-wall.

The pertinence of the model is assessed using two sets of data for a Mach 0.9 jet. One corresponds to a direct numerical simulation (DNS) of a Reynolds number 3600 turbulent jet and the other to a large eddy simulation (LES) of a Reynolds number 4×10^5 jet. Both time-averaged and time-dependent amplitudes and spatial extents are extracted from the velocity field of the numerical data. Computing the sound field generated by the wave-packet models we find for both simulations that while the wave-packet with a time-averaged envelope shows discrepancies of more than an order of magnitude with the sound field, when the wave-packet 'jitters' in a way similar to the intermittency displayed by the simulations, we obtain agreement to within 1.5 dB at low axial angles. This shows that the 'jitter' of the wave-packet is a salient source feature, and one which should be modelled explicitly.

1. Introduction

Estimation of the sound radiation from a turbulent flow, using an acoustic analogy, requires the solution of a propagation equation, assuming some given form for a corresponding source term. This form must be such that the sound

* Corresponding author at: Institut Pprime, CNRS – Université de Poitiers – ENSMA, UPR 3346, 43 route de l'Aérodrome, 86036 Poitiers, France. Tel.: +33549453820; fax: +33549453663.
E-mail address: andre.cavalieri@univ-poitiers.fr (A.V.G. Cavalieri).
[1] Current address: Department of Engineering, University of Cambridge, Trumpington Street, Cambridge CB2 1PZ, UK.

0022-460X/$ - see front matter
doi:10.1016/j.jsv.2011.04.007

producing kinematic structure of the turbulence is approximated in a physically pertinent manner. When Lighthill first provided us with a theoretical foundation from which to model, study and understand jet noise, turbulence, both generally and in the specific case of the round jet, was considered to comprise a space–time chaos, devoid of any underlying order. The standard at that time for the kinematic description of turbulence structure could be found in turbulence theories such as that of Batchelor [1]: Attempts to understand and model turbulence were based on the Reynolds averaged Navier–Stokes equations, where the only conceptual constructs invoked, aside from those expressed in the conservation equations, are those required for closure (Boussinesq's notion of eddy viscosity, for instance) on one hand, and, on the other, the flow entities supposed to participate in the physical process associated with the various terms that appear in the RANS equations: fluctuation energy is 'produced', 'transported', 'dissipated' by virtue of interactions between stochastic flow 'scales' or 'eddies'. Source terms in acoustic analogies were constructed in accordance with this conceptual picture of turbulence. Lighthill assumed a statistical distribution of uncorrelated eddies throughout the source region; and this led to the well known U^8 power law for an isothermal turbulent jet [2].

However, predictions based on Lighthill's analogy, using such kinematical models for the turbulence, do not explain all of the features of subsonic jet noise: at low emission angles (with respect to the downstream jet axis) the U^8 power law does not hold for example, and the narrower spectral shape is generally not well predicted. This of course does not necessarily imply that there is anything wrong with the acoustic analogy as a theoretical framework for jet noise, as is sometimes suggested in the literature. It simply means that the models used for the source and propagator have not been adequately appropriated to the physical mechanisms which are at work in a turbulent jet.

An acoustic analogy constitutes an exact rearrangement of the fluid mechanics equations. If a flow solution is known exactly, an accurate calculation of the sound field can be obtained, regardless of the source–propagator split. This has been demonstrated by means of direct numerical simulation (hereafter DNS). Colonius et al. [3], for instance, calculated sound generation by a mixing layer using Lilley's analogy, Freund [4] used Lighthill's analogy to determine the acoustic field of a Mach 0.9 jet. More recently both Samanta et al. [5] and Sinayoko et al. [6] have used Goldstein's [7] generalisation of the acoustic analogy to explore other source–propagator splits. In all cases the correct sound field can be retrieved.

However, despite the possibility of accurate calculation of the acoustic fields, the source terms obtained from DNS have not, to date, clearly revealed which features of a turbulent jet underpin the production of sound. It is therefore not clear how the turbulence of a jet should be manipulated and modified in order to reduce noise. Some broad guidelines can of course be provided. The solution of an acoustic analogy will place the far-field sound energy in relation to certain turbulence quantities, such as the mean velocity field, the integral space- and time-scales, convection velocities, etc. And we thereby have an indication of how changes in these turbulence quantities will impact the radiated sound power. But we do not currently have tools capable of clarifying what kind of actuation, or design modification, will lead to a desired change in such time-averaged quantities; the space- and time-local physical processes which underpin these statistical measures are not clearly understood, and so we are generally obliged to operate on a trial and error basis. The evolution of fluid mechanics, and aeroacoustics, will see the implementation of real-time, closed-loop control; and the aforesaid time-averaged quantities will be of little use in this context. It will be necessary to directly model, both kinematically and dynamically, the space- and time-local characteristics of flow events which generate sound. This paper, and others by the first two authors, are motivated by this necessity.

Efforts to understand and model the space- and time-local behaviour of turbulence would be in vain were it not for the underlying order which is now known to exist in most turbulent flows: soon after the first attempts by Lighthill and his successors to predict the sound radiated by turbulent jets a change occurred in the way turbulence is perceived. Turbulent flows were observed to be more ordered than had previously been believed, and a new conceptual flow entity was born, sometimes referred to as a 'coherent structure', or, alternatively, a 'wave-packet'. Mollo-Christensen was one of the first to report such order in the case of the round jet: '…although the velocity signal is random, one should expect to see intermittently a rather regular spatial structure in the shear layer' [8]. A series of papers followed, confirming these observations and postulating on the nature of this order ([9–11] to cite just a few). Stability theory was evoked as a possible theoretical framework for the modelling of such flow behaviour, and kinematical and/or dynamical models for coherent structures, based on ideas derived from stability theory, can be found, for instance, in the works of Michalke [12,13], Crow [14], Crigthon and Gaster [15], Tam and Morris [16], Mankbadi and Liu [17] and Crighton and Huerre [18]: coherent turbulent structures are modelled by means of a hydrodynamic stability analysis of the mean flow; for slowly spreading mean flows solutions comprise waves which amplify spatially and then decay. From the point of view of sound production, the salient features of such flow organisation, as identified by the said modelling efforts, are the process of amplification and decay, and the high level of axial coherence, which makes of these structures a non-compact, 'semi-infinite antenna for sound' [8]. This *spatial modulation* can help to explain, for instance, the results of Laufer and Yen [19], whose excited low Mach number jet showed *superdirective* radiation.

A further feature of the unsteadiness associated with the orderly part of a turbulent jet is its intermittency. The above citation from Mollo-Christensen recognises this. Crow and Champagne observed, by means of flow visualisation, the appearance of a train of coherent 'puffs' of turbulence. These were characterised by an average Strouhal number of 0.3, but the authors noted how 'three or four puffs form and induct themselves downstream, an interval of confused flow ensues, several more puffs form, and so on'. Further experimental evidence of this kind of intermittency can be found in the work of Broze and Hussain [20], who observed that even when a forcing at St=0.4 is applied at the nozzle exit, significant jitter remains in the flow velocity signature.

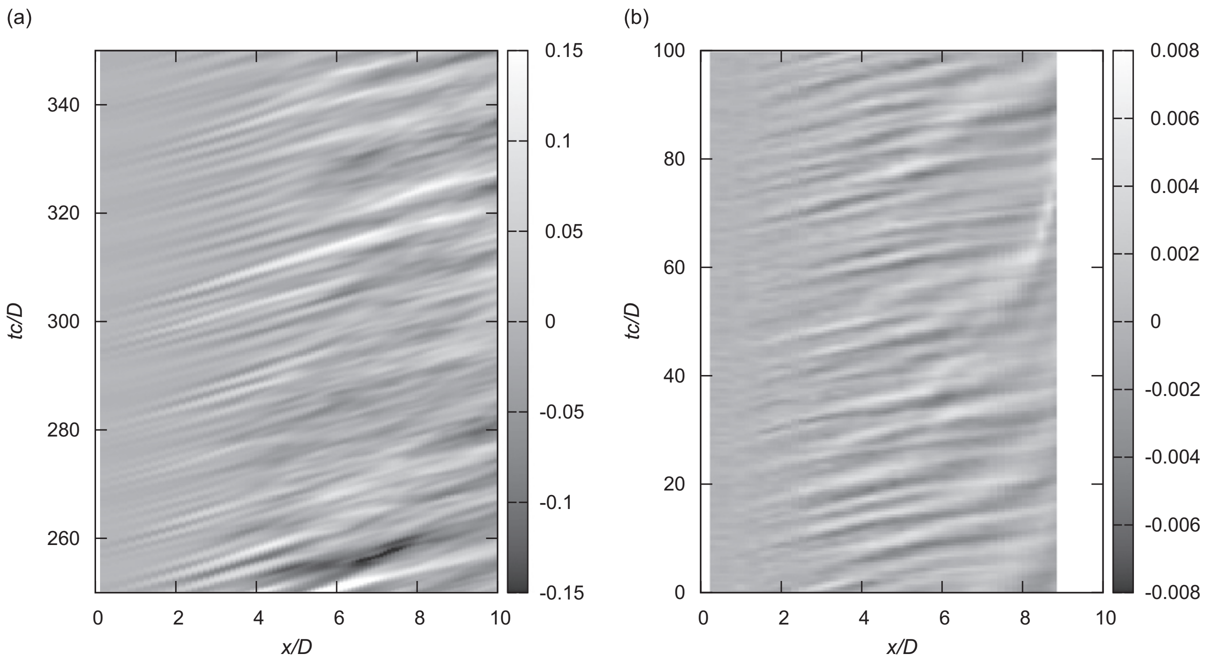

Fig. 1. Jittering wave-packets in numerical and experimental subsonic jet data: (a) azimuthal mean of the streamwise velocity in the lipline of a jet DNS [21] and (b) near pressure field of a coaxial jet [22].

An illustration of the space–time flow structure that we here loosely qualify as a jittering wave-packet is provided in Figs. 1(a) and (b). We see in Fig. 1(a) a space–time plot of the azimuthal mean of the streamwise component of the velocity, taken from the Mach 0.9 jet DNS of Freund [21]. A pattern of convected waves is observed from $x \approx D$ to $x \approx 6D$. These are characterised by some average frequency, but they undergo a modulation which is both spatial and temporal: the maximum amplitude of the wave changes in time, as does the position where it breaks down.

It is more difficult to access such information experimentally, as PIV systems do not currently provide sufficient temporal resolution. However, the near-field pressure contains the footprint of evanescent waves generated by convected hydrodynamic coherent structures, and nearfield microphone arrays (such as used by Picard and Delville [23], Suzuki and Colonius [24], Tinney and Jordan [22], Reba et al. [25]) can be used to measure this footprint. Fig. 1(b) shows the near pressure field of a coaxial jet measured by Tinney and Jordan [22]. A similar space–time structure to that observed in Fig. 1(a) DNS is observed.[2]

The analysis and/or calculation of sound radiation by such spatio-temporal structure can be performed in the frequency domain. The flow quantities are Fourier transformed in time, and the calculations are performed separately for each frequency component, which is periodic by definition and therefore cannot represent temporal jitter; the signature of jittering events is in this case spread across a range of frequencies. This approach is chosen, for instance, by Morris [26] and Reba et al. [25] and is perfectly adequate for the evaluation of source models and for sound prediction.

If, on the other hand, we are interested in determining the instantaneous features of a jet that generate sound (which closed-loop controllers will be required to manipulate in order to reduce noise), with a view to understanding flow mechanisms and thence constructing more sophisticated models, an analysis in the time domain can be advantageous, for it is no longer necessary to project the flow data onto infinitely extended basis functions. Such an approach proved useful in the analysis by Cavalieri et al. [27] of the noise-controlled mixing layers of Wei and Freund [28]. The noise reduction in the controlled flow was seen to be caused by a temporally localised action of the control; this prevented a space–time localised flow event and an associated space–time localised energy burst in the acoustic field. A number of other studies can be cited where time-domain analysis allowed a provision of insight which would not have been possible using spectral analysis: experimental studies include those of Juvé et al. [29], Guj et al. [30], Hileman et al. [31] and Kœnig et al. [32] for example; numerical examples can be found in the work of Kastner et al. [33] and Bogey and Bailly [34]. Fig. 2 shows a scalogram taken from Kœnig et al., where time-local high-amplitude energy bursts in the acoustic field at 30° can be seen at $t \approx 0.323$, 0.338, and 0.392 s.

In addition, therefore, to the *spatial modulation* evoked earlier, the ordered part of a turbulent jet is seen to comprise *temporal modulation*, or 'jitter'. The only works, to the best of our knowledge, where such behaviour has been explicitly

[2] It is worth pointing out that the Reynolds number of the DNS is 3600, while that of the experiment is 5×10^6!

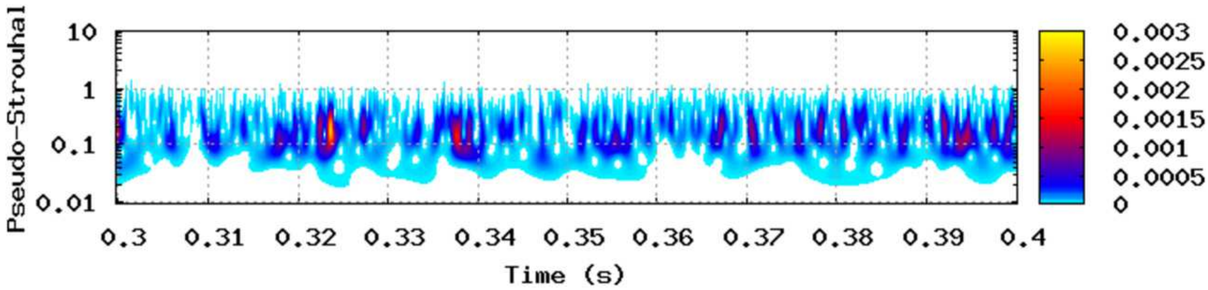

Fig. 2. Scalogram of the far-field pressure of a Mach 0.9 jet at 30° from the jet axis. Taken from Kœnig et al. [32].

modelled, are those of Ffowcs Williams and Kempton [35] and Sandham et al. [36]. In the present work we wish to evaluate how space–time modulation such as that shown in Figs. 1(a) and (b) impacts the radiated sound field (Fig. 2). We follow the ideas of Ffowcs Williams and Kempton [35], who introduced some jitter in the phase speed of a convected wave, but maintained a fixed envelope function. Our contribution is in the evaluation of the effect of temporal variations of this envelope function, which are observable in Figs. 1(a) and (b). We propose three source models whose basic form is that of a convected instability wave, but one which undergoes modulation in both space and time; in this sense, our model includes both the characteristics of Crow's [14] and Sandham et al.'s [36] models.

In order to validate our models we have chosen to use Lighthill's acoustic analogy [2]. The simplicity of this analogy, compared for instance with those of Lilley [37] or Goldstein [7], means that we are able to obtain most of the results analytically, and this permits a comprehensive exploration of the parameter space of the jittering wave-packet models. Furthermore, the availability of an analytical time domain Green's function for Lighthill's analogy means that the effect of intermittent temporal variations can be obtained without the application of a Fourier transform, which might mask the intermittent bursts, as it did in the case of Wei and Freund's optimal controlled mixing-layer, by spreading their signature over a large frequency range [28,27].

The work we pursue here is, largely, an exercise in system reduction. We are interested in the simplest possible representation of the jet, as a source of sound, but which provides an acceptably accurate prediction of the radiated sound field. This raises the question of *optimal source description* and *robustness* of the formulation used to describe the sound generation process; these two issues are closely related.

The question of the robustness of acoustic analogies is an interesting one, that has been addressed by Samanta et al. [5] in an *ad hoc* manner. The solutions of different acoustic analogies are calculated for the same direct numerical simulation of a two-dimensional mixing layer. The sound fields computed by all analogies show good agreement with the DNS. The flow fields are then artificially modified so as to introduce errors in the source $\mathbf{q}$; this is done through a manipulation of the coefficients of POD modes of the full solution. Errors result in the calculation of the radiated sound; for most cases similar errors are obtained for the different formulations, but for one of the cases (division of the first POD mode coefficient by 2) Lighthill's analogy presents greater errors than the other formulations for the sound radiation in the upstream direction.

The problem can be thought of as follows. Consider the integral solution of an acoustic analogy, written in the general form $\mathcal{L}\mathbf{q} = p$. The parameter space of the source $\mathbf{q}$ is expressed in terms of an orthonormal basis and possesses an inner product; such is the case, for instance, for the POD basis of Samanta et al. If we now consider the eventual impact of the introduction of a small disturbance (modification) to the source, $\delta\mathbf{q}$ (as done by Samanta et al. for a number of different analogies), we are interested in the impact that this will have on the acoustic field, i.e. δp. The problem comes down to the following situation: if $\delta\mathbf{q} \parallel \nabla\mathcal{L}$ then the sound field will be sensitive to small perturbations in the source, $\delta\mathbf{q}$. $\delta\mathbf{q}$ is in this case aligned with the direction of maximum sensitivity of the operator $\mathcal{L}$ in the parameter space considered. If, on the other hand, $\delta\mathbf{q} \perp \nabla\mathcal{L}$, then changes in $\mathbf{q}$ will have no impact on the sound field, p.

This shows that the arbitrary introduction of disturbances to, and subsequent comparison of, two different analogies cannot provide an unambiguous assessment, in an absolute sense, of the relative robustness of the two formulations. For, if the gradients $\nabla\mathcal{L}_1$ and ∇L_2 have different directions in the parameter space, one will always be able to find a perturbation which causes one operator to appear less robust than the other. This shows that, while the study of Samanta et al. is of considerable interest as a first step in addressing this question of the robustness of acoustic analogies, it does not allow a conclusive evaluation in this regard; the said authors recognise that the conclusions of their work are particular to the studied flow and to the proposed disturbances.

The approach that we follow in the present paper amounts to an *ad hoc*, physics-based, filtering (or system reduction) of flow data such that directions in the source parameter space that are irrelevant for the peak sound radiation at low emission angles are removed. The system reduction is achieved in a number of ways. For example, by means of reasoning based on the source compactness we choose to suppress the radial dimension of the jet—this choice is associated with the Lighthill formulation of the problem; the choice of a convected wave *ansatz*, on the other hand, is based on observation (by us and past researchers), as is the wave-packet 'jitter'. The success of the jittering wave-packet *ansatz* in reproducing the low angle radiation indicates that we have identified a robust source representation for the operator that we consider.

The paper is organised as follows. In Section 2 we obtain an analytical solution for the sound radiation of a wave-packet whose spatial and temporal modulations are given by Gaussian functions; Section 3 presents numerical results for a source model based on the reduction of the spatial extent of modulation during a certain period of time. Finally, we obtain in Section 4 an analytical expression for a wave-packet whose amplitude and spatial extent both change slowly with time, and a comparison of the model results with DNS (Freund [21]) and LES data (Daviller [38]; see also Cavalieri et al. [39]) is presented in Section 5.

We see that the intermittent wave-packet can produce directive sound radiation, such as is observed in jets. We furthermore show how intermittency increases the radiated power for a given fixed source fluctuation level. We then use velocity data extracted from the DNS and the LES to compare the sound radiation of two wave-packets: one whose amplitude and spatial extent is time-averaged and a second where the same quantities 'jitter' in the same way as velocity data taken from the simulations. The time-averaged wave-packet shows a discrepancy of more than an order of magnitude when compared with the DNS and the LES, while the 'jittering' wave-packet agrees to within 1.5 dB for downstream radiation. This illustrates how the 'jittering' of the 'coherent structures' of the flow is a salient source feature, and it suggests that, where simplified modelling strategies are concerned, an effort should be made to model this source parameter explicitly.

Finally, the role played by such wave-packet jitter in a supersonic scenario is assessed in Appendix C. We find that, while it is a salient feature for convectively subsonic flows, when the convective Mach number is greater than one the jitter ceases to be so important, as would be expected from an analysis in the frequency–wavenumber space.

2. Temporally localised amplitude change of a wave-packet

In Lighthill's analogy, the acoustic field is given, for a three-dimensional flow, as

$$p(\mathbf{x},t) = \frac{1}{4\pi}\iiint\left[\frac{1}{|\mathbf{x}-\mathbf{y}|}\frac{\partial^2 T_{ij}}{\partial y_i \partial y_j}(\mathbf{y},\tau)\right]_{\tau = t-|\mathbf{x}-\mathbf{y}|/c} \mathrm{d}\mathbf{y}, \tag{1}$$

where T_{ij} is Lighthill's stress tensor. We wish to write down as simple an expression as possible to model the source term, but one which is capable of reproducing some of the features of jet noise at shallow angles to the jet axis. Thus we model T_{ij} only with the T_{11} term since it can be shown [40] that the radiation in the far field comes only from the component of Lighthill's tensor which is aligned with the radiation direction; at low axial angles we expect the efficiency of T_{11} to be higher than the other components of the tensor. We present nonetheless the results of our model for higher angles. Although these results will probably be in this case an underestimation of the radiated sound, the present results can be superposed with appropriate models using the other components of Lighthill's stress tensor to yield the radiated sound field at higher axial angles.

Furthermore, we only use the part of T_{11} that is linear in the velocity fluctuations. This choice is based on results of the analysis by Freund [4] and Bodony and Lele [41], who have performed full propagations of the Lighthill source terms based on a DNS and LES calculations, respectively. Their work showed that for the radiation of unheated Mach 0.9 and Mach 2 jets the linear term dominates at the peak frequencies at low angles. For instance, in Freund's calculation the contribution of the linear term at St$=$0.2 at an angle of 30° is 10 dB higher than that of the quadratic term.

The linear term is sometimes argued to correspond to *propagation* effects, whereby the mean-flow convects and refracts *acoustic* perturbations, rather than to sound generation. However, in our view the physical meaning of these linear terms remains an open question. For example, in terms of incompressible turbulence mechanisms, the hydrodynamic pressure fluctuations can be obtained by means of a Poisson equation, the linear components of whose source term dominate the peak region of the *turbulence* pressure spectrum [42]; in this situation these linear terms clearly have nothing to do with flow-acoustic interaction. Additionally, since an acoustic analogy is based, as discussed in the introduction, on the splitting of the equations into a base flow and superimposed disturbances, interpretation of the different terms in the equations depends on the analogy which is used. In a recent study, Sinayoko et al. [6] compared the source terms and solutions corresponding to two acoustic analogy formulations, one comprising a *non-radiating* unsteady base flow and another a time-averaged base flow. In the former case the solution is purely acoustic, whereas in the latter the solution, which contains linear terms of the kind considered in this paper, is dominated by hydrodynamics.

We therefore here consider the linear part of T_{11}, which the aforesaid study shows to be predominantly hydrodynamic, without delving further into its physical meaning. Furthermore, recent studies by Freund [4] and Bodony and Lele [41] show how this term dominates low-angle radiation at peak frequencies. The present theoretical developments remain nonetheless extensible to source terms which are nonlinear in the velocity fluctuations, as the basic functional forms will remain the same.

To evaluate the effect of temporal amplitude changes, we define a wave-packet which is localised in time, with amplitude A given by

$$A(\tau) = \mathrm{e}^{-\tau^2/\tau_c^2}. \tag{2}$$

We model T_{11} by

$$T_{11}(\mathbf{y},\tau) = 2\rho_0 U\tilde{u}\,\frac{\pi D^2}{4}\,\delta(y_2)\delta(y_3)\mathrm{e}^{\mathrm{i}(\omega\tau - k y_1)}\mathrm{e}^{-y_1^2/L^2}\mathrm{e}^{-\tau^2/\tau_c^2}, \tag{3}$$

where ρ_0 is the density of the undisturbed fluid, U is the jet velocity, $\tilde{u}$ is the maximum amplitude of velocity fluctuations in the wave-packet, D is the jet diameter and $\delta(\,)$ represents the Dirac delta distribution. The convection is represented by the frequency ω and the wavenumber k, with the convection velocity calculated as ω/k. This convected wave is modulated both in space and time; the envelopes are two Gaussian functions, and the amplitude modulation is defined by the spatial and temporal parameters L and τ_c. This expression is similar to that used by Lele [43] for modelling shock-cell noise sources in supersonic jets, although in that work a slightly different version of the source, without the double derivative, was used.

We use a complex-valued expression for T_{11} in the present work; it is implied in the following that the real part of the radiated pressure should be considered. Furthermore, the volume distribution of T_{11} is simplified by its concentration on a line, which can be seen by the two δ distributions in Eq. (3). This simplification can be justified if the source is compact in the radial direction; Appendix A provides a more detailed justification of this simplification.

Samples of the spatial and temporal variation of T_{11} are shown in Fig. 3. For both L and τ_c tending to infinity, the T_{11} component of Lighthill's stress tensor in Eq. (3) models a purely convected wave, as shown in Fig. 3(a). With τ_c tending to infinity, and for a finite value of L, we get a wave-packet that is periodic in time (Fig. 3(b)); this corresponds to Crow's [14] model. If we have finite values for both L and τ_c, the model represents a wave-packet that is localised in time, as shown in Fig. 3(c). Finally, if both L and τ_c are small, compared, respectively, to the convected wavelength and period, our model represents a small isolated turbulent event (Fig. 3(d)).

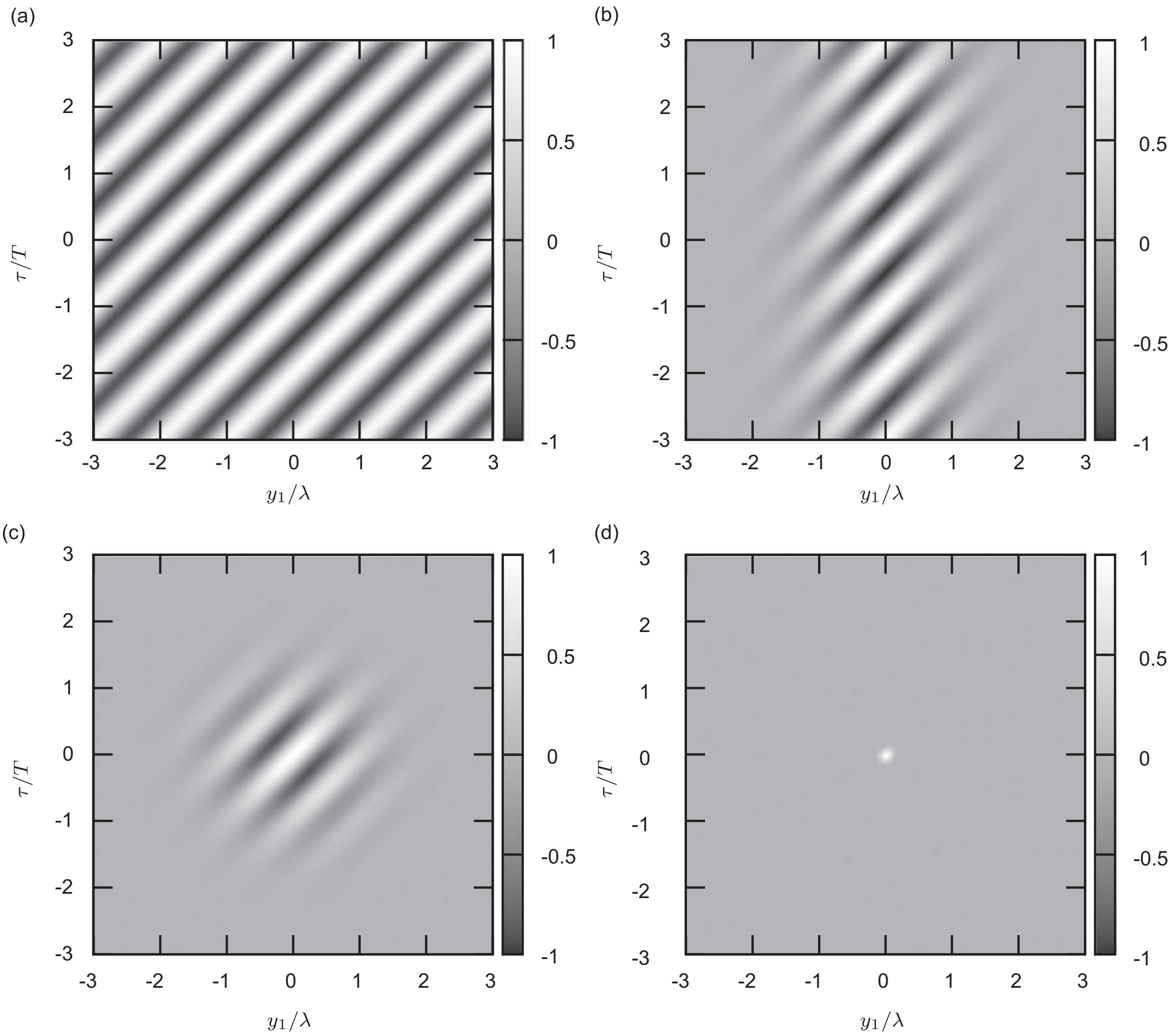

Fig. 3. Sample T_{11} distributions: (a) $L/\lambda \to \infty$, $\tau_c/T \to \infty$, (b) $L/\lambda = 1$, $\tau_c/T \to \infty$, (c) $L/\lambda = 1$, $\tau_c/T = 1$ and (d) $L/\lambda = 0.1$, $\tau_c/T = 0.1$.

Inserting Eq. (3) into Eq. (1) and making a far-field assumption gives us

$$p(\mathbf{x},t) = \frac{\rho_0 U\tilde{u}D^2\cos^2\theta}{8c^2|\mathbf{x}|}\frac{\partial^2}{\partial t^2}\left\{ e^{i\omega(t-|\mathbf{x}|/c)-(t-|\mathbf{x}|/c)^2/\tau_c^2}\int_{-\infty}^{\infty} f(y_1)\,dy_1 \right\}, \tag{4}$$

with

$$f(y_1) = e^{i(\omega y_1\cos\theta/c - ky_1)}e^{-y_1^2/L^2-(y_1\cos\theta)^2/c^2\tau_c^2}e^{-2y_1\cos\theta(t-|\mathbf{x}|/c)/c\tau_c^2}, \tag{5}$$

where c is the speed of sound in the undisturbed fluid and θ is the angle of $\mathbf{x}$ to the jet axis.

The calculation of the integral of Eq. (5) leads to an analytical expression for the pressure in the far field:

$$p(\mathbf{x},t) = PQe^{i\omega t_r - t_r^2/\tau_c^2 - L^2/4\tau_c^2\gamma^2[(ck-\omega\cos\theta)\tau_c^2-2it_r\cos\theta]^2}, \tag{6}$$

with

$$t_r = t - \frac{|\mathbf{x}|}{c}, \tag{7}$$

$$P = \frac{\rho_0 U\tilde{u}D^2\tau_c cL\sqrt{\pi}\cos^2\theta}{4c^2|\mathbf{x}|\gamma} \tag{8}$$

$$Q = \left\{ \left[i\omega - 2\frac{t_r}{\tau_c^2} + \frac{iL^2\cos\theta}{\tau_c^2\gamma^2}[(ck-\omega\cos\theta)\tau_c^2 - 2it_r\cos\theta] \right]^2 - \frac{2c^2}{\gamma^2} \right\} \tag{9}$$

and

$$\gamma = \sqrt{\tau_c^2c^2 + L^2\cos^2\theta}. \tag{10}$$

If we calculate the limit with $\tau_c \to \infty$ to Eqs. (6)–(10), we will have

$$\gamma \to \tau_c c \tag{11}$$

and

$$P \to \frac{\rho_0 U\tilde{u}D^2L\sqrt{\pi}\cos^2\theta}{4c^2|\mathbf{x}|}, \tag{12}$$

which, after substitution in Eq. (6), leads as expected to a result that corresponds to Crow's [14] (see also Crighton [40]) model,

$$p(\mathbf{x},t) = -\frac{\rho_0 U\tilde{u}M_c^2(kD)^2L\sqrt{\pi}\cos^2\theta}{8|\mathbf{x}|}e^{-L^2k^2(1-M_c\cos\theta)^2/4}e^{i\omega(t-|\mathbf{x}|/c)}, \tag{13}$$

where M_c is the convective Mach number given by $\omega/(kc)$.

The analytical expression of Eqs. (6)–(10) is compared to a numerical evaluation of Eq. (1), obtained by numerical integration of the analytical derivative of T_{11} at the exact value of the retarded time. Sample calculations were made for a jet Mach number equal to 0.9, where the phase speed of the convected wave was taken as $0.6U$ and the maximal amplitude of velocity fluctuation, $\tilde{u}$, as $0.1U$. The frequency f was chosen so as to correspond to a Strouhal number $\mathrm{St}=0.3$, where $\mathrm{St}=fD/U$. The temporal variation of the pressure at a point at $R=100D$ and $\theta=30$ is shown in Fig. 4, and the directivity at $R=100D$ is shown in Fig. 5. Very close agreement is found between the analytical and numerical results.

Figs. 4 and 5 show the general trends of the intermittency effect in sound radiation by a temporally localised wave-packet: as τ_c is decreased, which means that the source fluctuation energy is concentrated in a smaller time interval, the sound radiation also becomes concentrated in a similar interval, but presents higher intensity peaks, as shown in Fig. 4. The increase of sound radiation occurs at all angles, as shown in Fig. 5, and as τ_c decreases, the radiation pattern approaches that of an axial quadrupole. We see also in Figs. 5(a) and (b) that for moderate temporal modulations a directive behaviour, similar to Crow's model [14], is obtained.

To quantitatively evaluate how intermittency increases the sound radiation by the turbulent structures, we define an efficiency ratio based on the radiated acoustic energy, given by

$$E_A = \int_0^{\infty}\int_{\Omega}\frac{p^2}{\rho_0 c}\,dS(\mathbf{x})\,dt, \tag{14}$$

with the surface integral calculated over a spherical surface Ω in the far field, and the turbulent kinetic energy, or 'source' energy, given by

$$E_S = \frac{1}{T}\int_0^{\infty}\int_{V_S}\frac{\rho_0 u^2}{2}\,d\mathbf{y}\,d\tau, \tag{15}$$

where the volume integral is over the source region V_S.

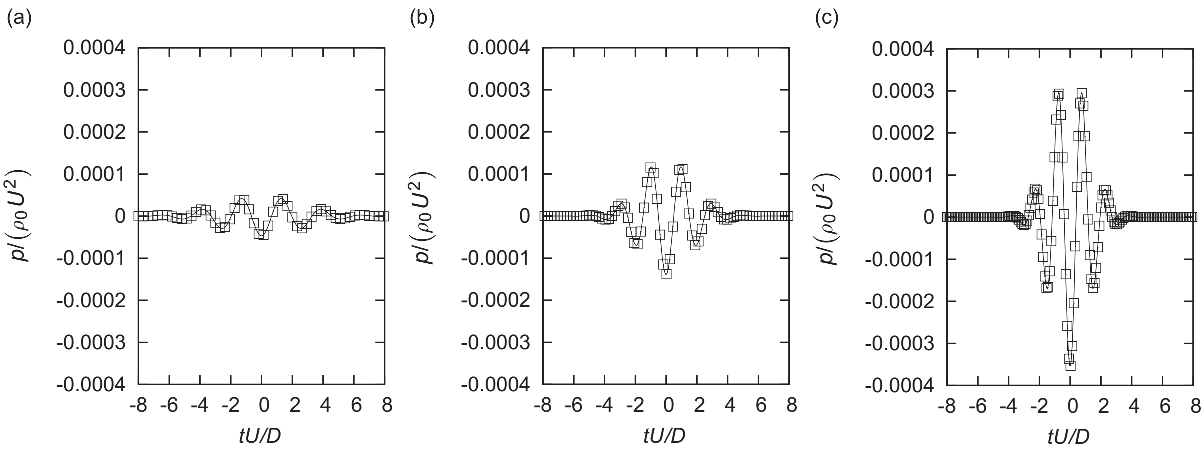

Fig. 4. Far-field pressure for $\theta=30^\circ$ and $L/\lambda=1$, with: (a) $\tau_c/T=1$, (b) $\tau_c/T=0.5$ and (c) $\tau_c/T=0.2$. Lines show analytical results, and symbols show numerical computations.

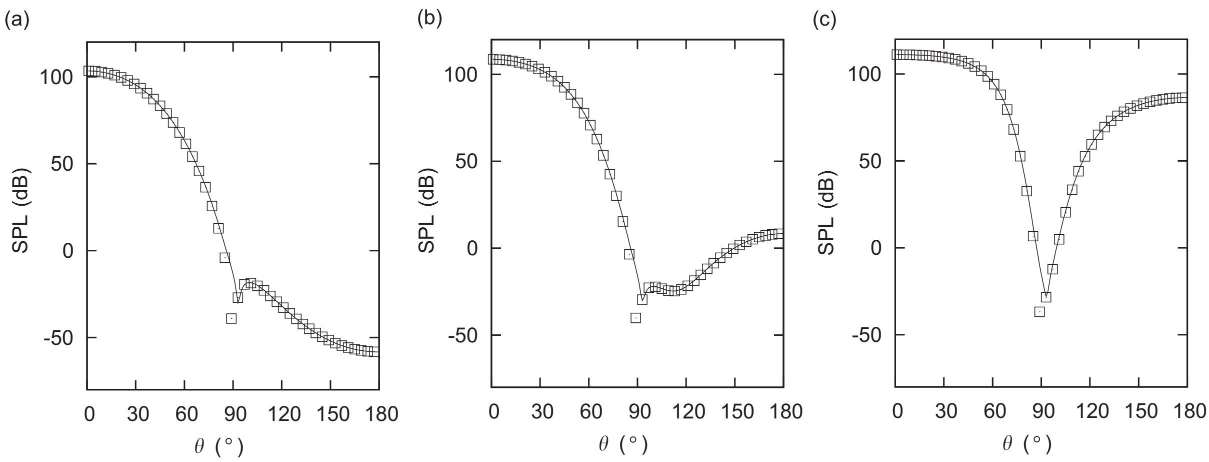

Fig. 5. Directivity for $L/\lambda=1$, with: (a) $\tau_c/T=1$, (b) $\tau_c/T=0.5$ and (c) $\tau_c/T=0.2$. Decibel scale referenced to $(2\times10^{-5}\ \mathrm{Pa})/(\rho_0U^2)$. Lines show analytical results, and symbols show numerical computations.

The efficiency ratio E_A/E_S measures the amount of source fluctuation energy that 'escapes' to the far acoustic field as sound. Figs. 6(a)–(c) show the efficiency ratio for wave-packets at $M=0.3$, 0.6, and 0.9, respectively, for several values of L and τ_c. In Fig. 6(c) we see that at $M=0.9$, for a given spatial modulation, that is, for a fixed L, a localisation in time (decrease in τ_c) increases the efficiency of the source, especially for low spatial growth rates ($L/\lambda>1$)—note that the contour levels are logarithmic. The same is also true for the $M=0.3$ and 0.6 wave-packets; however, the intermittency effect is less pronounced, as seen in Figs. 6(a) and (b). These observations agree with the results of Sandham et al. [36], who showed that for a wavy wall problem, extended infinitely in space ($L\to\infty$ in our model), rapid time variations of the amplitude (which corresponds to low values of τ_c) can lead to efficient sound radiation, especially at high subsonic convective Mach numbers. We extend this conclusion to the present case, where both space and time modulations of the convected wave are allowed in the model.

3. Temporally localised envelope truncation

In order to provide temporal changes in the spatial extent of the envelope function, we model T_{11} as

$$T_{11}(\mathbf{y},\tau)=2\rho_0U\tilde{u}\,\frac{\pi D^2}{4}\,\delta(y_2)\delta(y_3)\mathrm{e}^{\mathrm{i}(\omega\tau-ky_1)}\mathrm{e}^{-y_1^2/L^2(\tau)}. \tag{16}$$

With this expression the peak amplitude of the convected wave is kept constant, but the characteristic length of the envelope, L, changes with time. We model the changes in L as

$$L(\tau)=L_0-\kappa\mathrm{e}^{-(\tau-\tau_0)^2/\tau_L^2}, \tag{17}$$

4482 A.V.G. Cavalieri et al. / Journal of Sound and Vibration 330 (2011) 4474–4492

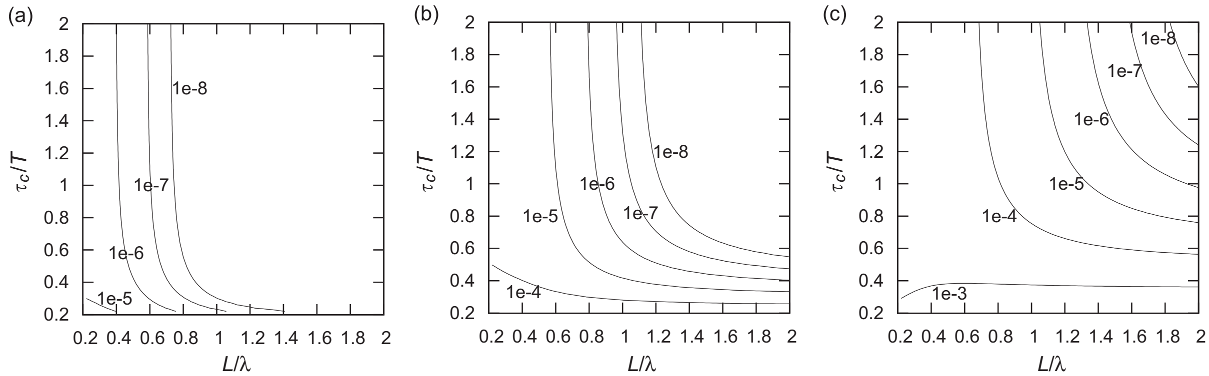

Fig. 6. Acoustic efficiency of the intermittent wave-packet for: (a) $M=0.3$, (b) $M=0.6$ and (c) $M=0.9$.

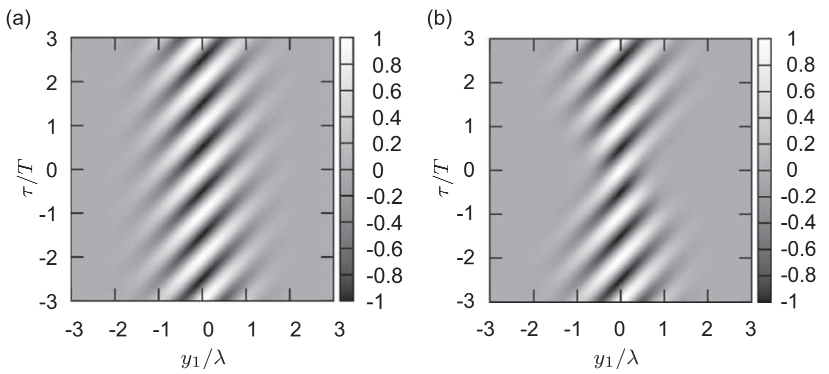

Fig. 7. Example of the source with: (a) $\kappa=0$ and (b) $\kappa=L_0/2$ and $\tau_L=T$.

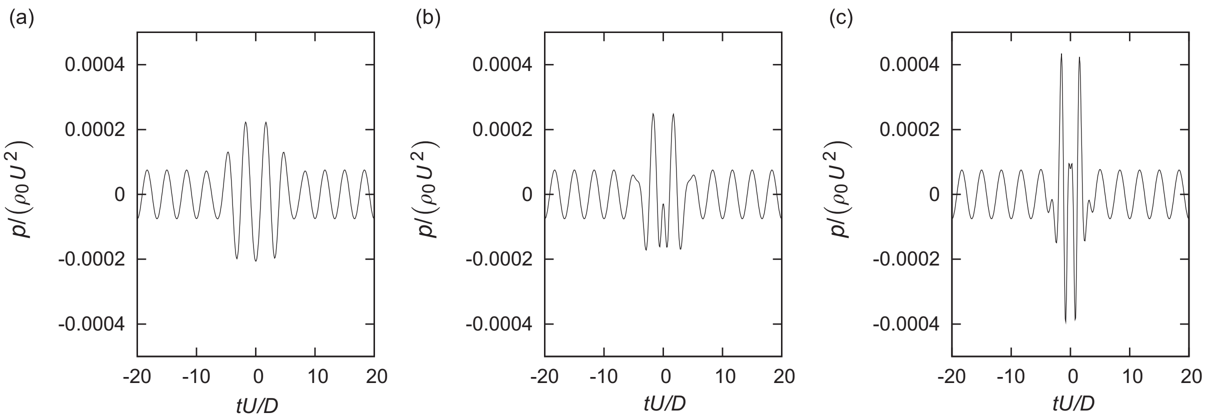

Fig. 8. Far-field pressure at $\theta=30^\circ$ for $\kappa=L_0/2$ and: (a) $\tau_L=T$, (b) $\tau_L=T/2$ and (c) $\tau_L=T/5$.

where L_0 is an initial envelope width and κ is the maximum envelope reduction, which happens at $\tau=\tau_0$. This reduction of the envelope happens during an interval characterised by the temporal scale τ_L, and has the shape of a Gaussian function. Examples of this source shape are shown in Fig. 7; for $\kappa=0$ (Fig. 7a) we have a periodic wave-packet, as in Fig. 3(b), and for $\kappa>0$ (Fig. 7b), we have the temporally localised truncation.

For this source shape, the radiated sound field is periodic before the change in the envelope. When L begins to differ significantly from L_0, there is a change in the radiation, which is increased for positive κ. Fig. 8 shows the results of the numerical integration of Eq. (1) with the source given by Eqs. (16) and (17) for a point at $\theta=30^\circ$ to the jet axis. For this sample calculation, the same numerical values of Section 2 were used; additionally, we used $L_0=\lambda$ and $\kappa=L_0/2$.

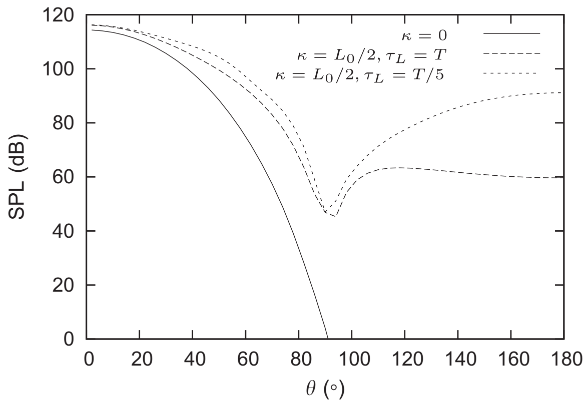

Fig. 9. Directivity for wave-packets with temporally localised envelope reduction. Decibel scale referenced to $(2 \times 10^{-5}$ Pa$)/(\rho_0 U^2)$.

The results show that as we decrease the values of τ_L, which means that the truncation of the wave-packet is faster, the sound radiation is increased.

Fig. 9 shows the directivity of the sources of Fig. 7. The effect of the truncation of the wave-packet structure is seen as an increase of the sound levels at all angles; this increase is more significant for the higher axial angles. For fast reduction of the wave-packet envelope (low τ_L) the noise increase is intensified: even though the sources with envelope reduction have less turbulent kinetic energy, their radiation is increased when compared to the periodic wave-packet.

The present model can be related to the work of Kastner et al. [33], whose analysis of data from DNS of a Re=3600, M=0.9 jet showed that intense noise generation happens at times where a structure resembling an instability wave is truncated; a wave-packet model, periodic in time, of this truncated wave is proposed in that work, leading to an increase of radiation at all angles. Here, the source model of Eq. (16) explicitly accounts for the temporally localised nature of such a truncation, and the radiation results confirm that such truncation leads to a noise intensification in the acoustic field.

4. Wave-packet with slowly varying amplitude and spatial extent

In order to account for both temporal changes in the wave-packet amplitude and axial extension, and to provide a framework where it is possible to fit the wave-packet parameters with numerical data, we now model the T_{11} component Lighthill's stress tensor as

$$T_{11}(\mathbf{y},\tau) = 2\rho_0 U\tilde{u}\,\frac{\pi D^2}{4}\,\delta(y_2)\delta(y_3)A(\tau)\mathrm{e}^{\mathrm{i}(\omega\tau - ky_1)}\mathrm{e}^{-y_1^2/L^2(\tau)}, \tag{18}$$

where we allow temporal variations of the amplitude A, as in Section 2, and also temporal changes in L, as in Section 3.

Using this expression in Eq. (1), with the far-field assumption, leads to

$$p(\mathbf{x},t) = \frac{\rho_0 U\tilde{u}D^2\cos^2\theta}{8c^2|\mathbf{x}|}\frac{\partial^2}{\partial t^2}\int_{-\infty}^{\infty} A\left(t - \frac{|\mathbf{x}| - y_1\cos\theta}{c}\right)\mathrm{e}^{\mathrm{i}[\omega(t-(|\mathbf{x}|-y_1\cos\theta)/c)-ky_1]}\mathrm{e}^{-y_1^2/L^2(t-(|\mathbf{x}|-y_1\cos\theta)/c)}\,\mathrm{d}y_1. \tag{19}$$

If the amplitude A and the characteristic length of the envelope, L, change slowly when evaluated at retarded-time differences $(y_1\cos\theta/c)$ along the wave-packet, as detailed in Appendix B, we can consider axial compactness for these functions in the integration, such that

$$A\left(t - \frac{|\mathbf{x}| - y_1\cos\theta}{c}\right) \approx A\left(t - \frac{|\mathbf{x}|}{c}\right) \tag{20}$$

and

$$L\left(t - \frac{|\mathbf{x}| - y_1\cos\theta}{c}\right) \approx L\left(t - \frac{|\mathbf{x}|}{c}\right). \tag{21}$$

If * is used to denote a function evaluated at the retarded time $t - |\mathbf{x}|/c$, we have

$$p(\mathbf{x},t) = \frac{\rho_0 U\tilde{u}D^2\cos^2\theta}{8c^2|\mathbf{x}|}\frac{\partial^2}{\partial t^2}\left\{A^*\int \mathrm{e}^{\mathrm{i}[\omega(t-(|\mathbf{x}|-y_1\cos\theta)/c)-ky_1]}\mathrm{e}^{-y_1^2/(L^*)^2}\,\mathrm{d}y_1\right\}. \tag{22}$$

Evaluation of this integral, considering that the temporal changes in L and in A are slower than those related to the harmonic oscillation in ω, leads to

$$p(\mathbf{x},t) = -A^*\frac{\rho_0 U\tilde{u}M_c^2(kD)^2L^*\sqrt{\pi}\cos^2\theta}{8|\mathbf{x}|}\mathrm{e}^{-(L^*)^2k^2(1-M_c\cos\theta)^2/4}\mathrm{e}^{\mathrm{i}\omega(t-|\mathbf{x}|/c)}. \tag{23}$$

4484 A.V.G. Cavalieri et al. / Journal of Sound and Vibration 330 (2011) 4474–4492

This means that for sufficiently slow temporal changes in A and in L, the radiated sound field at a given time t is that of a wave-packet whose amplitude and envelope corresponds to the values A^* and L^*, that is, *to the wave-packet at the retarded time* $t-|\mathbf{x}|/c$ (compare with Eq. (13)).

5. Evaluation of the model using simulation data

In order to now assess the degree to which these simplified models can reproduce the main characteristics of the downstream radiation from subsonic jets we use numerical data of Mach 0.9 jets, taken from a direct numerical simulation of an unheated jet at Re=3600 [21] and from a large eddy simulation of a Mach 0.9 isothermal jet at Re $= 4 \times 10^5$ ([38]; see also [39]), to furnish the third model with instantaneous values for A and L. These are obtained from the azimuthal mean (the axisymmetric Fourier mode) of the streamwise velocity on the jet lipline. The use of this lipline data as input for the present line source model is justified in Appendix A.

For both the DNS and the LES data[3] the peak frequency of the axisymmetric mode at 3.5D from the jet exit is St ≈ 0.4, and this frequency is used in Eq. (23). An average convection Mach number ($M_c = 0.555M_j$ for the DNS, and $M_c = 0.543M_j$ for the LES) was determined from the slope of the peak in the $k_1-\omega$ spectrum of the azimuthal mean of the streamwise velocity at the lipline. To obtain the envelope parameters, we first filter the velocity field in the frequency range $0.3 \leq \mathrm{St} \leq 0.5$. The parameters $A(\tau)$ and $L(\tau)$ are then obtained by Gaussian fits, at each instant τ, to a short-time Fourier series, similar to the procedure of Tadmor et al. [48] and Joe et al. [49], using a central frequency of St=0.4:

$$u(y_1,t) = A_1(y_1,t)\cos(\omega t) + B_1(y_1,t)\sin(\omega t), \tag{24}$$

where the A_1 and B_1 coefficients are given by

$$A_1(y_1,t) = \frac{2}{T}\int_{t-T/2}^{t+T/2} u(y_1,\tau)\cos(\omega\tau)\,\mathrm{d}\tau, \tag{25}$$

$$B_1(y_1,t) = \frac{2}{T}\int_{t-T/2}^{t+T/2} u(y_1,\tau)\sin(\omega\tau)\,\mathrm{d}\tau, \tag{26}$$

and the instantaneous amplitude of the oscillations is given as $\sqrt{A(y_1,t)^2 + B(y_1,t)^2}$. The moving window width T is taken as the period of oscillation in ω. In this way, the temporal oscillations of the velocity are described as sines and cosines whose amplitudes change in time, but slowly when compared to the period T of the oscillation.

We then calculate instantaneous lengths and amplitudes using the Gaussian fits for each instantaneous envelope. The fits are effected using the instantaneous amplitude over the range $D \leq y_1 \leq 5.5D$, where 5.5D corresponds to end of the potential core for both calculations. Some sample fits for the LES are shown in Fig. 10. The Gaussian fits are a reasonable approximation, in particular at times when high envelope amplitudes occur.

The sound propagation results of the source model are shown in Fig. 11; the acoustic data considered is the axisymmetric mode of the pressure on a cylindrical surface in the acoustic region of the computations. For the DNS (Fig. 11a) this surface is at four diameters from the jet axis, and for the LES (Fig. 11b) it is at nine diameters from the axis. Therefore, in Fig. 11 high values of x_1/D correspond to low axial angles. The SPL is calculated with a frequency range from St=0.3 to 0.5, consistent with the filtering applied to the velocity data.

We include in Fig. 11 numerical results of the calculation without the far-field assumption, since the data is on cylindrical surfaces that are not in the far acoustic field. There is agreement to within 1.5 dB for low axial angles between both calculations and the wave-packet with an ‘unsteady envelope’, i.e. the wave-packet of Eq. (18) equipped with the instantaneous values of A and L.

In Fig. 11 there are also results for a wave-packet with a steady envelope, whose parameters A and L were kept constant in time and equal to the ensemble average of the instantaneous Gaussian fits. The predicted sound levels are much lower than those obtained for the instantaneous wave-packet, leading to significant differences between the model and the acoustic data from the DNS and the LES. The reason for this is the neglect of the wave-packet ‘jitter’, which was seen for the model problems in Sections 2 and 3 to enhance sound radiation.

It is known that models based on Gaussian functions can often be sensitive to small parametric changes. Such a lack of robustness can cast doubt as to the ability of the model to truly reproduce the physical mechanisms it is designed to mimic. In order to test the robustness of the jittering wave-packet model, and thereby confirm its utility as a conceptual handle where the production of sound by coherent structures in subsonic jets is concerned, we evaluated, numerically, the sound radiated by a similar kind of source structure, but where the function $1/[1+(y_1^4/L^4(\tau))]$ was used to represent the spatial envelope. This fit led to a sound prediction again to within 1.5 dB of the LES results for the low axial angles, showing that the present results are not due to a particular choice of envelope function and thereby further confirming the physical pertinence of the jittering wave-packet model.

[3] This large eddy simulation has been validated using three different sets of experimental data [44–46] and another comprehensively validated simulation [47]; a more complete validation is reported by Daviller [38] and so only a restricted ensemble of validation information is given here, in Appendix D.

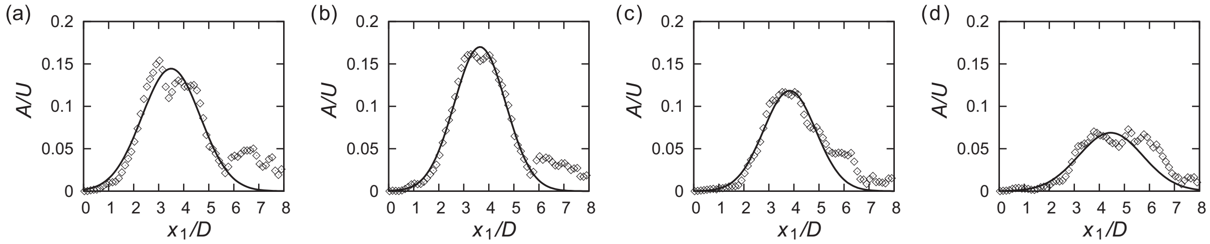

Fig. 10. Instantaneous amplitude of the filtered streamwise velocity for the large eddy simulation (symbols) and instantaneous Gaussian fits (full lines) at tc/D=(a) 3.2, (b) 6.4, (c) 9.6 and (d) 12.8.

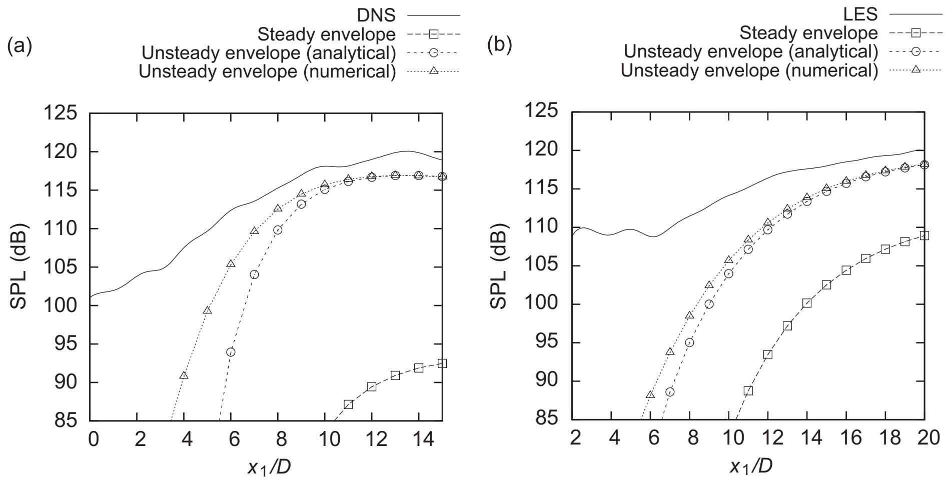

Fig. 11. Comparison between wave-packet models and numerical data of Mach 0.9 jets: (a) DNS [21] and (b) LES [38]. SPL taken for the axisymmetric mode of the acoustic pressure for $0.3 \le \mathrm{St} \le 0.5$.

6. Conclusion

An analytical expression for the radiated far-field pressure by a temporally localised wave-packet is presented, and results are found to agree well with those obtained by a numerical calculation. The effect of temporal modulation is seen to comprise an enhancement of sound radiation at all angles. A directive radiation pattern is obtained for moderate temporal modulations. This result extends that of Sandham et al. [36].

Numerical results for a wave-packet whose axial extent changes in time also show enhanced sound radiation, and, again, directive radiation. A third model is then proposed which includes temporal changes in both the amplitude and spatial extent of the wave-packet. Its physical pertinence is assessed and confirmed by parametrising the model using data extracted from a DNS and an LES of Mach 0.9 jets: we obtain far-field sound levels which are within 1.5 dB of the acoustic pressure computed by the simulations, whereas when time-averaged wave-packet parameters are used the discrepancy is greater than 10 dB. Such jitter is shown, in Appendix C, to only be important for jets which are convectively subsonic; in the convectively supersonic case jitter does not enhance sound radiation in the same way, because all of the fluctuation energy of the wave-packet already lies in the radiating sector of frequency–wavenumber space; jitter here mostly just spreads the spectral tail of the function into non-radiating regions of the spectrum.

The present results encourage further study of intermittent events in both flow and acoustic fields of subsonic jets, and have potential to contribute to the enhancement of source imaging methodologies on one hand, and, on the other, to provide guidance for reduced-complexity kinematic, dynamic modelling and control of sound sources in these flows.

Acknowledgements

The present work is supported by CNPq, National Council of Scientific and Technological Development—Brazil. Numerical data: DNS and LES kindly provided, respectively, by Jonathan B. Freund and Guillaume Daviller.

Appendix A. Slowly changing surface-distributed wave-packet

In this appendix we derive an expression for a wave-packet distributed over a cylindrical surface on the jet lipline; additionally, we study the sound radiation of different Fourier azimuthal modes for the wave-packet. We express the T_{11} component of Lighthill's tensor for a given azimuthal mode m as

$$T_{11}(\mathbf{y},\tau)=\rho_0 U\tilde{u}R\delta(r-R)A(\tau)e^{i(\omega\tau-ky_1)}e^{-y_1^2/L(\tau)^2}C_m e^{im\phi}. \tag{A.1}$$

With this expression in Eq. (1), we have

$$p(\mathbf{x},t)=\frac{\rho_0 U\tilde{u}R^2}{4\pi c^2|\mathbf{x}|}\frac{\partial^2}{\partial t^2}\iint A\left(t-\frac{|\mathbf{x}-\mathbf{y}|}{c}\right)e^{i[\omega(t-|\mathbf{x}-\mathbf{y}|/c)-ky_1]}e^{-y_1^2/L^2(t-|\mathbf{x}-\mathbf{y}|/c)}C_m e^{im\phi}\,d\phi\,dy_1. \tag{A.2}$$

We suppose without loss of generality that the observer is at $\Phi=0$ and $x_2=0$ in cartesian coordinates, being $\Phi=\tan^{-1}(x_2/x_3)$. The distance can be expressed, with a far-field assumption, as

$$|\mathbf{x}-\mathbf{y}|\approx|\mathbf{x}|-y_1\cos\theta-R\cos\phi\sin\theta, \tag{A.3}$$

where θ is the angle of $\mathbf{x}$ to the jet axis.

If we suppose additionally that the temporal changes in A and in L are slow if evaluated at retarded-time differences $(y_1\cos\theta/c)$ along the wave-packet, as in Appendix B, we can perform similar approximations as in Section 4:

$$A\left(t-\frac{|\mathbf{x}|-y_1\cos\theta-R\cos\phi\sin\theta}{c}\right)\approx A\left(t-\frac{|\mathbf{x}|}{c}\right), \tag{A.4}$$

$$L\left(t-\frac{|\mathbf{x}|-y_1\cos\theta-R\cos\phi\sin\theta}{c}\right)\approx L\left(t-\frac{|\mathbf{x}|}{c}\right). \tag{A.5}$$

Using the notation * meaning evaluation at the average retarded time $(t-|\mathbf{x}|/c)$, we have

$$p(\mathbf{x},t)=\frac{\rho_0 U\tilde{u}R^2}{4\pi c^2|\mathbf{x}|}\frac{\partial^2}{\partial t^2}\iint A^* e^{i[\omega(t-(|\mathbf{x}|-y_1\cos\theta-R\cos\phi\sin\theta)/c)-ky_1]}e^{-y_1^2/(L^*)^2}C_m e^{im\phi}\,d\phi\,dy_1. \tag{A.6}$$

This integral can be rearranged to

$$p(\mathbf{x},t)=\frac{\rho_0 U\tilde{u}R^2}{4\pi c^2|\mathbf{x}|}\frac{\partial^2}{\partial t^2}\int_{-\infty}^{\infty}A^* e^{i[\omega(t-(|\mathbf{x}|-y_1\cos\theta)/c)-ky_1]-y_1^2/(L^*)^2}\,dy_1\int_0^{2\pi}C_m e^{i(m\phi-\omega(R\cos\phi\sin\theta/c))}\,d\phi. \tag{A.7}$$

The evaluation of the azimuthal integral

$$I_1=\int_0^{2\pi}e^{i(m\phi-\omega(R\cos\phi\sin\theta/c))}\,d\phi, \tag{A.8}$$

which can be expressed as

$$I_1=\int_0^{2\pi}e^{i(m\phi)}e^{(-i\pi\mathrm{St}M\cos\phi\sin\theta)}\,d\phi \tag{A.9}$$

indicates the efficiency of the azimuthal mode m in radiating to the far acoustic field.

Since the Bessel functions J_m have the property

$$J_m(x)=\frac{1}{2\pi i^m}\int_0^{2\pi}e^{ix\cos\phi}e^{im\phi}\,d\phi \tag{A.10}$$

we can write

$$I_1=(-i)^m 2\pi J_m(\pi\mathrm{St}M\sin\theta). \tag{A.11}$$

For St $M\sin\theta=0$ the I_1 integral yields 2π for $m=0$, and 0 for all other values of m. This means that, if we neglect retarded time differences along the azimuthal direction, only axisymmetric wave-packets can radiate. In other words, if the wave-packet diameter D is compact (recall that $D/\lambda=\mathrm{St}M$), or if the observation angle θ is small, only the axisymmetric wave-packet has significant radiation. This is always true for $\theta=0$ and $\theta=\pi$, i.e. for an observer in the jet axis, which is a known result [12,50,51].

We show in Fig. A1 the results for the I_1 integral, divided by $(-i)^m$ to yield a real quantity. We see that the integral of $m=0$ decays from its compact value of 2π, eventually goes to zero, and then oscillates. The integrals for the higher azimuthal modes are zero at the compact limit, as expected from the properties of the Bessel functions; they go from zero to a certain value, which is of the same order of the $m=0$ integral, and then oscillate.

For the numerical values $\theta=\pi/6$, $M=0.9$ and St$=0.4$, we have St$M\sin\theta=0.18$, and in this case, as seen in Fig. A1, we can, if we have similar amplitudes C_m for the different m values, neglect all modes $m>0$ and consider the compact limit ($I_1=2\pi$ for $m=0$) as a first approximation; the I_1 integral for $m=1$ and the present numerical values yields a sound intensity 10 dB lower than that for $m=0$, being the integrals for higher m modes even lower than that. There is experimental evidence of the similar C_m amplitudes in the work of Suzuki and Colonius [24], who detect instability waves

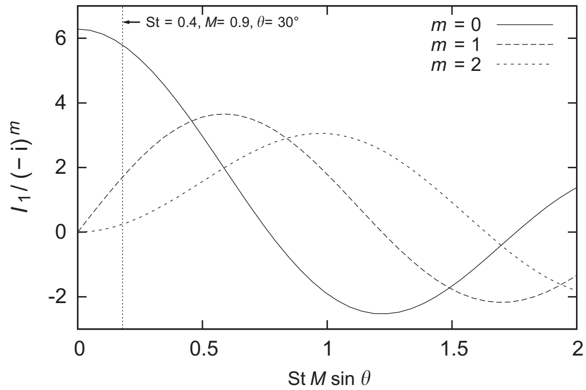

Fig. A1. Results for the I_1 integral.

in the near field of a jet with a beamforming algorithm, and find comparable peak amplitudes for modes $m=0$ and 1, with slightly higher values for $m=0$; amplitudes of the mode $m=2$ are somewhat lower.

If we retain only the axisymmetric wave-packet and approximate I_1 as 2π, we have

$$p(\mathbf{x},t)=\frac{\rho_0 U\tilde{u}R^2}{2c^2|\mathbf{x}|}\frac{\partial^2}{\partial t^2}\int A^* C_0 \mathrm{e}^{\mathrm{i}[\omega(t-(|\mathbf{x}|-y_1\cos\theta)/c)-ky_1]}\mathrm{e}^{-y_1^2/(L^*)^2}\,\mathrm{d}y_1, \tag{A.12}$$

and integration gives

$$p(\mathbf{x},t)=-C_0A^*\frac{\rho_0 U\tilde{u}M_c^2(kD)^2L^*\sqrt{\pi}\cos^2\theta}{8|\mathbf{x}|}\mathrm{e}^{-(L^*)^2k^2(1-M_c\cos\theta)^2/4}\mathrm{e}^{\mathrm{i}\omega(t-|\mathbf{x}|/c)}, \tag{A.13}$$

which, combining the constant C_0 with the amplitude A, is exactly the same result of Section 4 shown in Eq. (23). This means that for low values of the parameter StMsinθ, the use of a wave-packet concentrated on a line leads to the same result as a surface wave-packet, justifying therefore the use in Section 5 of a line distribution of T_{11}, whose amplitude is fitted to the azimuthal mean of the u fluctuation on the jet lipline.

Appendix B. Quantification of compactness of the amplitude and spatial extent

In Section 4, an approximation was made to the wave-packet amplitude and spatial extent, which were considered as slowly varying functions. In order to quantify the maximum temporal scale of these functions that allows these approximations, we will model them as complex exponentials whose frequency is different from the ω value for the convected wave. For convenience, we repeat here Eq. (19):

$$p(\mathbf{x},t)=\frac{\rho_0 U\tilde{u}D^2\cos^2\theta}{8c^2|\mathbf{x}|}\frac{\partial^2}{\partial t^2}\int_{-\infty}^{\infty}A\left(t-\frac{|\mathbf{x}|-y_1\cos\theta}{c}\right)\mathrm{e}^{\mathrm{i}[\omega(t-(|\mathbf{x}|-y_1\cos\theta)/c)-ky_1]}\mathrm{e}^{-y_1^2/L^2(t-(|\mathbf{x}|-y_1\cos\theta)/c)}\,\mathrm{d}y_1. \tag{B.1}$$

Considering the amplitude variations as a complex exponential in ω_A, we have

$$A\left(t-\frac{|\mathbf{x}|-y_1\cos\theta}{c}\right)=\mathrm{e}^{\mathrm{i}\omega_A(t-|\mathbf{x}|/c)}\mathrm{e}^{-\mathrm{i}\omega_A(y_1\cos\theta)/c}. \tag{B.2}$$

Although the integral in the Eq. (B.1) extends from $-\infty$ to ∞, the presence of a Gaussian envelope inside the integral limits the region of significant values of the integrand; thus, we can take the y_1 values to be between $\pm 2L_{ref}$, where L_{ref} is a reference value for the spatial extent of the envelope, for instance its ensemble average.

Therefore, to be able to write

$$A\left(t-\frac{|\mathbf{x}|-y_1\cos\theta}{c}\right)\approx A\left(t-\frac{|\mathbf{x}|}{c}\right) \tag{B.3}$$

as an appropriate approximation, we should have

$$\frac{2\omega_A L_{ref}\cos\theta}{c}\ll 1. \tag{B.4}$$

This can be thought of as a compactness condition for the amplitude function A that allows the utilisation of the approximation in Eqs. (20) or (B.3). A similar development can be made for the spatial extent, leading to an analogous result for a frequency ω_L,

$$\frac{2\omega_L L_{ref}\cos\theta}{c}\ll 1. \tag{B.5}$$

Thus, the expression of Eq. (23) for the radiated pressure can be applied if the oscillations of the functions A and L have temporal scales that corresponds to the conditions (B.4) and (B.5), respectively.

More general temporal functions $A(\tau)$ and $L(\tau)$ can be expressed in terms of their Fourier transforms $\hat{A}(\omega)$ and $\hat{L}(\omega)$, such that

$$A(\tau)=\frac{1}{2\pi}\int_{-\infty}^{\infty}\hat{A}(\omega)\mathrm{e}^{\mathrm{i}\omega\tau}\,\mathrm{d}\omega, \tag{B.6}$$

$$L(\tau)=\frac{1}{2\pi}\int_{-\infty}^{\infty}\hat{L}(\omega)\mathrm{e}^{\mathrm{i}\omega\tau}\,\mathrm{d}\omega. \tag{B.7}$$

Hence, the foregoing analysis is possible for each component $\hat{A}(\omega)\mathrm{e}^{\mathrm{i}\omega\tau}$ and $\hat{L}(\omega)\mathrm{e}^{\mathrm{i}\omega\tau}$. In this case, the compactness condition for the A and L functions is that their Fourier transforms only have energy content for frequencies lower than the limiting values of conditions (B.4) and (B.5).

Appendix C. Results for supersonic convection speeds

Although the analysis of the current paper focuses on subsonic convection speeds, there is no restriction for the convection Mach number used in the proposed models. In order to evaluate the effect of temporal variations of the wave-packet parameters for supersonic convection speeds we have applied the wave-packet model of Section 2, with temporally localised changes in the amplitude, for a supersonic Mach number. We show in Fig. C1 a comparison of the acoustic efficiency E_A/E_S, defined in Section 2, for Mach numbers of 0.9 and 2, considering the convecting Mach number to be 0.6 times the jet Mach number.

We notice that while there are significant changes in the radiation efficiency of the wave-packet with subsonic convection speed with changes in space–time modulations (Fig. C1(a)), this is not the case for $M=2$. In Fig. C1(b) we see an almost constant acoustic efficiency for $M=2$, whose order is 10^{-2}. This suggests that the jitter in the wave-packet parameters is much less important for supersonic speeds than in the subsonic case.

This can be further explored with an analysis of the source in frequency–wavenumber ($\omega-\mathbf{k}$) space. A known result of Lighthill's analogy is that when the source is Fourier transformed in time and space the only radiating part presents (see Crighton [40])

$$|\omega|=|\mathbf{k}|c, \tag{C.1}$$

where

$$|\mathbf{k}|=\sqrt{k_1^2+k_2^2+k_3^2}. \tag{C.2}$$

Since the present wave-packet source, defined in Eq. (3), is concentrated on a line, its energy is uniformly distributed for the k_2 and k_3 wavenumber components, for the Fourier transforms in k_2 and k_3 of the Dirac distributions $\delta(y_2)$ and $\delta(y_3)$ are constant and equal to 1. In this case, the condition of (C.1) is satisfied for the energy content of the source in the frequency–wavenumber sector given by

$$|\omega|\geq|k_1|c. \tag{C.3}$$

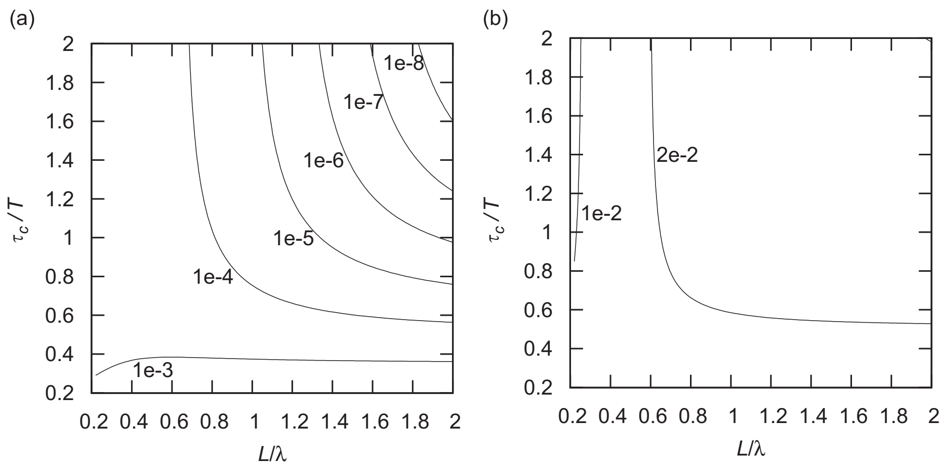

Fig. C1. Acoustic efficiency of the intermittent wave-packet for: (a) $M=0.9$ and (b) $M=2$.

Examples of the frequency–wavenumber spectra for subsonic and supersonic convection speeds are shown, respectively, in Figs. C2 and C3. The radiating sector, defined in Eq. (C.3), and the non-radiating one are labeled in the figures.

We note for the subsonic case that for large spatial and temporal source envelopes, as shown in Fig. C2(a), most of the source energy is in the non-radiating sector of the frequency–wavenumber spectrum. The distribution is centered in the frequency and wavenumber of the subsonic convected wave; therefore, the center is in the non-radiating sector. The sound radiation is solely due to the small 'tail' above the limit $\omega = k_1 c$. If the source envelope is narrower, either in space (Fig. C2b) or in time (Fig. C2c), the energy distribution in the frequency–wavenumber spectrum is flattened, respectively, in the k_1 and the ω directions. In both cases, more source energy is now in the radiating sector, since there are significant increases of the radiating 'tail' of the source energy. This relates to the increase of orders of magnitude for the acoustic efficiency observed in Fig. C1(a) for low values of L and τ_c.

For the supersonic case with large envelopes in Fig. C3(a), most of the source energy is already in the radiating sector, for now the frequency and wavenumber of the convected wave, which mark the center of the energy distribution, are already in the radiating part of the spectrum.

Narrow envelopes in space or time, shown, respectively, in Figs. C3(b) and C3(c), flatten the distribution, as in the subsonic case. However, now the 'tail' is extended to the non-radiating sector, and most of the source energy still remains in the radiating part of the frequency–wavenumber spectrum. The changes in the radiating efficiency are slight, and the differences of orders of magnitude observed in the subsonic case are no longer present, as seen in Fig. C1(b).

The present results suggest thus that while the jittering of the wave-packet parameters changes significantly sound radiation for subsonic convection speeds, it would have a negligible effect on sound radiation for supersonic convection speeds.

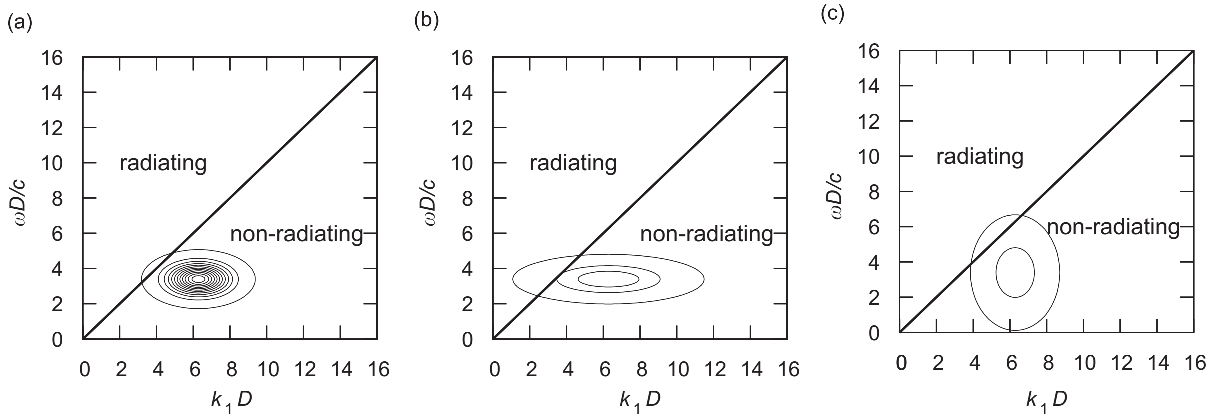

Fig. C2. Examples of frequency–wavenumber spectra of the source for M=0.9 with: (a) $L=\lambda, \tau_c=T$, (b) $L=0.5\lambda, \tau_c=T$ and (c) $L=\lambda, \tau_c=0.4T$. The same contours were used for all subfigures. The thick line represents $\omega = k_1 c$.

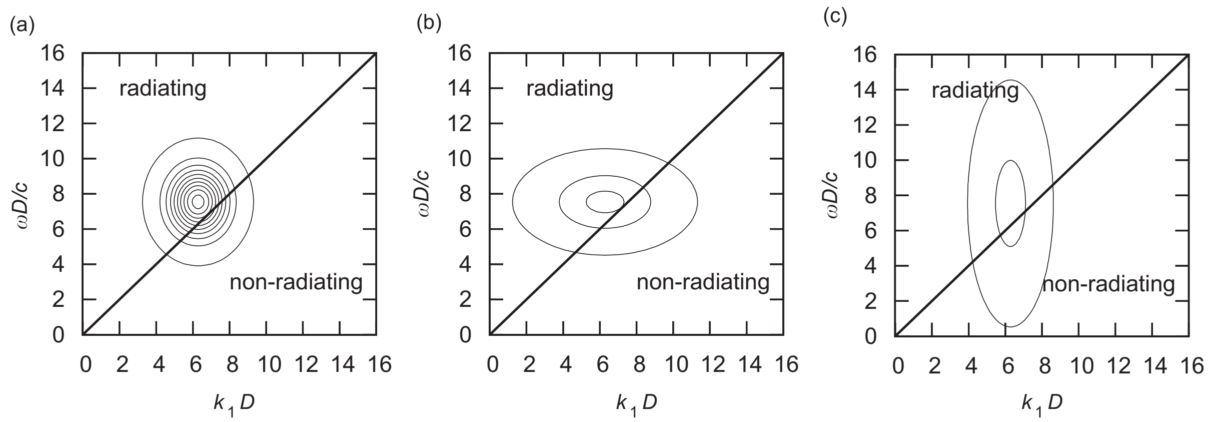

Fig. C3. Examples of frequency–wavenumber spectra of the source for M=2 with: (a) $L=\lambda, \tau_c=T$, (b) $L=0.5\lambda, \tau_c=T$ and (c) $L=\lambda, \tau_c=0.4T$. The same contours were used for all subfigures. The thick line represents $\omega = k_1 c$.

Appendix D. Validation of the large eddy simulation

We present in this Appendix some results of the validation of the LES of a Mach 0.9 jet used in the present work. We focus on only the velocity components as these are used to obtain the parameters of the model in Section 5.

In Fig. D1 we see comparisons of the rms values of the velocity with the results of Jordan et al. [45] and Bridges [44]. We note that the initial conditions are not matched; thus the inflow excitation does not reproduce exactly the boundary layers in the nozzle of the experiments, which can be expected due to the absence of the nozzle geometry in the present LES. However, for the downstream points, the rms values of the present calculation are close to the experimental ones, especially for the maximum values of u_{rms}.

Fig. D2 presents comparisons of the convection velocity, which is compared to both the experiment of Bridges [44] and to the LES of Bodony [52] at the jet axis (Fig. D2a) and the lipline (Fig. D2b). Close agreement is verified for both positions.

The axial correlation lenghtscales for the streamwise velocity are compared to experimental data in Fig. D3. Besides some differences in the region close to the jet nozzle, the present results match closely the experimental values obtained by Fleury et al. [53] and are higher than the values of Bridges [44].

In Fig. D4 we see spectra in the far acoustic field for a point at 72D from the jet exit and at $\theta = 45^\circ$ from the jet downstream axis, compared to the experimental results of Tanna [46] and to the LES of Bodony [52] (see also [54]). We note that the present calculation agrees with the experimental results for Strouhal numbers ranging from 0.07 to 1. On the other hand, for lower frequencies the present calculation overestimates the sound. The experimental spectrum peak is nonetheless well calculated in the present simulation, and this peak is the focus of the comparison made in Section 4.

The spectra for both large eddy simulations decrease in an abrupt manner for high frequencies when compared to the experimental data. This is due to the limitations in spatial discretisation of the domain of the LES that necessitates the use of subgrid modelling.

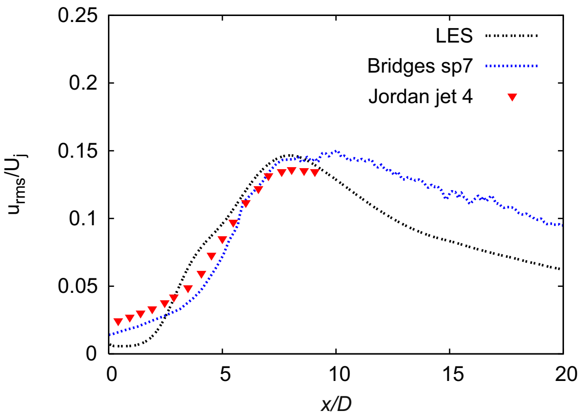

Fig. D1. RMS values of the streamwise velocity component on the jet lipline.

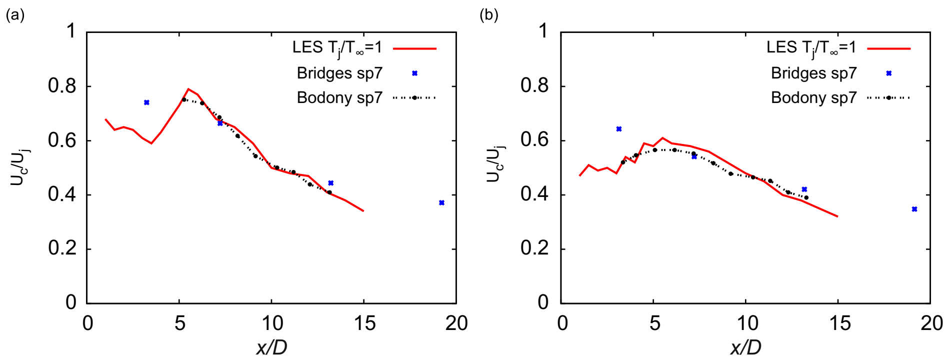

Fig. D2. Convection speed on (a) the jet centerline and (b) lipline.

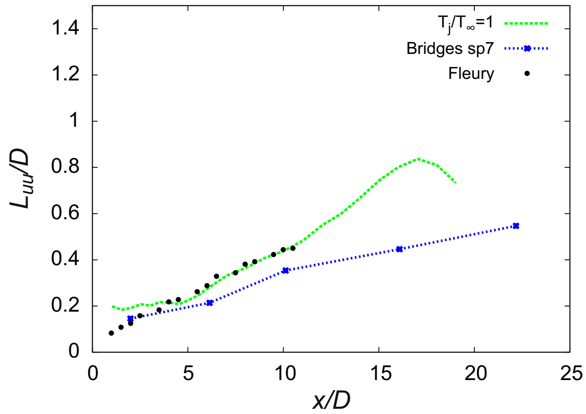

Fig. D3. Axial correlation lengthscale for the streamwise velocity.

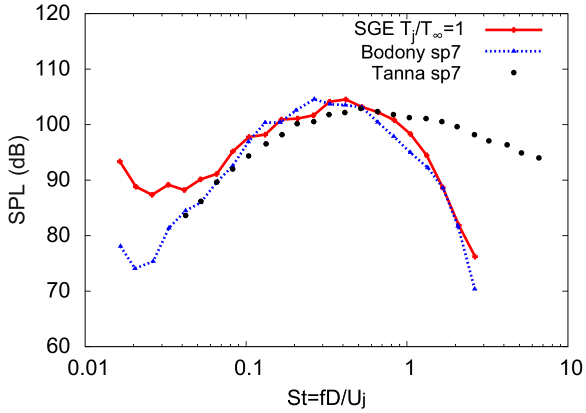

Fig. D4. 1/3-octave spectra at 72D from the jet exit for $\theta = 45^\circ$.

References

[1] G.K. Batchelor, *The Theory of Homogeneous Turbulence*, Cambridge University Press, 1953.
[2] M.J. Lighthill, On sound generated aerodynamically. I. General theory, in: *Proceedings of the Royal Society of London. Series A, Mathematical and Physical Sciences*, 1952, pp. 564–587.
[3] T. Colonius, S.K. Lele, P. Moin, Sound generation in a mixing layer, *Journal of Fluid Mechanics* 330 (1997) 375–409.
[4] J.B. Freund, Noise-source turbulence statistics and the noise from a Mach 0.9 jet, *Physics of Fluids* 15 (2003) 1788–1799.
[5] A. Samanta, J.B. Freund, M. Wei, S.K. Lele, Robustness of acoustic analogies for predicting mixing-layer noise, *AIAA Journal* 44 (11) (2006) 2780–2786.
[6] S. Sinayoko, A. Agarwal, Z. Hu, Flow decomposition and aerodynamic sound generation, *Journal of Fluid Mechanics* 668 (2011) 335–350.
[7] M.E. Goldstein, A generalized acoustic analogy, *Journal of Fluid Mechanics* 488 (2003) 315–333.
[8] E. Mollo-Christensen, Jet noise and shear flow instability seen from an experimenter's viewpoint (similarity laws for jet noise and shear flow instability as suggested by experiments), *Journal of Applied Mechanics* 34 (1967) 1–7.
[9] S.C. Crow, F.H. Champagne, Orderly structure in jet turbulence, *Journal of Fluid Mechanics* 48 (3) (1971) 547–591.
[10] G.L. Brown, A. Roshko, On density effects and large structure in turbulent mixing layers, *Journal of Fluid Mechanics* 64 (4) (1974) 775–816.
[11] C.J. Moore, The role of shear-layer instability waves in jet exhaust noise, *Journal of Fluid Mechanics* 80 (2) (1977) 321–367.
[12] A. Michalke, A wave model for sound generation in circular jets, Technical Report, Deutsche Luft- und Raumfahrt, November 1970 ⟨http://elib.dlr.de/63062/⟩.
[13] A. Michalke, An expansion scheme for the noise from circular jets, *Zeitschrift für Flugwissenschaften* 20 (1972) 229–237.
[14] S.C. Crow, Acoustic gain of a turbulent jet, *Physiological Society Meeting*, vol. 6, University of Colorado, Boulder, Paper IE, 1972.
[15] D.G. Crighton, M. Gaster, Stability of slowly diverging jet flow, *Journal of Fluid Mechanics* 77 (2) (1976) 397–413.
[16] C.K.W. Tam, P.J. Morris, The radiation of sound by the instability waves of a compressible plane turbulent shear layer, *Journal of Fluid Mechanics* 98 (2) (1980) 349–381.
[17] R. Mankbadi, J. Liu, Sound generated aerodynamically revisited: large-scale structures in a turbulent jet as a source of sound, *Philosophical Transactions of the Royal Society of London. Series A, Mathematical and Physical Sciences* 311 (1516) (1984) 183–217.
[18] D.G. Crighton, P. Huerre, Shear-layer pressure fluctuations and superdirective acoustic sources, *Journal of Fluid Mechanics* 220 (1990) 355–368.
[19] J. Laufer, T.-C. Yen, Noise generation by a low-Mach-number jet, *Journal of Fluid Mechanics* 134 (1983) 1–31.
[20] G. Broze, F. Hussain, Nonlinear dynamics of forced transitional jets: periodic and chaotic attractors, *Journal of Fluid Mechanics* 263 (1994) 93–132.
[21] J.B. Freund, Noise sources in a low-Reynolds-number turbulent jet at Mach 0.9, *Journal of Fluid Mechanics* 438 (2001) 277–305.
[22] C.E. Tinney, P. Jordan, The near pressure field of co-axial subsonic jets, *Journal of Fluid Mechanics* 611 (2008) 175–204.

[23] C. Picard, J. Delville, Pressure velocity coupling in a subsonic round jet, *International Journal of Heat and Fluid Flow* 21 (3) (2000) 359–364.
[24] T. Suzuki, T. Colonius, Instability waves in a subsonic round jet detected using a near-field phased microphone array, *Journal of Fluid Mechanics* 565 (2006) 197–226.
[25] R. Reba, S. Narayanan, T. Colonius, Wave-packet models for large-scale mixing noise, *International Journal of Aeroacoustics* 9 (4) (2010) 533–558.
[26] P.J. Morris, A note on noise generation by large scale turbulent structures in subsonic and supersonic jets, *International Journal of Aeroacoustics* 8 (4) (2009) 301–315.
[27] A.V.G. Cavalieri, P. Jordan, Y. Gervais, M. Wei, J.B. Freund, Intermittent sound generation and its control in a free-shear flow, *Physics of Fluids* 22 (11) (2010) 115113.
[28] M. Wei, J.B. Freund, A noise-controlled free shear flow, *Journal of Fluid Mechanics* 546 (2006) 123–152.
[29] D. Juvé, M. Sunyach, G. Comte-Bellot, Intermittency of the noise emission in subsonic cold jets, *Journal of Sound and Vibration* 71 (1980) 319–332.
[30] G. Guj, M. Carley, R. Camussi, A. Ragni, Acoustic identification of coherent structures in a turbulent jet, *Journal of Sound and Vibration* 259 (5) (2003) 1037–1065.
[31] J.I. Hileman, B.S. Thurow, E.J. Caraballo, M. Samimy, Large-scale structure evolution and sound emission in high-speed jets: real-time visualization with simultaneous acoustic measurements, *Journal of Fluid Mechanics* 544 (2005) 277–307.
[32] M. Kœnig, A.V.G. Cavalieri, P. Jordan, J. Delville, Y. Gervais, D. Papamoschou, M. Samimy, S.K. Lele, Farfield pre-filtering and source-imaging for the study of jet noise, in: *16th AIAA/CEAS Aeroacoustics Conference and Exhibit*, Stockholm, Sweden, 2010.
[33] J. Kastner, M. Samimy, J. Hileman, J.B. Freund, Comparison of noise mechanisms in high and low Reynolds number high-speed jets, *AIAA Journal* 44 (10) (2006) 2251–2258.
[34] C. Bogey, C. Bailly, An analysis of the correlations between the turbulent flow and the sound pressure fields of subsonic jets, *Journal of Fluid Mechanics* 583 (2007) 71–97.
[35] J.E. Ffowcs Williams, A.J. Kempton, The noise from the large-scale structure of a jet, *Journal of Fluid Mechanics* 84 (4) (1978) 673–694.
[36] N.D. Sandham, C.L. Morfey, Z.W. Hu, Sound radiation from exponentially growing and decaying surface waves, *Journal of Sound and Vibration* 294 (1) (2006) 355–361.
[37] G.M. Lilley, On the noise from jets, *AGARD CP* 131 (1974) 1–13.
[38] G. Daviller, Etude numérique des effets de temperature dans les jets simples et coaxiaux, Ph.D. Thesis, École Nationale Supérieure de Mécanique et d'Aérotechnique, Poitiers, France, 2010 (in French).
[39] A.V.G. Cavalieri, G. Daviller, P. Comte, P. Jordan, G. Tadmor, Y. Gervais, Using LES to explore sound-source mechanisms in jets, *Procedia Engineering* 6 (2010) 104–113.
[40] D.G. Crighton, Basic principles of aerodynamic noise generation, *Progress in Aerospace Sciences* 16 (1) (1975) 31–96.
[41] D.J. Bodony, S.K. Lele, Low-frequency sound sources in high-speed turbulent jets, *Journal of Fluid Mechanics* 617 (2008) 231–253.
[42] W.K. George, P.D. Beuther, R.E.A. Arndt, Pressure spectra in turbulent free shear flows, *Journal of Fluid Mechanics* 148 (1984) 155–191.
[43] S.K. Lele, Phased array models of shock-cell noise sources, in: *11th AIAA/CEAS Aeroacoustics Conference (26th Aeroacoustics Conference)*, 2005, pp. 1–20.
[44] J. Bridges, Effect of heat on space–time correlations in jet, *12th AIAA Aeroacoustics Conference*, vol. AIAA 2006-2534, 2006.
[45] P. Jordan, Y. Gervais, J.-C. Valière, H. Foulon, Final result from single point measurement, Project Deliverable D3.4, JEAN-EU Fifth Framework Program G4RD-CT2000-00313, Laboratoire d'Études Aérodynamiques, 2002.
[46] H. Tanna, An experimental study of jet noise. Part I: turbulent mixing noise, *Journal of Sound and Vibration* 50 (3) (1977) 405–428.
[47] C. Bogey, C. Bailly, Computation of a high Reynolds number jet and its radiated noise using large eddy simulation based on explicit filtering, *Computers and Fluids* 35 (10) (2006) 1344–1358.
[48] G. Tadmor, D. Bissex, B. Noack, M. Morzynski, T. Colonius, K. Taira, Temporal-harmonic specific pod mode extraction, *AIAA Paper 2008-4190, Fourth AIAA Flow Control Conference*, Seattle, Washington, 2008.
[49] W. Joe, T. Colonius, D. MacMynowski, Optimized waveforms for feedback control of vortex shedding, *Active Flow Control II, Notes on Numerical Fluid Mechanics and Multidisciplinary Design* 108 (2010) 391–404.
[50] A. Michalke, H.V. Fuchs, On turbulence and noise of an axisymmetric shear flow, *Journal of Fluid Mechanics* 70 (1975) 179–205.
[51] U. Michel, The role of source interference in jet noise, in: *15th AIAA/CEAS Aeroacoustics Conference (30th Aeroacoustics Conference)*, 2009, pp. 1–15.
[52] D.J. Bodony, Aeroacoustic Prediction of Turbulent Free Shear Flows, Ph.D. Thesis, Stanford University, 2004.
[53] V. Fleury, C. Bailly, E. Jondeau, M. Michard, D. Juvé, Space-time correlations in two subsonic jets using dual-PIV measurements, *AIAA Journal* 46 (10) (2008) 2498–2509.
[54] D.J. Bodony, S.K. Lele, On using large-eddy simulation for the prediction of noise from cold and heated turbulent jets, *Physics of Fluids* 17 (8) (2005) 085103.

Chapter V

Axisymmetric superdirectivity in subsonic jets

The analysis of the preceding chapters presents evidence that the sound radiated by subsonic jets at low polar angles may be associated with a wave-packet structure, especially when the axisymmetric mode of the far-field pressure is considered.

Based on this, we perform measurements in the acoustic field of jets so as to ascertain if the different azimuthal modes of the far-field pressure can be associated with wavepackets in the flow.

Unlike the previous chapters, the present analysis is done in the frequency domain. In an experiment, one always has information limited by the number of available sensors, and this makes it harder, though not impossible, to analyse the emission of acoustic bursts in the time domain, combining information in the velocity and acoustic fields, as done in chapters II and III. For a first assessment on wave-packet radiation by subsonic jets, we thus analyse our measurements using their spectral content, which is explored separately for each azimuthal mode.

We present in the following pages a pre-print version of the article "Axisymmetric superdirectivity in subsonic jets", accepted for publication in the Journal of Fluid Mechanics.

Under consideration for publication in J. Fluid Mech. 1

Axisymmetric superdirectivity in subsonic jets

ANDRÉ V. G. CAVALIERI[1,2], PETER JORDAN[1], TIM COLONIUS[3] AND YVES GERVAIS[1]

[1]Institut Pprime, Poitiers, France

[2]Instituto Tecnológico de Aeronáutica, São José dos Campos, Brazil

[3]California Institute of Technology, Pasadena, CA

(Received ?? and in revised form ??)

We present experimental results for the acoustic field of jets with Mach numbers between 0.35 and 0.6. An azimuthal ring array of six microphones, whose polar angle, θ, was progressively varied, allows the decomposition of the acoustic pressure into azimuthal Fourier modes. In agreement with past observations, the sound field for low polar angles (measured with respect to the jet axis) is found to be dominated by the axisymmetric mode, particularly at the peak Strouhal number. The axisymmetric mode of the acoustic field can be clearly associated with an axially *non-compact source*, in the form of a wavepacket: the sound pressure level for peak frequencies is found be *superdirective* for all Mach numbers considered, with exponential decay as a function of $(1 - M_c \cos\theta)^2$. While the mode $m = 1$ spectrum scales with Strouhal number, suggesting that its energy content is associated with turbulence scales, the axisymmetric mode scales with Helmholtz number—the ratio between source length scale and acoustic wavelength. The axisymmetric radiation has a stronger velocity dependence than the higher order azimuthal modes, again in agreement with predictions of wave-packet models. We estimate the axial extent of the source of the axisymmetric component of the sound field to be of the order of 6 to 8 jet diameters. This estimate is obtained in two different ways, using, respectively, the directivity shape and the velocity exponent of the sound radiation. The analysis furthermore shows that compressibility plays a significant role in the wave-packet dynamics, even at this low Mach number. Velocity fluctuations on the jet centerline are reduced as the Mach number is increased, an effect that must be accounted for in order to obtain a correct estimation of the velocity dependence of sound radiation. Finally, the higher-order azimuthal modes of the sound field are considered, and a model for the low-angle sound radiation by helical wavepackets is developed. The measured sound for azimuthal modes 1 and 2 at low Strouhal numbers is seen to correspond closely to the predicted directivity shapes.

1. Introduction

Sound generation by subsonic turbulent jets is a problem comprising coupling between the turbulent motions of the jet and the less complex acoustic motions of the sound field. A difference in complexity is apparent in both the structure of the equations that model the two different kinds of motion, and in the experimentally measured fluctuations in the near and far fields.

If we consider, for instance, the azimuthal dependence of the fluctuations in each region, considerably fewer azimuthal Fourier modes are necessary to represent the sound field

31]

than are needed to represent the turbulence (Michalke & Fuchs 1975; Fuchs & Michel 1978). Many researchers have interpreted this low-order azimuthal structure of the sound field as evidence of a corresponding low-order *sound-producing* turbulence structure (see for instance Crow & Champagne 1971; Moore 1977; Juvé *et al.* 1979; Hussain & Zaman 1981; Brown & Bridges 2006; Tinney & Jordan 2008).

A candidate source model for the coherent structures is an axially-extensive wave packet. This model can be motivated theoretically by linear stability theory applied to a steady jet base flow, and physically justified by means of a scale-separation argument. The acoustically-important features of the wave packet are its frequency, wavelength, axial amplification, saturation and downstream decay; the saturation is not necessarily associated with non-linearity, and can be accounted for in a linear framework by appealing to the slow spread of the mean flow (Gudmundsson & Colonius 2011). While Mollo-Christensen (1963, 1967) observed and discussed these features from the point of view of both hydrodynamic stability theory and aeroacoustics, Crow (1972) (see also Crighton 1975) was first to propose a source model, using the framework of Lighthill's (1952) acoustic analogy. The radiation of such sources, for subsonic convection speeds, is highly directive and concentrated at low polar angles (measured with respect to the downstream jet axis).

Similar studies were undertaken by Crighton & Huerre (1990), who evaluated the directivity pattern of different envelope functions for the convected wave, and by Sandham *et al.* (2006), who showed that *temporal* modulation of such convected wave-packets can further enhance sound radiation. Other variants, proposed by Ffowcs Williams & Kempton (1978) and Cavalieri *et al.* (2011*b*), allow inclusion of the intermittency that is observed in high Reynolds number, turbulent jets, i.e. the appearance and disappearance of the trains of turbulent 'puffs' observed by Crow & Champagne (1971).

All of the above models have in common their directivity: sound radiation is concentrated at low polar angles with exponential decay at higher polar angles. The term *superdirectivity* was used by Crighton & Huerre (1990) to describe this characteristic of the sound field, and they showed that acoustic non-compactness is a requirement for such radiation.

Experimentally, there is not, for the moment, a complete consensus regarding the relationship between the superdirectivity of wave-packet models and the sound field of subsonic jets; while the latter does present higher sound intensities at low polar angles, it does not have exponential decay as a function of θ. Superdirectivity has been observed in a forced jet by Laufer & Yen (1983), where forcing was effected at a Strouhal number, based on the momentum thickness, of $\mathrm{St}_{\delta 2} = 0.017$. The excited jet comprised subharmonics of the forcing frequency, and the directivity of the subharmonic sound radiation was observed to decay exponentially with $(1 - M_c \cos\theta)^2$, in agreement with the directivity of the models of Crow (1972) and Ffowcs Williams & Kempton (1978). However, the excitation frequency corresponds to a Strouhal number, based on the jet diameter, of $\mathrm{St} = 5.8$, which is much higher than the Strouhal numbers of the most energetic part of the sound field radiated by free turbulent jets. It is therefore difficult to affirm that Laufer and Yen's experiment corresponds to what occurs in unforced jet flows; the mechanism they studied is most likely restricted to low Mach number jets with laminar boundary layers at the nozzle exit, as discussed by Bridges & Hussain (1987).

On the other hand, Cavalieri *et al.* (2011*a*) have shown, with numerical data from a LES of a Mach 0.9 jet, that a simplified wave-packet *Ansatz*, fitted with velocity data from the LES, can reproduce the radiated sound for the axisymmetric mode of the simulation to within 1.5dB at low polar angles. Furthermore, the axisymmetric mode was found to be highly directive, dominating sound radiation at low polar angles, as found experimentally by Fuchs & Michel (1978) and Juvé *et al.* (1979). These results suggest that the signature of a wave-packet source structure may be observable in high Reynolds number jets if the axisymmetric radiation is isolated from the other azimuthal modes present in the acoustic field.

The objective of the present work is to investigate, experimentally, if such superdirective wave-packet signatures are present in the acoustic field of *unforced* subsonic jets. We decompose the acoustic field measured by a microphone ring array into azimuthal Fourier modes. We then examine the directivity and spectra of each azimuthal mode; polar spacings of $\Delta\theta = 5°$ are used at low emission angles, in order to obtain good angular resolution of the directivity of the different azimuthal modes, and to detect the expected high variations in acoustic intensity. We focus particularly on the axisymmetric mode, in an effort to characterise its structure and ascertain if it is consistent with existing wave-packet models.

In our evaluation of the experimental data we consider a model problem wherein the free-space wave equation is driven by a simplified line source; the form of the source is consistent with Lighthill's acoustic analogy. The model problem considered is not, of course, intended to correspond to the real flow, or to contain all of the physics of jet noise production; its purpose is to allow us to test hypotheses. On one hand we want to check for consistency between experimentally-observed features of the sound field and hypothesised, acoustically-important, features of the flow. On the other hand, we wish to rule out source features that are not consistent with the sound field: for example, a superdirective sound field at low Mach number cannot be produced by an acoustically compact source; an extended axial source region, with significant interference effects, is required to generate such an acoustic field (Crighton & Huerre 1990), and one of the conclusions of the analysis is that the sound radiated to low polar angles is indeed dominated by such as source.

The paper is organised as follows. In § 2 we describe the experimental setup. In § 3 there is a brief review of pertinent results concerning wave-packet sound radiation. This is followed by a presentation and general discussion of the experimental results in § 4. We first focus on the results for the Mach 0.6 jet and show that the axisymmetric mode dominates the peak frequency acoustic field at low polar angles, and the SPL for $\mathrm{St} = 0.2$ is shown to be in agreement with the superdirectivity predicted by non-compact wave-packet models. The same characteristics are observed for the lower Mach number jets ($M = 0.4$, $M = 0.5$). Next, the axial extent of the source is estimated using the wave-packet model of Crow (1972). In § 4.3 we explore the scaling of the different azimuthal modes as a function of Strouhal and Helmholtz numbers to evaluate non-compactness effects on the spectral shape of the individual modes. We consider in § 4.4 the velocity dependence of the different azimuthal modes; the analysis provides a second estimate of the source axial extent which is consistent with the one made using the directivity (provided compressibility effects are correctly accounted for). Extrapolation of the present results to higher subsonic Mach numbers suggests that the dominance of the axisymmetric mode will be further enhanced as the Mach number is increased.

While the main focus of the present work is the axisymmetric mode, results for higher order modes are also shown to be compatible with wavepacket radiation. A theoretical framework is developped in Appendix B, and in § 5 we present comparisons of a model of sound radiation by helical wavepackets with the present experimental results.

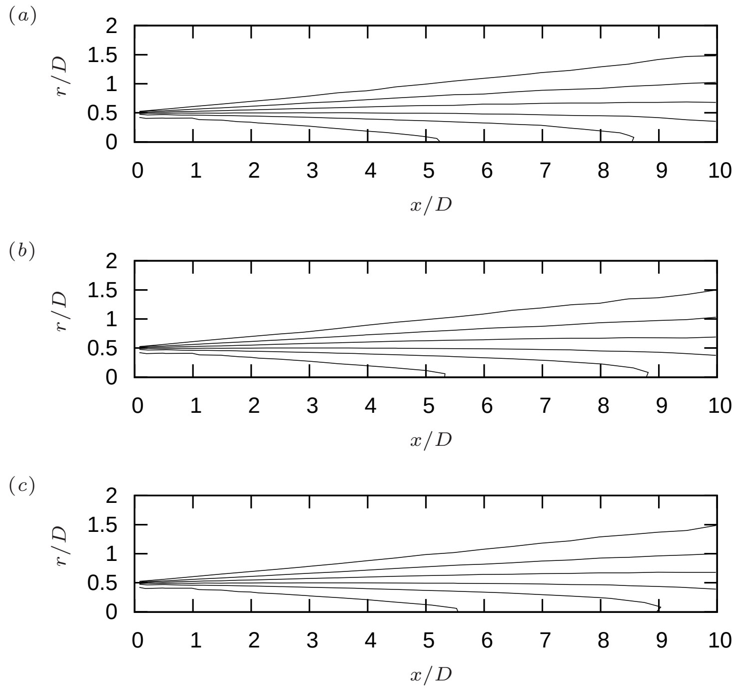

FIGURE 1. Mean axial velocity $\bar{u}_x$ fields for (a) $M = 0.4$, (b) $M = 0.5$ and (c) $M = 0.6$. Contours are equally spaced from $0.1U$ to $0.99U$.

2. Experimental setup

The experiments were performed in the 'Bruit et Vent' anechoic facility at the Centre d'Etudes Aérodynamiques et Thermiques (CEAT), Institut Pprime, Poitiers, France. A photo of the setup is shown in figure 3. Acoustic measurements were made for unheated jets, with acoustic Mach numbers ($M = U/c$, where U is the jet exit velocity and c the ambient sound speed) in the range $0.35 \leqslant M \leqslant 0.6$ with an increment of 0.05. The nozzle diameter, D, was 0.05m. With these conditions, the Reynolds number, $\rho UD/\mu$, varies from 3.7×10^5 to 5.7×10^5, where ρ and μ are, respectively, the density and the viscosity at the nozzle exit. All but the lowest velocity lead to a Reynolds number above 4×10^5, which was seen by Viswanathan (2004) as a critical number above which sound radiation attains asymptotic spectral shapes.

The velocity field is considered in cylindrical coordinates (x, r, ϕ), where x is aligned with the jet axis, r is the radius and ϕ the azimuthal angle; spherical coordinates (R, θ, Φ) are used for the acoustic field, where R is the radius, θ is the polar angle measured from the downstream jet axis and Φ is the azimuthal angle. For both systems, the origin is at the nozzle exit. The three velocity components are denoted u_x, u_r and u_ϕ.

A convergent section was located upstream of the jet exit, with an area contraction of 31. This was followed by a straight circular section of length 150mm; a boundary layer trip was used to force transition 135mm upstream ($2.7D$) of the nozzle exit. Extensive hot-wire velocity measurements were made throughout the jet, including the nozzle exit plane. An *in situ* calibration of the hot wire was performed using Pitot tube measurements as reference values (Tutkun *et al.* 2009). The mean axial velocity fields are shown in figure 1 for Mach numbers of 0.4, 0.5 and 0.6. Aside from a slight lengthening of the potential core as the Mach number is increased, there are only small differences between the normalised mean velocity profiles for these jets.

M	δ (mm)	δ/D	δ_2 (mm)	δ_2/D
0.4	4.5	$9.0 \cdot 10^{-2}$	0.477	$9.5 \cdot 10^{-3}$
0.5	4.25	$8.5 \cdot 10^{-2}$	0.401	$8.0 \cdot 10^{-3}$
0.6	4.25	$8.5 \cdot 10^{-2}$	0.396	$7.9 \cdot 10^{-3}$

TABLE 1. Boundary layer thickness δ and momentum thickness δ_2 at the nozzle exit

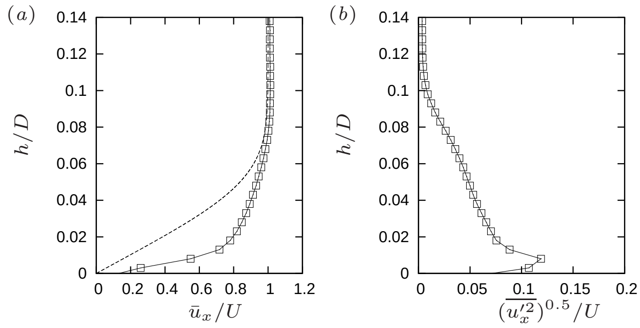

FIGURE 2. Boundary layer profiles at the nozzle exit for the Mach 0.5 jet: (a) mean velocity and (b) rms value. Dashed line in (a) is Blasius profile.

Radial profiles of the velocity field in the nozzle exit plane were obtained with high spatial resolution both upstream and downstream of the exit plane in order to discern the character of the boundary layer. The results, shown in figure 2, indicate that the boundary layers (Bridges & Hussain 1987) are turbulent. The boundary layer and momentum thicknesses at the nozzle exit are shown in table 1. For these estimates, the Crocco-Busemann relation for unitary Prandtl number was used to determine the density across the boundary layer.

Six microphones were deployed on an azimuthal ring in the acoustic field with a fixed angle θ to the downstream jet axis. The setup is shown in figure 3. The ring has a diameter of $35D$. The entire array was displaced incrementally along the jet axis in order to characterise the sound field as a function of θ. On account of the resulting differences in the distance, R, between the nozzle exit and the microphones, a $1/R$ scaling is applied to the acoustic pressure in order to rescale the measurements to a fixed distance of $R = 35D$. The circumferential homogeneity of the acoustic field was verified by comparing spectra of the individual microphones, shown in figure 3(b). The pressure from the six microphones was used to decompose the far acoustic field into azimuthal Fourier modes. The procedure is described in Appendix A, where we also use the coherence between neighbouring microphones to assess the accuracy of the Fourier series. This evaluation shows the procedure is appropriate up to Strouhal number of unity for the present microphone ring, which is the range of frequencies we focus on in the present work.

3. Sound radiation by an axisymmetric wave-packet

In this section we recall the results of Crow (1972) (see also Crighton 1975, sec. 10) for a simple wave-packet source. The results of this model are used for analysis of the experimental results presented in the following sections. The model is based on the acoustic analogy of Lighthill (1952). The continuity and Navier-Stokes equations are combined and rewritten as an inhomogeneous free-space wave equation with nonlinear source terms (*a*) (*b*)

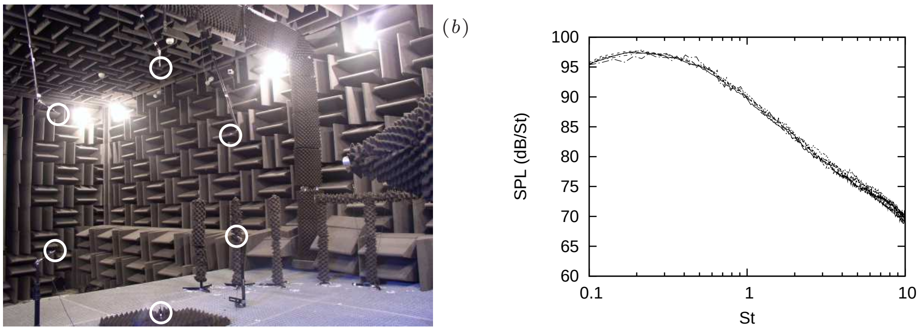

FIGURE 3. (*a*) Experimental setup (microphones are highlighted with white circles); (*b*) spectra of the six microphones at $\theta = 30°$ and $M = 0.6$

(Lighthill's stress tensor T_{ij}) on the right-hand side that depend on turbulent fluctuations:

$$\frac{\partial^2 \rho}{\partial t^2} - c^2 \nabla^2 \rho = \frac{\partial^2 T_{ij}}{\partial x_i \partial x_j} \tag{3.1}$$

with

$$T_{ij} = \rho u_i u_j + (p - c^2 \rho)\delta_{ij}. \tag{3.2}$$

In the spirit of the Lighthill's theory, the problem considered is an *analog* to a compressible, turbulent flow. The source terms on the right-hand side of eq. (3.1) are considered as given, and the radiated sound can be calculated, for a free jet, using the free-field Green's function.

In Crow's model, the wave equation is driven by a simplified line source S_{xx}, constructed using the axisymmetric part of the T_{xx} term alone (i.e. a distribution of axially-aligned, longitudinal quadrupoles), as

$$S_{xx}(x, m = 0, \omega) = \int T_{xx}(x, r, m = 0, \omega) r \mathrm{d}r. \tag{3.3}$$

where m is the azimuthal Fourier mode, and ω the frequency, so that the far-field pressure is given, as shown in Appendix B, as

$$p(R, \theta, m = 0, \omega) = -\frac{k_a^2 \cos^2 \theta \mathrm{e}^{-\mathrm{i}k_a R}}{2R} \int_{-\infty}^{\infty} S_{xx}(x, m = 0, \omega) \mathrm{e}^{-\mathrm{i}k_a x \cos\theta} \mathrm{d}x, \tag{3.4}$$

where k_a is the acoustic wavenumber ω/c.

This line source model comprises a convected wave of frequency ω and wavenumber k, modulated by a Gaussian with characteristic length L,

$$S_{xx}(x, m = 0, \omega) = \rho_0 U \hat{u}_x \frac{D^2}{4} \mathrm{e}^{-\mathrm{i}kx} \mathrm{e}^{-\frac{x^2}{L^2}}, \tag{3.5}$$

where ρ_0 is the density of the undisturbed fluid and $\hat{u}_x$ the streamwise velocity fluctuation amplitude, which is obtained by the radial integration in eq. (3.3) of a radially-constant T_{xx}, given as

$$T_{xx}(x, r, m = 0, \omega) = 2\rho_0 U \hat{u}_x \mathrm{e}^{-\mathrm{i}kx} \mathrm{e}^{-\frac{x^2}{L^2}} \tag{3.6}$$

between 0 and $D/2$. An envelope function given by a Gaussian, as in eq. (3.6), is supported by the near-field measurements of forced jets by Laufer & Yen (1983), and of unforced, heated jets with Mach numbers ranging from 0.9 to 1.58 (Reba *et al.* 2010). Gaussian envelopes were also seen to match envelopes taken from the velocity field of large eddy simulations of cold $M = 0.9$ jets (Cavalieri *et al.* 2011*b*). Finally, the experimental near-field pressure results presented by Gudmundsson & Colonius (2011), including an unheated jet at $M = 0.5$ and $\mathrm{Re} = 7 \times 10^5$, suggest that a Gaussian envelope may be appropriate to model wavepackets in jets with the operating conditions of the present work.

The line source approximation in eq. (3.6) can be justified in Lighthill's analogy for the axisymmetric part of the source if we consider radial compactness, i.e. the jet diameter is much smaller than the acoustic wavelength, as shown in Appendix B. This is the case for low values of the Strouhal and Mach numbers.

Furthermore, in a linear problem, such as Lighthill's, a given azimuthal component of the source generates the same azimuthal mode in the sound field. This assumption has been used, for instance, by Michalke (1970, 1972) or Mankbadi & Liu (1984), and is also shown in the derivation of Appendix B. The line-source model in eq. (3.6) is therefore solely related to the axisymmetric radiation. A similar model for helical wavepackets is presented in § 5.

Evaluation of the far field pressure in the time domain leads to

$$p(R, \theta, m = 0, t) = -\frac{\rho_0 U \tilde{u} M_c^2 (kD)^2 L \sqrt{\pi} \cos^2\theta}{8R} \mathrm{e}^{-\frac{L^2 k^2 (1 - M_c \cos\theta)^2}{4}} \mathrm{e}^{\mathrm{i}\omega\left(t - \frac{R}{c}\right)}, \tag{3.7}$$

where M_c is the Mach number based on the phase velocity U_c of the convected wave. The acoustic intensity in the far acoustic field can be calculated as $p^2/(\rho_0 c)$.

The models of Ffowcs Williams & Kempton (1978) and Cavalieri *et al.* (2011*b*), which include jitter in this source shape, also present the same exponential function $\exp(-L^2 k^2 (1 - M_c \cos\theta)^2/4)$ for the pressure. This exponential polar variation is referred to as *superdirectivity* (Crighton & Huerre 1990).

We note that superdirectivity results if the characteristic length, L, of the Gaussian is large compared to the convected wavelength, i.e. $kL = 2\pi L/\lambda_c \gg 1$. The superdirectivity can thus be seen to result from axial interference in an axially-extended source comprising more than one oscillation wavelength. For subsonic convection velocities, the interference between regions of positive and negative source strength results in the sound field being beamed towards low angles, an almost complete cut-off occurring at high polar angles. This is illustrated in figure 4, where source shapes and corresponding directivities are plotted for different values of kL, considering $M_c = 0.36$. For the compact limit, $kL \to 0$, the directivity of the source is given by $\cos^4\theta$ for the acoustic intensity. For small values of the characteristic length, L, the dependence of the directivity on L is weak. However, as the axial interference becomes significant, the directivity changes considerably, becoming increasingly concentrated at low axial angles, as can be seen in figure 4(b) for $kL = 6$. In this case, the directivity shape is dominated by the exponential term in eq. (3.7), and is close to a straight line when plotted as a function of $(1 - M_c \cos\theta)^2$. For this source extent, as shown in figure 4(a), there is interference between three neighbouring wavefronts in the source, leading to the observed superdirectivity.

A further effect of non-compactness can be seen in the velocity dependence of sound radiation. A compact source will lead to a U^8 velocity dependence of the acoustic intensity. But as non-compact effects become significant, the velocity dependence changes, and may be other than a power law; indeed, the expression in eq. (3.7) is not a power law in the velocity. Figure 4(c) shows the velocity exponent, n, of the acoustic intensity for $M = 0.5$, evaluated using eq. (3.7). For this calculation we assume constant Strouhal number and source extent, L/D. We note that a compact wave-packet, with, for example

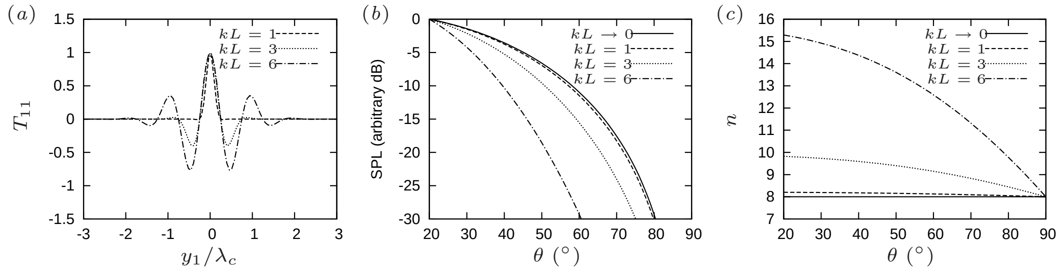

FIGURE 4. (a) Wave-packet shapes, (b) corresponding directivities for $M_c = 0.36$ with values at $\theta = 20^\circ$ were fixed at 0dB, and (c) velocity exponents, taken with a derivative around $M_c = 0.3$.

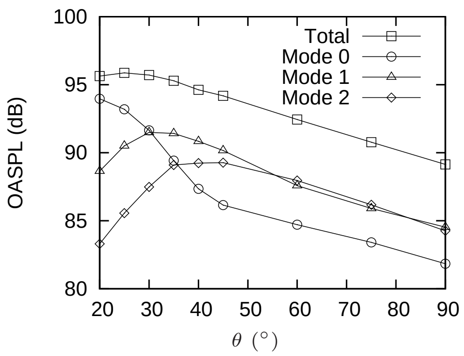

FIGURE 5. Directivity for the $M = 0.6$ jet

$kL = 1$, has a velocity exponent close to 8 for all angles; increases in L lead to higher velocity exponents, especially for lower axial angles.

4. Experimental results and analysis

4.1. *Mach 0.6 jet*

Figure 5 shows the directivity of the Mach 0.6 jet for the measured angles, as well as the contributions of the different azimuthal modes. The axisymmetric mode presents a marked directivity towards the low axial angles. Indeed, there is a 7.8 dB increase in the sound intensity between 45° and 20°. The other azimuthal modes increase more gradually over $45^\circ \leqslant \theta \leqslant 90^\circ$, with a slope close that of the axisymmetric mode in the same angular sector. For lower angles, modes 1 and 2 decay with decreasing angle. Similar directivities for the azimuthal modes 0, 1 and 2 have been observed in a large eddy simulation of a Mach 0.9 jet (Cavalieri *et al.* 2011a).

Spectra for angles 20°, 30° and 40° are shown in figure 6. The increase of mode 0 is mostly concentrated in the lower frequencies. For Strouhal numbers greater than 1 there is still a dominance in the total spectra of modes 1 and 2.

To evaluate the directivity of the spectral peak, the SPL for St = 0.2 is shown in figure 7. We see that for this frequency there is an even higher directivity of mode 0, with an increase of 15.4 dB between 45° and 20°, i.e. a factor of 34 in the acoustic intensity.

As presented in § 3, models representing the wave-packet form of axisymmetric coherent structures in jets predict an exponential change of sound intensity with $(1 - M_c \cos\theta)^2$. Figure 7(b) presents the SPL at St = 0.2 as a function of this parameter, considering M_c to be equal to $0.6M$; changes in M_c from 0.5 to 0.7 were seen to have little impact on the directivity shape. The constant slope in the sector $20^\circ \leqslant \theta \leqslant 45^\circ$ indicates that

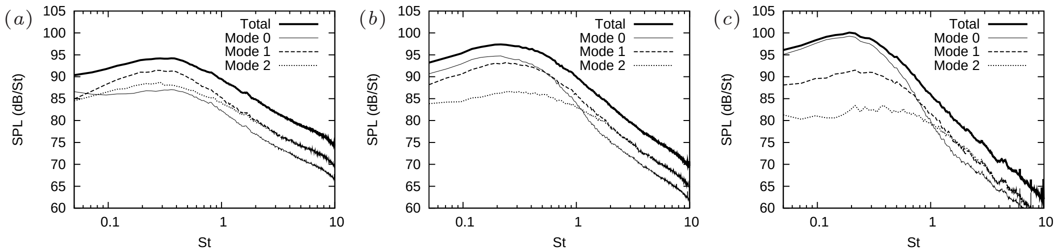

FIGURE 6. Spectra of individual modes for (*a*) $\theta = 40°$, (*b*) $\theta = 30°$ and (*c*) $\theta = 20°$

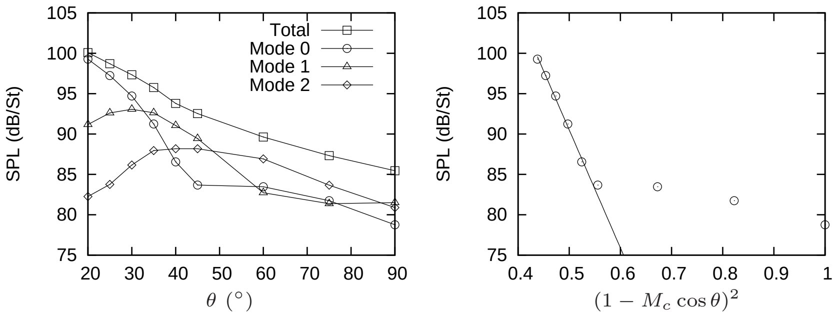

FIGURE 7. SPL for St = 0.2 for the Mach 0.6 jet as a function of (*a*) θ and (*b*) $(1 - M_c \cos\theta)^2$.

there is indeed an exponential change. Furthermore, since these models are based on a line source distribution, the radiated sound field is axisymmetric. The comparison with the experimental mode 0 is thus justified.

The directivity shape of azimuthal modes 1 and 2 in figure 7 is shown in § 5 to be compatible with a source constituted of helical wavepackets, which do not produce superdirective radiation. Further discussion of the higher azimuthal modes is postponed to § 5, where a model for the sound radiation by helical wavepackets is developed.

The superdirectivity observed for the axisymmetric mode is present for a range of frequencies near the peak as can be seen in figure 8. We note that for $0.1 \leqslant \mathrm{St} \leqslant 0.3$ the directivity changes very little, and a linear fit made for St = 0.2 closely matches the directivity for both St = 0.1 and St = 0.3. For higher frequencies, we note that as the angle is increased, the SPL tends to the same exponential decay observed for the peak frequency. As the frequency is increased, this decay is progressively less significant: whereas a decay of 15.4dB between 20° and 45° is observed for St = 0.2, for St = 0.4 we have a decay of 10.7dB, and for St = 0.6 we have 7.7dB (now between 25° and 45°, for the maximum level is obtained for $\theta = 25°$). Although the decay at higher St differ from that at St = 0.2, the high-frequency directivity remains exponential, as seen in figure 9 for St = 0.4, 0.6 and 0.8, but with progressively lower slopes. The deviations from the straight lines for low angles (20 and 25 degrees) that are measured for higher frequencies may be due to propagation effects; this is discussed in more detail in the following section.

The results of figure 8 and the mode-0 spectra shown in figure 6 suggest that the results for St = 0.2 are representative of a range of frequencies around the spectral peak.

4.2. *Lower Mach numbers*

The trends observed in the $M = 0.6$ jet were also found for the lower Mach number flows. Figures 10 and 11 show spectra for $M = 0.4$ and $M = 0.5$, respectively. The results are similar to the $M = 0.6$ jet. However, we note that as the Mach number is reduced, the dominance of the axisymmetric mode at, say, $\theta = 20°$ or $\theta = 30°$ is decreased. This

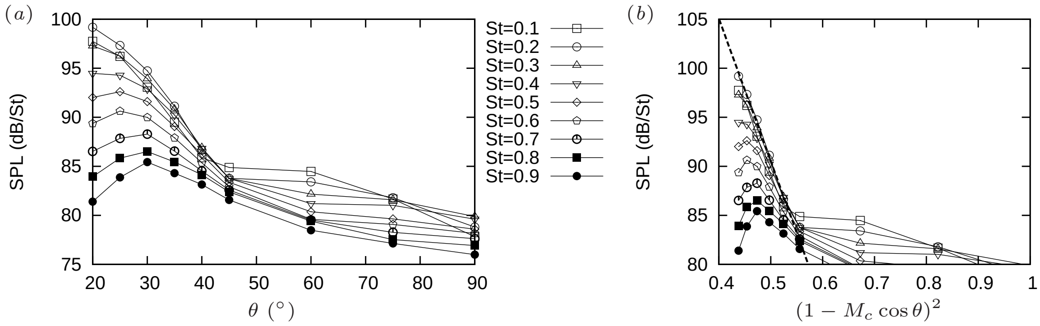

FIGURE 8. Directivity for the axisymmetric mode as a function of Strouhal number and of (a) θ and (b) $(1 - M_c \cos\theta)^2$.

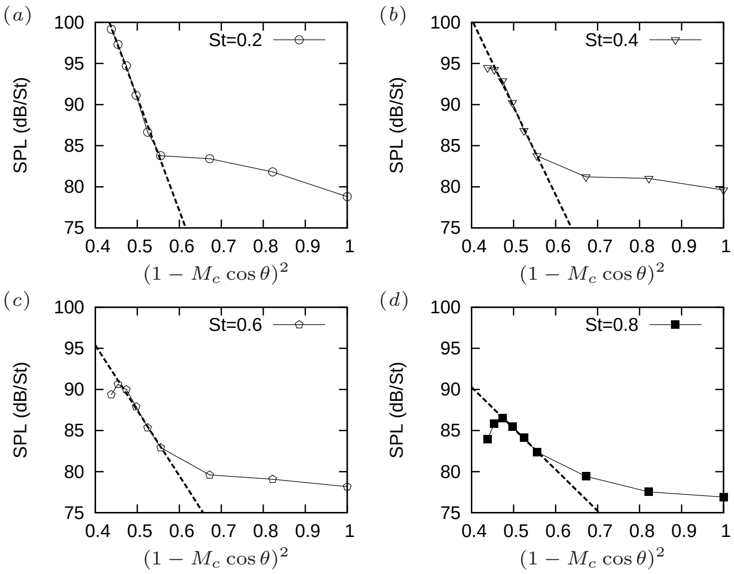

FIGURE 9. Directivity for the axisymmetric mode as a function of $(1 - M_c \cos\theta)^2$ for (a) St $= 0.2$, (b) St $= 0.4$, (c) St $= 0.6$ and (d) St $= 0.8$.

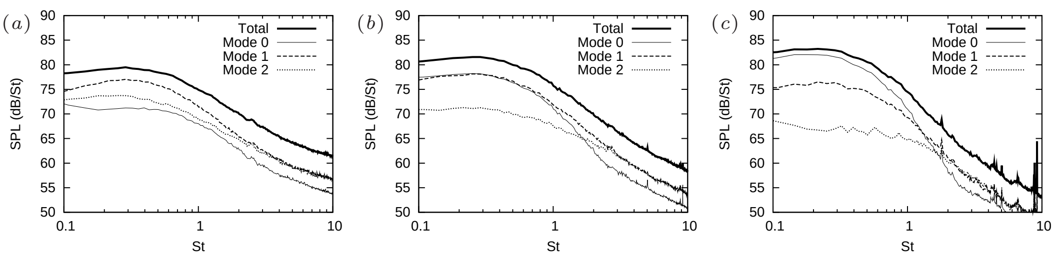

FIGURE 10. Spectra of individual modes for $M = 0.4$ and (a) $\theta = 40^\circ$, (b) $\theta = 30^\circ$ and (c) $\theta = 20^\circ$

effect in the OASPL is shown in figure 12, and for the SPL at St $= 0.2$ in figure 13. For convenience, we replot, in both figures, the results for the $M = 0.6$ jet.

For $M = 0.4$ to $M = 0.6$, the SPL at St $= 0.2$ is shown as a function of $(1 - M_c \cos\theta)^2$ in figure 14. We note once more the same trends for all three Mach numbers, with an exponential decay of the acoustic intensity as a function of $(1 - M_c \cos\theta)^2$, indicating again the superdirectivity of the axisymmetric mode.

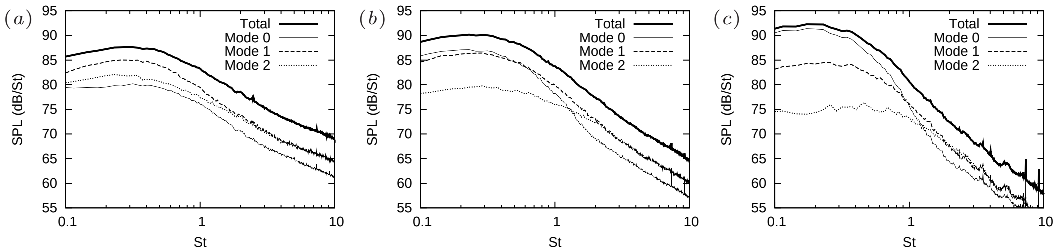

FIGURE 11. Spectra of individual modes for $M = 0.5$ and (a) $\theta = 40°$, (b) $\theta = 30°$ and (c) $\theta = 20°$

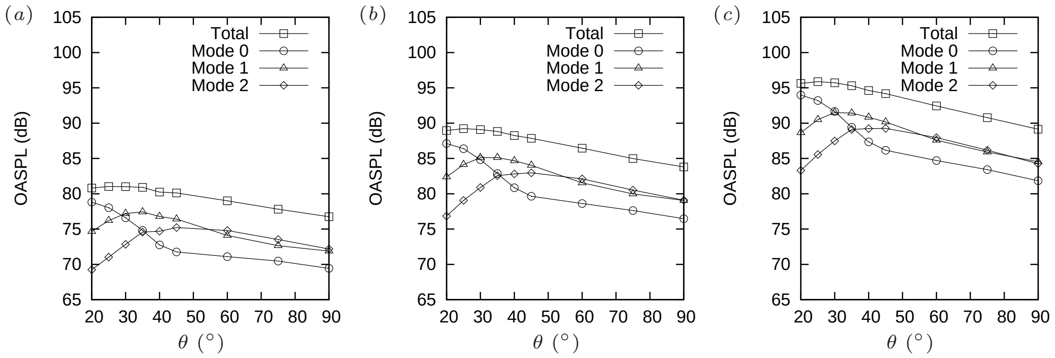

FIGURE 12. Directivity for (a) $M = 0.4$, (b) $M = 0.5$ and (c) $M = 0.6$.

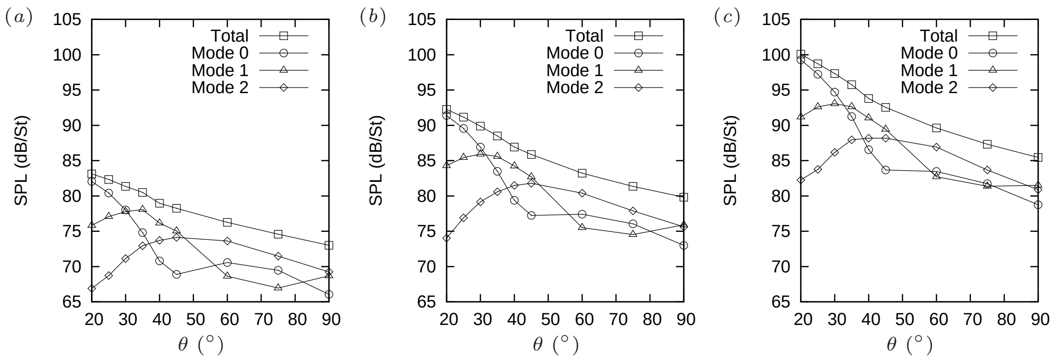

FIGURE 13. SPL for $\mathrm{St} = 0.2$ (a) $M = 0.4$, (b) $M = 0.5$ and (c) $M = 0.6$.

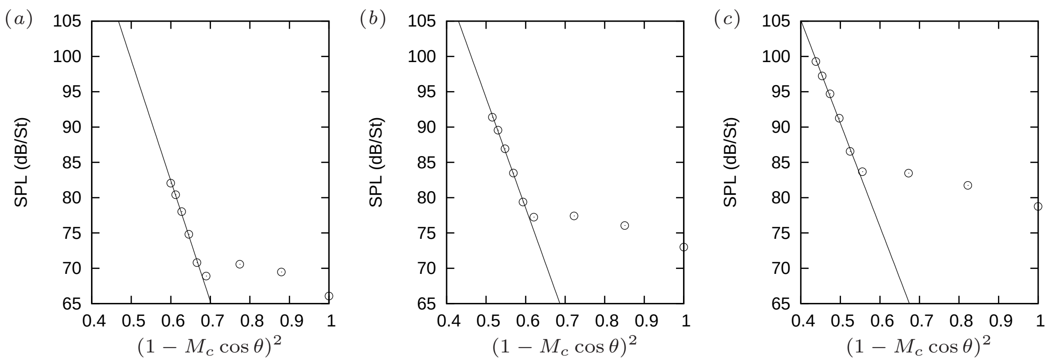

FIGURE 14. SPL of the axisymmetric mode for $\mathrm{St} = 0.2$ and (a) $M = 0.4$, (b) $M = 0.5$ and (c) $M = 0.6$.

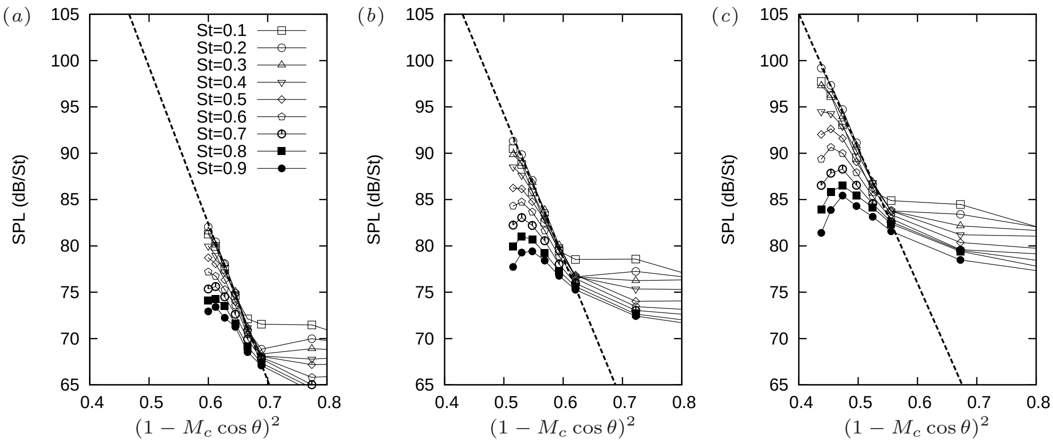

FIGURE 15. SPL of the axisymmetric mode as a function of $(1 - M_c \cos\theta)^2$ for (a) $M = 0.4$, (b) $M = 0.5$ and (c) $M = 0.6$.

M	SPL($\theta = 20°$) − SPL($\theta = 45°$)(dB)	kL	L/D
0.4	13.2	6.50	3.10
0.5	14.1	6.34	3.03
0.6	15.4	6.40	3.06

TABLE 2. Estimation of source extent using the axisymmetric mode at St = 0.2

The behaviour observed at other frequencies is shown in figure 15 for $M = 0.4$ and $M = 0.5$. The $M = 0.6$ results are repeated for convenience. We note that for the three cases the directivity shapes for St = 0.1 and 0.3 closely followm the straight line fitted for St = 0.2, showing that superdirectivity is present over a range of frequencies. Moreover, as the Mach number decreases, a broader range of frequencies have directivities close to that of the St = 0.2 component: the change of slope observed with increasing St, shown in figure 9 for $M = 0.6$, is less significant at lower Mach numbers.

Another feature of the directivity shapes in figure 15 is that for high frequencies there is a departure from the superdirective behaviour, a reduction of SPL occurring at the lower angles. This is especially marked for $M = 0.6$ at Strouhal numbers of 0.5 and above. For lower Mach numbers the effect is significantly reduced. A possible explanation can be given in terms of propagation effects such as refraction by the mean shear, which tends to decrease the sound at low polar angles, especially at higher Mach number. This is not accounted for by the simplified model of eqs. (3.6) and (3.7), which is based on Lighthill's analogy. This point merits further study, but is outside the scope of the present work.

Since the directivity for St = 0.2 is exponential between $\theta = 20°$ and $\theta = 45°$, we can use the measured exponential decay rate to estimate the wave-packet axial extent, L/D, via the wave-packet *Ansatz* described in § 3 and an assumed value of $U_c/U = 0.6$. A best fit of the experimental data then results in the estimated values of L/D given in Table 2

The use of Crow's wave-packet model results in a consistent estimation of L/D for all three Mach numbers, with a value close to 3. In turn, this value of L/D indicates that the wave-packet extends over an axial region of 6–8 jet diameters, similar to the result shown in figure 4(a) for $kL = 6$ (setting $U_c/U = 0.6$ and St = 0.2, $\lambda_c = 3D$). This modulation is such that *three* oscillations are present in the source; i.e. there is

M	SPL($\theta = 20°$) − SPL($\theta = 45°$)(dB)	kL	L/D
0.4	11.8	5.94	1.42
0.5	11.8	5.48	1.31
0.6	10.7	4.75	1.13

Table 3. Estimation of source extent using the axisymmetric mode at St = 0.4

M	SPL($\theta = 25°$) − SPL($\theta = 45°$)(dB)	kL	L/D
0.4	8.8	5.18	0.82
0.5	8.3	4.50	0.72
0.6	7.7	3.92	0.62

Table 4. Estimation of source extent using the axisymmetric mode at St = 0.6

M	SPL($\theta = 30°$) − SPL($\theta = 45°$)(dB)	kL	L/D
0.4	6.1	4.38	0.46
0.5	5.1	3.16	0.42
0.6	4.1	1.81	0.29

Table 5. Estimation of source extent using the axisymmetric mode at St = 0.8

significant axial interference, as discussed in § 3, leading to the observed superdirectivity in the radiated sound field.

The above estimate of the axial source extent is in agreement with results reported by Hussain & Zaman (1981), who educed, using phase-averaged measurements in a jet excited at St = 0.3, a flow pattern comprising a train of three coherent structures, characterised by regions of closed vorticity contours, and spanning a region of up to 7 jet diameters from the nozzle exit. This also agrees with the experimental observations of Tinney & Jordan (2008), who studied the near pressure field of unforced coaxial jets, and found a subsonically convected wave extending up to 8 secondary jet diameters downstream of the nozzle exit. In their study, the first two POD modes of the near-field pressure had the shape of a sine and a cosine modulated by an envelope function comprising three oscillation cycles.

The same estimation was performed using the directivities observed at St = 0.4, 0.6 and 0.8, and the results are shown in tables 3, 4 and 5, respectively. For the Mach 0.4 jet the estimated source extent for St = 0.4 is roughly half that estimated for St = 0.2. Since the wavelength of the convected wave is also halved as the Strouhal number is increased, this means that in this case the source also presents *three* spatial oscillations. As the Mach number is increased the estimated values of L/D are reduced; however, this does not mean that the source becomes compact, since we are still far from the $kL \to 0$ limit, as seen in § 3. Estimation of the source extent for St = 0.6 shows similar trends to those observed at St = 0.4. The estimated values of L/D become lower as the Mach is increased, but the wave-like behaviour of the source is preserved.

For St = 0.8 the source extent is substantially reduced at higher Mach, and for $M = 0.6$ we have a value of kL of 1.8, approaching the compact limit. However, the apparent "cone of silence" observed in this case (see figure 15) suggests that the estimation of the source extent may be biased here by flow-acoustic effects.

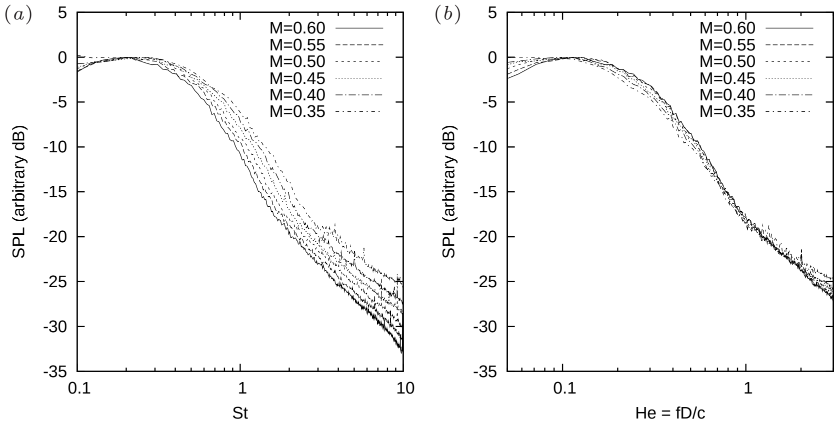

FIGURE 16. Spectral shapes for azimuthal mode 0 and $\theta = 30°$ as a function of (*a*) Strouhal number and (*b*) Helmholtz number.

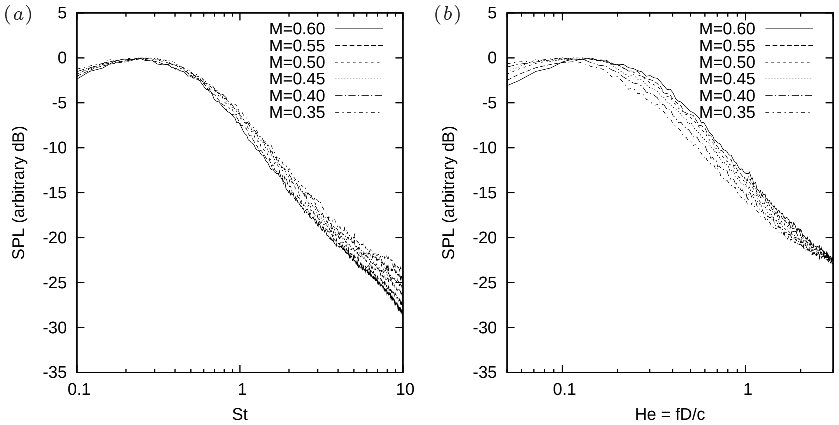

FIGURE 17. Spectral shapes for azimuthal mode 1 and $\theta = 30°$ as a function of (*a*) Strouhal number and (*b*) Helmholtz number.

4.3. *Spectral shape for the different azimuthal modes*

We now examine the scaling of the spectra with Mach number. Figures 16 and 17 show, respectively for the axisymmetric and first azimuthal mode, the spectra normalised by their maximum values, and plotted versus either Strouhal number, fD/U, or Helmholtz number, fD/c. The spectra of the axisymmetric component of the sound field collapse better when plotted as a function of Helmholtz number, whereas azimuthal mode 1 collapses better when plotted as a function of Strouhal number.

The Helmholtz number is related to the source compactness, as $\mathrm{He} = D/\lambda$, where λ is the acoustic wavelength. If the source extent is comparable to the acoustic wavelength, the Helmholtz number will play a significant role, for it is a measure of the interference effects from the different parts of the source; discussion of the significance of the Helmholtz number for aeroacoustic applications can be found in the work of Fuchs & Armstrong (1978). The scaling of the axisymmetric mode with the Helmholtz number suggests again that the non-compactness of the source plays an important role in the radiation of sound to low axial angles. The scaling of low angle spectra with Helmholtz number (without separation into azimuthal modes) has been observed previously by Lush (1971), Tanna (1977) and Viswanathan (2004). We show here that as the axisymmet-

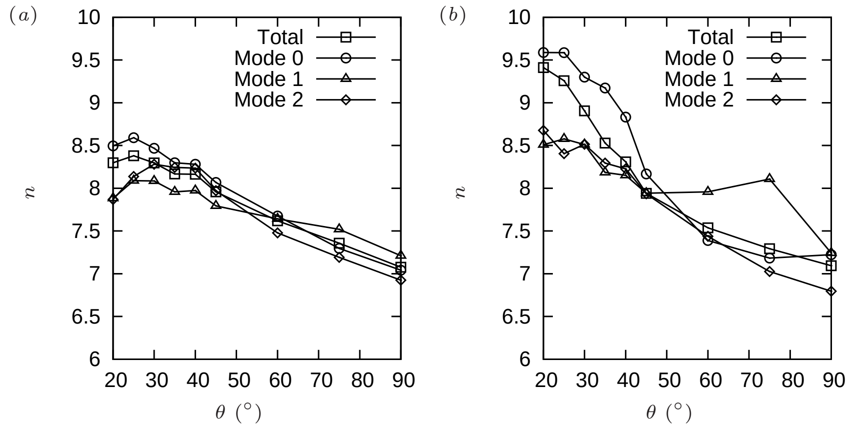

FIGURE 18. Velocity exponent n obtained by fits of the (a) OASPL and (b) SPL for St = 0.2.

ric mode accounts for most of the radiation at these angles, the He scaling in the total spectrum is predominantly due to the axisymmetric component. On the other hand, the Strouhal scaling found, for instance at 90° to the jet axis, can be related to the mode-1 scaling with St, seen in figure 17(a), as at higher angles the axisymmetric radiation is no longer dominant.

4.4. *Velocity dependence of the sound radiation for each azimuthal mode*

Close examination of figure 12 shows that the velocity dependence of the OASPL at each angle is not the same for the different azimuthal modes. Such variations are also observed in the SPL for St = 0.2, shown in figure 13. In order to evaluate this velocity dependence as a function of both θ and azimuthal mode, we performed fits of both OASPL and SPL for St = 0.2 as

$$\mathrm{OASPL(dB)}(m,\theta) = a(m,\theta) + 10n(m,\theta)\log_{10}(M), \tag{4.1}$$

$$\mathrm{SPL(dB/St)}(m,\theta) = a(m,\theta) + 10n(m,\theta)\log_{10}(M), \tag{4.2}$$

respectively, to obtain velocity scalings of the sound radiation, as in previous work (Zaman & Yu 1985; Viswanathan 2006; Bogey *et al.* 2007). This was done for the total values of OASPL and SPL, and also for the individual contributions of azimuthal modes 0, 1 and 2. Results are shown in figure 18.

The velocity exponents for OASPL shown in figure 18(a) do not show clear trends among the different azimuthal modes for higher angles. However, we note that for low angles the mode-0 exponent is higher than both that of the other azimuthal modes and of the total spectrum. If we extrapolate these trends for higher Mach numbers, we can expect that for low angles the mode-0 dominance in OASPL will be even more pronounced.

Considering the velocity dependence of SPL for St = 0.2 alone, shown in figure 18(b), these effects are even more marked, the velocity exponent of the axisymmetric mode for low angles being considerably higher than that of the other modes. This, as shown in § 3, is another indication of non-compactness of the source.

Naive use of the values obtained for n for St = 0.2 to estimate the source length based on the wave-packet model of § 3 leads to a source extent of $L/D \approx 1.5$ (source extent of 3–4 jet diameters) which is roughly half that estimated in § 4.3 based on the directivity. However, the derivation of the velocity exponent with the Crow (1972) wave-packet model assumes that the source extent and maximum amplitude do not change with

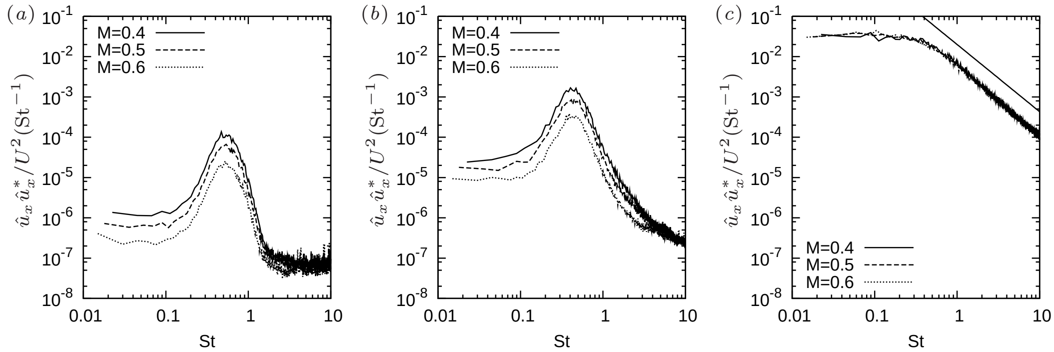

FIGURE 19. Velocity spectra on the jet centerline for (a) $x = 2D$ and (b) $x = 4D$, and (c) on the jet lipline for $x = 2D$. The straight line in (c) represents a $-5/3$ slope

increasing Mach number, and it also assumes a constant ratio between convection and jet speeds. Moreover, compressibility affects the development of the velocity fluctuations as a function of Mach number (see Lele 1994 and references therein for studies on compressible mixing layers). Linear stability theory also predicts lower growth rates as the Mach number is increased (see, for instance, reviews by Michalke 1984 and Morris 2010).

Velocity spectra on the jet centerline are shown in fig. 19 for $x = 2D$ and $x = 4D$. The centerline spectrum is chosen to highlight the axisymmetric mode of the velocity fluctuations† We see that for both axial positions the amplitude of the velocity fluctuations, when normalised by the jet velocity, *decreases* as the Mach number is increased. This can be attributed to the lower growth rate predicted by stability theory for higher Mach numbers, since the differences in the mean velocity profiles are slight (see figure 1) and could not cause such a significant effect. The reduction of the normalised amplitude for higher Mach numbers was also observed by Armstrong *et al.* (1977) and Suzuki & Colonius (2006) in experimental results for the near-field pressure. On the other hand, for the velocity spectra on the jet lipline, shown in figure 19(c), the results for the three Mach numbers collapse. The variation of the Mach number from 0.4 to 0.6 has therefore a significant effect on the evolution of the axisymmetric mode, but no detectable effect on the full jet turbulence.

This suggests that in order to appropriately account for the velocity dependence in the axisymmetric wave-packet model of § 3, one should account for the reduction of the normalised amplitude $\hat{u}_x/U$ as the Mach number is increased, leading to lower velocity exponents than the results of fig. 4(c). To perform an estimation of the source extent that accounts for compressibility effects in the evaluation of n, we have plotted in figure 20 the power spectral density for the centerline velocity for St $= 0.2$. We note that the decrease in the power can be roughly approximated by the straight line in the figure with a slope of -1.8. Using this expression in the evaluation of the velocity exponent n of the sound radiation of Crow's wave-packet model we obtain the results shown in figure 20(b). The exponents for $kL = 6$ are close to the experimental values in the angular range $20° \leqslant \theta \leqslant 45°$ where superdirectivity was observed, consistent with the value of kL educed from the directivity in § 4.2.

† In stability theory the boundary conditions on the jet centerline are of zero transverse velocity and arbitrary finite streamwise velocity for $m = 0$, and zero streamwise velocity for all higher order azimuthal modes (Batchelor & Gill 1962); therefore, we expect the centerline spectrum to be representative of the axisymmetric mode; indeed, such measurements have been used in the past for comparison with stability results (Crow & Champagne 1971; Michalke 1971; Crighton & Gaster 1976).

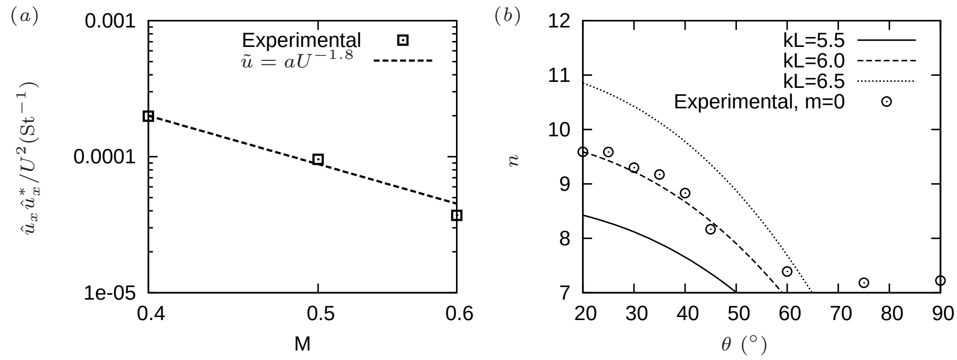

FIGURE 20. (a) Velocity dependence of the power spectral density of the centerline velocity at $x = 4D$ for St = 0.2, (b) Velocity exponent of sound radiation by wave-packets assuming $\tilde{u} = aU^{-1.8}$

Although the use of a velocity exponent n is useful to scale jet data at different Mach numbers and predict the increase of sound level as the jet velocity inreases, it should be noted that non-compact sources, such as are described by the wave-packet model of eq. (3.7), lead to a velocity dependence for the sound intensity that departs from a U^n form. As the Mach number range of the present tests is not comprehensive, a conclusive answer is not presently available regarding the precise form of the velocity dependence for the different azimuthal modes. Deviations from a U^n law can be seen in the results of Lush (1971), which spanned Mach numbers from 0.3 to 1.

5. Sound radiation by helical wavepackets

The far-field sound radiation from a given azimuthal mode of the T_{xx} component of Lighthill's stress tensor, derived in Appendix B, is

$$p(R, \theta, m, \omega) = -\frac{\mathrm{i}^m k_a^2 \cos^2\theta \mathrm{e}^{-\mathrm{i}k_a R}}{2R} \int \mathrm{e}^{\mathrm{i}k_a x \cos\theta} \mathrm{d}x \int T_{xx}(x, r, m, \omega) \times J_m(k_a r \sin\theta) r \mathrm{d}r. \qquad (5.1)$$

The line source approximation, used in the analysis of the preceding section, and derived in Appendix B for the axisymmetric mode, cannot be applied for the other azimuthal modes. The reason is the presence of $\sin\theta$ in the argument of the Bessel function in eq. (5.1); even though equivalent line sources can be obtained after the radial integration, a different line distribution is obtained for each polar angle, and hence no single line source is valid for all θ.

Another difference when we evaluate the sound radiation for a helical mode is that the radial distribution of fluctuations plays a significant role, even for small frequencies and Mach numbers. The Bessel functions of first kind of order m are proportional to x^m for low x; thus, for the axisymmetric mode they can be approximated as constant, whereas for the other azimuthal modes their precise shape will influence the result of the radial integral in eq. (5.1). Moreover, the assumption that the axial velocity fluctuations do not change radially, used in Crow's model, can only be used for the axisymmetric mode, since for helical modes the axial velocity fluctuation on the jet centerline is zero (Batchelor & Gill 1962).

In order to obtain the directivity of the sound radiated by the helical modes, we

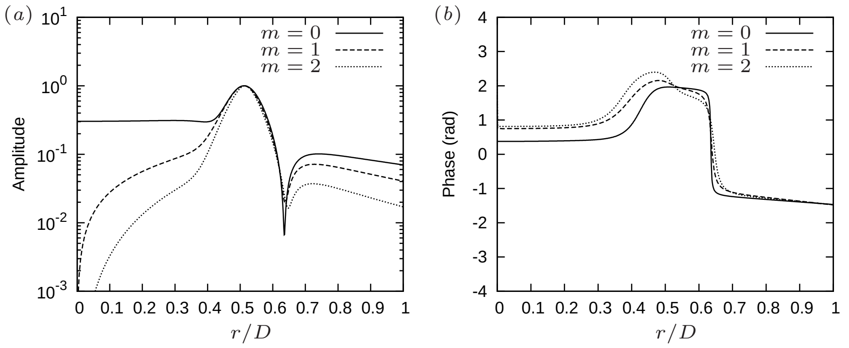

FIGURE 21. Axial velocity eigenfunctions obtained with linear stability theory for $x = D$ and St $= 0.2$: (a) amplitude and (b) phase.

consider the radial structure of T_{xx}, modelling it as

$$T_{xx}(x, r, m, \omega) = 2\rho_0 \bar{u}_x(r) \hat{u}_x(r, m, \omega) \mathrm{e}^{-\mathrm{i}kx} \mathrm{e}^{-\frac{x^2}{L^2}}, \tag{5.2}$$

where $\bar{u}_x(r)$ was taken as the mean velocity profile at $x = D$, and the velocity fluctuations $\hat{u}_x(r, m, \omega)$ were modelled as linear instability waves of frequency ω and azimuthal mode m. A linear spatial stability analysis is performed, based on a parallel shear-flow whose mean velocity profile is that measured at $x = D$, and the most unstable mode used in order to model the radial structure of the source. Radial distributions of velocity fluctuations obtained in this way have previously been seen to closely match experimental results for forced jets (Cohen & Wygnanski 1987; Petersen & Samet 1988), and there is evidence of similar agreement of instability wave models for unforced jets (Gudmundsson & Colonius 2011).

The linear spatial instability calculation was performed assuming parallel, compressible, inviscid flow, as in Michalke (1984). Numerical results were obtained with a Runge-Kutta integration in a shooting procedure, and the present results were seen to reproduce growth rates and convection velocities of the cited paper. Radial eigenfunctions so obtained are shown in figure 21. The eigenfunctions have a near-zero amplitude close to the jet lipline. This low amplitude is seen in figure 21(b) to correspond to a position where the phase has an jump of π. The two sides of the jet mixing layer present a phase opposition for the axial velocity, a feature observed in forced jets (Cohen & Wygnanski 1987; Petersen & Samet 1988), but also in natural, turbulent jets (Lau *et al.* 1972).

The source defined in eq. (5.2) was used in eq. (5.1) to obtain the radiated sound field for azimuthal modes 0, 1 and 2 as

$$p(R, \theta, m, \omega) = -\frac{\mathrm{i}^m \rho_0 k_a^2 \cos^2\theta \mathrm{e}^{-\mathrm{i}k_a R}}{R} \int \mathrm{e}^{\left[\mathrm{i}(k_a x \cos\theta - kx) - \frac{x^2}{L^2}\right]} \mathrm{d}x \int \bar{u}_x(r) \times \hat{u}_x(r, m, \omega) J_m(k_a r \sin\theta) r \mathrm{d}r. \tag{5.3}$$

The convection wavenumber k was taken as the real part of the wavenumber predicted by the stability calculation. Equation (5.2) has two parameters: a free amplitude for $\hat{u}_x(r, m, \omega)$ and the wave-packet characteristic length L. The free amplitude was determined so as to match the SPL values at $\theta = 30°$, and L was chosen to provide the best agreement with the other angles. Results are presented in figure 22, and the wave-packet parameters summarised in table 6. The calculated sound radiation of the wave-packets closely fits the directivity shape in the experiment for the three azimuthal modes.

The determination of kL for the axisymmetric mode, which was done in § 4.2, is repeated here, and despite the difference between the convection speed assumed in § 4.2

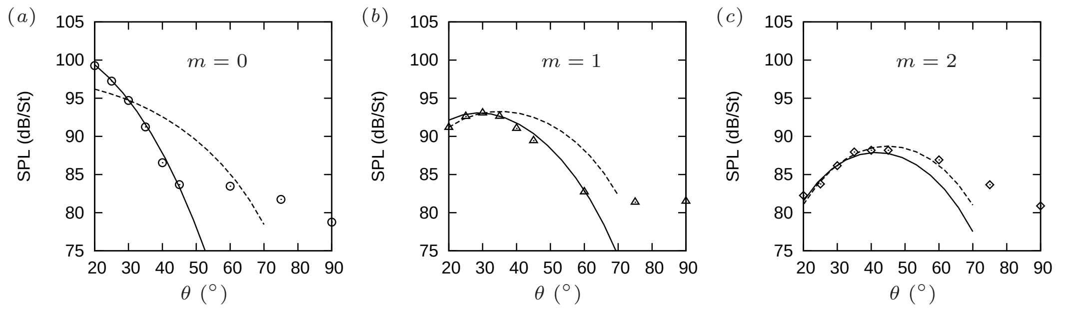

FIGURE 22. Comparison of experimental results (points) with sound radiation from wave-packet models (full lines) for $M = 0.6$, $\mathrm{St} = 0.2$ and (*a*) $m = 0$, (*b*) $m = 1$ and (*c*) $m = 2$. Dashed lines show results assuming axial compactness ($kL \to 0$).

Azimuthal mode	U_c/U	kL
0	0.97	6.0
1	0.72	3.3
2	0.63	2.3

TABLE 6. Wave-packet parameters for $M = 0.6$ and $\mathrm{St} = 0.2$.

(0.6 times the jet velocity) and the value predicted by instability theory at $x = D$ (0.97U) there is little change in the estimated value of kL (compare with table 2), showing that the conclusions of § 4 do not depend on the assumption of a particular value for the convection velocity.

Figure 22 also illustrates the changes in the directivity as a function of the azimuthal mode. As m is increased, for low θ the function $J_m(kr \sin\theta)$ causes a "cut-off" of the radiated sound. This cut-off is due to the azimuthal interference in the source. In the limit $\theta = 0$ only the axisymmetric mode radiates to the far field (Michalke & Fuchs 1975), since $J_m(0)$ is equal to 1 for $m = 0$ and 0 for all other m.

The azimuthal interference for the helical modes causes the sound field to lose its superdirective behaviour for higher m, with increasing cut-off with m. It is thus not surprising that superdirectivity was verified only for the axisymmetric mode, as shown in § 4. The results shows however, again, that with appropriately chosen parameters the directivity shape is very closely matched by a wave-packet model.

Finally, we note that the spatial extents estimated for both helical wavepackets are significantly lower than that of the axisymmetric component. Although values of kL around 3, as in table 6 for $m = 1$, still correspond to non-compact sources (see § 3), their influence on the radiated sound is lower than for the axisymmetric mode, which may explain the Strouhal number scaling observed in § 4.3 for $m = 1$.

To study the influence of axial non-compactness of the estimated wave-packets on the sound radiation, we have included in figure 22 dashed lines with the results for an axially compact source. We see that for $m = 0$ and $m = 1$ the axial extent of the source is significant for sound radiation, and neglect of it leads to errors on the directivity shape, particularly for the axisymmetric mode, as discussed in § 4. However, for $m = 2$ the low value of kL is such that the differences between the wave-packet model and a compact source are quite small, and axial interference does not play a significant role in this case.

Results of the sound radiation by helical wavepackets for other values of the Strouhal and Mach numbers are shown in figures 23 and 24, for azimuthal modes 1 and 2, respectively. In each calculation the radial eigenfunction of linear instability corresponding to

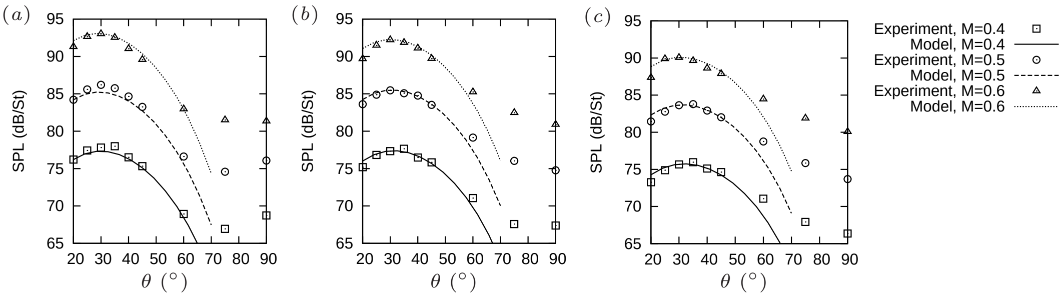

FIGURE 23. Comparison of experimental results with sound radiation from wave-packet models for azimuthal mode 1 and (*a*) St = 0.2, (*b*) St = 0.4 and (*c*) St = 0.6

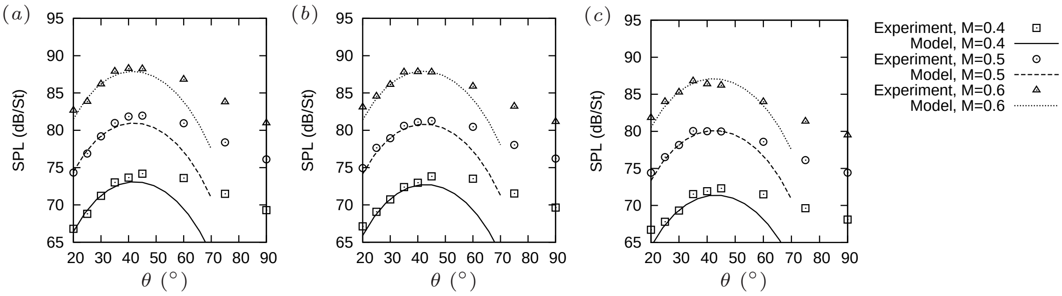

FIGURE 24. Comparison of experimental results with sound radiation from wave-packet models for azimuthal mode 2 and (*a*) St = 0.2, (*b*) St = 0.4 and (*c*) St = 0.6

Azimuthal mode	$kL(\mathrm{St}=0.2)$	$kL(\mathrm{St}=0.4)$	$kL(\mathrm{St}=0.6)$
1	3.3	2.8	2.6
2	2.3	2.1	1.9

TABLE 7. Wave-packet parameters for the three Mach numbers in figures 23 and 24.

the values of St and M was used. As before, the free amplitude of $\hat{u}_x$ is determined so as to match the radiated sound for $\theta = 30°$, and the value of L is chosen to match the directivity shape. However, we kept the same value of kL for the three Mach numbers to constrain the model, avoiding an excess of parameters to fit the experiments. The values of kL for Strouhal numbers of 0.2, 0.4 and 0.6 are shown in table 7 for azimuthal modes 1 and 2.

The results in figures 23 and 24 are close to the experimental results and present the same trends of the measurements. This confirms that the sound radiation at low angles for a range of Strouhal and Mach numbers has the directivity of helical wavepackets.

6. Conclusion

An experimental investigation of the azimuthal components of the sound radiated by subsonic jets in the Mach number range $0.35 \leqslant M \leqslant 0.6$ has been carried out using a ring array comprising six microphones. For this Mach number range the axisymmetric mode is seen to be highly directive, large increases in intensity being observed as the angle to the downstream jet axis is decreased. This trend is more marked for the peak frequencies. The observed increase is such that the axisymmetric mode dominates the sound radiation for low polar angles.

An exponential change of SPL with the paramater $(1-M_c\cos\theta)^2$ is predicted by wave-packet models, using an axially non-compact source distribution. The non-compactness leads to interference between different regions of the source; the sound radiation is, as a result, concentrated at low angles, and, for subsonic convection velocities, decreases exponentially as $(1-M_c\cos\theta)^2$ is increased. This effect has been observed for the axisymmetric mode, a decay of 15.4dB being seen for the peak frequency. With this value, and a wave-packet *Ansatz*, the axial extent of the source has been estimated to be of the order of 6-8 jet diameters for the $M = 0.4$, 0.5 and 0.6 jets. Further evidence of the importance of the non-compactness of the source for the axisymmetric mode is observed in a Helmholtz scaling of the axisymmetric mode and in a velocity dependence with an exponent of 9.6 for low angles.

The analysis is extended to inlcude higher order azimuthal modes, and a model is proposed for sound radiation to low polar angles by helical wavepackets. The superdirective radiation, characteristic of the axisymmetric mode, is changed due to the azimuthal interference in the source, which reduces the radiation for low θ. The model presents favorable comparisons with measurements for modes 1 and 2, showing that the sound field for helical modes also correspond to wave-packet radiation. However, the educed source extents are decreased for higher azimuthal modes, and, for mode 2, are close to the compact limit.

Since the present Mach number range is below most aeronautical applications, it is useful to evaluate the trends with increasing M. Recalling that the velocity exponent n in eqs. (4.1) and (4.2) and in figure 18 reflects the increment of the radiated sound as M is increased, the observations in the present work allow the following scenario to be postulated with regard to the effect of increasing jet Mach number on the radiated sound:

(*a*) As the jet Mach number is increased, the sound radiation of the axisymmetric mode grows faster than the sound field of the higher order modes (figure 18*a*);

(*b*) The increase in the axisymmetric radiation is even more pronounced near the spectral peak (figure 18*b*);

(*c*) The velocity increase therefore causes the sound radiation at low angles to be dominated by the axisymmetric mode, especially at the peak Strouhal number.

These trends suggest that at higher subsonic Mach numbers the observed axisymmetric radiation will have increased importance. Furthermore, the results suggest that the axisymmetric radiation can be appropriately modelled if, instead of considering the turbulent field to be formed by stochastic eddies with random phase (Lee & Ribner 1972; Crighton 1975), the axial interference over a non-compact source region is taken into account (see for instance Michalke 1970; Michel 2009). Some of the shortcomings in acoustic analogies may be overcome if we use appropriate source models for the large scale structures in jets, accounting for axially-extended wavepackets such as we have studied here.

For modelling purposes, we can think of the axial source interference in two ways, which are not mutually exclusive. The first is in an average sense: we look for an averaged mutual interference between the different positions of a jet, and particularly for its average effect in the sound field. For this evaluation, correlations and cross-spectra are appropriate measures, and, especially in the near field, as shown by Tinney & Jordan (2008) and Reba *et al.* (2010), these prove to be significant over a region extending several jet diameters from the nozzle exit. Furthermore, since for many practical applications determination of the radiated spectra is sufficient, this can be accomplished by coupling such correlation data with an acoustic analogy, as done, for example, by Karabasov *et al.* (2010), among others, or with a Kirchhoff surface, as shown by Reba *et al.* (2010). For such an approach, stability calculations may constitute an appropriate dynamic model, and indeed it has been shown that reasonable predictions can be obtained for the radiated sound at low angles (Colonius *et al.* 2010).

A second approach for studying such source interference effects involves an instantaneous perspective. Since a turbulent jet is intermittent, source interference changes with time. This leads to periods when the interference is destructive, during which we have periods of “relative quiet”; or, periods during which the destructive interference may be less significant, resulting in high-energy temporally-localised bursts in the acoustic field (Hileman *et al.* 2005; Kœnig *et al.* 2010). Experimental evaluation of the instantaneous interference between coherent structures in a flow is not an easy task, but such endeavours appear worthwhile considering the additional physical insight to be gained in terms of the dynamic law of jet noise source mechanisms. Furthermore, as seen by Cavalieri *et al.* (2010), the details of the mutual interference in the source region can be crucial for the understanding of differences between uncontrolled, noisy flows and their controlled, quieter counterparts.

This work was partially supported by CNPq, National Council of Scientific and Technological Development – Brazil, and through the EU-Russian program ORINOCO (FP7-AAT-2010-RTD-Russia; project number 266103). The authors thank Joël Delville and Carine Fourment-Cazenave for their work during the experiments.

Appendix A. Azimuthal decomposition of the acoustic field

A.1. *Definitions*

We present here the azimuthal Fourier series applied for the far-field pressure. The coefficients of a Fourier series in Φ are given by

$$p(R,\theta,m,t) = \frac{1}{2\pi}\int_{-\pi}^{\pi} p(R,\theta,\Phi,t)\mathrm{e}^{\mathrm{i}m\Phi}\mathrm{d}\Phi, \tag{A 1}$$

and the reconstruction of the pressure signal is

$$p(R,\theta,\Phi,t) = \sum_{m=-\infty}^{\infty} p(R,\theta,m,t)\mathrm{e}^{-\mathrm{i}m\Phi} \tag{A 2}$$

with the property

$$p(R,\theta,-m,t) = p^*(R,\theta,m,t) \tag{A 3}$$

since the pressure is a real-valued function.

In particular, we have for $\Phi = 0$ the reconstruction

$$p(R,\theta,\Phi=0,t) = \sum_{m=-\infty}^{\infty} p(R,\theta,m,t), \tag{A 4}$$

and each azimuthal component is given by

$$p_0(R,\theta,\Phi=0,t) = p(R,\theta,m=0,t), \tag{A 5}$$

$$p_m(R,\theta,\Phi=0,t) = p(R,\theta,m,t) + p(R,\theta,-m,t) \text{ if } m \neq 0. \tag{A 6}$$

The azimuthal components p_m so defined are real-valued. The use of $\Phi = 0$ for the reconstruction is without loss of generality due to the circumferential homogeneity of the acoustic field of axisymmetric jets.

A.2. *Evaluation of the accuracy of the Fourier series*

In the present work we have used a ring of six microphones in the far field to determine the azimuthal Fourier modes of the acoustic pressure. In order to evaluate if the spacing of $\varphi = 60°$ between microphones is appropriate, we evaluate the coherence function

$$C(\varphi,\omega) = \frac{|W(\varphi,\omega)|^2}{S_{pp}(\Phi_0,\omega)S_{pp}(\Phi_0+\varphi,\omega)} \tag{A 7}$$

where S_{pp} is the power spectral density of a single microphone and W is the cross spectral density between two microphones spaced azimuthally of φ, given as

$$W(\varphi,\omega) = \hat{p}(\Phi,\omega)\hat{p}^*(\Phi+\varphi,\omega), \tag{A 8}$$

where averaging between Fourier transforms of segments of the time series is implicit, and the spherical coordinates R and θ have been dropped for compactness.

The relationship between the coherence function and the azimuthal Fourier series can be obtained as follows. Using eq. (A 2), the spatio-temporal correlation of two microphones spaced of φ with a time lag of τ can be written as

$$p(\Phi,t)p(\Phi+\varphi,t+\tau) = \sum_{m=0}^{\infty} p_m(t)p_m(t+\tau)\cos(m\varphi) \tag{A 9}$$

since the correlation function is even in φ and does not depend on Φ due to the circumferential homogeneity of the jet.

We take the temporal average of both sides and use the correlation theorem to obtain

$$\hat{p}(\Phi,\omega)\hat{p}^*(\Phi+\varphi,\omega) = \sum_{m=0}^{\infty} |\hat{p}_m(\omega)|^2\cos(m\varphi) \tag{A 10}$$

such that $\hat{p}_m(\omega)$ can be obtained by the cross spectral density as

$$|\hat{p}_0(\omega)|^2 = \frac{1}{2\pi}\int_0^{2\pi} \hat{p}(\Phi,\omega)\hat{p}^*(\Phi+\varphi,\omega)\mathrm{d}\varphi \tag{A 11}$$

$$|\hat{p}_m(\omega)|^2 = \frac{1}{\pi}\int_0^{2\pi} \hat{p}(\Phi,\omega)\hat{p}^*(\Phi+\varphi,\omega)\cos(m\varphi)\mathrm{d}\varphi \text{ if } m \neq 0. \tag{A 12}$$

Now consider that the integral is calculated numerically; for instance, eq. (A 12) is approximated as

$$|\hat{p}_m(\omega)|^2 = \frac{1}{2\pi}\sum_{\varphi} \hat{p}(\Phi,\omega)\hat{p}^*(\Phi+\varphi,\omega)\cos(m\varphi)\Delta\varphi. \tag{A 13}$$

If the coherence function is zero for all but $\varphi = 0$ for some frequency ω, the microphone spacing is lower than the azimuthal coherence length. In this case, the result will be

$$|\hat{p}_0(\omega)|^2 = \frac{1}{2\pi}|\hat{p}(\Phi,\omega)|^2\Delta\varphi \tag{A 14}$$

and

$$|\hat{p}_m(\omega)|^2 = \frac{1}{\pi}|\hat{p}(\Phi,\omega)|^2\Delta\varphi \text{ if } m \neq 0. \tag{A 15}$$

for all m, which is not an accurate result: an uniform distribution in azimuthal modes is obtained only for a function with zero azimuthal coherence length, but for all physical quantities this length will be finite. This result is only an artifact of the azimuthal spacing.

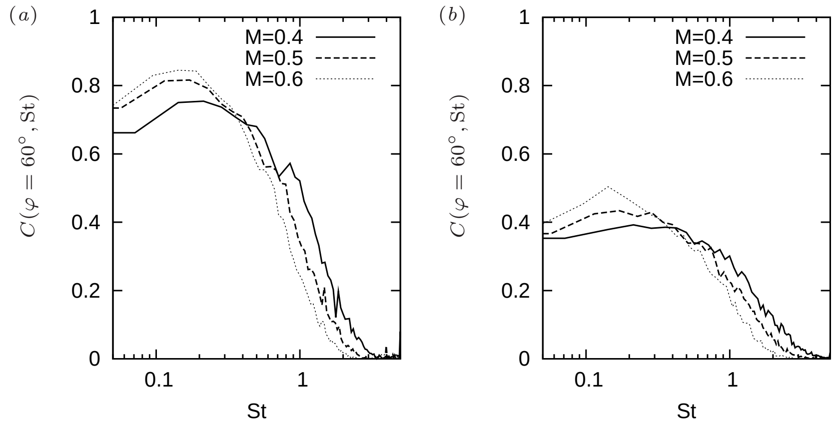

FIGURE 25. Coherence between microphones with azimuthal spacing of $\varphi = 60^\circ$ for (*a*) $\theta = 20^\circ$ and (*b*) $\theta = 30^\circ$.

Hence, to obtain meaningful results for the azimuthal Fourier series, the coherence should be non-zero for the microphone spacing φ.

Coherence results are shown in figure 25 for $\theta = 20^\circ$ and 30°. We see that for both polar angles the coherences are significant for Strouhal numbers up to 1, and decay to zero for St ≈ 2. This validates the analysis in § 4 and § 5, done mostly for Strouhal numbers lower than unity. However, care should be taken in analysing higher frequencies, which we avoid in the present work. For such task an azimuthal ring with a higher number of microphones would be necessary.

Appendix B. The line-source approximation for low-angle radiation

The purpose of the present Appendix is to show, using Lighthill's analogy, the steps that allow to write the solution of the radiated sound at low polar angles to be expressed, in certain cases, as the radiation by a line source, such as the Crow's model in eq. (3.6).

The solution of Lighthill's equation for the pressure p in the frequency domain is given in $\mathbf{x}$ as

$$p(\mathbf{x},\omega) = \iiint \frac{\partial^2 T_{ij}}{\partial y_i \partial y_j}(\mathbf{y},\omega)\frac{\exp\left(-\mathrm{i}k_a|\mathbf{x}-\mathbf{y}|\right)}{4\pi|\mathbf{x}-\mathbf{y}|}\mathrm{d}\mathbf{y}, \tag{B 1}$$

where $k_a = \omega/c$ is the acoustic wavenumber and a time factor of $\exp(\mathrm{i}\omega t)$ is implied.

If we are interested in the radiation to low polar angles, we can consider the T_{11} term of Lighthill's tensor alone as a first approximation. It can be shown that only the quadrupoles aligned with the radiation direction generate sound in the far acoustic field (Crighton 1975), and for low angles these quadrupoles can be approximated by the T_{11} term. Another reason is that while the velocity fluctuations in the three directions have similar amplitudes in a jet, the mean streamwise velocity is more than an order of magnitude higher than the transverse components. The use of T_{11} alone to calculate sound radiation for low angles was used in the models of Cavalieri *et al.* (2011*b*), and led to good agreement with results of a large eddy simulation.

We rewrite the source in cylindrical coordinates (x, r, ϕ) and the observer in spherical coordinates (R, θ, Φ). The far-field approximation gives a distance between source and observer equal to $R - x\cos\theta - r\sin\theta\cos(\phi - \Phi)$, leading to

$$p(R,\theta,\Phi,\omega) = \frac{1}{4\pi R}\iiint \frac{\partial^2 T_{xx}}{\partial x^2}(x,r,\phi,\omega)\mathrm{e}^{-\mathrm{i}k_a(R - x\cos\theta - r\sin\theta\cos(\phi-\Phi))}r\mathrm{d}x\mathrm{d}r\mathrm{d}\phi. \tag{B 2}$$

The double derivative can be passed from Lighthill's tensor to the Green's function, as shown, for instance, by Goldstein (1976). This gives

$$p(R,\theta,\Phi,\omega) = \frac{1}{4\pi R}\iiint T_{xx}(x,r,\phi,\omega) \times\frac{\partial^2}{\partial x^2}\left[\mathrm{e}^{-\mathrm{i}k_a(R-x\cos\theta-r\sin\theta\cos(\phi-\Phi))}\right] r\mathrm{d}x\mathrm{d}r\mathrm{d}\phi. \tag{B 3}$$

The azimuthal dependence of T_{xx} can be expanded in an azimuthal Fourier series. Taking the mode m of T_{xx} leads to

$$p(R,\theta,\Phi,\omega) = \frac{1}{4\pi R}\iiint T_{xx}(x,r,m,\omega)\mathrm{e}^{-\mathrm{i}m\phi} \times\frac{\partial^2}{\partial x^2}\left[\mathrm{e}^{-\mathrm{i}k_a(R-x\cos\theta-r\sin\theta\cos(\phi-\Phi))}\right] r\mathrm{d}x\mathrm{d}r\mathrm{d}\phi, \tag{B 4}$$

which can be manipulated to give

$$p(R,\theta,\Phi,\omega) = \frac{\mathrm{e}^{-\mathrm{i}m\Phi}}{4\pi R}\iiint T_{xx}(x,r,m,\omega)\mathrm{e}^{-\mathrm{i}m(\phi-\Phi)} \times\frac{\partial^2}{\partial x^2}\left[\mathrm{e}^{-\mathrm{i}k_a(R-x\cos\theta-r\sin\theta\cos(\phi-\Phi))}\right] r\mathrm{d}x\mathrm{d}r\mathrm{d}\phi. \tag{B 5}$$

Integration in cylindrical coordinates gives

$$p(R,\theta,\Phi,\omega) = \mathrm{e}^{-\mathrm{i}m\Phi}\frac{\mathrm{e}^{-\mathrm{i}k_aR}}{4\pi R}\int\mathrm{d}x\int T_{xx}(x,r,m=0,\omega) \times\frac{\partial^2}{\partial x^2}\left[\mathrm{e}^{\mathrm{i}(k_a x\cos\theta)}\right] r\mathrm{d}r\int \mathrm{e}^{-\mathrm{i}m(\phi-\Phi)}\mathrm{e}^{\mathrm{i}k_a r\sin\theta\cos(\phi-\Phi)}\mathrm{d}\phi \tag{B 6}$$

From the integral representation of the Bessel functions J_m with integer m (Morse & Ingard 1968)

$$J_m(x) = \frac{1}{2\pi\mathrm{i}^m}\int_0^{2\pi}\mathrm{e}^{ix\cos\phi}\cos(m\phi)\mathrm{d}\phi, \tag{B 7}$$

we can deduce the azimuthal integral to be equal to $2\pi\mathrm{i}^m J_m(k_a r\sin\theta)$. This leads to

$$p(R,\theta,\Phi,\omega) = -\mathrm{e}^{-\mathrm{i}m\Phi}\frac{\mathrm{i}^m k_a^2\cos^2\theta\mathrm{e}^{-\mathrm{i}k_aR}}{2R}\int\mathrm{e}^{\mathrm{i}k_a x\cos\theta}\mathrm{d}x\int T_{xx}(x,r,m,\omega) \times J_m(k_a r\sin\theta)r\mathrm{d}r. \tag{B 8}$$

In eq. (B 8) we see that an azimuthal mode m of T_{xx} leads to a $\mathrm{e}^{-\mathrm{i}m\Phi}$ factor in the radiated pressure, showing that there is a direct correspondence between the azimuthal modes in the source and in the acoustic field, such that

$$p(R,\theta,m,\omega) = -\frac{\mathrm{i}^m k_a^2\cos^2\theta\mathrm{e}^{-\mathrm{i}k_aR}}{2R}\int\mathrm{e}^{\mathrm{i}k_a x\cos\theta}\mathrm{d}x\int T_{xx}(x,r,m,\omega) \times J_m(k_a r\sin\theta)r\mathrm{d}r. \tag{B 9}$$

where $p(R,\theta,m,\omega)$ is the coefficient of azimuthal mode m of the radiated pressure.

For the axisymmetric mode, eq. (B 9) gives

$$p(R,\theta,m=0,\omega) = -\frac{k_a^2\cos^2\theta\mathrm{e}^{-\mathrm{i}k_aR}}{2R}\int\mathrm{e}^{\mathrm{i}k_a x\cos\theta}\mathrm{d}x\int T_{xx}(x,r,m=0,\omega) \times J_0(k_a r\sin\theta)r\mathrm{d}r. \tag{B 10}$$

If $k_a r \sin\theta \ll 1$, we can make a further approximation by taking $J_0(k_a r \sin\theta)$ to be 1†. Noting that

$$k_a r \sin\theta = 2\pi \mathrm{St} M \frac{r}{D} \sin\theta \tag{B 11}$$

and considering the radial integration in eq. (B 8) has significant values for values of r not much larger than D, the approximation of $J_0(k_a r \sin\theta)$ as 1 is reasonable for low values of the radiation angle and of the Strouhal and Mach numbers.

The far-field pressure is then given as

$$p(R,\theta,m=0,\omega) = -\frac{k_a^2 \cos^2\theta \mathrm{e}^{-\mathrm{i}k_a R}}{2R} \int \mathrm{e}^{\mathrm{i}k_a x \cos\theta} \mathrm{d}x \int T_{xx}(z,r,m=0,\omega) r \mathrm{d}r, \tag{B 12}$$

and the axisymmetric source can be approximated as a line distribution of quadrupoles with intensity

$$S_{xx}(x,m=0,\omega) = \int T_{xx}(x,r,m=0,\omega) r \mathrm{d}r. \tag{B 13}$$

This or similar approximations have been used in a number of works in the litterature (Crow 1972; Ffowcs Williams & Kempton 1978; Cavalieri *et al.* 2011*b*). The far-field pressure is given as

$$p(R,\theta,m=0,\omega) = -\frac{k_a^2 \cos^2\theta \mathrm{e}^{-\mathrm{i}k_a R}}{2R} \int S_{xx}(x,m=0,\omega) \mathrm{e}^{-\mathrm{i}k_a x \cos\theta} \mathrm{d}x. \tag{B 14}$$

REFERENCES

Armstrong, R. R., Fuchs, H. V. & Michalke, A. 1977 Coherent structures in jet turbulence and noise. *AIAA Journal* **15**, 1011–1017.

Batchelor, G. K. & Gill, A. E. 1962 Analysis of the stability of axisymmetric jets. *Journal of Fluid Mechanics* **14** (04), 529–551.

Bogey, C., Barré, S., Fleury, V., Bailly, C. & Juvé, D. 2007 Experimental study of the spectral properties of near-field and far-field jet noise. *International Journal of Aeroacoustics* **6** (2), 73–92.

Bridges, J. E. & Hussain, A. K. M. F. 1987 Roles of initial condition and vortex pairing in jet noise. *Journal of Sound and Vibration* **117** (2), 289–311.

Brown, C. A. & Bridges, J. 2006 Acoustic efficiency of azimuthal modes in jet noise using chevron nozzles. *Tech. Rep.*. National Aeronautics and Space Administration.

Cavalieri, A. V. G., Daviller, G., Comte, P., Jordan, P., Tadmor, G. & Gervais, Y. 2011*a* Using large eddy simulation to explore sound-source mechanisms in jets. *Journal of Sound and Vibration* **330** (17), 4098–4113.

Cavalieri, A. V. G., Jordan, P., Agarwal, A. & Gervais, Y. 2011*b* Jittering wave-packet models for subsonic jet noise. *Journal of Sound and Vibration* **330** (18-19), 4474–4492.

Cavalieri, A. V. G., Jordan, P., Gervais, Y., Wei, M. & Freund, J. B. 2010 Intermittent sound generation and its control in a free-shear flow. *Physics of Fluids* **22** (11), 115113.

Cohen, J. & Wygnanski, I. 1987 The evolution of instabilities in the axisymmetric jet. part 1. the linear growth of disturbances near the nozzle. *Journal of Fluid Mechanics* **176**, 191–219.

Colonius, T., Samanta, A. & Gudmundsson, K. 2010 Parabolized stability equation models of large-scale jet mixing noise. *Procedia Engineering* **6**, 64–73.

Crighton, D. G. 1975 Basic principles of aerodynamic noise generation. *Progress in Aerospace Sciences* **16** (1), 31–96.

Crighton, D. G. & Gaster, M. 1976 Stability of slowly diverging jet flow. *Journal of Fluid Mechanics* **77** (2), 397–413.

† More precisely, since $J_0(x) \approx 1 - x^2/4$ for small x, the approximation of $J_0(k_a r \sin\theta)$ as 1 is reasonable if $k_a^2 r^2 \sin^2\theta/4 \ll 1$.

Crighton, D. G. & Huerre, P. 1990 Shear-layer pressure fluctuations and superdirective acoustic sources. *Journal of Fluid Mechanics* **220**, 355–368.

Crow, S. C. 1972 Acoustic gain of a turbulent jet. In *Phys. Soc. Meeting, Univ. Colorado, Boulder, paper IE*, , vol. 6.

Crow, S. C. & Champagne, F. H. 1971 Orderly structure in jet turbulence. *Journal of Fluid Mechanics* **48** (3), 547–591.

Ffowcs Williams, J. E. & Kempton, A. J. 1978 The noise from the large-scale structure of a jet. *Journal of Fluid Mechanics* **84** (4), 673–694.

Fuchs, H. V. & Armstrong, R. R. 1978 Turbulent source coherence and Helmholtz number as aerodynamic noise parameters. *Structure and Mechanisms of Turbulence II* pp. 189–201.

Fuchs, H. V. & Michel, U. 1978 Experimental evidence of turbulent source coherence affecting jet noise. *AIAA Journal* **16** (9), 871–872.

Goldstein, M. E. 1976 Aeroacoustics. *New York, McGraw-Hill International Book Co., 1976. 305 p.* .

Gudmundsson, K. & Colonius, T. 2011 Instability wave models for the near-field fluctuations of turbulent jets. *Journal of Fluid Mechanics* **689**, 97–128.

Hileman, J. I., Thurow, B. S., Caraballo, E. J. & Samimy, M. 2005 Large-scale structure evolution and sound emission in high-speed jets: real-time visualization with simultaneous acoustic measurements. *Journal of Fluid Mechanics* **544**, 277–307.

Hussain, A. K. M. F. & Zaman, K. B. M. Q. 1981 The 'preferred mode' of the axisymmetric jet. *Journal of Fluid Mechanics* **110**, 39–71.

Juvé, D., Sunyach, M. & Comte-Bellot, G. 1979 Filtered azimuthal correlations in the acoustic far field of a subsonic jet. *AIAA Journal* **17**, 112.

Karabasov, S., Afsar, M. Z., Hynes, T. P., Dowling, A. P., McMullan, W. A., Pokora, C. D., Page, G. J. & McGuirk, J. J. 2010 Jet Noise: Acoustic analogy informed by large eddy simulation. *AIAA journal* **48** (7), 1312–1325.

Kœnig, M., Cavalieri, A. V. G., Jordan, P., Delville, J., Gervais, Y., Papamoschou, D., Samimy, M. & Lele, S. K. 2010 Farfield pre-filterering and source-imaging for the study of jet noise. In *16th AIAA/CEAS Aeroacoustics Conference and Exhibit*. Stockholm, Sweden.

Lau, J. C., Fisher, M. J. & Fuchs, H. V. 1972 The intrinsic structure of turbulent jets. *Journal of Sound and Vibration* **22** (4), 379–384.

Laufer, J. & Yen, T.-C. 1983 Noise generation by a low-Mach-number jet. *Journal of Fluid Mechanics* **134**, 1–31.

Lee, H. K. & Ribner, H. S. 1972 Direct correlation of noise and flow of a jet. *The Journal of the Acoustical Society of America* **52**, 1280.

Lele, S. K. 1994 Compressibility effects on turbulence. *Annual Review of Fluid Mechanics* **26** (1), 211–254.

Lighthill, M. J. 1952 On sound generated aerodynamically. I. General theory. *Proceedings of the Royal Society of London. Series A, Mathematical and Physical Sciences* pp. 564–587.

Lush, P. A. 1971 Measurements of subsonic jet noise and comparison with theory. *Journal of Fluid Mechanics* **46** (03), 477–500.

Mankbadi, R. & Liu, J. T. C. 1984 Sound generated aerodynamically revisited: large-scale structures in a turbulent jet as a source of sound. *Philosophical Transactions of the Royal Society of London. Series A, Mathematical and Physical Sciences* **311** (1516), 183–217.

Michalke, A. 1970 A wave model for sound generation in circular jets. *Tech. Rep.*. Deutsche Luft- und Raumfahrt.

Michalke, A. 1971 Instabilitat eines Kompressiblen Runden Freistrahls unter Berucksichtigung des Einflusses der Strahlgrenzschichtdicke. *Zeitschrift für Flugwissenschaften* **19**, 319–328; English translation: NASA TM 75190, 1977.

Michalke, A. 1972 An expansion scheme for the noise from circular jets. *Zeitschrift für Flugwissenschaften* **20**, 229–237.

Michalke, A. 1984 Survey on jet instability theory. *Progress in Aerospace Sciences* **21**, 159–199.

Michalke, A. & Fuchs, H. V. 1975 On turbulence and noise of an axisymmetric shear flow. *Journal of Fluid Mechanics* **70**, 179–205.

Michel, U. 2009 The role of source interference in jet noise. In *15th AIAA/CEAS Aeroacoustics Conference(30th Aeroacoustics Conference)*, pp. 1–15.

Mollo-Christensen, E. 1963 Measurements of near field pressure of subsonic jets. *Tech. Rep.*. Advisory Group for Aeronautical Research and Development, Paris, France.

Mollo-Christensen, E. 1967 Jet noise and shear flow instability seen from an experimenter's viewpoint(Similarity laws for jet noise and shear flow instability as suggested by experiments). *Journal of Applied Mechanics* **34**, 1–7.

Moore, C. J. 1977 The role of shear-layer instability waves in jet exhaust noise. *Journal of Fluid Mechanics* **80** (2), 321–367.

Morris, P. J. 2010 The instability of high speed jets. *International Journal of Aeroacoustics* **9** (1), 1–50.

Morse, P. M. & Ingard, K. U. 1968 *Theoretical acoustics*. McGraw-Hill Book Company.

Petersen, R. A. & Samet, M. M. 1988 On the preferred mode of jet instability. *Journal of Fluid Mechanics* **194** (1), 153–173.

Reba, R., Narayanan, S. & Colonius, T. 2010 Wave-packet models for large-scale mixing noise. *International Journal of Aeroacoustics* **9** (4), 533–558.

Sandham, N. D., Morfey, C. L. & Hu, Z. W. 2006 Sound radiation from exponentially growing and decaying surface waves. *Journal of Sound and Vibration* **294** (1), 355–361.

Suzuki, T. & Colonius, T. 2006 Instability waves in a subsonic round jet detected using a near-field phased microphone array. *Journal of Fluid Mechanics* **565**, 197–226.

Tanna, H. K. 1977 An experimental study of jet noise Part I: Turbulent mixing noise. *Journal of Sound and Vibration* **50** (3), 405–428.

Tinney, C. E. & Jordan, P. 2008 The near pressure field of co-axial subsonic jets. *Journal of Fluid Mechanics* **611**, 175–204.

Tutkun, M., George, W. K., Foucaut, J. M., Coudert, S., Stanislas, M. & Delville, J. 2009 In situ calibration of hot wire probes in turbulent flows. *Experiments in Fluids* **46** (4), 617–629.

Viswanathan, K. 2004 Aeroacoustics of hot jets. *Journal of Fluid Mechanics* **516**, 39–82.

Viswanathan, K. 2006 Scaling laws and a method for identifying components of jet noise. *AIAA Journal* **44** (10), 2274.

Zaman, K. B. M. Q. & Yu, J. C. 1985 Power spectral density of subsonic jet noise. *Journal of Sound and Vibration* **98** (4), 519–537.

Chapter VI

Instability waves in unforced turbulent jets

In the analysis of the previous chapter, we showed that the acoustic field at low axial angles is consistent with a wave-packet source of low azimuthal wavenumber, in agreement with the studies of numerical simulations in chapters III and IV.

We continue our experimental work by taking measurements of the velocity field of the same jets used in the experiments of chapter V. The focus is on the analysis of the lower-order azimuthal modes in the velocity field ($m = 0$ and 1), which are dominant in the acoustic field for low polar angles. The wave-packet structure is assessed by the comparison of experimental results with linear Parabolised Stability Equations.

We present in the following a preliminary version of the paper "Instability waves in unforced turbulent jets", to be presented in the 18th AIAA/CEAS Aeroacoustics Conference in June 2012.

18th AIAA/CEAS Aeroacoustic Conference and Exhibit, 4-6 June 2010, Colorado Springs, Colorado

Instability waves in unforced turbulent jets detected with time-resolved, stereoscopic PIV

André V. G. Cavalieri[1]*, Daniel Rodríguez[2,3]†,
Peter Jordan[1]‡, Tim Colonius[2]§, Yves Gervais[1]¶

[1] *Institut Pprime, Poitiers, France*

[2] *California Institute of Technology, Pasadena, CA*

[3] *Universidad Politecnica de Madrid, Spain*

We study the velocity field of unforced, high-Reynolds-number subsonic jets, with turbulent boundary layers at the nozzle exit, so as to discern the presence of instability waves in such flows and their relationship to the radiated sound. The velocity field is obtained by single-point hot-wire measurements, and at cross-stream planes with stereoscopic, time-resolved PIV, allowing, in this last case, the Fourier decomposition of the field in frequency and azimuthal Fourier modes. Low angle sound radiation is measured with a microphone ring at polar angle, $\theta = 20°$, to the downstream jet axis, simultaneously with the PIV acquisition. Azimuthal wavenumber spectra for velocity and far-field pressure have different behaviours, velocity peaking at high azimuthal modes (scaling with local momentum thickness) whereas far-field pressure is predominantly axisymmetric, suggesting that radial compactness tends to an increased relative acoustic efficiency of the axisymmetric mode in the flow. This is confirmed by significant correlations, around 10%, between mode-0 velocity and mode-0 far-field pressure, values significantly higher than previous two-point correlation results in the literature for subsonic jets. The axisymmetric and first helical modes in the velocity field are then compared with the solution of linear Parabolised Stability Equations (PSE) (where the experimental mean velocity field is used as the base flow) to ascertain if these modes correspond to linear instability waves. For all but the lowest frequencies close agreement is obtained for the spatial amplification on the jet axis until the end of the potential core. The radial shapes of the linear PSE results also agree with the experimental results for the same region. This suggests that even though the studied unforced jets are of broadband behaviour and present a wide range of turbulent scales, the evolution of the lower frequencies and azimuthal modes can be modelled as linear instabilities of the mean velocity profile, and these are associated to the radiated sound at low polar angles.

I. Introduction

Since the first observations of coherent structures in turbulent jets,[1,2] instability waves, or wavepackets, have been postulated as a possible sound source mechanism in free jets.[1,3–6] These are characterised by a hydrodynamic wave with amplitude growth, saturation and decay, and an axial extent much larger than the characteristic turbulence lengthscale. For this reason, wavepackets lead to non-compact source models for sound generation, which represent a significant departure from turbulence models as stochastic eddies, as was supposed at the time of Lighthill.[7]

As an aside to the aforementioned studies, we should mention that most of the early successful comparisons between instability waves and experiments[8,9] involved *forced jets*, which present phase-locked disturbances that are more easily measured experimentally, and the extension of the conclusions taken from the

*PhD student, Institut Pprime, 43 rue de l'Aérodrome, 86036 Poitiers, France.
†Marie Curie COFUND fellow, California Institute of Technology.
‡Research Scientist, Institut Pprime, 43 rue de l'Aérodrome, 86036 Poitiers, France.
§Professor, California Institute of Technology.
¶Professor, Institut Pprime, 40 avenue du Recteur Pineau, 86022 Poitiers, France.

analysis of these flows to their unforced counterparts is not straightforward. For natural jets, modelling of fluctuations as azimuthally-coherent instability waves may be facilitated, though, when applied to the near-field pressure, which is known to have a simpler structure than the turbulent velocity field. For instance, pressure inside a turbulent jet has its fluctuation energy content concentrated in few low-order azimuthal modes, in contrast to the velocity field.[10,11] The same is the case for the pressure surrounding a jet,[12] and measurements using line arrays of microphones in this region reveal the structure of a hydrodynamic wave extending several jet diameters downstream of the nozzle exit.[13,14]

Recent results showing agreement between linear instability-wave models and the near-field pressure of natural jets[15,16] show that this region can indeed be modelled quite accurately as a superposition of linear instability waves with different frequencies and azimuthal modes. It is thus tempting to affirm that such waves are also present inside the turbulent velocity field. On the other hand, if this is true, the extent to which turbulent velocity fluctuations can be modelled as linear waves is not clear. The hydrodynamic waves may have small amplitudes, without a clear signature in the velocity field of an unforced jet. Such a signature is clear for forced jets[1,8,9,17] and for transitional flows, i.e. jets with laminar boundary layers at the nozzle exit.[18–21] In both cases the velocity field is dominated by coherent structures, at least for small distances from the nozzle exit. However, this is not the case for natural jets with turbulent boundary layers at the nozzle exit, which are flows closer to the aeronautical applications.

Gudmundsson and Colonius[16] present a comparison between results of linear Parabolised Stability Equations (hereafter PSE) and the velocity field of jets, obtained using PIV in cross sections of a jet. Since in that work the PIV measurements were not time resolved, comparison for individual frequencies was not possible, and the instability waves needed to be superposed prior to comparison with experiment. The results show nonetheless an encouraging agreement, which motivated us to design an experiment for frequency-dependent comparisons between instability wave models and measurements.

In this work we present experimental results that thus probe further into the velocity fields of unforced, turbulent jets so as to determine if velocity fluctuations of low azimuthal wavenumber may be modelled as linear instability waves. To model such waves, we use linear PSE, as in the work of Gudmundsson and Colonius,[16] which allow wavepackets in slowly-diverging flows to be modelled. Linear PSE is used here as a reference model for hydrodynamic waves resulting from the Kelvin-Helmholtz instability in the initial region of a jet. Although several results presented here may seem as a validation of linear PSE (and are indeed so), our view is that, more than that, they represent an asessment of the presence of such linear waves in a turbulent jet, and of the possibility of applying a linear model for turbulent velocity fluctuations, the experimental mean velocity profile being used as a base flow for linearisation.

As a further motivation for this study, the jets analysed in the present work were seen previously to lead to an acoustic field consistent with sound radiation by non-compact wavepackets with low azimuthal wavenumber; most notably, the sound field at low polar angles is mostly axisymmetric, with the characteristic *superdirectivity* expected for wave-packet radiation.[22] This suggests that an axisymmetric wavepacket inside the turbulent field causes low-angle radiation, and here we investigate this by a detailed study of the axisymmetric part of the velocity field and its connection to the radiated sound, which is assessed by correlations between individual azimuthal modes.

This work is organised as follows. The experimental setup is described in section II. In section III.A we evaluate the dominant azimuthal wavenumbers in both velocity and acoustic fields, and the relationship between individual azimuthal modes in the turbulence and in the far-field pressure is investigated with correlations in section III.B.

We then evaluate if the axisymmetric and first helical modes in the velocity field of jets can be modelled as linear instability waves, calculated using linear PSE. A brief description of the computational approach is presented in section IV.A. We then perform comprehensive comparisons of this model with the experimental results. For our evaluations, we first take advantage of the symmetry properties of circular jets, and perform a comparison of the axisymmetric mode on the jet centerline, using hot-wire results, in section IV.B. To obtain results for helical modes, and at radial positions other than the centerline, we have performed stereoscopic time-resolved PIV measurements on cross-stream planes at several axial stations. The confrontation of the experimental results with the linear instability results are presented in section IV.C, with a discussion on the presence of such waves in turbulent jets.

II. Experimental setup

The experiments were performed in the 'Bruit et Vent' anechoic facility at the Centre d'Etudes Aérodynamiques et Thermiques (CEAT), Institut Pprime, Poitiers, France. We have carried out velocity measurements of subsonic jets with acoustic Mach numbers equal to 0.4, 0.5 and 0.6. The nozzle diameter, D, was 0.05m. With these conditions, the Reynolds number, $\rho U D/\mu$, varies from 4.2×10^5 to 5.7×10^5, where ρ and μ are, respectively, the density and the viscosity at the nozzle exit.

A convergent section was located upstream of the jet exit, with an area contraction of 31. This was followed by a straight circular section of length 150mm; a boundary layer trip was used to force transition 135mm upstream ($2.7D$) of the nozzle exit. Hot-wire results for the boundary layer at the nozzle exit are shown in figure 1, showing a typical turbulent profile. The present jet setup was previously used for acoustic measurements with an azimuthal microphone ring.[22]

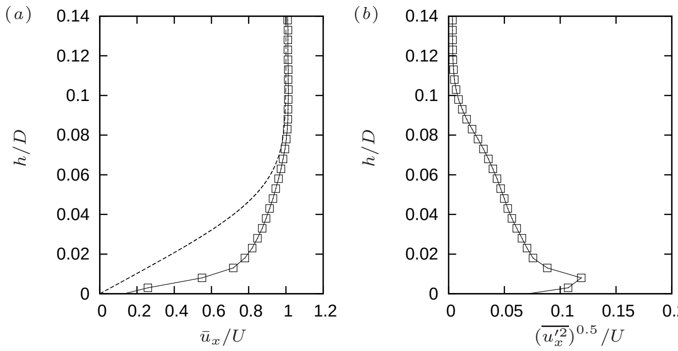

Figure 1. Boundary layer profiles at the nozzle exit for the Mach 0.5 jet: (*a*) mean velocity and (*b*) rms value. Dashed line in (*a*) is Blasius profile.

Velocity measurements were obtained using a traversing single hot wire and with stereoscopic, time-resolved particle image velocimetry (TR-PIV). The hot wire was calibrated *in situ* using the procedure described by Tutkun *et al.*,[23] with a traversing Pitot tube giving the mean axial velocity.

The stereoscopic TR-PIV experiments were done with a setup similar to Kœnig *et al.*[24] The measurements are performed in cross-stream planes, as in Tinney *et al.*[25] and Kœnig *et al.*[24] Two cameras are placed at an angle of 45° to the laser plane, one placed upstream and the other downstream of the plane. The flow was seeded with oil smoke. The sampling frequency is 5kHz, which corresponds to St = 1.82, 1.46 and 1.21 for the $M = 0.4$, 0.5 and 0.6 jets, respectively. A total of 19414 image pairs were recorded. Image-processing consisted of a five-pass correlation routine with 64x64 pixel correlation for the first pass, 16x16 pixel for the final pass and with a 50% correlation overlap at each pass, done with LaVision software Davis 8; this leads to velocity fields with 114×102 velocity vectors. This grid was subsequently interpolated to cylindrical coordinates to allow the expansion of the velocity field in azimuthal Fourier modes.

We have also measured the acoustic pressure with an azimuthal ring of nine microphones at a polar angle $\theta = 20°$, with a distance R to the nozzle exit equal to 42.3D. These measurements were done simultaneously with the TR-PIV experiment, which allowed calculation of flow-acoustic correlations in two ways: the first was between a single point in the velocity field and a single microphone, as often done in the litterature;[26–30] the second was between a given azimuthal mode in velocity and acoustic fields. This last approach has a theoretical motivation, detailed in section III.B, and allows the determination of correlations between instability waves in the flow and the radiated sound field.

As an evalution of the errors in the present experiment, the TR-PIV results for the axial velocity at $x/D = 2$ for the $M = 0.4$ jet are compared in figure 3 to the measurements taken with the traversing Pitot tube and hot wire. Close agreement is found for both the mean and rms values of the velocity.

The sampling frequency of 5kHz was the maximum possible value with the available equipment. To evaluate the effect of aliasing in spectra obtained from the TR-PIV measurements, these are compared in figure 3 to hot-wire spectra. For positions close to the jet lipline, such as shown in figures 3(b) and (c), the difference between TR-PIV and hot-wire spectra is slight. However, on the jet axis (figure 3a) the difference becomes significant, particularly for frequencies far from the peak. In addition to the aliasing errors, inside the potential core the amplitudes of velocity fluctuations are much lower than in the regions of turbulent

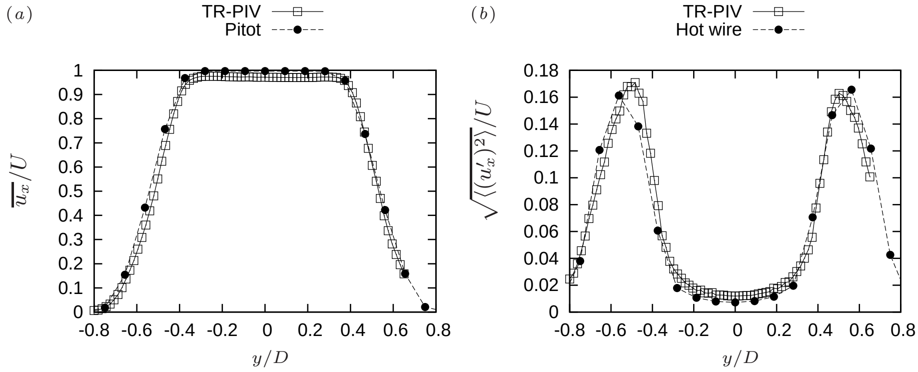

Figure 2. Comparison of (a) mean and (b) rms value of the axial velocity at $x/D = 2$ for the $M = 0.4$ jet using the different experimental techniques of the present work

flow, leading to a reduction of the signal-to-noise ratio if one considers that the noise in PIV measurements is uniformly distributed in space. In agreement with this, the errors in the determination of spectra from TR-PIV results are reduced for downstream positions on the jet centerline, as seen in figure 3(d).

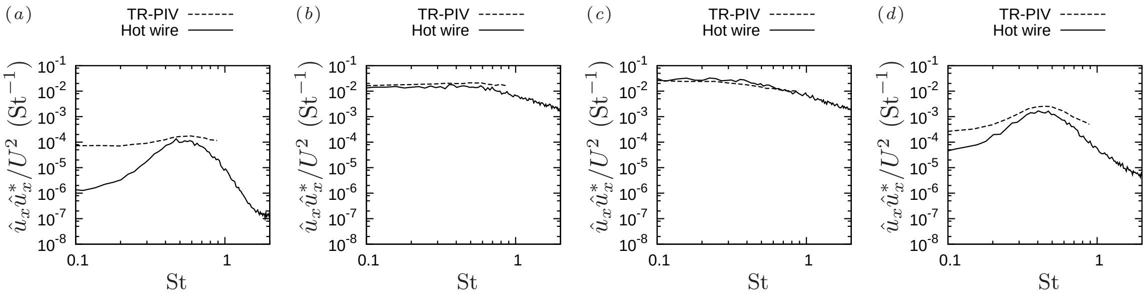

Figure 3. Comparison of hot wire and PIV spectra at (*a*) $x/D = 2$, $r/D = 0$, (*a*) $x/D = 2$, $r/D = 0.48$, (*a*) $x/D = 2$, $r/D = 0.57$ and (*d*) $x/D = 4$, $r/D = 0$.

To avoid significant errors due to aliasing in the TR-PIV results, we focus the analysis of the $M = 0.4$ jet measurements on the Strouhal number range of $0.3 \leq \mathrm{St} \leq 0.7$. For higher Mach numbers, aliasing becomes significant, even for this Strouhal number range; however, its effect is apparently uniform for all radial positions, as shown in Appendix A, where we see also that a correction of the PIV results based on hot-wire measurements leads to close agreement between velocity results for $M = 0.6$ and linear PSE solutions.

III. Azimuthal content of the velocity and acoustic fields

III.A. Dominant azimuthal wavenumbers for velocity and far-field pressure

To present a view of the characteristic turbulent structures in the velocity field of the the present jets, we present in figure 4 snapshots of the instantaneous axial velocity fluctuations in a cross section of the Mach 0.4 jet. Azimuthally-coherent structures, such as the ones modelled by linear instability models, are hardly visible in this visualisation, which is dominated by smaller-scale eddies with the characteristic turbulent length scale. The simple observation of the fields in figure 4 shows that the present jets are not dominated by coherent structures such as forced jets,[1,17] and, at first sight, does not suggest the existence of instability waves of low azimuthal wavenumber in such flows.

On the other hand, application of an azimuthal Fourier series to the turbulent field reveals that some energy is contained in lower azimuthal modes, and even for the axisymmetric mode. Figure 5 shows the energy of the fluctuations of axial velocity on the jet lipline, resolved as a function of the azimuthal wavenumber. We notice in figure 5(a) that the most energetic azimuthal mode is around 11 for the near nozzle region ($x/D = 1$). For downstream positions, lower azimuthal modes of velocity become more important, and the

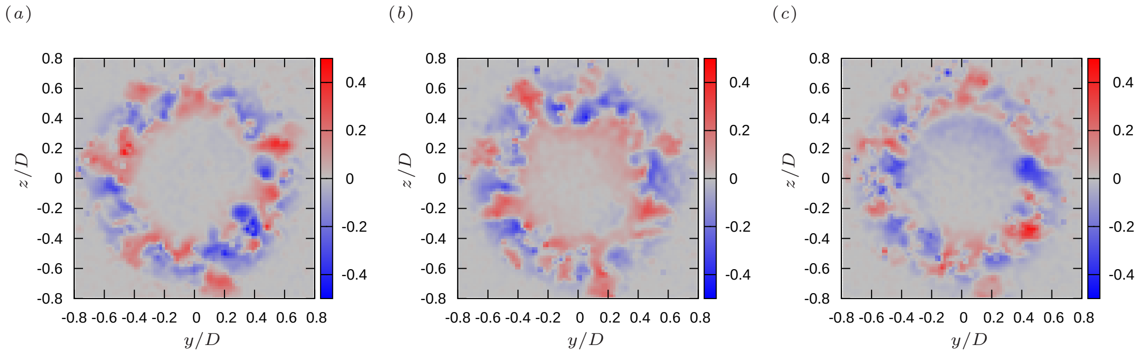

Figure 4. Sample instantaneous experimental axial velocity fluctuations at $x/D = 2$ for the Mach 0.4 jet

peak shifts to $m = 4$ for $x/D = 3$.

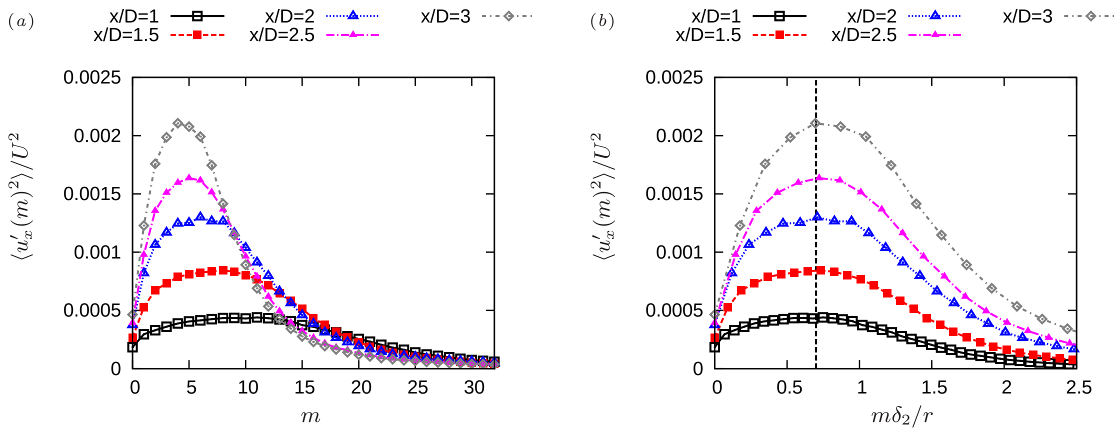

Figure 5. Energy of axial velocity fluctuations on the jet lipline as a function of azimuthal wavenumber scaled with (a) radius r and (b) local momentum thickness δ_2. Dashed line in (b) refers to $m\delta_2/r = 0.7$.

Rescaling of the azimuthal wavenumber with the local momentum thickness δ_2 for each axial station, as in figure 5(b), shows that the peak azimuthal wavenumber scales with δ_2, similar to what happens in turbulent boundary layers (the results of Tomkins and Adrian[31] show a peak for spanwise wavenumber of $k_z\delta_2 \approx 1$).

Presented in this way, the velocity field pictured in figure 4 is formed by a number of turbulent eddies. The large-scale, energy-containing structures have azimuthal coherence related to the local momentum thickness. However, we note in figure 5 that the energy for the lower azimuthal modes (e.g. $m = 0$ or 1) is not zero, despite such modes not being readily visible in an instantaneous view of the jet.

In contrast to the energy at high azimuthal wavenumbers in the velocity field, a number of experimental results[12,22,32,33] show that the radiated sound field at low polar angles is dominated by low azimuthal modes, especially for low frequencies. Figure 6 shows the far-field spectrum at $\theta = 20°$ resolved into azimuthal modes for the present $M = 0.4$ jet (the acoustic field of this jet, and of the other jets studied in the present work, is documented in detail by Cavalieri *et al.*[22]). We see that the low-frequency part of the radiated sound is dominated by the axisymmetric mode, with lower sound radiation with increasing m.

Theoretically, the difference of the dominant azimuthal wavenumbers in the turbulent and in the acoustic fields can be understood by noting that for low frequencies a condition of *radial compactness* is satisfied by the jet: the diameter is significantly lower than the acoustic wavelength. In these cases, higher azimuthal modes will have low acoustic efficiency due to the destructive interference in the $\exp(im\phi)$ factor in the acoustic source.

Use of cylindrical coordinates and azimuthal modes in Lighthill's analogy allows the quantification of this

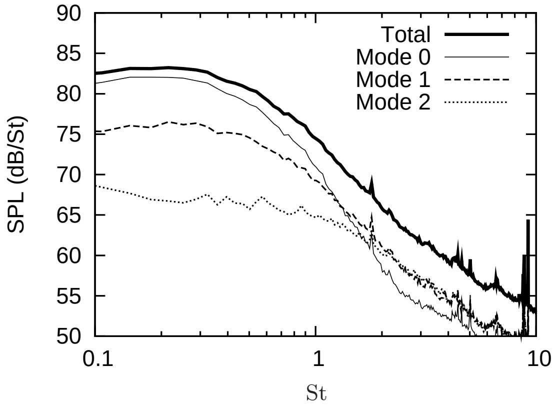

Figure 6. Spectra of individual modes in the far acoustic field for $M = 0.4$ and $\theta = 20°$. Taken from Cavalieri *et al.*[22]

effect. For low acoustic angles, consideration of azimuthal mode m and frequency ω of the T_{xx} component of Lighthill's stress tensor leads to

$$p(R, \theta, m, \omega) = -\frac{i^m k_a^2 \cos^2\theta e^{-ik_a R}}{2R} \int e^{ik_a x \cos\theta} dx \int T_{xx}(x, r, m, \omega) J_m(k_a r \sin\theta) r dr, \qquad (1)$$

where k_a is the acoustic wavenumber ω/c. The Bessel function of the first kind J_m results from azimuthal integration, and leads to a lower efficiency of high azimuthal modes, as explored previously in the litterature.[5,10,34,35]

This effect is illustrated in figure 7. Noting that $k_a r = 2\pi \mathrm{St} M r/D$, we see that the ordinate in the figure is the ratio of $J_m(k_a r \sin\theta)$ to $J_0(k_a r \sin\theta)$ in decibels, and indicates the efficiency of mode m relative to the axisymmetric mode for sound radiation at $\theta = 30°$. We note that for low Strouhal numbers this acoustic efficiency decays quite fast with increasing azimuthal wavenumber m, which suggests that low azimuthal modes in the turbulent field account for most of the sound generation at these low frequencies and polar angles, in spite of their lower energy.

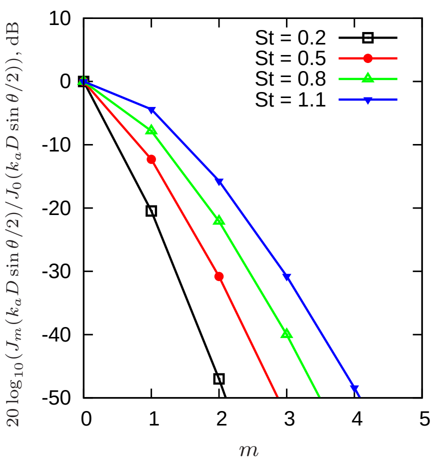

Figure 7. Acoustic efficiency for sound radiation at $\theta = 30°$ by the azimuthal mode m relative to the axisymmetric mode, for a ring source at $r = D/2$ in a $M = 0.6$ jet.

III.B. Correlations between axisymmetric modes of velocity and far-field sound

Based on the observed contrast between the dominant azimuthal modes in the velocity and far-field pressure, and on the theoretical higher acoustic efficiency of lower azimuthal modes, we have investigated the relationship between azimuthal modes in the jet and in the acoustic field with the computation of correlations between velocity and far-field pressure at $\theta = 20°$. We present first two-point correlations, defined as

$$C_{u_x,p}(x,r,R,\theta,\tau) = \frac{1}{t_f}\int_0^{t_f} u_x(x,r,\phi,t)p(R,\theta,\phi,t+\tau)\mathrm{d}t. \tag{2}$$

These correlations ignore the difference in the azimuthal content between velocity and pressure fields, and would amount to an attempt to correlate a high azimuthal wavenumber in the velocity field to a low one in the acoustic field.

If we assume instead a relationship between *azimuthal modes* in the velocity and in the acoustic field, such as in eq. (1), it makes sense to correlate, instead, the axisymmetric modes of velocity and far-field pressure, as

$$C^0_{u_x,p}(x,r,R,\theta,\tau) = \frac{1}{t_f}\int_0^{t_f} u_x(x,r,m=0,t)p(R,\theta,m=0,t+\tau)\mathrm{d}t, \tag{3}$$

which isolates the axisymmetric mode of the axial velocity before correlation with the axisymmetric part of the far-field sound.

Results of the two-point correlations, as in eq. (2), are presented in figures 8 and 9, for the $M = 0.4$ and $M = 0.6$ jets, respectively. The correlation results have a typical noise level around 0.02. This is due to the reduced number of TR-PIV samples (19414). We see that the two-point correlations in figures 8 and 9 are low, without an apparent peak above the noise level.

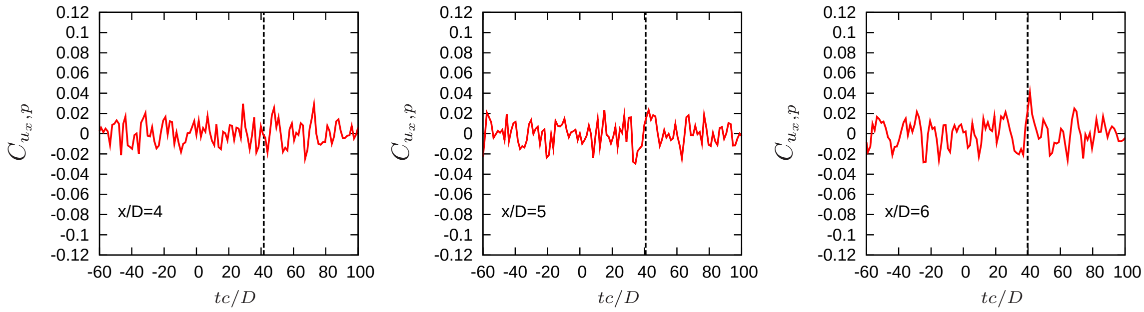

Figure 8. Two-point correlations for the $M = 0.4$ jet, taken with a velocity measurement at $r = D/4$ and far-field pressure at $\theta = 20°$. The dashed line indicates propagation time without flow-acoustic effects.

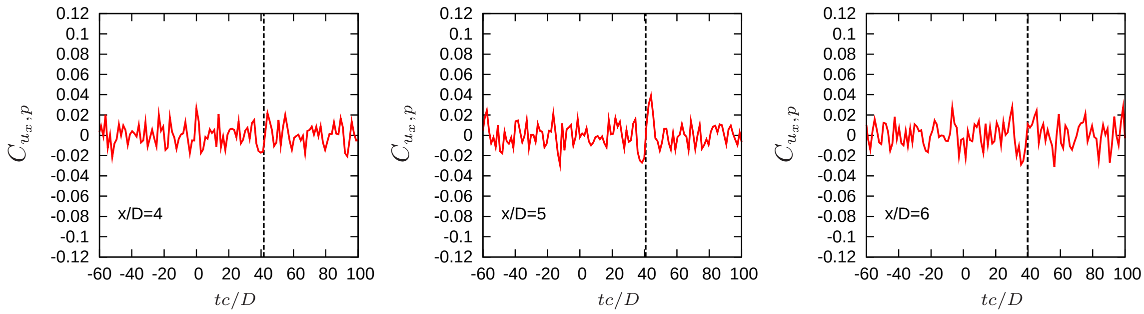

Figure 9. Two-point correlations for the $M = 0.6$ jet, taken with a velocity measurement at $r = D/4$ and far-field pressure at $\theta = 20°$. The dashed line indicates propagation time without flow-acoustic effects.

Computation of correlations between axisymmetric modes, as in eq. (3), leads to the results shown in figure 10 and 11. The correlations are now well above the noise level, and are of order of 10% for the $M = 0.6$ jet, which is significantly higher than values obtained by two-point correlations in previous studies of subsonic turbulent jets.[27,29]

In addition, previous studies showed a strong decay of two-point correlations when the reference position is moved away from the jet centerline; an example is the work of Panda *et al.*[29] In Panda *et al.*'s experiment, all correlations of subsonic jets taken at $r/D = 0.45$ were below the experimental noise level. Here we still see significant correlations for several radial positions, as illustrated in figure 12. These results support the

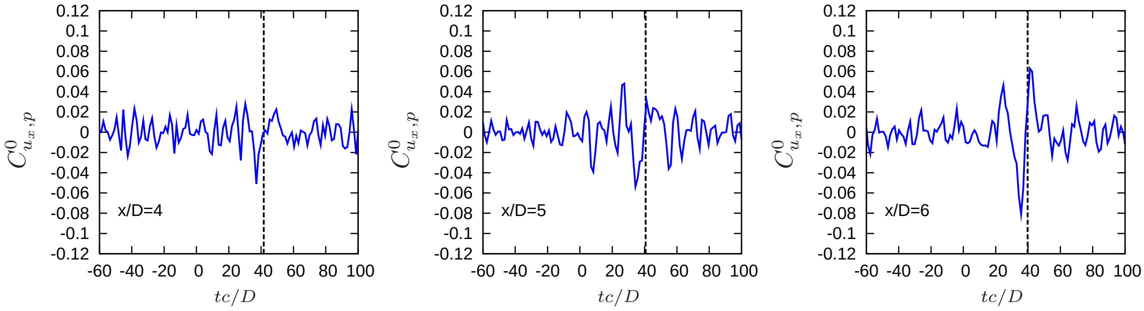

Figure 10. Correlations between mode-0 axial velocity at $r = D/4$ and mode-0 far-field pressure at $\theta = 20°$ for the $M = 0.4$ jet. The dashed line indicates average propagation time without flow-acoustic effects.

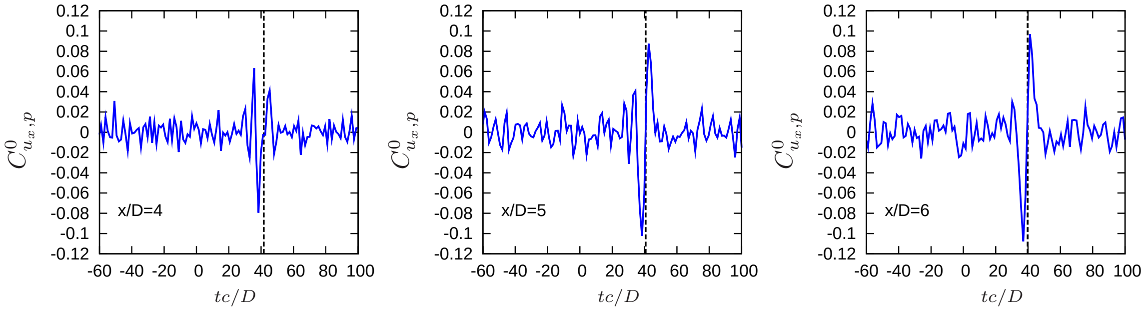

Figure 11. Correlations between mode-0 axial velocity at $r = D/4$ and mode-0 far-field pressure at $\theta = 20°$ for the $M = 0.6$ jet. The dashed line indicates average propagation time without flow-acoustic effects.

idea that the azimuthally-coherent part of the velocity field, which also happens to be radially-coherent, has higher acoustic efficiency, and, despite being less energetic than the dominant azimuthal wavenumbers, is the dominant source of low-angle sound radiation.

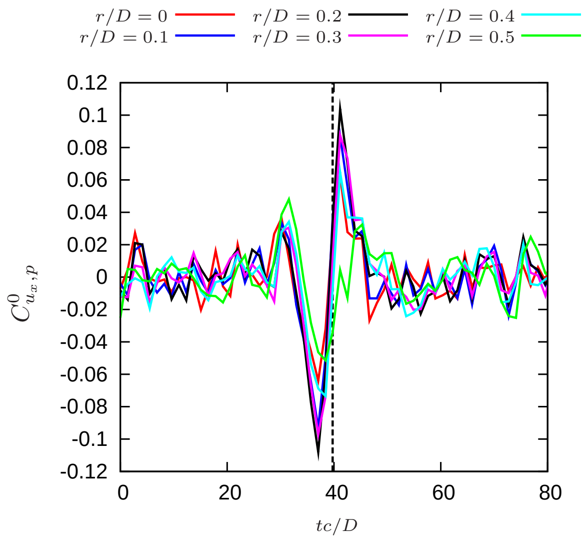

Figure 12. Correlations between mode-0 axial velocity and mode-0 far-field pressure for different radial positions. Results taken at the axial station $x/D = 6$ of the $M = 0.6$ jet

Noting that most of the acoustic field at $\theta = 20°$ is axisymmetric,[22] the present results show the significance of the axisymmetric *velocity* mode for sound radiation at low polar angles, and confirm the theoretical predictions. However, care should be taken in the interpretation of these correlation results, since we see that correlations are significant over a region which is extended in both x and r; even when C^0 is used to account for individual azimuthal modes, the correlation is performed between a ring in the flow and a second ring in the acoustic field, and thus no information is obtained about the extended axial structure of the noise source.

The observations in the present section motivate the research for an appropriate model for the lower-order azimuthal modes in a jet, which we develop in the next section as linear instability waves.

IV. Detection of linear instability waves in the velocity field

Previous experimental observations of the present jets[22] have shown that the measured acoustic radiation is compatible with a wave-like, non-compact source with low azimuthal wavenumber, and the results of the preceding section show further evidence linking the axisymmetric part of the velocity field and the radiated sound.

In the present section we investigate the lower azimuthal modes of the velocity field to ascertain if they can be modelled as instability waves. We use as a reference solution for linear instability waves a computation based on linear Parabolised Stability Equations[36] using the experimental mean field as a base flow.

Most of the results of the present section refer to the $M = 0.4$ jet, since this is the most favourable case for comparison with TR-PIV results due to the aliasing in the experiment. Further comparisons with the $M = 0.5$ and $M = 0.6$ jets are shown in Appendix A.

IV.A. Linear Parabolised Stability Equations (PSE)

Instability waves in the jets were modelled using linear PSE, following the approach described by Gudmundsson and Colonius.[16] We describe the PSE approach briefly in the present section; more details can be found in the cited paper.

PSE represent a generalisation of the parallel-flow linear stability theory for flows with a mild variation on the streamwise direction. For a free jet, the total flow field q is decomposed into a mean (time-averaged) and axisymmetric component $\bar{q}$ and its fluctuations

$$q = \bar{q} + q', \tag{4}$$

where $q = [u_x, u_r, u_\phi, T, \rho]^T$ is the vector of fluid variables. The fluctuating part is then written as a sum of Fourier modes in the azimuthal direction and in frequency

$$q'(x, r, \theta, t) = \sum_{\omega} \sum_{m=-M}^{M} \chi_{m\omega}(x, r)\ \exp(\mathrm{i}(m\phi - \omega t)), \tag{5}$$

where $\chi_{m\omega}$ is the modal function corresponding to the mode (m, ω).

The mean flow is a function of the axial and radial directions (x, r), but a slow variation of its properties along the axial direction is assumed. This assumption permits the decomposition of $\chi_{m\omega}$ into a slowly varying shape function (that evolves in the same scale as the mean flow) and a rapidly varying wave-like part:

$$\chi_{m\omega}(x, r) = A_{m\omega}(x) \cdot \hat{q}_{m\omega}(x, r) = \exp\left(\mathrm{i} \int_x \alpha_{m\omega}(\xi)\ d\xi\right) \cdot \hat{q}_{m\omega}(x, r). \tag{6}$$

Here $\alpha_{m\omega}(x)$ is a complex axial wavenumber, for which a mild variation is also assumed. It is important to stress that the separation in scales between the mean flow, and the modal shape functions on one hand, and the modal wavelengths associated with $\alpha_{m\omega}$ on the other is a necessary hypothesis in the derivation of the PSE. However, for low frequencies the wavelength can be comparable to the extent of the potential core.

We introduce the previous decomposition into the compressible Navier-Stokes, continuity and energy equations. After subtraction of the terms corresponding to the mean flow, and neglecting quadratic terms on the fluctuations, we arrive at the system of equations

$$\left(\mathcal{L}^0 - \mathrm{i}n\omega\mathcal{L}^t + \mathcal{L}^x\frac{\partial}{\partial x} + \mathcal{L}^r\frac{\partial}{\partial r} + \mathrm{i}m\frac{\mathcal{L}^\theta}{r} + \right)\hat{q}$$
$$+\frac{1}{Re_a}\left(\mathcal{V}^0 + \mathcal{V}^x\frac{\partial}{\partial x} + \mathcal{V}^r\frac{\partial}{\partial r} + \mathrm{i}m\frac{\mathcal{V}^\theta}{r} + \mathcal{V}^{xx}\frac{\partial^2}{\partial x^2} + \mathcal{V}^{rr}\frac{\partial^2}{\partial r^2}\right.$$
$$\left.-m^2\frac{\mathcal{V}^{\theta\theta}}{r^2} + \mathcal{V}^{xr}\frac{\partial^2}{\partial x\partial r} + \mathrm{i}m\frac{\mathcal{V}^{r\theta}}{r}\frac{\partial}{\partial r} + \mathrm{i}m\frac{\mathcal{V}^{x\theta}}{r}\frac{\partial}{\partial x}\right)\hat{q} \quad = \quad \frac{\hat{F}_{mn}}{A_{mn}}. \tag{7}$$

The linear operators $\mathcal{L}$ and $\mathcal{V}$ can be found elsewhere.[37] For brevity, the subscripts have been dropped from the shape function and wavenumber in the previous expression. The left-hand-side on (7) is a linear spatial operator for the mode (m, ω), and each frequency-azimuthal mode component evolves independently of the others. Following from the slow axial variation assumed for $\hat{q}$, the second axial derivatives on the viscous terms are neglected, so that the system of equations can be integrated along the x-direction. The decomposition of (6) is ambiguous in that the evolution of χ can be absorbed into either the shape function $\hat{q}_{m\omega}$ or the complex amplitude $A_{m\omega}$ corresponding to the wave-like behavior. Following Herbert,[36] the normalisation condition

$$\int_0^\infty \hat{q}^* \frac{\partial \hat{q}}{\partial x} r \, dr = 0, \tag{8}$$

where the superscript $*$ denotes complex conjugation, is imposed individually to every mode, removing the exponential dependence on the shape function $\hat{q}$.

The characteristic boundary conditions of Thompson[38] are used for the outer boundary, while centerline conditions are derived following Mohseni and Colonius.[39] The same approach of Gudmundsson and Colonius[16] was applied to obtain numerical solutions of the system of equations (7). The reader is referred to that paper for further details on the computational method.

Adequate boundary conditions are required at the inlet, especially for $\hat{q}$ and α, for each mode. The complex amplitudes $A_{m\omega}$ can be rescaled after the computations in order to fit experimental measurements, as linear PSE results are independent of the modal amplitudes and phases. A 'local' spatial linear instability eigenvalue problem (EVP) can be derived from the equations (7); from its solution, the dominant inflectional instability eigenmode is taken as initial condition for $\hat{q}$ and α.

IV.B. Comparison with experimental velocity fluctuations on the jet centerline

The linear modes have a free amplitude, and this has been adjusted using the velocity spectra on the jet centerline. There the kinematic boundary conditions are zero transverse velocity and finite axial velocity for azimuthal mode 0, zero axial velocity and finite transverse velocity for mode 1, and zero velocities for all higher modes.[40] As the velocity measurements were performed with a single hot wire, we expect that in the potential core the measurements will be of the axial velocity, allowing thus the comparison between the mode 0 from linear PSE and the hot wire spectra.

Figure 13 shows comparison, between linear PSE and experiment, of the amplitude for the streamwise velocity component for the Mach 0.4 jet. The free constant multiplying linear PSE amplitudes was chosen by matching amplitudes at $x/D = 2$. Between the nozzle exit and the end of the potential core ($x/D \approx$ 5–5.5) there is an amplification of four orders of magnitude of the fluctuation energy in the experiment. In this region there is close agreement between linear PSE and the experimental values for Strouhal numbers of 0.3–0.9.

We note in figure 13 differences between the modelled instability waves and the experimental results for points downstream of the end of the potential core. Similar behaviour was also observed in previous work by Suzuki and Colonius[15] and Gudmundsson and Colonius.[16] In these papers the discrepancies were attributed to fluctuations that were uncorrelated with the upstream instability waves. Proper Orthogonal Decomposition (POD) was applied to obtain modes correlated axially, and the use of the first POD modes allowed uncorrelated oscillations to be filtered, improving significantly the agreement at downstream positions. However, since the hot-wire measurements are single-point we could not apply a POD to these results to verify if this also appplies also for the current experiments.

For the two lower Strouhal numbers, 0.1 and 0.2, shown in figures 13(a) and (b), linear PSE underpredicts the growth rate of the axisymmetric mode. This was also the case in other works[15,16] and as shown in

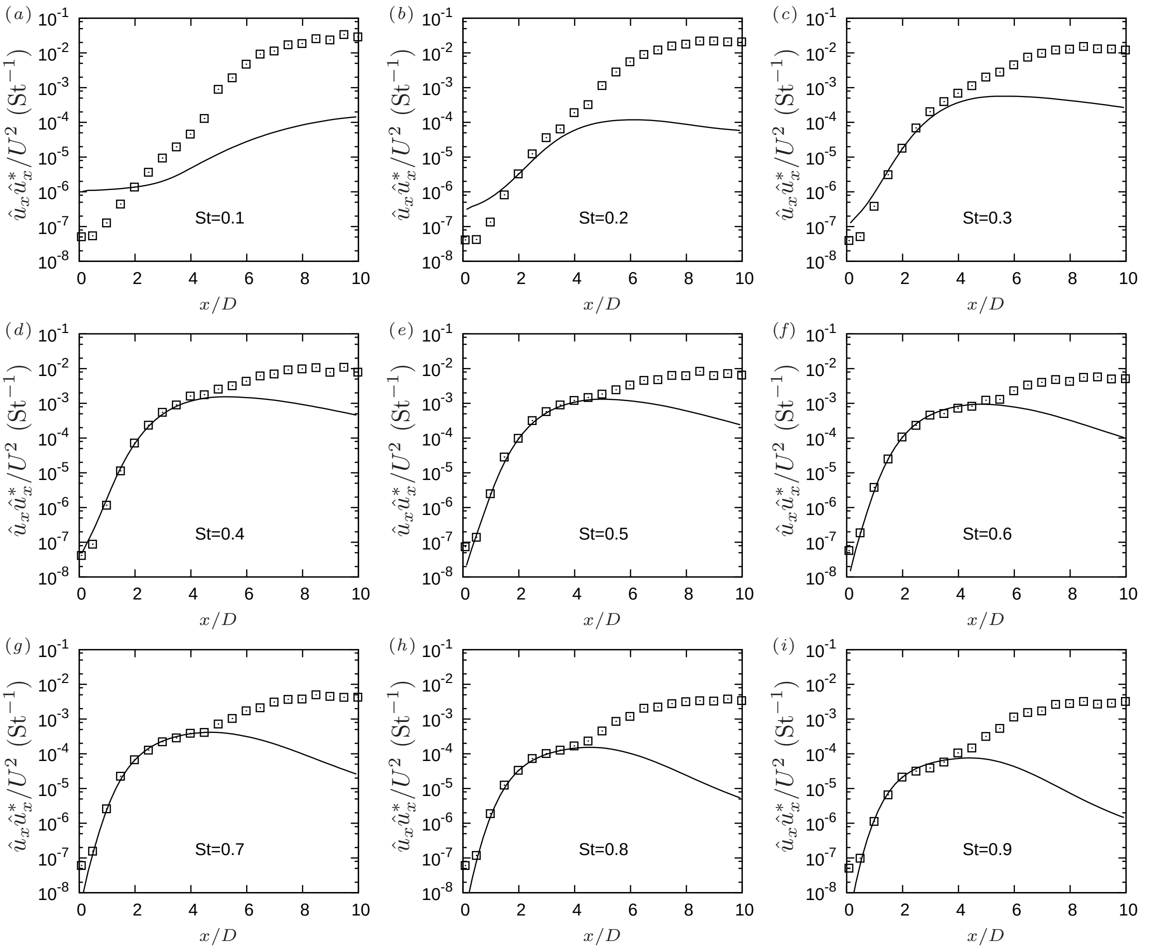

Figure 13. Comparison between linear PSE (lines) for $m = 0$ and experimental velocity fluctuations on the centerline (symbols) for the $M = 0.4$ jet. Subfigures (a)–(i) refer respectively to Strouhal numbers from 0.1 to 0.9 with increments of 0.1.

Appendix A, is also verified for the higher Mach numbers. These discrepancies have been attributed in the cited papers to increased non-parallel effects for these lower frequencies, since the potential core length becomes comparable to the wavelength for these Strouhal numbers, which invalidates the hypotheses in the PSE derivation shown in section IV.A. The lack of agreement at low Strouhal numbers may also be due to non-linear effects; such a possibility has been considered by Sandham and Salgado[41] and Suponitsky *et al.*,[42] who show in computations how the non-linear interaction between waves at higher Strouhal numbers may affect the development of low-St velocity fluctuations and change the radiated sound field. The present results do not, however, allow us to discern between these two possibilities to explain the said discrepancies.

Similar agreement is found for the other jets over the same St range; this is shown in Appendix A. However, due to the compressibility effects discussed by Cavalieri *et al.*,[22] the normalised amplitudes of the linear PSE modes on the jet centerline become lower as the Mach number is increased. This is shown in figure 14 for three Strouhal numbers. We note that the amplitudes near the nozzle exit are quite close, and lower growth rates due to compressibility lead to decreases in amplitudes for higher Mach numbers. The linear PSE modes are seen to correctly model these observed trends in the experimental fluctuations.

IV.C. Cross-stream planes

Velocity measurements using time-resolved PIV in cross-stream planes of the jet allow application of a Fourier transform in time and of a Fourier series in azimuth, leading to a decomposition of the velocity field in both frequency and azimuthal wavenumber, such as in eq. (5). This allows in turn comparison of experiment with

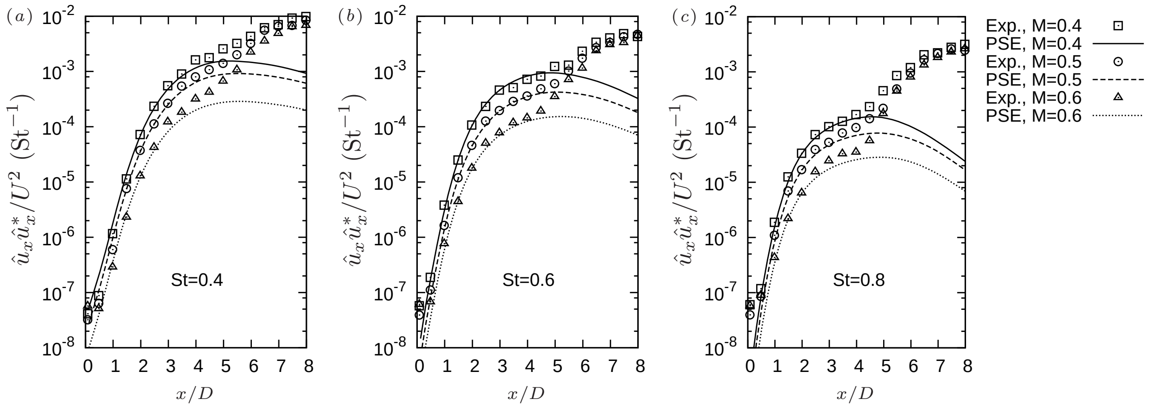

Figure 14. Compressibility effect in the velocity fluctuations and in the linear PSE amplitudes for (*a*) St $= 0.4$, **(*b*)** St $= 0.6$ **and (*c*)** St $= 0.8$**.**

linear PSE results for each (ω, m) pair at several axial and radial positions.

We show first comparisons for the axisymmetric mode at $x/D = 2$ in section IV.C.1 to explain some of the general features of both experiment and PSE solution. The first helical mode is compared to linear PSE at the same axial station in section IV.C.2. Finally, the axial development of instability waves is studied in section IV.C.3. All comparisons in the present section were made for the $M = 0.4$ jet.

Throughout this section, comparisons are restricted to the Strouhal number range of 0.3—0.7. Comparisons for Strouhal numbers of 0.1 and 0.2, not shown here, did not show good agreement with linear instability wave models, similarly to what was verified for the hot-wire data in section IV.B.

IV.C.1. Axisymmetric mode at x/D=2

The stereoscopic TR-PIV results were compared to the radial shapes of the PSE solutions for azimuthal modes $m = 0$, 1. We begin the study of linear instability waves by looking at the axisymmetric mode of the $M = 0.4$ jet in the present section, focusing first on jet cross section at $x/D = 2$. In all comparisons of the axisymmetric mode obtained by TR-PIV results we have used the linear PSE results with amplitudes for u_x matched using the hot-wire spectra at $x/D = 2$ and $r/D = 0$; hence, no further adjustement was performed to match the PIV results. Figure 15 shows a comparison of the axial velocity fluctuations at this station for $m = 0$.

As seen in section III.A, the fluctuation energy of the axisymmetric mode close to the jet lipline is much lower than the overall flucutation energy, shown in dash-dot lines in figure 15. This is in contrast to the jet centerline, where all axial velocity fluctuations correspond, as expected, to the axisymmetric mode.

The comparison in figure 15 between PSE and experimental mode 0 shows a fair agreement. However, the PSE solution presents nearly zero amplitudes at a radial position close to the lipline (the precise position depends on the frequency). To understand the meaning of this zero amplitude, we see in figure 16 a comparison of the phase between experiment and linear PSE for Strouhal number of 0.7. We note that in the experiment there is a phase jump of π between the two sides of the mixing layer, a behaviour also represented by the PSE solution.

This phase opposition for the streamwise velocity is found in coherent, axisymmetric vortical structures obtained by phase averages of forced jets,[8,9,17] and was also seen previously in unforced jets.[43] This is illustrated in figure 16(b). At the radial position of the center of a vortex, shown with a dashed line, the axial velocity is zero; therefore, a forced jet consisting mostly of periodic vortex rings presents a nearly zero amplitude for the streamwise velocity at the radial position of the vortex centers. We can conjecture that the jitter of coherent structures in an unforced jet will lead to temporal changes in the radial position of the centers, so that the experimental amplitude is not zero.

Based on this conjecture, in an attempt to obtain an average structure of the streamwise velocity without jitter, we have applied spectral POD in the radial direction to extract the correlated part of the fluctuations,

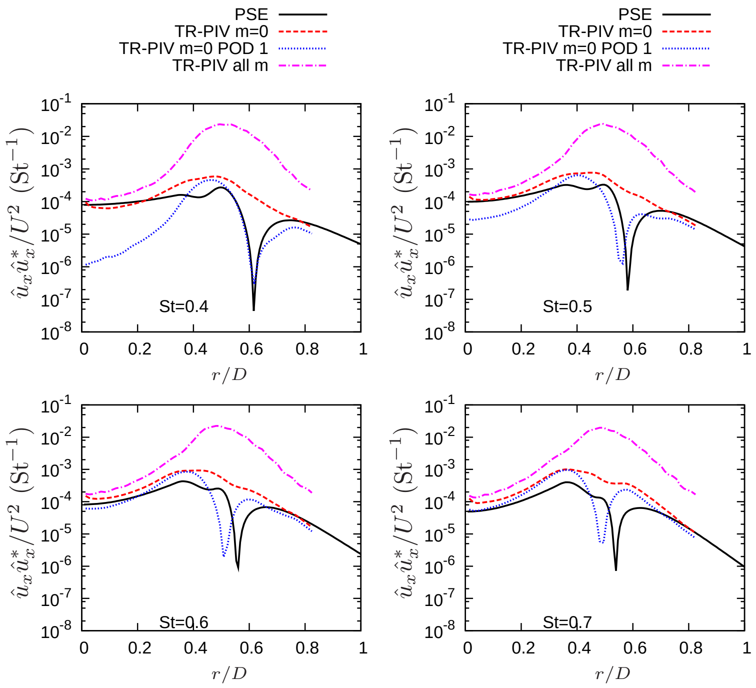

Figure 15. Comparison between u_x from linear PSE and experiment for $m = 0$, $M = 0.4$ and $x/D = 2$

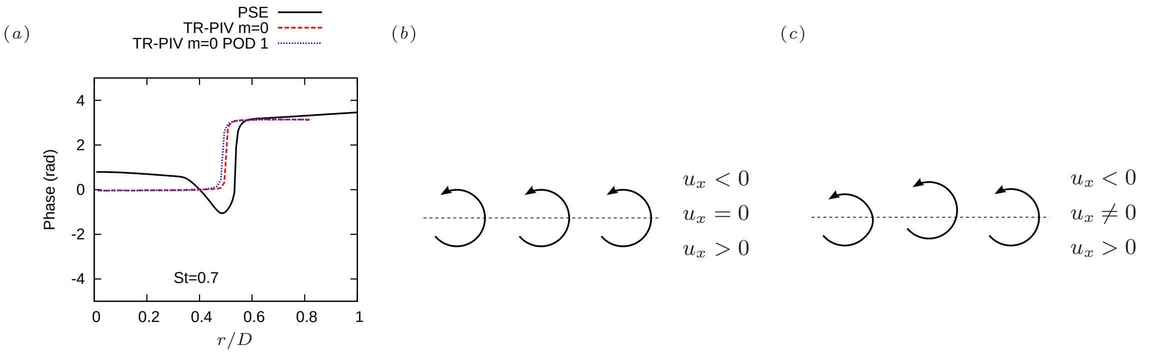

Figure 16. (*a*) Phases of the streamwise velocity for the axisymmetric mode at $\mathrm{St} = 0.7$ and $x/D = 2$(phase is fixed as zero at $r/D = 0.4$); (*b*) sketch representing the phase difference across a mixing layer with a developping Kelvin-Helmholtz instability; (*c*) effect of jitter in the position of vortex centers

using the same approach described by Jung *et al.*,[44] which amounts to solving the integral equation

$$\int R_{x,x}(x,r,r',m,\omega)\xi_x(x,r',m,\omega)r'\mathrm{d}r' = \lambda(x,m,\omega)\xi_x(x,r,m,\omega) \tag{9}$$

where ξ is an eigenfunction (POD mode), λ is the corresponding eigenvalue and and $R_{x,x}$ is given by

$$R_{x,x}(x,r,r',m,\omega) = u_x(x,r,m,\omega)u_x^*(x,r',m,\omega). \tag{10}$$

This kernel $R_{x,x}(x,r,r',m,\omega)r$ is not Hermitian; an auxiliar Hermitian kernel was obtained, as in Jung *et al.*,[44] by multiplying the integral equation (9) by $\sqrt{r}$ and considering $R_{x,x}(x,r,r',m,\omega)\sqrt{r'r}$ as the kernel and $\xi_x(x,r,m,\omega)\sqrt{r'}$ as the eigenfunction.

The POD defined in eq. (9) was done for each velocity component independently. We have also applied a POD with the three velocity components in the kernel, as done by Delville,[45] and results are shown in Appendix B. However, for the presentation of the results we have preferred the scalar POD, since, as shown in Appendix B, the vectorial POD led to nearly identical results, but with the velocity components split into different modes, suggesting that a single physical phenomenon was separated in different POD modes. The scalar POD was considered less ambiguous, and, as will be seen, linear instability waves were consistently detected using the first scalar POD mode for each velocity component.

Throughout this section we have used the projection of the experimental results onto the mode with highest energy, obtained by

$$\mathrm{POD}(u_x) = \sqrt{\lambda^{(1)}}\xi_x^{(1)}, \tag{11}$$

where $\lambda^{(1)}$ is the highest eigenvalue and $\xi_x^{(1)}$ the corresponding eigenfunction, was used to extract the coherent part of the velocity field, and is referred to as the "first POD mode" through the remainder of this paper.

This first POD mode for u_x is plotted in figures 15 and 16, where we see that this mode presents indeed an amplitude close to zero near the lipline, at the position of the phase jump. The position of this zero amplitude agrees closely with the PSE solution, as shown in figure 15.

The radial velocity is compared in figure 17. Note that linear PSE solutions have the same free constant multiplying all flow variables; therefore, no further adjustement is done for this comparison. The agreement between linear PSE and experiment is good, especially considering the first POD mode close to the centerline. Since the radial velocity should be zero on the centerline for $m = 0$, the present results suggest that POD acts in this case as a filter, removing some of the uncorrelated noise in the experimental results and leading to the correct trend for the radial velocity close to the centerline.

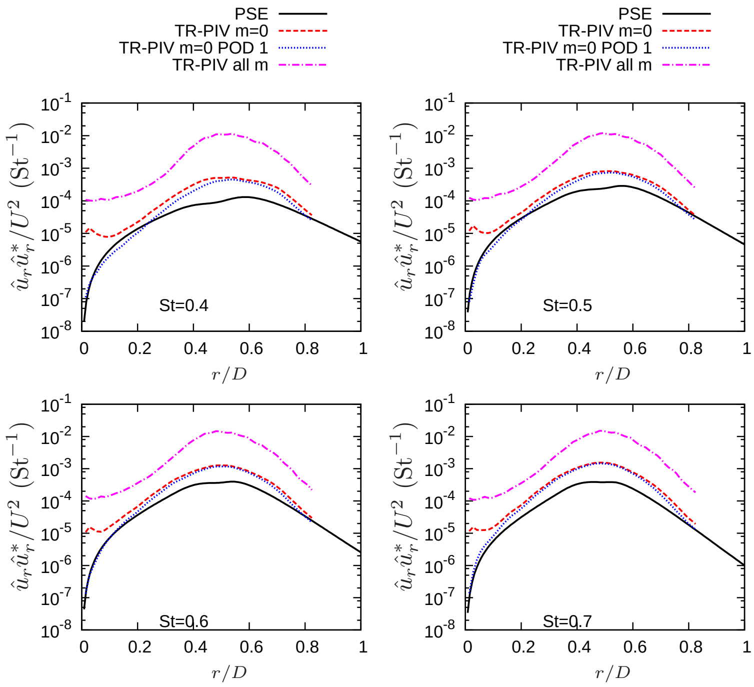

Figure 17. Comparison between u_r from linear PSE and experiment for $m = 0$, $M = 0.4$ and $x/D = 2$

IV.C.2. First helical mode at x/D=2

As in the axisymmetric case, linear PSE solutions have a free constant that is determined using experimental data. However, since the hot-wire measurments of axial velocity on the centerline cannot give information about helical modes, we have used the TR-PIV results at $x/D = 2$ to determine this free amplitude for $m = 1$. We define an inner product

$$\langle u(x,r,\omega,m), \varphi(x,r,\omega,m)\rangle = \int \big[u_x(x,r,\omega,m)\varphi_x^*(x,r,\omega,m) \\ + u_r(x,r,\omega,m)\varphi_r^*(x,r,\omega,m) + u_\phi(x,r,\omega,m)\varphi_\phi^*(x,r,\omega,m)\big]\, r\mathrm{d}r \tag{12}$$

between the experimental results and the linear PSE solutions, where φ refers to the velocity modelled by the PSE solution $\chi_{m\omega}$. If the velocity field can be expressed as

$$u(x, r, \omega, m) = b(x, \omega, m)\varphi(x, r, \omega, m), \tag{13}$$

the value of b can be determined as

$$b(x, \omega, m) = \frac{\langle u(x, r, \omega, m), \varphi(x, r, \omega, m)\rangle}{\|\varphi(x, r, \omega, m)\|^2}. \tag{14}$$

We have used the results at $x/D = 2$ to determine $b(x = 2D, \omega, m)$, and used this value of b as the free constant multiplying the linear PSE results for all values of x and r.

Figure 18 presents comparisons for the axial velocity at $x/D = 2$. The radial velocity in the same axial station is compared in figure 19. We note that, as for the axisymmetric mode, the solution of linear PSE presents a nearly zero amplitude close to the jet lipline, which compares favourably with the first POD mode calculated from the experimental data. The agreement between model and experiment is good for both the axial and radial velocity components, although for $m = 1$ the agreement is not as close as for the axisymmetric mode shown in section IV.C.1.

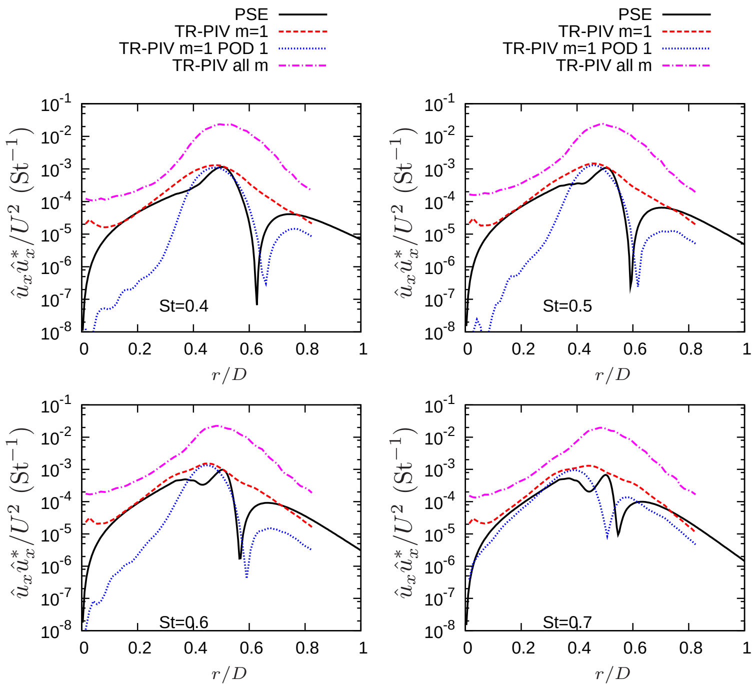

Figure 18. Comparison between u_x from linear PSE and experiment for $m = 1$, $M = 0.4$ and $x/D = 2$

IV.C.3. Axial development of instability waves

We illustrate the development of linear instability waves in the jet by comparing the linear PSE solution for Strouhal number of 0.5 to the experimental results for both the axisymmetric and first helical modes at axial stations ranging from $x/D = 1$ to $x/D = 8$. This comparison is shown for the axisymmetric mode in figure 20 for the axial velocity, and in figure 21 for the radial velocity fluctuations.

We see in figures 20 and 21 three distinct zones in the jet with regard to the development of instability waves. In a first region, exemplified with the results for $x/D = 1$ and $x/D = 1.5$, the velocity fluctuations present some differences from the linear instability model, suggesting that this near-nozzle region is characterised by a transition from the fluctuations internal to the nozzle to the Kelvin-Helmholtz instability observed downstream. This transition is more clearly seen in the fluctuations close to the jet lipline; on the centerline, the flow seems to conform earlier to a jet instability, at, say, $x/D = 0.5$, as seen in the hot-wire

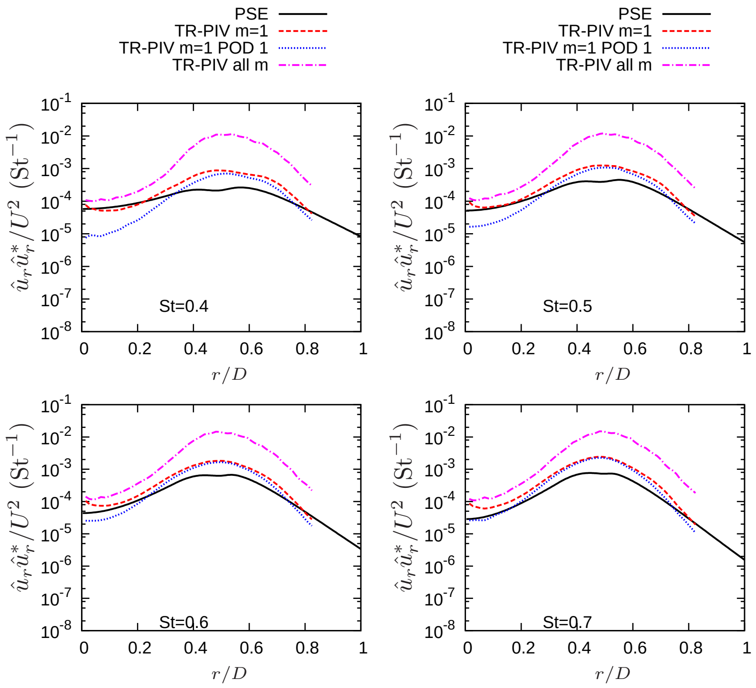

Figure 19. Comparison between u_r from linear PSE and experiment for $m = 1$, $M = 0.4$ and $x/D = 2$

results in section IV.B. Another possibility to explain results for low x is that in this region instability waves are indeed present, but do not dominate the velocity fluctuations, especially close to the lipline.

Between $x/D = 2$ and the end of the potential core ($x/D \approx 5.5$ for the $M = 0.4$ jet) the velocity fluctuations are closely matched by linear PSE, for both axial and radial velocity fluctuarions. However, for locations downstream of the end of the potential core, the agreement between the instability-wave model and the experiment becomes progressively worse, as exemplified in the results for $6 \leq x/D \leq 8$. The comparison of results in this region leads to three hypotheses:

H1. Downstream of the end of the potential core nonlinear effects become significant in the development of wavepackets, invalidating any linear instability-wave model;

H2. Linear instability waves persist for high x, but account only for a small part of the azimuthally-coherent overall energy;

H3. The instability-wave *Ansatz* no longer applies to describe velocity fluctuations in this region: downstream of the potential core the wavepackets degenerate into turbulence.

These hypotheses will be investigated in more detail in the near future, with further exploration of the experimental database. The third possibility seems less likely on account of the persistance of the Kelvin-Helmholtz shape of disturbance amplitudes, with a zero value close to the lipline for the first POD mode for stations well beyond the potential core, as seen in figure 20. Current work by our group includes nonlinear PSE computations in order to evaluate if inclusion of nonlinear interaction between wavepackets leads to better agreement in the downstream region.

Results representing the development of the instability wave for the helical mode at St $= 0.5$ are shown in figures 22 and 23, for the axial and radial velocity components, respectively. We observe an overall picture similar to the $m = 0$ results; however, for $m = 1$ the discrepancies between linear PSE and experiment start to become significant for $x/D \approx 4$ for the axial velocity (the radial velocity presents fair agreement up to $x/D = 5$).

To present these results, and also comparisons for other Strouhal numbers, in a more compact manner, we have used the inner product defined in eq. (12) to define a metric β of the agreement between linear PSE

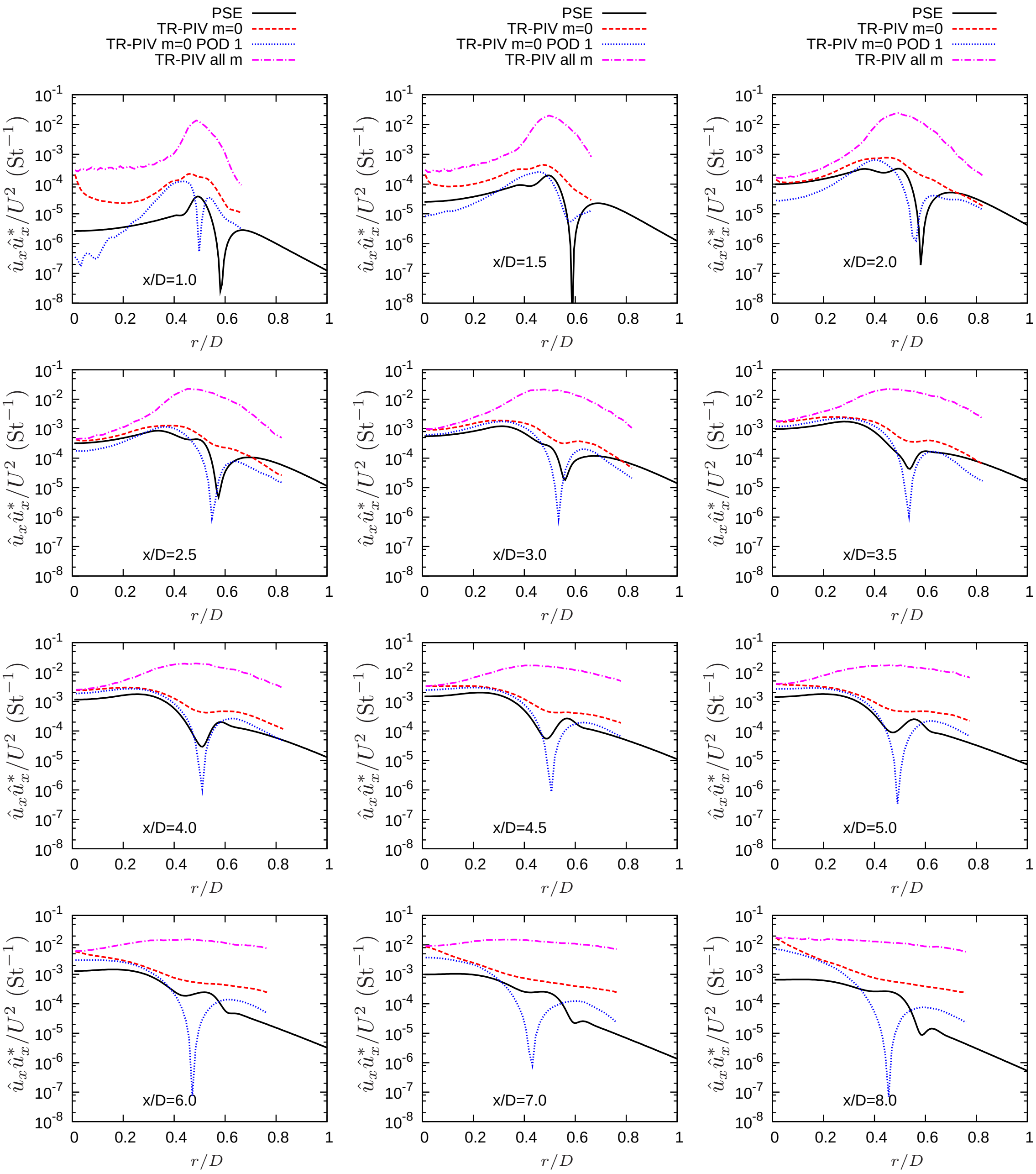

Figure 20. Comparison between u_x from linear PSE and experiment for $m = 0$, $M = 0.4$ and $\mathrm{St} = 0.5$. $x/D = 1$, 1.5, 2, 2.5, 3, 3.5, 4, 4.5, 5, 6, 7, 8

and experiment, similar to what is done by Gudmundsson and Colonius.[16] If we define

$$\beta(x, \omega, m) = \frac{\langle u(x, r, \omega, m), \varphi(x, r, \omega, m)\rangle}{\|u(x, r, \omega, m)\|\|\varphi(x, r, \omega, m)\|} \tag{15}$$

we have $0 \leq |\beta| \leq 1$, where $|\beta(x, \omega, m)| = 1$ means that linear PSE and experiment have exactly the same radial shapes for the three velocity components for given axial station, frequency and azimuthal mode. On the other hand, $|\beta(x, \omega, m)| = 0$ indicates orthogonality between model and experiment.

We have calculated the β metric using the first POD mode in eq. (15), since it allows the extraction of the coherent part of the instability wave from the experimental results. Results of the metric $|\beta|$ are shown

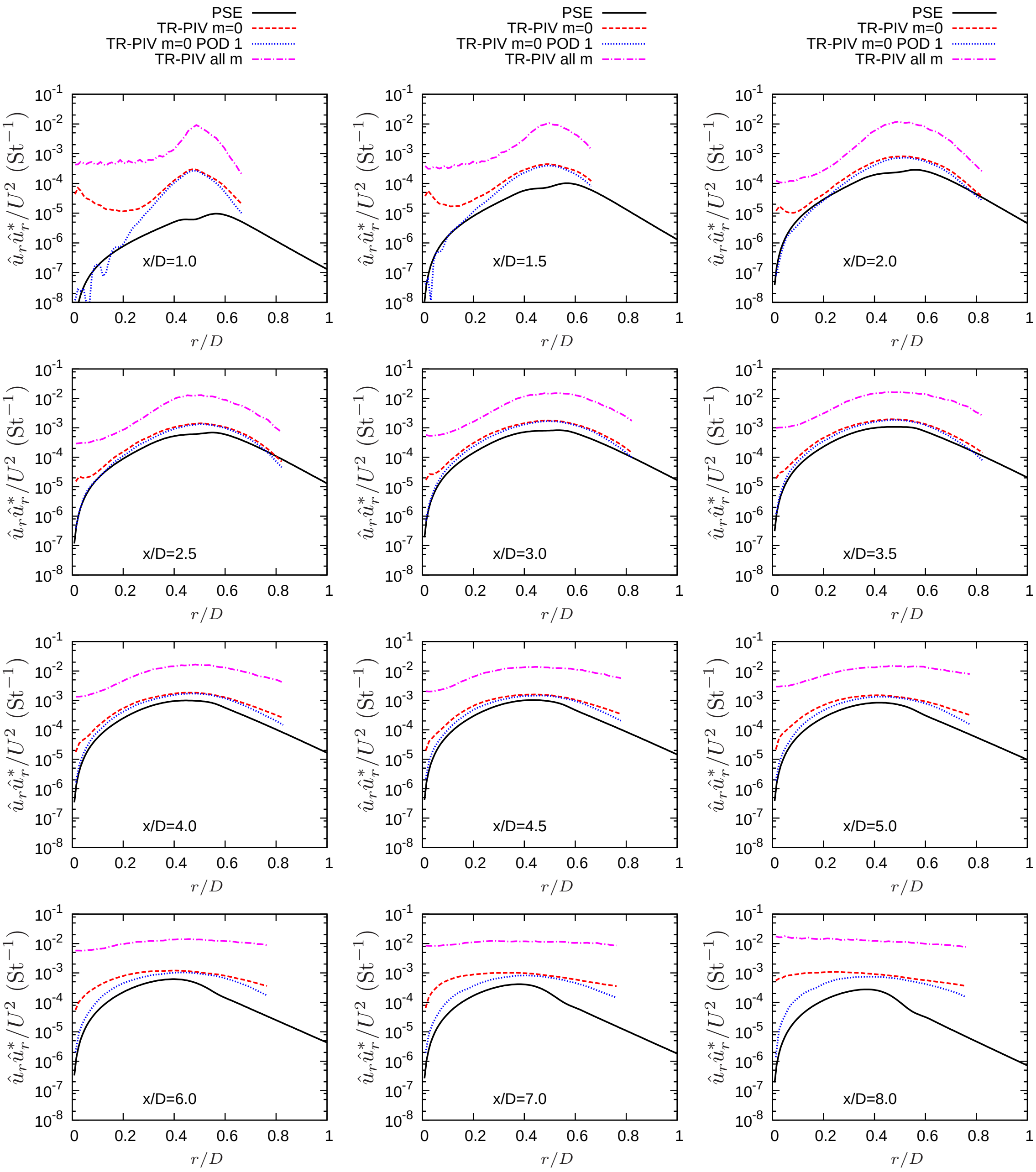

Figure 21. Comparison between u_r from linear PSE and experiment for $m = 0$, $M = 0.4$ and St $= 0.5$. $x/D = 1$, 1.5, 2, 2.5, 3, 3.5, 4, 4.5, 5, 6, 7, 8

in figures 24 (a) and (b), for azimuthal modes 0 and 1, respectively.

The agreement for the axisymmetric mode is in general better than for the first helical mode. The results in figure 24 show in all cases the three regions aforediscussed. In an initial region, agreement is somewhat worse; this is followed by a region upstream of the end of the potential core with close agreement between PSE and experiment, and at downstream positions discrepancies between model and experiment become significant.

On the other hand, we note that the values of β are *frequency-dependent*. Instability waves with high St tend match better the experimental results for low x, and the inverse happens at downstream positions,

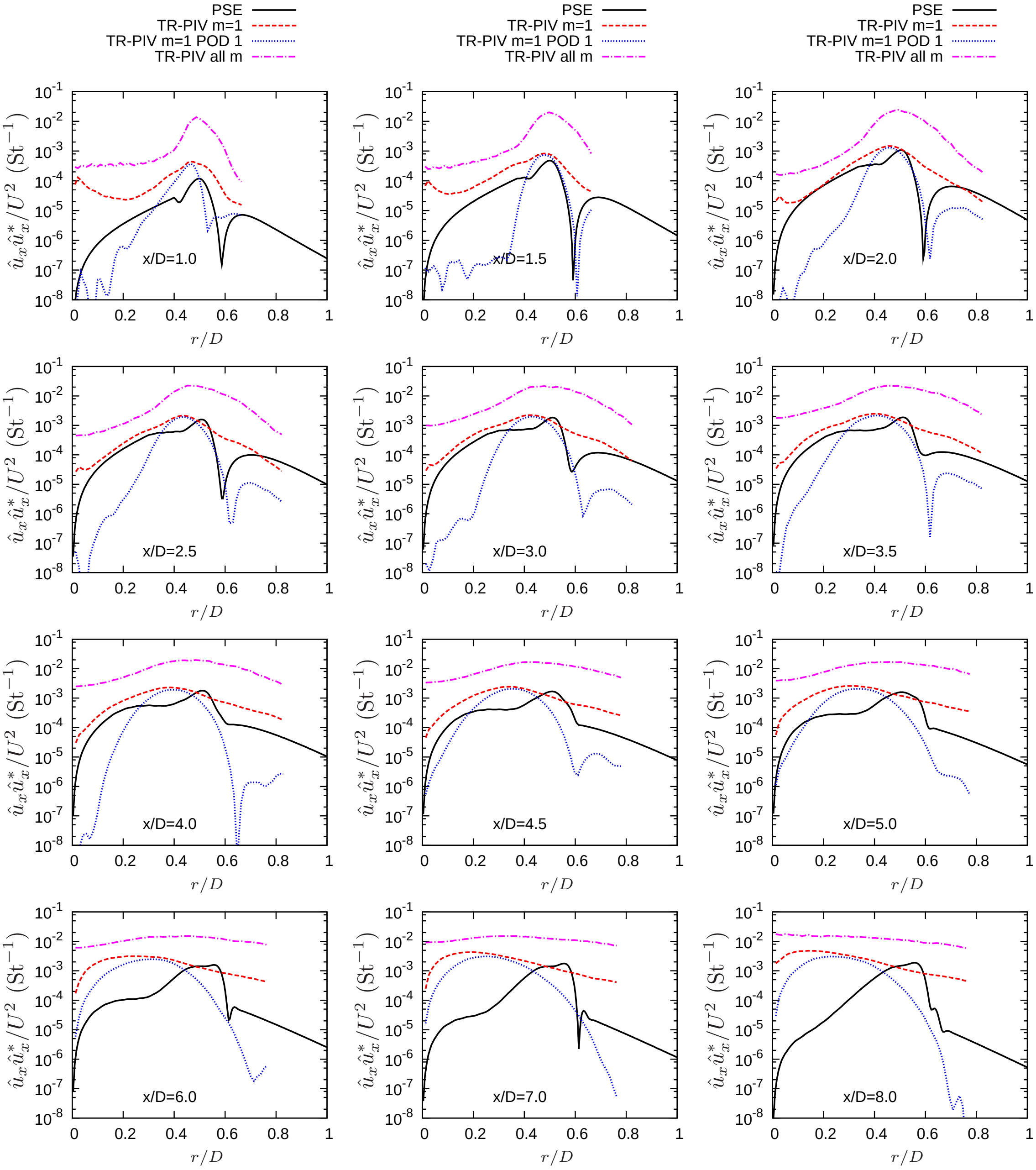

Figure 22. Comparison between u_x from linear PSE and experiment for $m = 1$, $M = 0.4$ and $\mathrm{St} = 0.5$. $x/D = 1$, 1.5, 2, 2.5, 3, 3.5, 4, 4.5, 5, 6, 7, 8

where agreement with low St is better. This trend is consistent with the growth rates expected for each axial station. For low values of x/D, the relatively thinner mixing layer will lead to a high frequency for maximum growth rate, and instability waves with high St will have a fast spatial growth near the nozzle exit. They tend thus to dominate early the overall fluctuations for a given frequency and azimuthal mode, while low-St waves, with lower growth rate, take a longer extent to have a significant contribution for the measured velocity fluctuations.

This situation is reversed downstream, since the velocity profile becomes progressively stable to high Strouhal numbers, whereas waves with low St are amplified in a longer extent of the jet. The decay of the

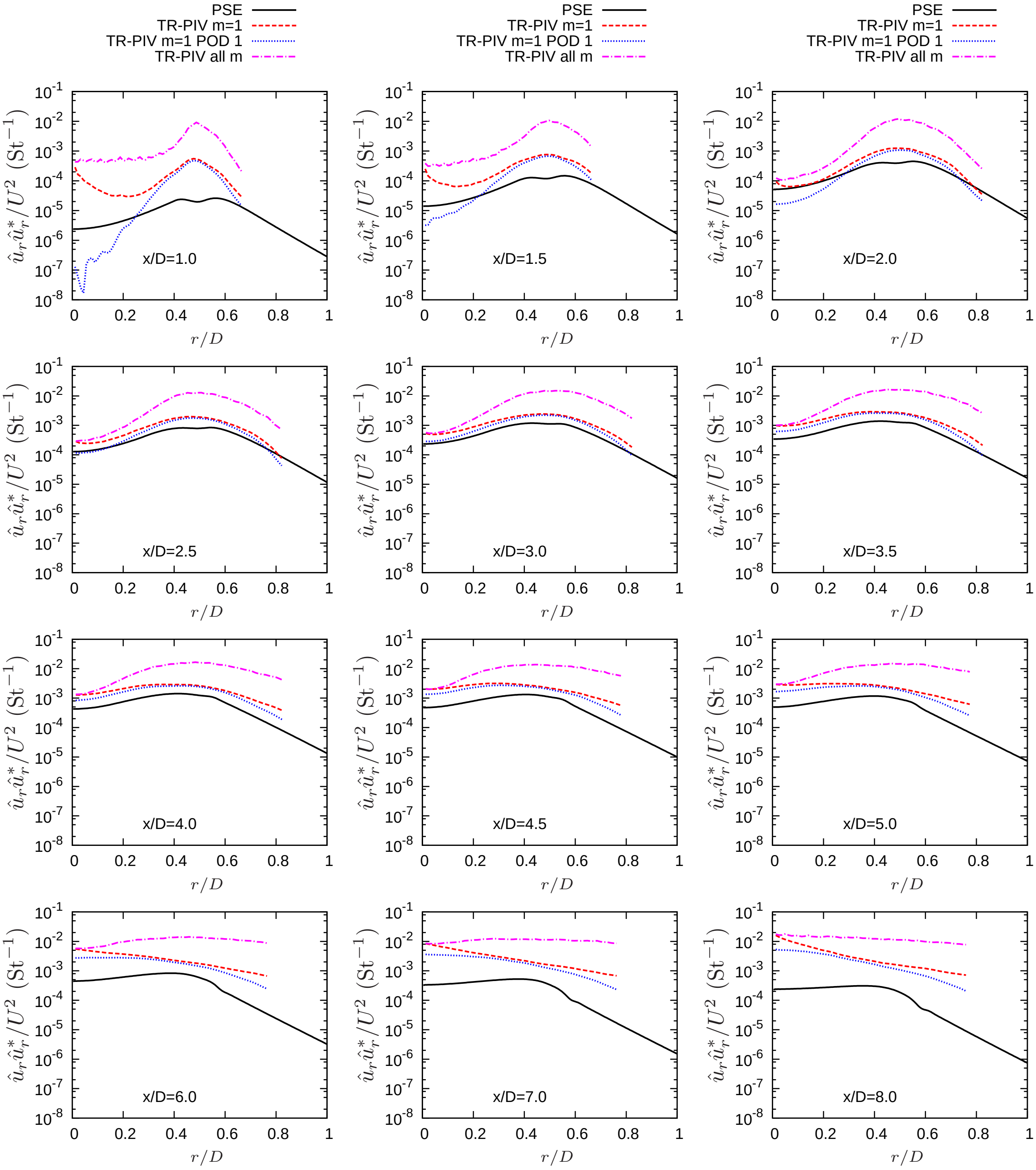

Figure 23. Comparison between u_r from linear PSE and experiment for $m = 1$, $M = 0.4$ and $\mathrm{St} = 0.5$. $x/D = 1$, 1.5, 2, 2.5, 3, 3.5, 4, 4.5, 5, 6, 7, 8

high-frequency disturbances suggests that the velocity field is no longer dominated, in the downstream region, by instability waves with high Strouhal number. The downstream persistance of low-frequency instability waves may explain their better agreement with the experimental results.

V. Conclusion and perspectives

We present a study of velocity fluctuations in turbulent subsonic jets without externally-imposed forcing, with time-resolved measurements allowing the extraction of azimuthal modes in the flow and in the acoustic

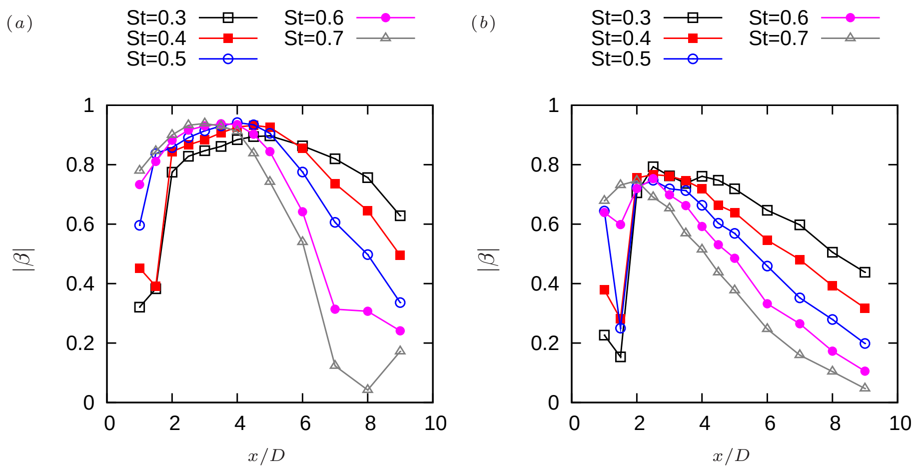

Figure 24. Absolute value of normalised inner product between linear PSE and experiment for (a) $m = 0$ and (b) $m = 1$.

field. The velocity field is seen to present significant energy for high azimuthal wavenumbers, whereas low-angle radiation is predominantly axisymmetric. On the other hand, the axisymmetric mode has non-zero amplitude, and when the axisymmetric part of the velocity field is isolated from the turbulence and correlated to the far-field sound, correlations of order of 10% are obtained, values significantly higher than two-point correlations obtained for these jets and other experiments for subsonic jets.

The velocity field is then studied to verify if this axisymmetric structure, and also the first helical mode, can be described as a superposition of linear instability waves. Linear PSE is used for this, providing a model for linear instability waves accounting for the slow divergence of the experimental mean velocity profiles. There is good agreement for azimuthal modes 0 and 1 until the end of the potential core, showing that linear instability waves are an appropriate model for the development of flucutations in such flows, and that these modes present a wave-packet structure, in agreement with source models identified using far-field information.[22,46,47]

The agreement found between linear PSE and the experimental velocity fluctuations is a further support of the contention that the fluctuations in turbulent jets, for low Strouhal numbers and azimuthal wavenumbers, can be described as linear instability waves with the mean field as a base flow, at least until the end of the potential core. Some nonlinearity is nonetheless implicit, since the base flow in the computations is the experimental mean field. The background turbulence can be seen to establish this mean field via the Reynolds stresses; this base flow now supports a linear Kelvin-Helmholtz instability leading to an extended hydrodynamic wavepacket.

The linearity of the velocity fluctuations contrasts with some numerical studies for low Reynolds number jets,[42,48] which show that non-linear effects are necessary to describe the evolution of near-field disturbances. In these transitional flows, most of the kinetic energy of fluctuations is related to azimuthally-coherent structures formed during laminar-turbulent transition; these high amplitudes lead to nonlinear effects on the wave-packet evolution, even close to the nozzle exit. However, as seen in section III.A, for a high Reynolds number jet with a turbulent boundary layer in the nozzle, as in the present case, only a small fraction of the turbulent kinetic energy is contained in the low azimuthal modes, which favors application of a linear approach.

The present results show that a part of the turbulent field of high Reynolds number jets can be obtained using the Navier-Stokes equations linearised using the mean velocity field. This is quite different from the general view of turbulence as an essentially nonlinear phenomenon. We doubt though that the dominant turbulent velocity fluctuations, of high azimuthal wavenumber, could be obtained with similar linearisations. On the other hand, if we are looking for the significant velocity fluctuations for sound generation, which have significantly lower energy, a linear wave-packet model appears to be appropriate to describe the evolution from the nozzle exit to the end of the potential core, at least in a statistical sense: we note that all comparisons between linear PSE and experiment were done using averaged spectra to obtain amplitudes and phases for each frequency and azimuthal mode. Linear PSE represents thus a good model for an "averaged jet".

Downstream of the end of the potential core, though, the model diverges from the experimental results.

This can be due, for instance, to significant nonlinear effects in this region, but also to a reduced contribution of the wavepacket to the overall azimuthally-coherent fluctuation energy. Current work involves extension to nonlinear PSE to account for nonlinear interaction of wavepackets, and also a more detailed study of the velocity field to study what happens downstream of the potential core.

Acknowledgments

We thank Carine Fourment-Cazenave, Patrick Braud and Joël Delville for their work during the experiments. This work was supported by CNPq, National Council of Scientific and Technological Development – Brazil, and through the EU-Russian program ORINOCO (FP7-AAT-2010-RTD-Russia; project number 266103).

Appendix A. Linear PSE comparisons for Mach 0.5 and 0.6

We show in figures 25 and 26 the comparison between the axisymmetric mode obtained with linear PSE and the experimental results for the axial velocity fluctuations on the jet centerline, respectively, for the $M = 0.5$ and 0.6 jets.

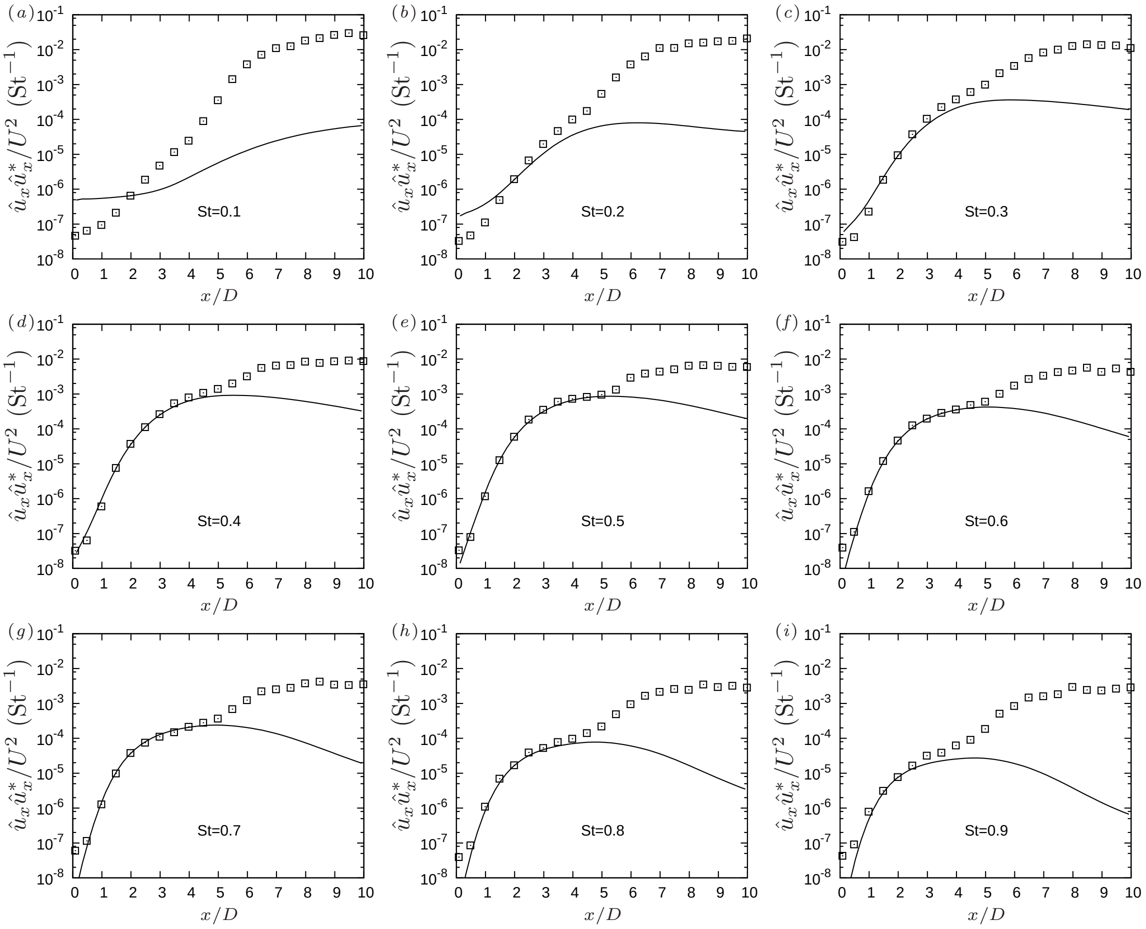

Figure 25. Comparison between linear PSE (lines) for $m = 0$ and experimental velocity fluctuations on the centerline (symbols) for the $M = 0.5$ jet. Subfigures (a)–(i) refer respectively to Strouhal numbers from 0.1 to 0.9 with increments of 0.1.

The observed trends for both jet Mach numbers are quite similar to the results for the $M = 0.4$ jet shown in figure 13. For Strouhal numbers between 0.3 and 0.9 there is close agreement between PSE and the experiment until the end of the potential core. Discussion on the possible reasons for the discrepancies

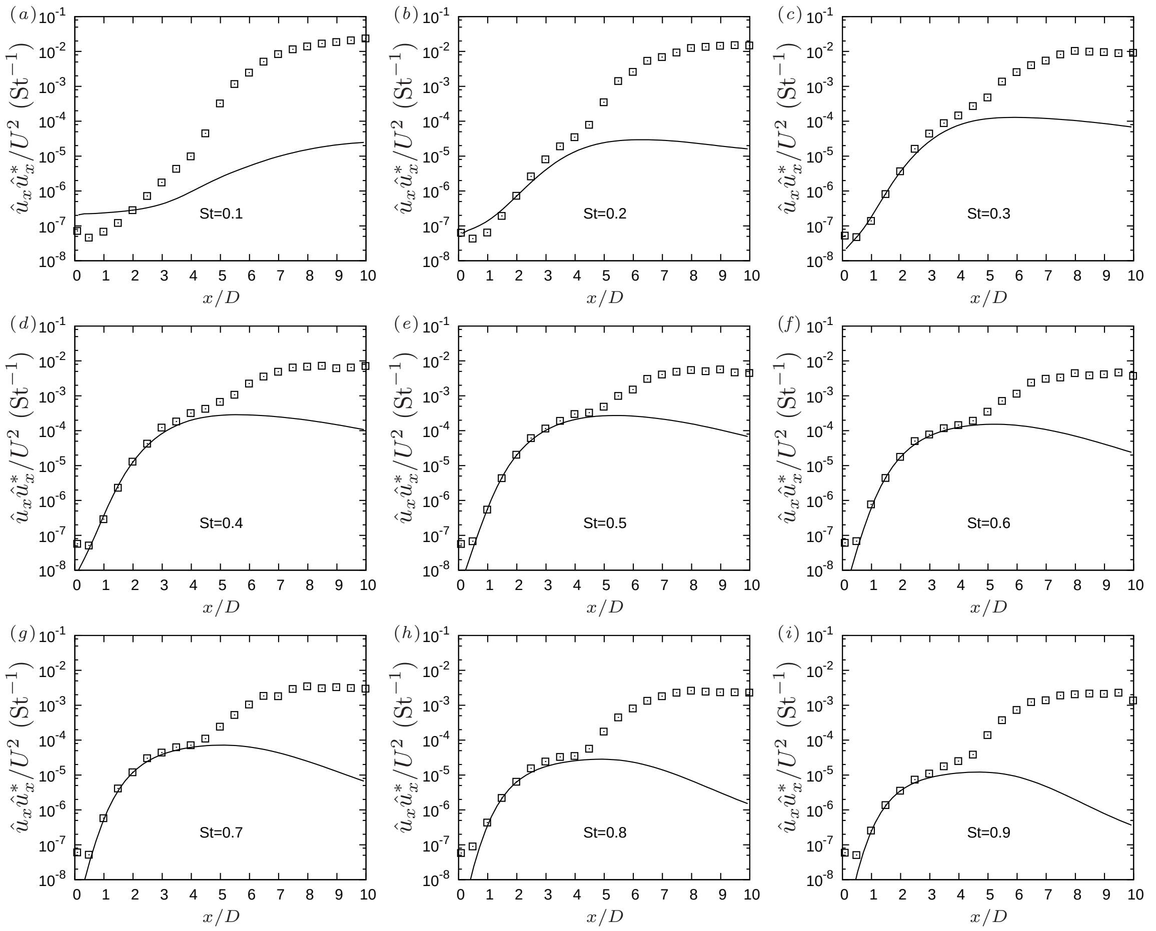

Figure 26. Comparison between linear PSE (lines) for $m = 0$ and experimental velocity fluctuations on the centerline (symbols) for the $M = 0.6$ jet. Subfigures (a)–(i) refer respectively to Strouhal numbers from 0.1 to 0.9 with increments of 0.1.

at lower frequencies is presented in section IV.B.

For comparison using the TR-PIV results, increasing the jet Mach number leads to higher aliasing, since the sampling rate was fixed at 5kHz for all experiments. As a result, the spectral estimates using TR-PIV are significantly higher than the corresponding hot-wire results.

Figures 27 and 28 present comparisons at $x/D = 3$ for the axisymmetric mode of the $M = 0.6$ jet, for the axial and radial velocity components, respectively. The radial shape of the PSE solution agrees closely with the first POD mode of the experiment. The measured amplitudes are higher than the PSE solution fitted with hot-wire spectra, but this amplitude change seems to be constant with radius.

We have performed an *ad hoc* correction for aliasing by defining a multiplicative constant for each frequency, which was obtained by dividing the hot-wire spectra on the jet centerline by the TR-PIV spectral estimate for u_x at the same position. This same constant was applied to all radial positions, and to both u_x and u_r. Results are shown in figures 29 and 30. The amplitudes are now quite close, indicating that the shifts in figures 27 and 28 are indeed related to aliasing in the experiments for high Mach number.

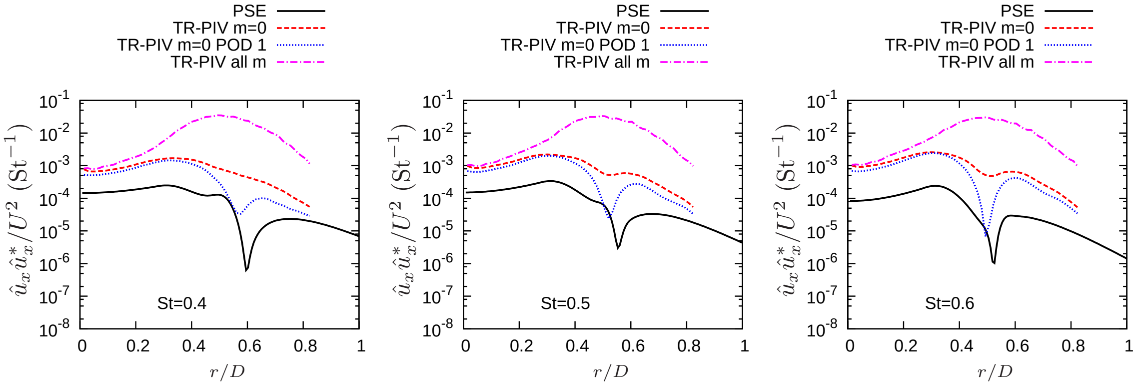

Figure 27. **Comparison between u_x from linear PSE and experiment for $m = 0$, $M = 0.6$ and $x/D = 3$**

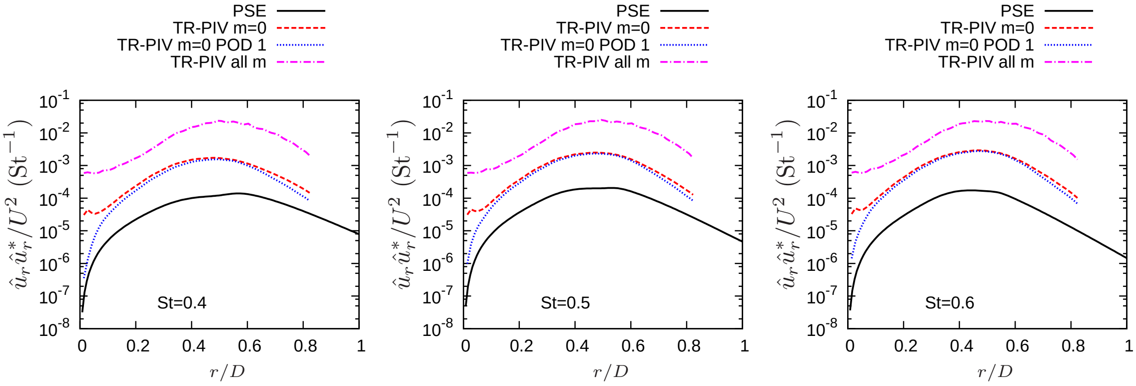

Figure 28. **Comparison between u_r from linear PSE and experiment for $m = 0$, $M = 0.6$ and $x/D = 3$**

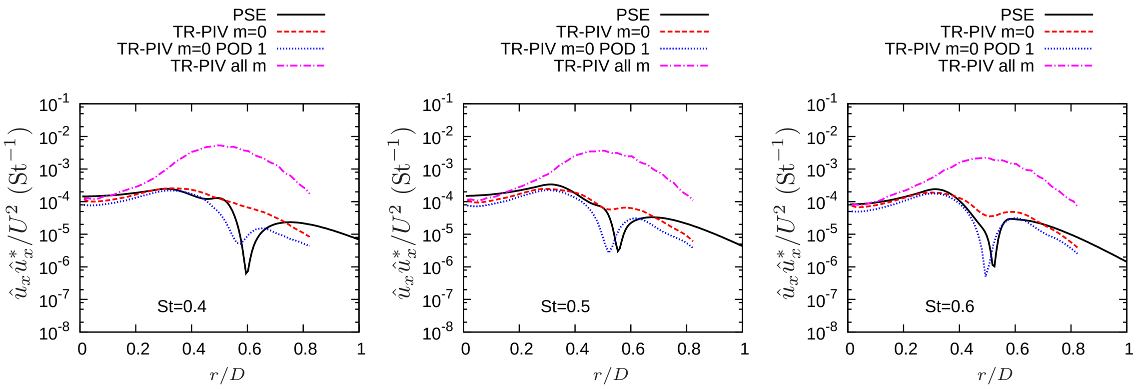

Figure 29. **Comparison between u_x from linear PSE and experiment (with aliasing correction) for $m = 0$, $M = 0.6$ and $x/D = 3$**

Appendix B. Comparison between scalar and vectorial POD

In this appendix, we compare modes obtained using the scalar POD defined by eq. (9) applied to each velocity component, and a vectorial POD, whose integral equation is given by

$$\int R_{i,j}(x, r, r', m, \omega)\xi_j(x, r', m, \omega)r'\mathrm{d}r' = \lambda(x, m, \omega)\xi_i(x, r, m, \omega) \tag{16}$$

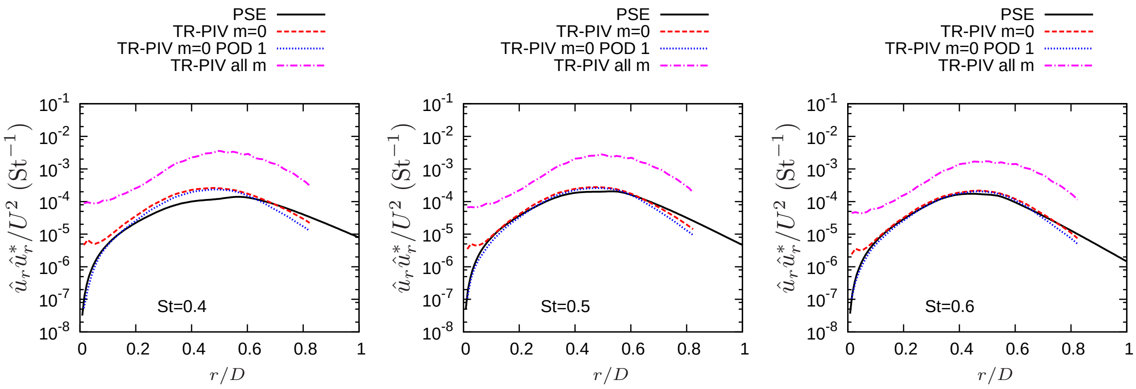

Figure 30. Comparison between u_r from linear PSE and experiment (with aliasing correction) for $m = 0$, $M = 0.6$ and $x/D = 3$

where subscripts i and j refer to the three velocity components u_x, u_r and u_ϕ, and $R_{i,j}$ is given by

$$R_{i,j}(x, r, r', m, \omega) = u_i(x, r, m, \omega) u_j^*(x, r', m, \omega). \tag{17}$$

This vectorial POD is calculated numerically using the approach described by Delville,[45] with a single $3N \times 3N$ matrix formed by computation of $R_{i,j}$ for the three velocity components using the N points in the radial direction. We have used an auxiliar Hermitian kernel, as done by Jung *et al.*[44] and described in section IV.C.1.

A sample comparison between results from scalar and vectorial POD is shown in figure 31. For the axial velocity fluctuations, shown in figure 31(a), we note an almost perfect superposition of the first scalar POD mode and the second vectorial POD mode. For the radial velocity, a similar superposition is found, this time with the first vectorial POD mode.

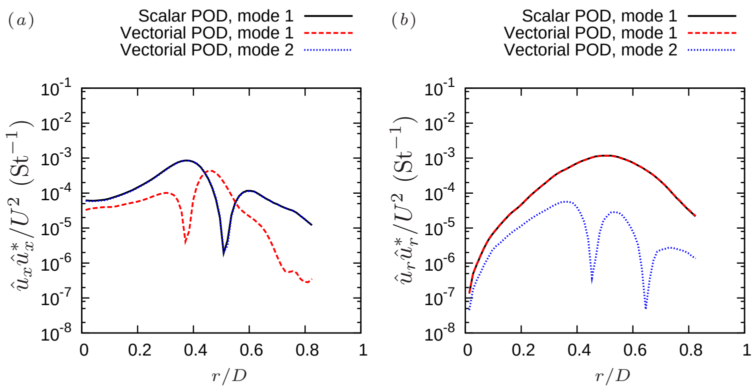

Figure 31. Comparison of scalar and vectorial POD applied to the $M = 0.4$ jet for $x/D = 2$, $m = 0$, St $= 0.6$. Note the superposed curves (first scalar mode is superposed to the second vectorial mode in a and to the first vectorial mode in b).

Since the first scalar POD modes of axial and radial velocity fluctuations were seen in section IV.C to correspond closely to linear stability waves, the results of figure 31 suggest that POD is separating a single physical phenomenon into two different orthogonal modes. This occurs most likely precisely due to the orthogonality requirement, since linear stability modes are known to be non-orthogonal.[49] In this case, orthogonal modes are not appropriate to describe the considered phenomenon.

Based these observations, we have chosen to use scalar POD for the analysis of the results presented in this paper, the first mode being used mostly as a filter of energetic, radially correlated fluctuations for each velocity component, instead of using vectorial POD.

References

[1]Crow, S. C. and Champagne, F. H., "Orderly structure in jet turbulence," *Journal of Fluid Mechanics*, Vol. 48, No. 3, 1971, pp. 547–591.

[2]Moore, C. J., "The role of shear-layer instability waves in jet exhaust noise," *Journal of Fluid Mechanics*, Vol. 80, No. 2, 1977, pp. 321–367.

[3]Michalke, A., "Instabilitat eines Kompressiblen Runden Freistrahls unter Berucksichtigung des Einflusses der Strahlgrenzschichtdicke," *Zeitschrift für Flugwissenschaften*, Vol. 19, 1971, pp. 319–328; English translation: NASA TM 75190, 1977.

[4]Crow, S. C., "Acoustic gain of a turbulent jet," *Phys. Soc. Meeting, Univ. Colorado, Boulder, paper IE*, Vol. 6, 1972.

[5]Mankbadi, R. and Liu, J. T. C., "Sound generated aerodynamically revisited: large-scale structures in a turbulent jet as a source of sound," *Philosophical Transactions of the Royal Society of London. Series A, Mathematical and Physical Sciences*, Vol. 311, No. 1516, 1984, pp. 183–217.

[6]Tam, C. K. W. and Burton, D. E., "Sound generated by instability waves of supersonic flows. Part 2. Axisymmetric jets," *Journal of Fluid Mechanics*, Vol. 138, No. -1, 1984, pp. 273–295.

[7]Lighthill, M. J., "On sound generated aerodynamically. I. General theory," *Proceedings of the Royal Society of London. Series A, Mathematical and Physical Sciences*, 1952, pp. 564–587.

[8]Cohen, J. and Wygnanski, I., "The evolution of instabilities in the axisymmetric jet. Part 1. The linear growth of disturbances near the nozzle," *Journal of Fluid Mechanics*, Vol. 176, 1987, pp. 191–219.

[9]Petersen, R. A. and Samet, M. M., "On the preferred mode of jet instability," *Journal of Fluid Mechanics*, Vol. 194, No. 1, 1988, pp. 153–173.

[10]Michalke, A. and Fuchs, H. V., "On turbulence and noise of an axisymmetric shear flow," *Journal of Fluid Mechanics*, Vol. 70, 1975, pp. 179–205.

[11]Armstrong, R. R., Fuchs, H. V., and Michalke, A., "Coherent Structures in Jet Turbulence and Noise," *AIAA Journal*, Vol. 15, 1977, pp. 1011–1017.

[12]Fuchs, H. V. and Michel, U., "Experimental evidence of turbulent source coherence affecting jet noise," *AIAA Journal*, Vol. 16, No. 9, 1978, pp. 871–872.

[13]Picard, C. and Delville, J., "Pressure velocity coupling in a subsonic round jet," *International Journal of Heat and Fluid Flow*, Vol. 21, No. 3, 2000, pp. 359–364.

[14]Tinney, C. E. and Jordan, P., "The near pressure field of co-axial subsonic jets," *Journal of Fluid Mechanics*, Vol. 611, 2008, pp. 175–204.

[15]Suzuki, T. and Colonius, T., "Instability waves in a subsonic round jet detected using a near-field phased microphone array," *Journal of Fluid Mechanics*, Vol. 565, 2006, pp. 197–226.

[16]Gudmundsson, K. and Colonius, T., "Instability wave models for the near-field fluctuations of turbulent jets," *Journal of Fluid Mechanics*, Vol. 689, 2011, pp. 97–128.

[17]Hussain, A. K. M. F. and Zaman, K. B. M. Q., "The 'preferred mode' of the axisymmetric jet," *Journal of Fluid Mechanics*, Vol. 110, 1981, pp. 39–71.

[18]Becker, H. A. and Massaro, T. A., "Vortex evolution in a round jet," *Journal of Fluid Mechanics*, Vol. 31, No. 03, 1968, pp. 435–448.

[19]Yule, A., "Large-scale structure in the mixing layer of a round jet," *Journal of Fluid Mechanics*, Vol. 89, No. 3, 1978, pp. 413–432.

[20]Laufer, J. and Yen, T.-C., "Noise generation by a low-Mach-number jet," *Journal of Fluid Mechanics*, Vol. 134, 1983, pp. 1–31.

[21]Violato, D. and Scarano, F., "Three-dimensional evolution of flow structures in transitional circular and chevron jets," *Physics of Fluids*, Vol. 23, No. 12, 2011, pp. 124104–124104.

[22]Cavalieri, A. V. G., Jordan, P., Colonius, T., and Gervais, Y., "Axisymmetric superdirectivity in subsonic jets," *17th AIAA/CEAS Aeroacoustics Conference and Exhibit*, Portland, OR, USA, June 5-8 2011.

[23]Tutkun, M., George, W. K., Foucaut, J. M., Coudert, S., Stanislas, M., and Delville, J., "In situ calibration of hot wire probes in turbulent flows," *Experiments in Fluids*, Vol. 46, No. 4, 2009, pp. 617–629.

[24]Kœnig, M., Fourment-Cazenave, C., Jordan, P., and Gervais, Y., "Jet noise reduction by fluidic injection from a rotating plug," *17th AIAA/CEAS Aeroacoustics Conference and Exhibit*, Portland, OR, USA, June 5-8 2011.

[25]Tinney, C. E., Glauser, M. N., and Ukeiley, L. S., "Low-dimensional characteristics of a transonic jet. Part 1. Proper orthogonal decomposition," *Journal of Fluid Mechanics*, Vol. 612, 2008, pp. 107.

[26]Lee, H. K. and Ribner, H. S., "Direct correlation of noise and flow of a jet," *The Journal of the Acoustical Society of America*, Vol. 52, 1972, pp. 1280.

[27]Schaffar, M., "Direct measurements of the correlation between axial in-jet velocity fluctuations and far field noise near the axis of a cold jet," *Journal of Sound and Vibration*, Vol. 64, No. 1, 1979, pp. 73–83.

[28]Juvé, D., Sunyach, M., and Comte-Bellot, G., "Intermittency of the noise emission in subsonic cold jets," *Journal of Sound and Vibration*, Vol. 71, 1980, pp. 319–332.

[29]Panda, J., Seasholtz, R. G., and Elam, K. A., "Investigation of noise sources in high-speed jets via correlation measurements," *Journal of Fluid Mechanics*, Vol. 537, 2005, pp. 349–385.

[30]Bogey, C. and Bailly, C., "An analysis of the correlations between the turbulent flow and the sound pressure fields of subsonic jets," *Journal of Fluid Mechanics*, Vol. 583, 2007, pp. 71–97.

[31]Tomkins, C. D. and Adrian, R. J., "Energetic spanwise modes in the logarithmic layer of a turbulent boundary layer," *Journal of Fluid Mechanics*, Vol. 545, 2005, pp. 141–162.

[32]Maestrello, L., "Two-point correlations of sound pressure in the far field of a jet: experiment," Tech. rep., National Aeronautics and Space Administration, 1976, NASA TM X-72835.

[33]Juvé, D., Sunyach, M., and Comte-Bellot, G., "Filtered azimuthal correlations in the acoustic far field of a subsonic jet," *AIAA Journal*, Vol. 17, 1979, pp. 112.

[34]Michalke, A., "A wave model for sound generation in circular jets," Tech. rep., Deutsche Luft- und Raumfahrt, November 1970.

[35]Cavalieri, A. V. G., Jordan, P., Agarwal, A., and Gervais, Y., "Jittering wave-packet models for subsonic jet noise," *Journal of Sound and Vibration*, Vol. 330, No. 18-19, 2011, pp. 4474–4492.

[36]Herbert, T., "Parabolized stability equations," *Annual Review of Fluid Mechanics*, Vol. 29, No. 1, 1997, pp. 245–283.

[37]Rodríguez, D., Aniruddha, S., Brès, G., and Colonius, T., "Parabolized stability equation models in turbulent supersonic jets," *18th AIAA/CEAS Aeroacoustics Conference and Exhibit*, Colorado Springs, CO, USA, June 4-6 2012.

[38]Thompson, K. W., "Time dependent boundary conditions for hyperbolic systems," *Journal of Computational Physics*, Vol. 68, No. 1, 1987, pp. 1–24.

[39]Mohseni, K. and Colonius, T., "Numerical Treatment of Polar Coordinate Singularities," *J. Comp. Phys.*, Vol. 157, 2000, pp. 787–795.

[40]Batchelor, G. K. and Gill, A. E., "Analysis of the stability of axisymmetric jets," *Journal of Fluid Mechanics*, Vol. 14, No. 04, 1962, pp. 529–551.

[41]Sandham, N. D. and Salgado, A. M., "Nonlinear interaction model of subsonic jet noise," *Philosophical Transactions of the Royal Society A*, Vol. 366, No. 1876, 2008, pp. 2745–2760.

[42]Suponitsky, V., Sandham, N., and Morfey, C., "Linear and nonlinear mechanisms of sound radiation by instability waves in subsonic jets," *Journal of Fluid Mechanics*, Vol. 658, 2010, pp. 509–538.

[43]Lau, J. C., Fisher, M. J., and Fuchs, H. V., "The intrinsic structure of turbulent jets," *Journal of Sound and Vibration*, Vol. 22, No. 4, 1972, pp. 379–384.

[44]Jung, D., Gamard, S., and George, W. K., "Downstream evolution of the most energetic modes in a turbulent axisymmetric jet at high Reynolds number. Part 1. The near-field region," *Journal of Fluid Mechanics*, Vol. 514, 2004, pp. 173–204.

[45]Delville, J., *La décomposition orthogonale aux valeurs propres et l'analyse de l'organisation tridimensionnelle des écoulements turbulents cisaillés libres*, Ph.D. thesis, Ph. D. thesis, Université de Poitiers, 1995.

[46]Papamoschou, D., "Wavepacket modeling of the jet noise source," *17th AIAA/CEAS Aeroacoustics Conference and Exhibit*, Portland, OR, USA, June 5-8 2011.

[47]Kœnig, M., Cavalieri, A. V. G., Jordan, P., Gervais, Y., and Papamoschou, D., "Far-field filtering for the study of jet noise: Mach and temperature effects," *17th AIAA/CEAS Aeroacoustics Conference and Exhibit*, Portland, OR, USA, June 5-8 2011.

[48]Mohseni, K., Colonius, T., and Freund, J. B., "An evaluation of linear instability waves as sources of sound in a supersonic turbulent jet," *Physics of Fluids*, Vol. 14, 2002, pp. 3593.

[49]Schmid, P. J., "Nonmodal stability theory," *Annual Review of Fluid Mechanics*, Vol. 39, 2007, pp. 129–162.

Conclusions and perspectives

1 Conclusions

1.1 Summary of main results

In the first part of this work, we have worked with numerical simulations: mixing layers in chapter II and a $M = 0.9$ jet in chapter III. In both cases we have applied a time-domain approach, where after detection of intermittent energy bursts in the acoustic field, we look at the state of the flow at times corresponding to the emission of the bursts. In both cases, we related the intermittent sound radiation to temporal changes in the interference pattern of convecting structures. For the mixing layer, a triple interaction of two-dimensional vortices opens up a long high-pressure zone in a flow otherwise nearly homogeneous in the axial direction. Application of optimal control prevents the emission of the acoustic burst by avoiding this triple interaction; the controlled mixing layer maintains its axial homogeneity and thus radiates less noise. In the case of the subsonic jet, the axisymmetric mode was seen to have a wave-packet structure that undergoes, intermittently, a sudden truncation downstream of the potential core, where axisymmetric structures tilt. This corresponds, as in the case of the mixing layer, to a temporal change in the envelope of convecting disturbances, with a decrease in the homogeneity leading to a burst in the radiated sound field.

A further aspect of the sound radiation in the large eddy simulation studied in chapter III was that most of the intermittent acoustic bursts were observed for the axisymmetric mode at low axial angles. In order to model the observed temporal changes in the structure of axisymmetric wavepackets, we have developed intermittent model sources in chapter IV. The inclusion of jitter in the wave-packet envelope is seen to increase sound radiation, with the emission of a burst, in agreement with the observations in chapters II and III. Finally, to check if the proposed model leads to a sound field consistent with that of the LES, we have fitted the model parameters using velocity data from the simulation. Calculation of the radiated sound using Lighthill's analogy led to good agreement with the sound pressure level at low polar angles in the LES. The same approach was also succesfully applied to the DNS of Freund [66].

The model developed in chapter IV provided a theoretical motivation to separately study each azimuthal mode in both the turbulent flow and in the acoustic field. Lower azimuthal modes, and the axisymmetric mode in particular, have high acoustic efficiency; and the wave-packet shape of mode 0, seen in chapters III and IV, leads to a strong directivity of axisymmetric bursts to low polar angles.

Chapters V and VI are devoted to experiments with turbulent subsonic jets, and present an investigation on wavepackets as noise sources in such flows. To deal with the experimental databases, we have worked in the frequency domain, in contrast with the time-domain approaches of the preceding chapters. This was motivated by a relative lack of information on the literature on the energy content of (ω, m) pairs in the turbulent and acoustic fields, where ω stands for the frequency and m for the azimuthal mode. Both parameters being fundamental for the acoustic efficiency of a wavepacket, as discussed in chapter IV, we have decided to perform measurements allowing Fourier decompositions in both time and azimuth. Moreover, due to the description of fluctuations as a function of both frequency and azimuthal wavenumber, linear stability theory (see review in section 1.3) can be used in the analysis as a dynamic model for wavepackets in the jets. The measurements, nonetheless, allow further analysis in the time domain as in the studies of numerical simulations, albeit with limitations on the available data. For instance, we applied the continuous wavelet transform to quantify the amount of intermittent energy in the different azimuthal modes of the sound field. This analysis, shown in the Appendix, confirmed the dominance of axisymmetric bursts at low axial angles and their strong directivity, suggested by the model in chapter IV.

The acoustic measurements studied in chapter V showed that the axisymmetric mode of the far-field pressure has the characteristic superdirective behaviour expected for radiation from an axisymmetric wave-packet (Crow [50]). This strong directivity is an indication that low-angle sound is related to an axisymmetric wavepacket with significant axial extension. The dependence of the radiated sound with the jet acoustic Mach number was also seen to be consistent with wave-packet radiation, but only after the compressibility efffects detected in the experiment are accounted for. Crow's model has been extended to allow helical wavepackets as sources, and azimuthal modes 1 and 2 in the acoustic field were seen to be consistent with the model.

For the same jets, wavepackets were detected for both the axisymmetric and the first helical mode in the velocity field in section VI, with close agreement with linear instability waves modelled using PSE. Additionally, correlation of far-field pressure with wavepackets in the flow, done in a mode-by-mode basis, led to values significantly higher than previous two-point results, showing the significance of azimuthally-coherent wavepackets for the radiated sound, in agreement with theory (Michalke [127]; Michalke & Fuchs [132]; see also discussion in section 2.1.1).

As a whole, the results presented in this thesis support the picture of wavepackets, generated by the linear Kelvin-Helmholtz instability of the mean turbulent flow, as the main sources of jet noise at low axial angles.

1.2 Open issues

In chapter VI we saw that azimuthal modes 0 and 1 for the velocity can be modelled as linear instability waves, at least up to the end of the potential core. However, for downstream stations the agreement between model and experiment becomes progressively worse, and hence the linear instability-wave model could not describe the full wave-packet envelope of amplification, saturation and decay.

We have nonetheless atempted to calculate the sound field radiated by instability waves modelled by linear PSE. To this end we have used Lighthill's analogy; we recall, as discussed by Cheung and Lele [36], that PSE cannot directly provide the radiated sound, since the employed *Ansatz* is appropriate for hydrodynamic waves but cannot, in general, describe acoustic waves. Alternatives to obtain the radiated sound include using the PSE solution in an acoustic analogy (as in Cheung and Lele [36]) or using the near-field pressure to obtain the far-field sound with a Kirchhoff surface (as done by Colonius *et al.* [43]). We have used the expressions derived in Appendix B of chapter V for low-angle radiation using Lighthill's analogy, which we repeat here for convenience: an equivalent line source S_{xx} is obtained as

$$S_{xx}(x,m=0,\omega) = 2\rho_0 \int_0^\infty \bar{u}_x(x,r) u_x(x,r,\omega) r \mathrm{d}r, \tag{VII.1}$$

where $u_x(x,r,\omega)$ is the axial velocity fluctuation taken from the PSE modes, and $\bar{u}_x(x,r)$ is the measured mean axial velocity. The far-field sound is calculated as

$$p(R,\theta,m=0,\omega) = -\frac{k_a^2 \cos^2\theta \mathrm{e}^{-\mathrm{i}k_a R}}{2R} \int S_{xx}(x,m=0,\omega) \mathrm{e}^{-\mathrm{i}k_a x \cos\theta} \mathrm{d}x. \tag{VII.2}$$

The calculation, though, led to significantly lower far-field amplitudes (discrepancies over

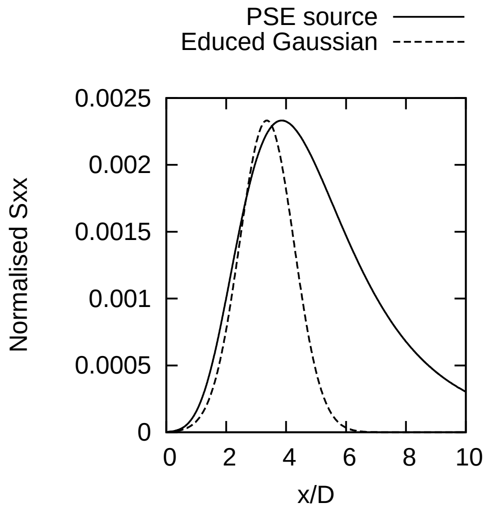

Figure VII.1 – Comparison of the absolute value of the radially-integrated source using eq. (VII.1) with envelope educed in chapter V, for $M = 0.4$ and $\mathrm{St} = 0.4$.

10dB) than the experimental results of chapter V. Use of a Kirchhoff surface did not change significantly this picture, and led to similar discrepancies. To understand such differences, we compare, in figure VII.1, the axial envelope of the radially-integrated PSE source with the envelope educed from far-field results in chapter V. We note that the two envelopes are close up to the saturation position; however, the PSE envelope has a much lower decay rate and has significant amplitudes for high x/D.

These different decay rates, which could be related to the lack of agreement between linear PSE does and the velocity fluctuations downstream of the potential core, may explain the errors in the calculated sound radiation using sources constructed from linear PSE. The modelled linear instability waves tend to remain coherent over a large axial extent, far beyond the potential core, which leads to low amplitudes of the radiated sound.

When the PSE source in fig. VII.1 is manipulated, with an envelope changed into the educed Gaussian, but with no changes in maximum amplitude or in phases, the radiated sound now agrees within 2dB at low polar angles.

These results suggest that the decay of instability waves is quite important for sound radiation. To model this decay, inclusion of nonlinear effects in PSE may lead to an improvement of the agreement for positions downstream of the potential core, but so far what happens in this region is not clear, and further analysis of the experimental database may help in the modelling of downstream phenomena.

On the other hand, the results presented here bring to mind the observations of chapter

III, where an intermittent truncation of a wavepacket was related to the emission of acoustic energy bursts to low polar angles. Our experimental results confirmed the significance of such acoustic bursts in our jets, as shown in the Appendix.

Regarding this kind of intermittent behaviour, a comment should be made on the statistical metrics obtained from the experiments. The analysis of chapters V and VI were performed using spectra of far-field pressure and turbulent velocity, respectively. Averaged spectra, from a large number of flow realisations, were used to obtain power spectral densities. In this sense, these studies display statistics representing average behaviours of the jet, either in the acoustic or in the turbulent field.

Intermittent changes in wavepackets can lead to an increase of the radiated sound, as exemplified in the jittering wave-packet models in chapter IV. We conjecture that such intermittent behaviour may lead to small changes in turbulent spectra, and, at the same time, significant modifications of the far-field sound. If this is true, the average behaviour of the turbulent field may not lead to the average far-field sound.

Some recent works display significant differences between turbulence- and acoustics-based statistics in jets. Freund and Colonius [69] applied POD to a computation of a Mach 0.9 jet with different inner products, and modes obtained using an inner product based on far-field acoustics are significantly different to those obtained with the standard product based on turbulent fluctuations. Similar conclusions were recently obtained by Kerhervé *et al.* [98], where Linear Stochastic Estimation was used to obtain a conditional average of the velocity, the far-field pressure being used as the condition; and by Schlegel *et al.* [175], where observable-inferred modes (OID) in free-shear flows were constructed using information from the acoustic field.

To obtain more information on turbulence intermittency, it seems appropriate to explore experimental data in both frequency and time domains, as done for the acoustic field in chapters II and III, and in the Appendix. A wave-packet description including jitter, as in IV, would permit evaluation of intermittency effects on the radiated sound. However, inclusion of experimental data in a jittering source model is not straightforward. It was done in an *ad hoc* manner in chapter IV, where a range of frequencies was described as a central one with modulations in amplitude and spatial extent. It is not clear how to do this with the full turbulent fluctuations, without filtering a specific frequency range; moreover, since experiments do not provide full information on the flow variables, some modelling would probably be necessary to approximate the spatio-temporal behaviour of the turbulent field.

1.3 Comments on the application of acoustic analogies

In the present work, Lighthill's acoustic analogy was used as a theoretical basis to study the properties of wavepacket models. A number of works point at conceptual flaws of such analogies (Doak [55], Fedorchenko [59]), and there is still an ongoing debate on the litterature on the merits acoustic analogies (see for instance, Spalart's analysis [178] on the work of Tam [183]).

It is our view that Lighthill's stress tensor T_{ij}, or any other source term coming from an acoustic analogy, cannot be interpreted as a "true source of aerodynamic sound". By definition, acoustic analogies deal with sound radiation problems which are analogous to aerodynamic sound generation; these acoustic problems are derived assuming propagation of infinitesimal disturbances on a given medium (flow at rest for Lighthill [116], parallel sheared flow for Lilley [118], more general base flows for Goldstein [76]). These simplified analog problems no longer model a turbulent flow; indeed, most of the turbulent fluctuations are not calculated, but supplied to the model in the form of a source term.

Nonetheless, this does not mean that acoustic analogies are of no interest. They represent a means of obtaining quantitative results for the acoustic field based on flow parameters. Moreover, the effect of a given structure of turbulent fluctuations on the radiated sound can be studied in a model problem using an acoustic analogy, and comparison of its radiation with experimental or numerical results is a consistency check for the model.

This was the approach chosen in the present work. The results of the wave-packet model in chapter IV were important in the design of the experiments of chapters V and VI. Lighthill's acoustic analogy, due to its simplicity, allowed the identification of physically significant parameters in the acoustic field and in the flow, and measurements confirmed the trends predicted by theory.

With the inherent complexity of turbulent flows, it is our view that a theoretical basis, and the acoustic analogy in particular if one studies sound generation, is quite useful, not by revealing "true noise sources", but by helping in the distillation of the salient features of such flows, which can be further explored by detailed analysis of numerical simulations, or by appropriate sensing in an experiment designed for that matter.

2 Perspectives

Wave-packet dynamics As already mentioned in this chapter, linear instability waves could not model the downstream decay of velocity fluctuations. An interesting perspective opened by the present work is the improvement of the linear PSE model, by inclusion of nonlinear interaction between wavepackets, using nonlinear PSE, or by modelling interactions with the background turbulence, with a model for Reynolds stresses, for instance. Further work on the experimental database presented in chapter VI appears promising.

Despite the differences in the downstream region, the comparison of velocity fluctuations with linear instability waves was quite favourable until the end of the potential core. Knowledge of this mechanism helps to propose or to understand jet noise mechanisms. For instance, Kœnig [101] verified that rotating microjets exiting a centerbody of the main jet led to a reduction of far-field noise; these microjets were seen to thicken the jet mixing layer, and analysis of the linear stability of the modified mean velocity profiles showed that the rotating microjets had a stabilising effect for axisymmetric disturbances.

The linear Kelvin-Helmholtz instability mechanism for the initial amplification of wavepackets may also shed light on the effect of nozzle-exit conditions on the radiated sound field. Near the nozzle, the range of unstable frequencies is determined by the mixing layer momentum thickness (see Michalke [131] or Petersen and Samet [154]). Thin mixing layers have a greater range of unstable frequencies than thick ones, and a jet with a thin boundary layer at the nozzle exit will in theory excite higher frequencies than one with a thick boundary layer. This is a tentative explanation for the augmentation of high-frequency sound in jet-noise facilities with significant contraction rates, discussed in section 2.2.4; convergents with high contraction rates will lead to favourable pressure gradients, and thinner boundary layers at the nozzle exit.

Another perspective is an investigation of the fluctuations that trigger the Kelvin-Helmholtz instability, which is of convective nature and is thus excited by upstream disturbances. For the experiments in the present work, it is likely that such fluctuations are related to the turbulent boundary layer inside the nozzle. Understanding of the mechanism by which fluctuations in the boundary layer couple with the downstream wavepackets may allow one to propose devices for passive or active control inside the nozzle.

Improvements on models of sound generation We saw in chapter V that for high frequencies and Mach numbers the axisymmetric sound changes from a superdirective radiation to a lobed pattern, with a reduction of acoustic intensities near the downstream jet axis recalling the cone of silence obtained when refraction by the sheared flow is accounted for. An investigation of the effects of flow-acoustic interactions would help to establish the reasons for this change of behaviour.

Most of the work in this thesis was related to the sound generation at low axial angles. Wavepackets, such as those modelled here, present highly directive sound generation, and their low acoustic intensities in the sideline direction suggests that they are not the most active mechanism of sound generation at $\theta = 90°$. The wave-packet models applied here use only the axial velocity fluctuation, and hence, by construction, have no far-field sound on the jet sideline. Modelling of radial and azimuthal velocities may change this picture, but it is not clear if a wave-packet model can lead to reasonable estimatives of the radiated sound at high polar angles.

However, for aeronautic applications, the jet is often below a wing, and the trailing edge scatters jet noise. When a surface with a trailing edge is present, even sources using axial velocity fluctuations, such as the wave-packet models of the present work, can lead to radiated sound normal to the jet, due to edge scattering [62].

Real-time jet noise control There has been significant improvement of the capabilities of flow control in experiments, and this is an active research topic. Numerical simulations are also used for that matter, and are a valuable tool for actuator and sensor design, for instance. Moreover, succesful implementation of flow control can greatly increase our knowledge of turbulence and of aeroacoustics, since one can analyse the differences between the baseline case and the actuated flow; an example is the optimally-controlled mixing layer of Wei and Freund [203], analysed in chapter II.

This last example showed the importance of accounting for intermittent behaviour in the flow for active control. Recent work by Kim *et al.* [99], using optimal control applied to large eddy simulation of jets, showed noise reductions by the decrease of the amplitude of intermittent bursts, similar to what is found in the mixing layer case.

These results suggest that for active, closed-loop control one should be able to deal with intermittent, temporally-localised descriptions of the flow. A model should be able to predict the radiated sound based on a short-time description of the flow, obtained by appropriate sensing. For this purpose, a wave-packet model including jitter, such as developped in chapter IV, may be viable to obtain a real-time prediction of the radiated sound, at least for a given frequency range.

Another issue related to flow control is the need of reduced-order models. A real-time, experimental setting would not afford the extensive numerical computations performed in simulations such as DNS or LES. It is thus essential to reduce the complexity of the problem and its computational cost in order that a model be useful for real-time flow control. Such a reduced order model should nonetheless retain the fundamental physics for sound generation.

A common approach for order reduction is the Galerkin method, based on the projection of the Navier-Stokes equations onto N spatial modes. This leads to a system of N ordinary differential equations, whose solution demands much less computational effort than the original system of partial differential equations. Some examples, derived assuming incompressible flow, include applications of Galerkin projections for turbulent boundary layers (Aubry *et al.* [6], Zhou and Sirovich [209], Rempfer [163]) flow over circular cylinders (Noack *et al.* [148]), spatial (Noack *et al.* [149]) and temporal (Wei and Rowley [204]) mixing layers. Galerkin projections can also be performed for compressible flows, as done by Rowley *et al.* [169] for the flow over a two-dimensional cavity.

Another possibility to obtain a reduced-order model is the calibration of the coefficients of the Galerkin system using flow data, which is more feasible when one has a limited amount of measurements of the flow variables. Examples of this approach include the works of Perret *et al.* [153] and Cordier *et al.* [44].

For the cited works, spatial modes are obtained by a proper orthogonal decomposition applied to the velocity field. Application of POD with a specified inner product ensures an optimal representation of a field in terms of the natural norm, which, for incompressible flow, amounts to the space integration of the turbulent kinetic energy. However, this optimality condition does not guarantee that the POD modes are an appropriate choice to model the dynamic behaviour of the flow (see, for instance, Rowley [168]). Furthermore, as seen in Appendix B of chapter VI, POD can split a single phenomenon into different modes due to the orthogonality constraint.

The results of chapter VI suggest that modes derived from the linear instability of the mean flow can provide an alternative to POD modes in the derivation of reduced-order modes. Unlike POD eigenfunctions, modes representing instability waves are selected using the flow dynamics; therefore, they clearly model specific physical phenomena.

The good agreement of linear instability waves with the velocity field of the jet also suggests that the upstream conditions should be modelled in a reduced-order dynamical system, since the cold jets studied here present convective instabilities (see discussion in the end of section 1.3). Such conditions, near or inside the nozzle, determine the initial amplitudes of waves that are amplified downstream. In light of the present results, inclusion of upstream disturbances as boundary conditions in the derivation of a reduced-order model seems important for the control of jets.

Appendix. Intermittency of the azimuthal components of the sound radiated by subsonic jets

We present in the following the paper "Intermittency of the azimuthal components of the sound radiated by subsonic jets", presented in the 17th AIAA/CEAS Aeroacoustics Conference in June 2011.

In this paper, we have applied the wavelet filter used in the simulations of chapter II and III to the experimental results of far-field pressure, studied in chapter V, to ascertain if the axisymmetric bursts of acoustic pressure, detected in the large-eddy simulation in chapter III, were also present in experiments of subsonic jets.

17th AIAA/CEAS Aeroacoustic Conference and Exhibit, 6-8 June 2010, Portland, Oregon

Intermittency of the azimuthal components of the sound radiated by subsonic jets

Maxime Kœnig[*], André V. G. Cavalieri[†], Peter Jordan[‡] and Yves Gervais[§]

Institut Pprime, Poitiers, France

We apply a filtering procedure, based on a continuous wavelet transform, to acoustic pressure and to the velocity field of an experimental Mach 0.6 jet in order to extract the intermittent bursts in the signals. With an intermittency measure based on this filter, it is possible to quantify the significance of these events in the total acoustic intensity. The acoustic pressure is measured by a ring of six azimuthal microphones, allowing decomposition of the sound field into azimuthal Fourier modes. The wavelet filtering is applied to each azimuthal mode, and the results show that the intermittent bursts occur mostly for the axisymmetric mode and for low polar angles. When high energy thresholds are used for the filtering, so as to retain only the most energetic bursts, more than 80 percent of the intermittent radiation is axisymmetric.

I. Introduction

The sound field radiated by a turbulent jet has been observed in a number of studies to comprise intermittent bursts.[1–3] Such bursts in the time series of the acoustic pressure are difficult, if not impossible, to detect just by the analysis of spectra. Nonetheless, this intermittency has proved to be a key feature of the sound generated by the 2D mixing layer of Wei and Freund,[4] who used optimal control in a direct numerical simulation in order to reduce the radiated sound. As shown by the analysis of Cavalieri *et al.*,[5] the uncontrolled mixing layer had intermittent acoustic bursts that were absent for the controlled flows. The continuous wavelet transform was shown in that paper to be useful for the objective detection of the intermittent bursts. As this intermittency was the feature suppressed by the optimal control, we may conjecture that intermittent bursts in the acoustic field of jets may be reduced by the application of appropriate actuation that targets the associated flow events.

An evaluation of the intermittency in the acoustic field can also be helpful in understanding how to model sound sources. Hileman *et al.*[3] have performed such an evaluation by dividing the acoustic pressure time series at 30° of a Mach 1.28 jet into loud noise generation events interspersed with periods of relative quiet. Cavalieri *et al.*[6] used a large eddy simulation (LES) of a Mach 0.9 jet to detect intermittent bursts in the acoustic field and to study jet motions associated with these events. Results showed that the intermittent bursts are mostly axisymmetric. The salient sound source feature related to the axisymmetric bursts was found to be the jitter of an axisymmetric wave-packet upstream of the end of the potential core. Models of such jittering wave-packets were developed by Cavalieri *et al.*,[7] and these models show that jitter both increases the efficiency of sound radiation and produces temporally-localised bursts for low axial angles in the acoustic field.

A detailed analysis of the intermittency characteristics of the far field pressure was presented by Kœnig *et al.*[8] The use of continuous wavelet transform, which have proved useful in previous studies,[5,6] showed that the pressure scalograms for the low angle radiation present temporally-localised energetic peaks. The introduction of a Global Intermittency Measure (GIM) in that paper allowed a quantitative evaluation of the intermittent energy content for each position in the acoustic field; in agreement with observations based on the scalograms, the GIM shows that low angle radiation is populated by intermittent bursts that make

*PhD student, Institut Pprime, 43 rue de l'Aérodrome, 86036 Poitiers, France.
†PhD student, Institut Pprime, 43 rue de l'Aérodrome, 86036 Poitiers, France.
‡Research Scientist, Institut Pprime, 43 rue de l'Aérodrome, 86036 Poitiers, France.
§Professor, Institut Pprime, 40 avenue du Recteur Pineau, 86022 Poitiers, France.

contributions to the overall fluctuation energy that are greater than what is found for such localised bursts at higher emission angles.

This paper extends these analyses to the azimuthal Fourier modes of the acoustic pressure field of subsonic jets. Using pressure measurements made with a 6-microphone ring, we decompose the pressure field into azimuthal Fourier modes. Considerably fewer azimuthal Fourier modes are necessary for description of the sound field than for description of the turbulence;[9,10] and many researchers have interpreted this low-order azimuthal structure of the sound field as evidence of a corresponding low-order *sound-producing* turbulence structure. One may indeed postulate that the coherent structures observed in jets (see for instance Crow & Champagne,[11] Moore,[12] Hussain & Zaman[13] or Tinney & Jordan,[14] among others) will produce such an azimuthally-coherent signature in the sound field. And it is this idea that is frequently the motivation for decomposition of the sound field into azimuthal Fourier modes (Maestrello,[15] Fuchs & Michel,[10] Juvé *et al.*,[16] Brown & Bridges[17] and Kopiev *et al.*[18]).

We then investigate the characteristics of each azimuthal mode by the separate determination of intermittency measures. We show that the intermittent bursts are mostly axisymmetric, confirming the analysis of the LES data.[6] This has important implications for noise source modelling, since the axisymmetric sound radiation is due uniquely to the axisymmetric part of the source[19] in Lighthill's acoustic analogy[20] or any other linearised analogy with an axisymmetric base flow. Therefore, a model of the axisymmetric structures in jets that includes their intermittency characteristics may constitute a model better adapted to mimic the real flow events implicated in the generation of jet noiseequipped for the quantitative prediction of jet noise, via to reproduce the bursts in the acoustic far field.; this can be important both from the perspecctive of real-timz control and modelling.

II. Experimental description

The experiments reported in this work were carried out in the Bruit et Vent anechoic facility at the Centre d'Etudes Aérodynamiques et Thermiques (CEAT), at the Institut Pprime in Poitiers, France. We have made measurements of the acoustic field of unheated jets, with acoustic Mach numbers $M = U/c_\infty$ ranging from 0.35 to 0.6 in intervals of 0.05. Velocity measurements were taken at Mach numbers of 0.4, 0.5 and 0.6. The nozzle exit measures 0.05m. With these conditions, the current measurements present a variation of Reynolds number $\rho UD/\mu$ from 3.7×10^5 to 5.7×10^5. A more detailed description of the experimental database is presented by Cavalieri *et al.*[21]

Six microphones were disposed as an azimuthal ring in the acoustic field of the jet, with the same angle θ to the downstream jet axis. The setup is shown in figure 1(a). The ring has a fixed diameter d equal to $35D$. Spectra of the six microphones for M=0.6 and $\theta = 30°$ are superposed in figure 1(b). The agreement between the spectra shows that there is no preferred azimuthal direction in the acoustic field and the hypothesis of circumferential homogeneity[9] is appropriate for the present experiment.

(a) (b)

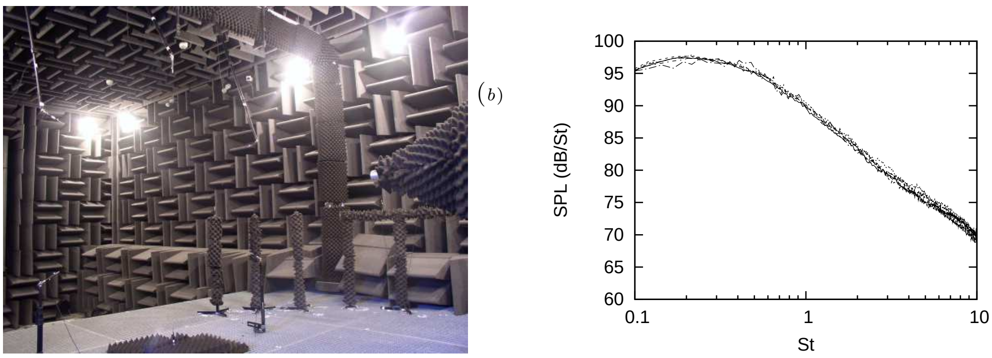

Figure 1. (a) Experimental setup; (b) spectra of the six microphones at $\theta = 30°$ and $M = 0.6$

III. Wavelet filtering

The continuous wavelet transform[22]

$$\tilde{p}(s,t) = \int_{-\infty}^{\infty} p(\tau)\psi(s,t-\tau)\mathrm{d}\tau, \tag{1}$$

is used to analyse the temporal structure of the sound field for each of the azimuthal modes. $\psi(s,t-\tau)$ is a family of wavelet functions, obtained by translation and dilatation of a mother wavelet function $\psi(1,t)$. We use the Paul wavelet with $q=4$ (see Kœnig *et al.*[8] for an evaluation of the wavelet transform results with different wavelet functions).

$$\psi(1,t-\tau) = \frac{2^q i^q q!}{\sqrt{\pi(2q)!}}[1-i(t-\tau)]^{-(q+1)}. \tag{2}$$

The result of the wavelet transform is a time-scale representation, or time-frequency. A sample segment of the scalogram of a microphone signal is shown in figure 2(a). There we note the occurrence of two energy bursts around $tU/D=7$ and $tU/D=13$. We apply a filter in the wavelet domain to retain the high-energy

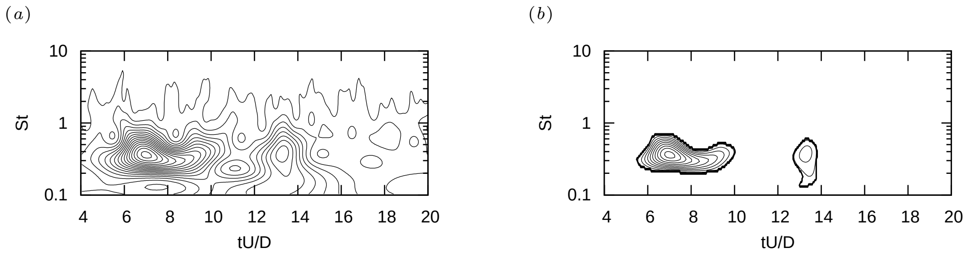

Figure 2. Scalograms of a segment of the (a) original and (b) filtered pressure signal. Contours range from $1\cdot10^{-5}\sigma^2$ to $8.1\cdot10^{-4}\sigma^2$ in steps of $5\cdot10^{-5}\sigma^2$. The thick contour in (b) is equal to $3\cdot10^{-4}\sigma^2$, the filtering threshold α.

bursts in the scalogram by defining an energy threshold α. We then decimate the wavelet coefficient to produce a filtered pressure field containing only the bursts whose energy in the wavelet domain is above $\alpha\sigma^2$:

$$\tilde{p_{\mathrm{f}}}(s,t) = \begin{cases} \tilde{p}(s,t) & \text{if } |\tilde{p}(s,t)|^2 > \alpha\sigma^2 \\ 0 & \text{if } |\tilde{p}(s,t)|^2 < \alpha\sigma^2 \end{cases} \tag{3}$$

where σ^2 is the mean square value of the pressure in the time domain. An example of this filtering with $\alpha = 3\cdot10^{-4}$ is shown in figure 2(b), where only the two said bursts around $tU/D=7$ and $tU/D=13$ are retained in the filtered scalogram.

We apply the wavelet transform for the pressure signal of a microphone and for each of its azimuthal Fourier modes. The coefficients of a Fourier series in ϕ are given by

$$C_m(t) = \frac{1}{2\pi}\int_{-\pi}^{\pi} p(t)\mathrm{e}^{im\phi}\mathrm{d}\phi, \tag{4}$$

and the reconstruction of the pressure signal for $\phi=0$ is given by

$$p(t) = \sum_{m=-\infty}^{\infty} C_m(t). \tag{5}$$

We have each azimuthal component for $\phi=0$ given by

$$p_0(t) = C_0(t), \tag{6}$$

$$p_m(t) = C_{-m}(t) + C_m(t) \text{ if } m \neq 0. \tag{7}$$

The use of $\phi=0$ for the reconstruction is without loss of generality, since there is no preferred azimuthal direction for turbulence or for sound generation.

In the present work we have used two different mean square value normalisations: by σ_m^2, the value of each azimuthal mode $p_m(t)$, and by σ_T^2, which corresponds the mean square value of the microphone signal $p(t)$. The use of σ_m is useful if one wants to compare the intermittency characteristics of each azimuthal mode as if they were unrelated signals. On the other hand, if one is interested in the significance of the intermittency of each azimuthal mode in the reconstruction of the total energy, it is better to normalise all azimuthal components by the total energy σ_T, to keep the superposition properties of the Fourier series.

The filtered pressure in the time domain is obtained by the inverse wavelet transform:

$$p_{\mathrm{f}}(t) = \frac{1}{C_\delta} \int_{0^+}^{\infty} \frac{\tilde{p}_{\mathrm{f}}(s,t)}{s^{3/2}} \mathrm{d}s. \tag{8}$$

Sample results are shown in figure 3 for the same microphone signal analysed in figure 2. We note that the filtering in the wavelet domain, shown in figure 2(b), leads to a decimation of the original signal. The only remaining pressure fluctuations are those corresponding to the bursts in the scalogram of figure 2(b).

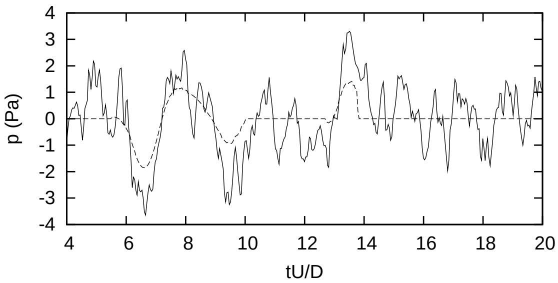

Figure 3. Pressure for the (——) original and (- - - -) filtered time series

IV. Acoustic results for the Mach 0.6 jet

We present here the results of the filtering operation described in the preceding section for $M = 0.6$ jet. We have used pressure signals of 10s, corresponding to a total non-dimensional time $tU/D = 40800$, sufficient to calculate probability distribution functions for the filtered bursts.

IV.A. Spectral content of the azimuthal modes

The pressure spectrum for the axial angle $\theta = 30°$ is shown in figure 4, as well as the spectra of the individual azimuthal Fourier modes.

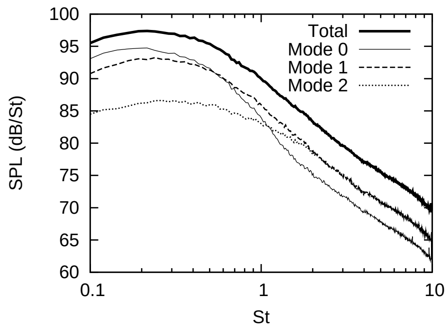

Figure 4. Total spectrum for the acoustic pressure and for its azimuthal components for $\theta = 30°$ and $M = 0.6$.

For this radiation angle, the axisymmetric mode dominates the sound radiation for the peak frequencies. This was also observed by Juvé *et al.*[16] for a Mach 0.4 jet. For higher Strouhal numbers, mode-1 and mode-2 radiation are dominant. For a detailed description on the spectral content of the azimuthal modes and their directivity, see Cavalieri *et al.*[21,23]

IV.B. Intermittency measures

We filtered the pressure signal, as well as its azimuthal modes, using the continuous wavelet transform as described in section III. To evaluate the intermittency of the signals, we calculate the energy of the filtered signal with a given threshold value α. High energy values in the filtered signals occur if the corresponding scalograms are composed of several energy bursts. Low energy for the filtered pressure is found when the signals do not present significant intermittent peaks in the scalogram. The energy of the filtered pressure and that of the azimuthal modes for $\theta = 20°$ is presented in figure 5.

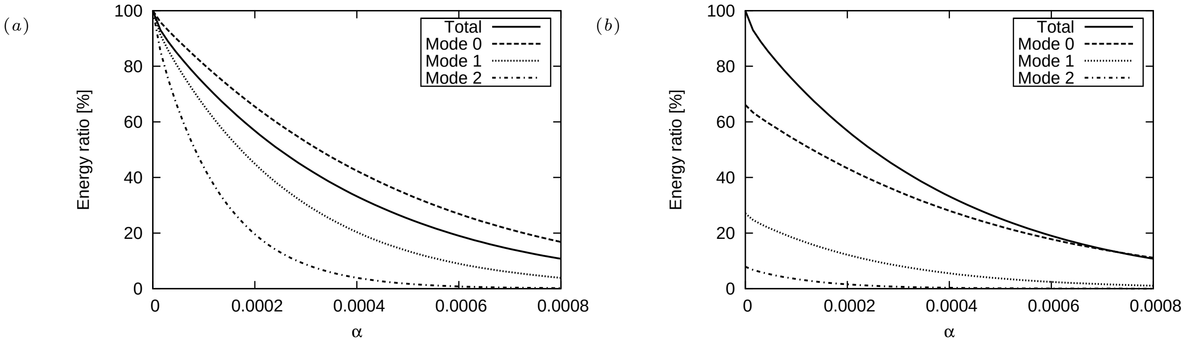

Figure 5. Energy of the filtered signals for $\theta = 20°$ as a function of threshold α with normalisation by (*a*) σ_m and (*b*) σ_T.

In figure 5(a) we have used the energy of each azimuthal mode, σ_m, in the normalisation of eq. (3). We note that the intermittency is present mostly for the axisymmetric mode, since for each threshold α a higher percent of the energy is retained by the filtering if compared to the other modes.

The normalisation of all the signals by the total energy σ_T leads to the results shown in figure 5(b). There, we note that for $\alpha = 0$ the energy ratios are different for each mode. Since $\alpha = 0$ in eq. (3) means no filter, these ratios correspond to the contribution of each azimuthal mode to the total energy of the unfiltered signal. The results of figure 5(b) show, in agreement with figure 5(a), higher intermittent energy for the axisymmetric mode. We note that for high α thresholds, above $6 \cdot 10^{-4}$, the filtered signal is almost completely axisymmetric.

Figures 6 and 7 show the results of the wavelet filt The normalisation of all the signals by the total energy σ_T leads to the results shown in figure 5(b). There, we note that for $\alpha = 0$ the energy ratios are different for each mode. Since $\alpha = 0$ in eq. (3) means no filter, these ratios correspond to the contribution of each azimuthal mode to the total energy of the unfiltered signal. The results of figure 5(b) show, in agreement with figure 5(a), higher intermittent energy for the axisymmetric mode. We note that for high α thresholds, above $6 \cdot 10^{-4}$, the filtered signal is almost completely axisymmetric.

Figures 6 and 7 show the results of the wavelet filtering for each azimuthal mode at polar angles $\theta = 30°$ and $\theta = 40°$, respectively. We note for $\theta = 30°$, shown in fig. 6 the same trends of the results for $\theta = 20°$: the intermittency of the pressure signal is mostly in the axisymmetric mode. However, for $\theta = 30°$ the energy of the filtered signals for a given threshold α is lower if compared to the filtering for $\theta = 20°$. As the polar angle is increased to 40°, the intermittency decreases, as seen in fig. 7, as little energy is retained for a given α if compared to the lower polar angles. This decrease in the intermittency with the increase of θ was observed by Kœnig *et al.*[8] For $\theta = 40°$ the different azimuthal modes behave in similar ways, with a slightly higher intermittent energy for mode 1.

We compare the filtering results for the axisymmetric mode at $\theta = 20°$, 30° and 40° in fig. 8. As the filtered energy for each threshold measures how peaky a scalogram is, the results of fig. 8 show that the presence of intermittent bursts decreases rather abruptly as the angle is increased. This indicates that these energy bursts are highly directive. As shown by Kœnig *et al.*[24] the directivity of these bursts changes exponentially with the polar angle, which suggests that they can be modelled using a wave-packet model[7,25,26] for the axisymmetric coherent structures in the jet.

The results of figures 5, 6 or 7 allow the determination of the energy of each azimuthal mode related to the total energy as the pressure is filtered with a given threshold. This is shown in figure 9 for $\theta = 30°$. The results show that the filtered events in the pressure are mostly comprised of axisymmetric bursts. As the energy threshold α is increased, this effect is even more noticeable, up to a point when more than 80 percent

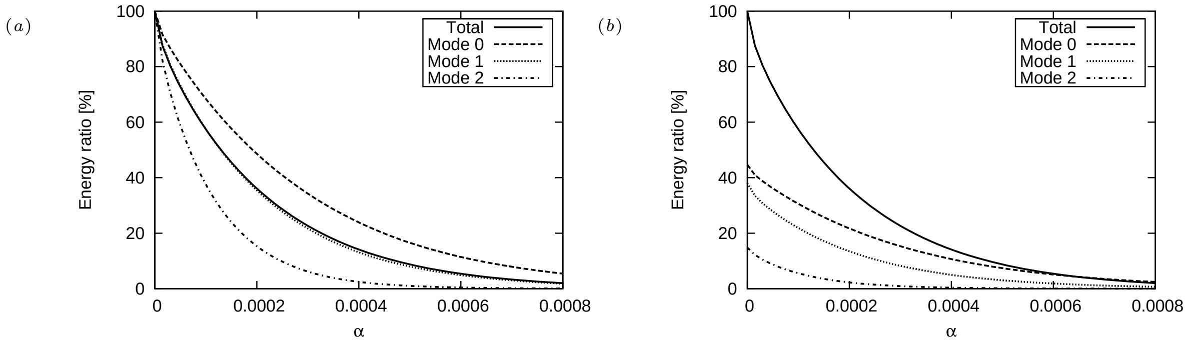

Figure 6. Energy of the filtered signals for $\theta = 30^\circ$ as a function of threshold α with normalisation by (*a*) σ_m and (*b*) σ_T.

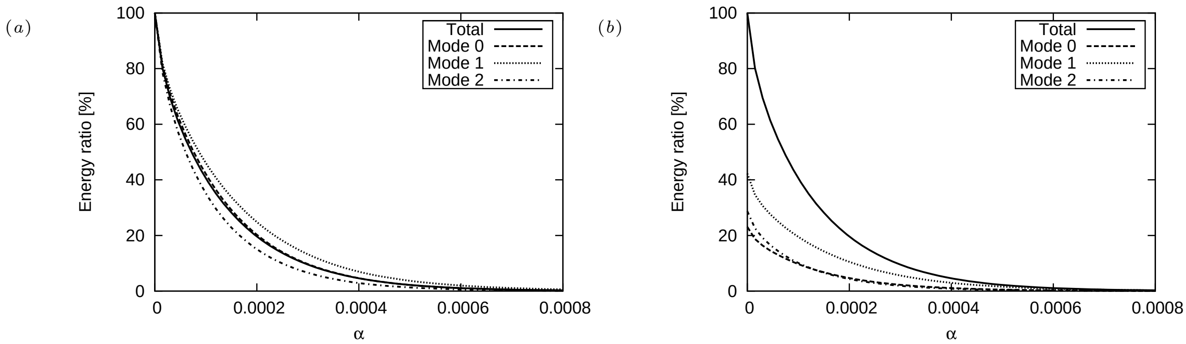

Figure 7. Energy of the filtered signals for $\theta = 40^\circ$ as a function of threshold α with normalisation by (*a*) σ_m and (*b*) σ_T.

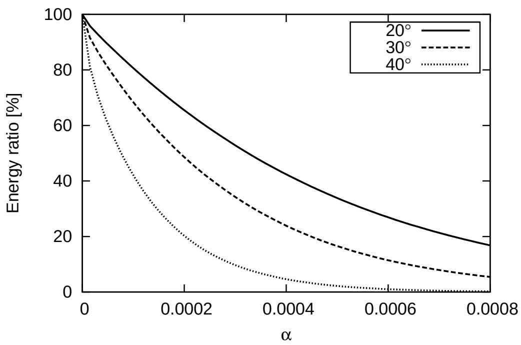

Figure 8. Energy of filtered mode-0 pressure signals

of the energy of the filtered pressure is given by the axisymmetric bursts. This agrees with the observations of Cavalieri *et al.*,[6] who applied the same techniques to the acoustic pressure of a large eddy simulation of a Mach 0.9 jet.

V. Conclusion

The application of a filter based on the continuous wavelet transform to extract coherent energy bursts in the acoustic field of a jet is proposed. This filter is applied to the azimuthal Fourier modes in the acoustic field of an experimental subsonic jet. The present results show that the bursts in the acoustic field, which account for a significant amount of the radiated energy,[8] are mostly axisymmetric. For high energy thresholds for

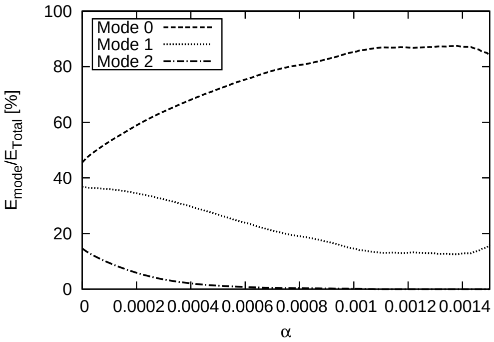

Figure 9. Energy contribution of the filtered azimuthal modes to the total filtered energy

the filtering, more than 80 percent of the burst energy is axisymmetric.

If we think on the possibilities for real-time, noise reduction control for subsonic jets, or on the understanding of the instantaneous mechanisms of sound production, the present results suggest that, as far as low angle radiation is concerned, focus on axisymmetric radiation tends to be more rewarding, for the intermittent energy bursts are mostly present for azimuthal mode 0. This allows the determination of times related to noise producing events,[3] the study of which can reveal the flow structures that are related to the emission of the acoustic energy bursts and that can be actuated by an appropriate control formulation.[4,5]

Acknowledgments

The present work was supported by SNECMA and CNPq, National Council of Scientific and Technological Development - Brazil.

References

[1]Juvé, D., Sunyach, M., and Comte-Bellot, G., "Intermittency of the noise emission in subsonic cold jets," *Journal of Sound and Vibration*, Vol. 71, 1980, pp. 319–332.

[2]Guj, G., Carley, M., Camussi, R., and Ragni, A., "Acoustic identification of coherent structures in a turbulent jet," *Journal of Sound and Vibration*, Vol. 259, No. 5, 2003, pp. 1037–1065.

[3]Hileman, J. I., Thurow, B. S., Caraballo, E. J., and Samimy, M., "Large-scale structure evolution and sound emission in high-speed jets: real-time visualization with simultaneous acoustic measurements," *Journal of Fluid Mechanics*, Vol. 544, 2005, pp. 277–307.

[4]Wei, M. and Freund, J. B., "A noise-controlled free shear flow," *Journal of Fluid Mechanics*, Vol. 546, 2006, pp. 123–152.

[5]Cavalieri, A. V. G., Jordan, P., Gervais, Y., Wei, M., and Freund, J. B., "Intermittent sound generation and its control in a free-shear flow," *Physics of Fluids*, Vol. 22, No. 11, 2010, pp. 115113.

[6]Cavalieri, A. V. G., Daviller, G., Comte, P., Jordan, P., Tadmor, G., and Gervais, Y., "Using large eddy simulation to explore sound-source mechanisms in jets," *to appear in Journal of Sound and Vibration*, 2011.

[7]Cavalieri, A. V. G., Jordan, P., Agarwal, A., and Gervais, Y., "Jittering wave-packet models for subsonic jet noise," *to appear in Journal of Sound and Vibration*, 2011.

[8]Kœnig, M., Cavalieri, A. V. G., Jordan, P., Delville, J., Gervais, Y., Papamoschou, D., Samimy, M., and Lele, S. K., "Farfield pre-filterering and source-imaging for the study of jet noise," *16th AIAA/CEAS Aeroacoustics Conference and Exhibit*, Stockholm, Sweden, June 7-9 2010.

[9]Michalke, A. and Fuchs, H. V., "On turbulence and noise of an axisymmetric shear flow," *Journal of Fluid Mechanics*, Vol. 70, 1975, pp. 179–205.

[10]Fuchs, H. and Michel, U., "Experimental evidence of turbulent source coherence affecting jet noise," *AIAA J*, Vol. 16, No. 9, 1978, pp. 871–872.

[11]Crow, S. C. and Champagne, F. H., "Orderly structure in jet turbulence," *Journal of Fluid Mechanics*, Vol. 48, No. 3, 1971, pp. 547–591.

[12]Moore, C. J., "The role of shear-layer instability waves in jet exhaust noise," *Journal of Fluid Mechanics*, Vol. 80, No. 2, 1977, pp. 321–367.

[13]Hussain, A. K. M. F. and Zaman, K. B. M. Q., "The 'preferred mode' of the axisymmetric jet," *Journal of Fluid Mechanics*, Vol. 110, 1981, pp. 39–71.

[14]Tinney, C. E. and Jordan, P., "The near pressure field of co-axial subsonic jets," *Journal of Fluid Mechanics*, Vol. 611, 2008, pp. 175–204.

[15]Maestrello, L., "Statistical properties of the sound and source fields of an axisymmetric jet," *American Institute of Aeronautics and Astronautics Conference*, Vol. 1, 1977.

[16]Juvé, D., Sunyach, M., and Comte-Bellot, G., "Filtered azimuthal correlations in the acoustic far field of a subsonic jet," *AIAA Journal*, Vol. 17, 1979, pp. 112.

[17]Brown, C. and Bridges, J., "Acoustic efficiency of azimuthal modes in jet noise using chevron nozzles," Tech. rep., National Aeronautics and Space Administration, 2006.

[18]Kopiev, V., Chernyshev, S., Faranosov, G., Zaitsev, M., and Belyaev, I., "Correlations of jet noise azimuthal components and their role in source identification," *16th AIAA/CEAS Aeroacoustics Conference and Exhibit*, Stockholm, Sweden, June 7-9 2010.

[19]Michalke, A., "A wave model for sound generation in circular jets," Tech. rep., Deutsche Luft- und Raumfahrt, November 1970.

[20]Lighthill, M. J., "On sound generated aerodynamically. I. General theory," *Proceedings of the Royal Society of London. Series A, Mathematical and Physical Sciences*, 1952, pp. 564–587.

[21]Cavalieri, A. V. G., Jordan, P., Colonius, T., and Gervais, Y., "Axisymmetric superdirectivity in subsonic jets," *17th AIAA/CEAS Aeroacoustics Conference and Exhibit*, Portland, OR, USA, June 5-8 2011.

[22]Farge, M., "Wavelet transforms and their applications to turbulence," *Annual Review of Fluid Mechanics*, Vol. 24, No. 1, 1992, pp. 395–458.

[23]Cavalieri, A. V. G., Rodríguez, D., Jordan, P., Colonius, T., and Gervais, Y., "Inlet conditions and wave-packets in subsonic jet noise," *Turbulence and Shear Flow Phenomena*, Ottawa, Canada, July 28-31 2011.

[24]Kœnig, M., Cavalieri, A. V. G., Jordan, P., Gervais, Y., and Papamoschou, D., "Far-field filtering for the study of jet noise: Mach and temperature effects," *17th AIAA/CEAS Aeroacoustics Conference and Exhibit*, Portland, OR, USA, June 5-8 2011.

[25]Crow, S. C., "Acoustic gain of a turbulent jet," *Phys. Soc. Meeting, Univ. Colorado, Boulder, paper IE*, Vol. 6, 1972.

[26]Ffowcs Williams, J. E. and Kempton, A. J., "The noise from the large-scale structure of a jet," *Journal of Fluid Mechanics*, Vol. 84, No. 4, 1978, pp. 673–694.

Bibliography

[1] R. J. Adrian. Conditional eddies in isotropic turbulence. *Physics of Fluids*, 22:2065, 1979. 9

[2] K. K. Ahuja. Correlation and prediction of jet noise. *Journal of Sound and Vibration*, 29(2):155–168, 1973. 31

[3] N. Andersson, L.E. Eriksson, and L. Davidson. Investigation of an isothermal Mach 0.75 jet and its radiated sound using large-eddy simulation and Kirchhoff surface integration. *International Journal of Heat and Fluid Flow*, 26(3):393–410, 2005. 67

[4] R. R. Armstrong, H. V. Fuchs, and A. Michalke. Coherent structures in jet turbulence and noise. *AIAA Journal*, 15:1011–1017, 1977. 6, 8, 11, 17, 109, 125

[5] R. J Astley and G. Gabard. Computational aero-acoustics (CAA) for aircraft noise prediction-Part A. *Journal of Sound and Vibration*, 330(16):3785–3786, 2011. xix

[6] N. Aubry, P. Holmes, J. Lumley, and E. Stone. The dynamics of coherent structures in the wall region of a turbulent boundary layer. *Journal of Fluid Mechanics*, 192:115–173, 1988. 159

[7] G. K. Batchelor. *The theory of homogeneous turbulence*. Cambridge University Press, 1953. 75

[8] G. K. Batchelor and A. E. Gill. Analysis of the stability of axisymmetric jets. *Journal of Fluid Mechanics*, 14(04):529–551, 1962. 10, 11, 109, 110, 133

[9] D. Bechert and E. Pfizenmaier. On wavelike perturbations in a free jet travelling faster than the mean flow in the jet. *Journal of Fluid Mechanics*, 72(2):341–352, 1975. 12

[10] H. A. Becker and T. A. Massaro. Vortex evolution in a round jet. *Journal of Fluid Mechanics*, 31(03):435–448, 1968. 125

[11] J.S. Bendat and A.G. Piersol. *Random data: analysis and measurement procedures*. Wiley-Interscience, 1986. 66

[12] D. J. Bodony. *Aeroacoustic prediction of turbulent free shear flows*. PhD thesis, Stanford University, 2004. 67, 70, 90

[13] D. J. Bodony and S. K. Lele. On using large-eddy simulation for the prediction of noise from cold and heated turbulent jets. *Physics of Fluids*, 17(8):085103, 2005. 32, 70, 90

[14] D. J. Bodony and S. K. Lele. Current status of jet noise predictions using large-eddy simulation. *AIAA journal*, 46(2):364, 2008. 32

[15] D. J. Bodony and S. K. Lele. Low-frequency sound sources in high-speed turbulent jets. *Journal of Fluid Mechanics*, 617:231–253, 2008. 33, 78

[16] C. Bogey and C. Bailly. Effects of inflow conditions and forcing on subsonic jet flows and noise. *AIAA journal*, 43(5):1000–1007, 2005. 34, 58

[17] C. Bogey and C. Bailly. Computation of a high Reynolds number jet and its radiated noise using large eddy simulation based on explicit filtering. *Computers & Fluids*, 35(10):1344–1358, 2006. 58, 84

[18] C. Bogey and C. Bailly. An analysis of the correlations between the turbulent flow and the sound pressure fields of subsonic jets. *Journal of Fluid Mechanics*, 583:71–97, 2007. 41, 76, 126

[19] C. Bogey and C. Bailly. Influence of nozzle-exit boundary-layer conditions on the flow and acoustic fields of initially laminar jets. *Journal of Fluid Mechanics*, 663:507–538, 2010. 31, 35

[20] C. Bogey, C. Bailly, and D. Juvé. Noise investigation of a high subsonic, moderate reynolds number jet using a compressible large eddy simulation. *Theoretical and Computational Fluid Dynamics*, 16(4):273–297, 2003. 32, 58, 67

[21] C. Bogey, S. Barré, V. Fleury, C. Bailly, and D. Juvé. Experimental study of the spectral properties of near-field and far-field jet noise. *International Journal of Aeroacoustics*, 6(2):73–92, 2007. 108

[22] M. Bouthier. Stabilité linéaire des écoulements presque parallèles. *Journal de Mécanique*, 11(4):599–621, 1972. 12, 13

[23] P. Bradshaw, D. H. Ferriss, and R. F. Johnson. Turbulence in the noise-producing region of a circular jet. *Journal of Fluid Mechanics*, 19(04):591–624, 1964. 4

[24] J. Bridges. Effect of heat on space-time correlations in jet. In *12th AIAA Aeroacoustics Conference*, volume AIAA 2006-2534, 8-10 May 2006. 69, 70, 84, 90

[25] J. E. Bridges and A. K. M. F. Hussain. Roles of initial condition and vortex pairing in jet noise. *Journal of Sound and Vibration*, 117(2):289–311, 1987. 28, 30, 41, 95, 98

[26] C. A. Brown and J. Bridges. Acoustic efficiency of azimuthal modes in jet noise using chevron nozzles. Technical report, National Aeronautics and Space Administration, 2006. 95

[27] G. L. Brown and A. Roshko. On density effects and large structure in turbulent mixing layers. *Journal of Fluid Mechanics*, 64(4):775–816, 1974. xi, 11, 75

[28] G. Broze and F. Hussain. Nonlinear dynamics of forced transitional jets: periodic and chaotic attractors. *Journal of Fluid Mechanics*, 263:93–132, 1994. 75

[29] M. Cabana, V. Fortuné, and P. Jordan. Identifying the radiating core of Lighthill's source term. *Theoretical and Computational Fluid Dynamics*, 22(2):87–106, 2008. 33

[30] A. V. G. Cavalieri, G. Daviller, P. Comte, P. Jordan, G. Tadmor, and Y. Gervais. Using LES to explore sound-source mechanisms in jets. *Procedia Engineering*, 6:104–113, 2010. 41, 78, 84

[31] A. V. G. Cavalieri, G. Daviller, P. Comte, P. Jordan, G. Tadmor, and Y. Gervais. Using large eddy simulation to explore sound-source mechanisms in jets. *Journal of Sound and Vibration*, 330(17):4098–4113, 2011. 55, 95, 101

[32] A. V. G. Cavalieri, P. Jordan, A. Agarwal, and Y. Gervais. Jittering wave-packet models for subsonic jet noise. In *AIAA Paper 2010-3957, 16th AIAA/CEAS Aeroacoustics Conference and Exhibit*, Stockholm, Sweden, June 7-9 2010. 41, 52, 57, 63, 65, 66

[33] A. V. G. Cavalieri, P. Jordan, A. Agarwal, and Y. Gervais. Jittering wave-packet models for subsonic jet noise. *Journal of Sound and Vibration*, 330(18-19):4474–4492, 2011. 73, 95, 100, 117, 119, 129

[34] A. V. G. Cavalieri, P. Jordan, T. Colonius, and Y. Gervais. Axisymmetric superdirectivity in subsonic jets. In *17th AIAA/CEAS Aeroacoustics Conference and Exhibit*, Portland, OR, USA, June 5-8 2011. 125, 126, 128, 129, 131, 132, 134, 144

[35] A. V. G. Cavalieri, P. Jordan, Y. Gervais, M. Wei, and J. B. Freund. Intermittent sound generation and its control in a free-shear flow. *Physics of Fluids*, 22(11):115113, 2010. 39, 57, 58, 76, 77, 115

[36] L. C. Cheung and S. K. Lele. Linear and nonlinear processes in two-dimensional mixing layer dynamics and sound radiation. *Journal of Fluid Mechanics*, 625:321, 2009. 36, 153

[37] B. T. Chu and L. S. G. Kovásznay. Non-linear interactions in a viscous heat-conducting compressible gas. *Journal of Fluid Mechanics*, 3(05):494–514, 1958. 24

[38] J. Cohen and I. Wygnanski. The evolution of instabilities in the axisymmetric jet. part 1. the linear growth of disturbances near the nozzle. *Journal of Fluid Mechanics*, 176:191–219, 1987. 12, 111, 124, 125, 135

[39] T. Colonius and J. B. Freund. Application of lighthill's equation to a mach 1.92 turbulent jet. *AIAA journal*, 38(2):368–370, 2000. 33

[40] T. Colonius and S. K. Lele. Computational aeroacoustics: progress on nonlinear problems of sound generation. *Progress in Aerospace Sciences*, 40(6):345–416, 2004. 32, 40

[41] T. Colonius, S. K. Lele, and P. Moin. Sound generation in a mixing layer. *Journal of Fluid Mechanics*, 330:375–409, 1997. 23, 32, 33, 40, 42, 52, 57, 75

[42] T. Colonius, A. Samanta, and K. Gudmundsson. Parabolized stability equation models of large-scale jet mixing noise. *Procedia Engineering*, 6:64–73, 2010. 115

[43] T. Colonius, A. Samanta, and K. Gudmundsson. Parabolized stability equation models of large-scale jet mixing noise. In *IUTAM Symposium on Computational Aero-Acoustics for Aircraft Noise Prediction*, Southampton, UK, March 29-31 2010. 153

[44] L. Cordier, E. Majd, B. Abou, and J. Favier. Calibration of POD reduced-order models using Tikhonov regularization. *International Journal for Numerical Methods in Fluids*, 63(2):269–296, 2010. 159

[45] D. G. Crighton. Basic principles of aerodynamic noise generation. *Progress in Aerospace Sciences*, 16(1):31–96, 1975. 16, 21, 24, 65, 78, 80, 88, 95, 98, 114, 117

[46] D. G. Crighton, A. P. Dowling, J. E. Ffowcs-Williams, M. Heckl, and F. G. Leppington. *Modern methods in analytical acoustics: lecture notes*. Springer, 1992. 12

[47] D. G. Crighton and M. Gaster. Stability of slowly diverging jet flow. *Journal of Fluid Mechanics*, 77(2):397–413, 1976. 12, 13, 75, 109

[48] D. G. Crighton and P. Huerre. Shear-layer pressure fluctuations and superdirective acoustic sources. *Journal of Fluid Mechanics*, 220:355–368, 1990. 21, 28, 75, 95, 96, 100

[49] W. O. Criminale, T. L. Jackson, and R. D. Joslin. *Theory and computation of hydrodynamic stability*. Cambridge Univ Pr, 2003. 9

[50] S. C. Crow. Acoustic gain of a turbulent jet. In *Phys. Soc. Meeting, Univ. Colorado, Boulder, paper IE*, volume 6, 1972. xv, 21, 28, 65, 75, 77, 79, 80, 95, 96, 98, 108, 119, 124, 152

[51] S. C. Crow and F. H. Champagne. Orderly structure in jet turbulence. *Journal of Fluid Mechanics*, 48(3):547–591, 1971. xi, 4, 7, 8, 9, 11, 13, 26, 75, 95, 109, 124, 125, 127

[52] G. Daviller. *Etude numérique des effets de temperature dans les jets simples et coaxiaux.* PhD thesis, Ecole Nationale Supérieure de Mécanique et d'Aérotechnique, Poitiers, France (in French), 2010. xiii, xxi, 78, 84

[53] G. Daviller, P. Jordan, and P. Comte. Toward source analysis of turbulent coaxial jets in large-eddy simulation. In *19 ème Congrès Francais de Mécanique*, Marseille, France, 24-28 août 2009. 57

[54] J. Delville. *La décomposition orthogonale aux valeurs propres et l'analyse de l'organisation tridimensionnelle des écoulements turbulents cisaillés libres.* PhD thesis, Université de Poitiers, 1995. 136, 148

[55] P. E. Doak. Analysis of internally generated sound in continuous materials: 2. a critical review of the conceptual adequacy and physical scope of existing theories of aerodynamic noise, with special reference to supersonic jet noise. *Journal of Sound and Vibration*, 25(2):263–335, 1972. 23, 156

[56] F. Ducros, P. Comte, and M. Lesieur. Large-eddy simulation of transition to turbulence in a boundary layer developing spatially over a flat plate. *Journal of Fluid Mechanics*, 326:1–36, 1996. 57

[57] D. Eschricht, P. Jordan, M. Wei, J. B. Freund, and F. Thiele. Analysis of noise-controlled shear-layers. In *13th AIAA/CEAS Aeroacoustics Conference(28th AIAA Aeroacoustics Conference)*, volume 211, 2007. 41, 44

[58] M. Farge. Wavelet transforms and their applications to turbulence. *Annual Review of Fluid Mechanics*, 24(1):395–458, 1992. 49, 50

[59] A. T. Fedorchenko. On some fundamental flaws in present aeroacoustic theory. *Journal of sound and vibration*, 232(4):719–782, 2000. 156

[60] J. E. Ffowcs Williams. The noise from turbulence convected at high speed. *Philosophical Transactions of the Royal Society of London. Series A, Mathematical and Physical Sciences*, 255(1061):469–503, 1963. 25

[61] J. E. Ffowcs Williams. Sound sources in aerodynamics–fact and fiction. *AIAA Journal*, 20(3):307–315, 1982. 16

[62] J. E. Ffowcs Williams and L. H. Hall. Aerodynamic sound generation by turbulent flow in the vicinity of a scattering half plane. *Journal of Fluid Mechanics*, 40(04):657–670, 1970. 158

[63] J. E. Ffowcs Williams and A. J. Kempton. The noise from the large-scale structure of a jet. *Journal of Fluid Mechanics*, 84(4):673–694, 1978. 21, 77, 100, 119

[64] V. Fleury. *Superdirectivité, bruit d'appariement et autres contributions au bruit de jet subsonique.* PhD thesis, Ecole Centrale de Lyon, 2006. 90

[65] V. Fortuné, E. Lamballais, and Y. Gervais. Noise radiated by a non-isothermal, temporal mixing layer. Part I: Direct computation and prediction using compressible DNS. *Theoretical and Computational Fluid Dynamics*, 18(1):61–81, 2004. 34

[66] J. B. Freund. Noise sources in a low-Reynolds-number turbulent jet at Mach 0.9. *Journal of Fluid Mechanics*, 438:277–305, 2001. xiv, xxi, 32, 33, 41, 58, 76, 78, 84, 152

[67] J. B. Freund. Noise-source turbulence statistics and the noise from a Mach 0.9 jet. *Physics of Fluids*, 15:1788–1799, 2003. 33, 75

[68] J. B. Freund. Adjoint-based optimization for understanding and suppressing jet noise. *Journal of Sound and Vibration*, 330:4114–4122, 2011. 35

[69] J. B. Freund and T. Colonius. Turbulence and sound-field POD analysis of a turbulent jet. *International Journal of Aeroacoustics*, 8(4):337–354, 2009. 155

[70] J. B. Freund, S. K. Lele, and P. Moin. Numerical simulation of a Mach 1.92 turbulent jet and its sound field. *AIAA Journal*, 38(11):2023–2031, 2000. 32

[71] H. V. Fuchs and R. R. Armstrong. Turbulent source coherence and Helmholtz number as aerodynamic noise parameters. *Structure and Mechanisms of Turbulence II*, pages 189–201, 1978. 107

[72] H. V. Fuchs and U. Michel. Experimental evidence of turbulent source coherence affecting jet noise. *AIAA Journal*, 16(9):871–872, 1978. 28, 95, 96, 125, 128

[73] W. K. George, P. D. Beuther, and R. E. A. Arndt. Pressure spectra in turbulent free shear flows. *Journal of Fluid Mechanics*, 148:155–191, 1984. 78

[74] M. E. Goldstein. Aeroacoustics. *New York, McGraw-Hill International Book Co., 1976. 305 p.*, 1976. 17, 23, 24, 118

[75] M. E. Goldstein. An exact form of Lilley's equation with a velocity quadrupole/temperature dipole source term. *Journal of Fluid Mechanics*, 443:231–236, 2001. 14, 36

[76] M. E. Goldstein. A generalized acoustic analogy. *Journal of Fluid Mechanics*, 488:315–333, 2003. 23, 24, 75, 77, 156

[77] M. E. Goldstein. On identifying the true sources of aerodynamic sound. *Journal of Fluid Mechanics*, 526:337–347, 2005. 24

[78] M. E. Goldstein. A theoretical basis for identifying the sound sources in a turbulent flow. *International Journal of Aeroacoustics*, 8(4):283–300, 2009. 24

[79] D. Gottlieb and E. Turkel. Dissipative two-four method for time dependent problems. *Mathematics of Computation*, 30(136):703–723, 1976. 57

[80] K. Gudmundsson and T. Colonius. Instability wave models for the near-field fluctuations of turbulent jets. *Journal of Fluid Mechanics*, 689:97–128, 2011. 13, 95, 100, 111, 125, 132, 133, 140

[81] G. Guj, M. Carley, R. Camussi, and A. Ragni. Acoustic identification of coherent structures in a turbulent jet. *Journal of Sound and Vibration*, 259(5):1037–1065, 2003. 57, 61, 76

[82] M. Harper-Bourne. Jet noise measurements: past and present. *International Journal of Aeroacoustics*, 9(4):559–588, 2010. 31

[83] M.E. Hayder and E. Turkel. High-order accurate solutions of viscous problem. In *AIAA paper 93-3074*, 1993. 57

[84] T. Herbert. Parabolized stability equations. *Annual Review of Fluid Mechanics*, 29(1):245–283, 1997. 13, 132, 133

[85] J. I. Hileman, B. S. Thurow, E. J. Caraballo, and M. Samimy. Large-scale structure evolution and sound emission in high-speed jets: real-time visualization with simultaneous acoustic measurements. *Journal of Fluid Mechanics*, 544:277–307, 2005. 30, 41, 50, 57, 61, 65, 76, 115

[86] P. Huerre and P. A. Monkewitz. Local and global instabilities in spatially developing flows. *Annual Review of Fluid Mechanics*, 22(1):473–537, 1990. 14

[87] A. K. M. F. Hussain and W. C. Reynolds. The mechanics of an organized wave in turbulent shear flow. *Journal of Fluid Mechanics*, 41(2):241–258, 1970. 8

[88] A. K. M. F. Hussain and K. B. M. Q. Zaman. Vortex pairing in a circular jet under controlled excitation. part 2. coherent structure dynamics. *Journal of Fluid Mechanics*, 101(03):493–544, 1980. 7, 8

[89] A. K. M. F. Hussain and K. B. M. Q. Zaman. The ‘preferred mode’ of the axisymmetric jet. *Journal of Fluid Mechanics*, 110:39–71, 1981. 7, 8, 26, 41, 95, 106, 125, 127, 135

[90] W. Joe, T. Colonius, and D. MacMynowski. Optimized waveforms for feedback control of vortex shedding. *Active Flow Control II, Notes on Numerical Fluid Mechanics and Multidisciplinary Design*, 108:391–404, 2010. 84

[91] P. Jordan and Y. Gervais. Subsonic jet aeroacoustics: associating experiment, modelling and simulation. *Experiments in Fluids*, 44(1):1–21, 2008. xx

[92] P. Jordan, Y. Gervais, J.-C. Valière, and H. Foulon. Final result from single point measurement. Project Deliverable D3.4,JEAN-EU 5th framework program G4RD-CT2000-00313, Laboratoire d’Études Aérodynamiques, 2002. 69, 70, 84, 90

[93] D. Jung, S. Gamard, and W. K. George. Downstream evolution of the most energetic modes in a turbulent axisymmetric jet at high Reynolds number. Part 1. The near-field region. *Journal of Fluid Mechanics*, 514:173–204, 2004. 136, 148

[94] D. Juvé, M. Sunyach, and G. Comte-Bellot. Filtered azimuthal correlations in the acoustic far field of a subsonic jet. *AIAA Journal*, 17:112, 1979. 29, 95, 96, 128

[95] D. Juvé, M. Sunyach, and G. Comte-Bellot. Intermittency of the noise emission in subsonic cold jets. *Journal of Sound and Vibration*, 71:319–332, 1980. 29, 30, 41, 57, 61, 76, 126

[96] S. Karabasov, M. Z. Afsar, T. P. Hynes, A. P. Dowling, W. A. McMullan, C. D. Pokora, G. J. Page, and J. J. McGuirk. Jet Noise: Acoustic analogy informed by large eddy simulation. *AIAA journal*, 48(7):1312–1325, 2010. 24, 114

[97] J. Kastner, M. Samimy, J. Hileman, and J. B. Freund. Comparison of noise mechanisms in high and low Reynolds number high-speed jets. *AIAA Journal*, 44(10):2251–2258, 2006. 41, 65, 76, 83

[98] F. Kerhervé, P. Jordan, A. V. G. Cavalieri, J. Deville, C. Bogey, and D. Juvé. Educing the source mechanism associated with downstream radiation in subsonic jets. *submitted to Journal of Fluid Mechanics*, 2012. 125, 155

[99] J. Kim, D. J. Bodony, and J. B. Freund. Aeroacoustics control of a turbulent Mach 1.3 jet using adjoint-based optimization. In *17th AIAA/CEAS Aeroacoustics Conference and Exhibit*, Portland, OR, USA, June 5-8 2011. 35, 158

[100] R. R. Kleinman and J. B. Freund. The sound from mixing layers simulated with different ranges of turbulence scales. *Physics of Fluids*, 20:101503, 2008. 26, 34

[101] M. Kœnig. *Réduction de bruit de jet par injection fluidique en corps central tournant.* PhD thesis, Ph. D. thesis, Université de Poitiers, 2011. xx, 157

[102] M. Kœnig, A. V. G. Cavalieri, P. Jordan, J. Delville, Y. Gervais, D. Papamoschou, M. Samimy, and S. K. Lele. Farfield pre-filterering and source-imaging for the study of jet noise. In *16th AIAA/CEAS Aeroacoustics Conference and Exhibit*, Stockholm, Sweden, June 7-9 2010. 57, 59, 60, 76, 77, 115

[103] M. Kœnig, A. V. G. Cavalieri, P. Jordan, Y. Gervais, and D. Papamoschou. Far-field filtering for the study of jet noise: Mach and temperature effects. In *17th AIAA/CEAS Aeroacoustics Conference and Exhibit*, Portland, OR, USA, June 5-8 2011. 144

[104] M. Kœnig, C. Fourment-Cazenave, P. Jordan, and Y. Gervais. Jet noise reduction by fluidic injection from a rotating plug. In *17th AIAA/CEAS Aeroacoustics Conference and Exhibit*, Portland, OR, USA, June 5-8 2011. 126

[105] L. S. G. Kovásznay. Turbulence in supersonic flow. *Journal of the Aeronautical Sciences*, 20(10):657–682, 1953. 24

[106] H. Lamb. *Hydrodynamics*. Cambridge Univ Pr, 1932. 10

[107] J. C. Lau, M. J. Fisher, and H. V. Fuchs. The intrinsic structure of turbulent jets. *Journal of Sound and Vibration*, 22(4):379–384, 1972. xi, 5, 9, 111, 135

[108] J. C. Lau, P. J. Morris, and M. J. Fisher. Measurements in subsonic and supersonic free jets using a laser velocimeter. *Journal of Fluid Mechanics*, 93:1–27, 1979. 2, 69

[109] J. Laufer and T.-C. Yen. Noise generation by a low-Mach-number jet. *Journal of Fluid Mechanics*, 134:1–31, 1983. 27, 33, 75, 95, 99, 125

[110] J. C. Laurence. Intensity, scale and spectra of turbulence in mixing region of free subsonic jet. Technical report, National Advisory Committee for Aeronautics, 1956. 4

[111] H. K. Lee and H. S. Ribner. Direct correlation of noise and flow of a jet. *The Journal of the Acoustical Society of America*, 52:1280, 1972. 29, 114, 126

[112] S. K. Lele. Compressibility effects on turbulence. *Annual Review of Fluid Mechanics*, 26(1):211–254, 1994. 109

[113] S. K. Lele. Phased array models of shock-cell noise sources. In *11th AIAA/CEAS Aeroacoustics Conference(26th Aeroacoustics Conference)*, pages 1–20, 2005. 63, 65, 79

[114] M. Lesieur and P. Comte. Favre filtering and macro- temperature in large-eddy simulations of compressible turbulence. *Comptes Rendus de l'Académie des Sciences*, 329(IIb):363–368, 2001. 57

[115] M. Lessen, J. A. Fox, and H. M. Zien. The instability of inviscid jets and wakes in compressible fluid. *Journal of Fluid Mechanics*, 21(01):129–143, 1965. 11

[116] M. J. Lighthill. On sound generated aerodynamically. I. General theory. *Proceedings of the Royal Society of London. Series A, Mathematical and Physical Sciences*, pages 564–587, 1952. 15, 16, 17, 40, 66, 75, 77, 95, 98, 124, 156

[117] M. J. Lighthill. On sound generated aerodynamically. II. Turbulence as a source of sound. *Proceedings of the Royal Society of London. Series A. Mathematical and Physical Sciences*, 222(1148):1, 1954. 17

[118] G. M. Lilley. On the noise from jets. *AGARD CP-131*, pages 13–1, 1974. 14, 23, 36, 77, 156

[119] G. Lodato, P. Domingo, and L. Vervisch. Three-dimensional boundary conditions for direct and large-eddy simulation of compressible viscous flows. *Journal of Computational Physics*, 227(10):5105–5143, 2008. 57

[120] P. A. Lush. Measurements of subsonic jet noise and comparison with theory. *Journal of Fluid Mechanics*, 46(03):477–500, 1971. 22, 25, 31, 107, 110

[121] L. Maestrello. Two-point correlations of sound pressure in the far field of a jet: experiment. Technical report, National Aeronautics and Space Administration, 1976. NASA TM X-72835. 28, 128

[122] L. Maestrello. Statistical properties of the sound and source fields of an axisymmetric jet. In *American Institute of Aeronautics and Astronautics Conference*, volume 1, 1977. 28

[123] M. R. Malik and C. L. Chang. Nonparallel and nonlinear stability of supersonic jet flow. *Computers & fluids*, 29(3):327–365, 2000. 13

[124] R. Mankbadi and J. T. C. Liu. A study of the interactions between large-scale coherent structures and fine-grained turbulence in a round jet. *Philosophical Transactions of the Royal Society of London. Series A, Mathematical and Physical Sciences*, 298(1443):541–602, 1981. 21

[125] R. Mankbadi and J. T. C. Liu. Sound generated aerodynamically revisited: large-scale structures in a turbulent jet as a source of sound. *Philosophical Transactions of the Royal Society of London. Series A, Mathematical and Physical Sciences*, 311(1516):183–217, 1984. 21, 75, 100, 124, 129

[126] A. Michalke. On the inviscid instability of the hyperbolic tangent velocity profile. *Journal of Fluid Mechanics*, 19(04):543–556, 1964. 10

[127] A. Michalke. A wave model for sound generation in circular jets. Technical report, Deutsche Luft- und Raumfahrt, November 1970. xvii, 18, 22, 28, 29, 100, 114, 153

[128] A. Michalke. Instabilitat eines Kompressiblen Runden Freistrahls unter Berucksichtigung des Einflusses der Strahlgrenzschichtdicke. *Zeitschrift für Flugwissenschaften*, 19:319–328; English translation: NASA TM 75190, 1977, 1971. 6, 12, 27, 109, 124

[129] A. Michalke. An expansion scheme for the noise from circular jets. *Zeitschrift für Flugwissenschaften*, 20:229–237, June 1972. 75, 100

[130] A. Michalke. Some remarks on source coherence affecting jet noise. *Journal of Sound and Vibration*, 87(1):1–17, 1983. 27

[131] A. Michalke. Survey on jet instability theory. *Progress in Aerospace Sciences*, 21:159–199, 1984. 109, 111, 157

[132] A. Michalke and H. V. Fuchs. On turbulence and noise of an axisymmetric shear flow. *Journal of Fluid Mechanics*, 70:179–205, 1975. xvii, 5, 8, 22, 86, 95, 112, 125, 129, 153

[133] U. Michel. The role of source interference in jet noise. In *15th AIAA/CEAS Aeroacoustics Conference(30th Aeroacoustics Conference)*, pages 1–15, 2009. 86, 114

[134] B. E. Mitchell, S. K. Lele, and P. Moin. Direct computation of the sound generated by vortex pairing in an axisymmetric jet. *Journal of Fluid Mechanics*, 383(1):113–142, 1999. 32, 33

[135] K. Mohseni and T. Colonius. Numerical treatment of polar coordinate singularities. *J. Comp. Phys.*, 157:787–795, 2000. 133

[136] K. Mohseni, T. Colonius, and J. B. Freund. An evaluation of linear instability waves as sources of sound in a supersonic turbulent jet. *Physics of Fluids*, 14:3593, 2002. 35, 144

[137] E. Mollo-Christensen. Measurements of near field pressure of subsonic jets. Technical report, Advisory Group for Aeronautical Research and Development, Paris, France, 1963. 95

[138] E. Mollo-Christensen. Jet noise and shear flow instability seen from an experimenter's viewpoint(Similarity laws for jet noise and shear flow instability as suggested by experiments). *Journal of Applied Mechanics*, 34:1–7, 1967. 4, 6, 18, 21, 75, 95

[139] E. Mollo-Christensen, M. A. Kolpin, and J. R. Martucelli. Experiments on jet flows and jet noise far-field spectra and directivity patterns. *Journal of Fluid Mechanics*, 18(2):285–301, 1964. 18, 25

[140] P. A. Monkewitz, D. W. Bechert, B. Barsikow, and B. Lehmann. Self-excited oscillations and mixing in a heated round jet. *Journal of Fluid Mechanics*, 213(1):611–639, 1990. 14

[141] P. A. Monkewitz and K. D. Sohn. Absolute instability in hot jets. *AIAA journal*, 26:911–916, 1988. 14

[142] C. J. Moore. The role of shear-layer instability waves in jet exhaust noise. *Journal of Fluid Mechanics*, 80(2):321–367, 1977. xi, 6, 7, 8, 11, 27, 75, 95, 124

[143] P. J. Morris. A note on noise generation by large scale turbulent structures in subsonic and supersonic jets. *International Journal of Aeroacoustics*, 8(4):301–315, 2009. 76

[144] P. J. Morris. The instability of high speed jets. *International Journal of Aeroacoustics*, 9(1):1–50, 2010. 109

[145] G. L. Morrison and D. K. McLaughlin. Instability process in low reynolds number supersonic jets. *AIAA Journal*, 18:793–800, 1980. 13

[146] P. M. Morse and K. U. Ingard. *Theoretical acoustics*. McGraw-Hill Book Company, 1968. 118

[147] J.W. Nichols and S.K. Lele. Global modes and transient response of a cold supersonic jet. *Journal of Fluid Mechanics*, 669(1):225–241, 2011. 15

[148] B. R. Noack, K. Afanasiev, M. Morzynski, G. Tadmor, and F. Thiele. A hierarchy of low-dimensional models for the transient and post-transient cylinder wake. *Journal of Fluid Mechanics*, 497(1):335–363, 2003. 159

[149] B. R. Noack, P. Papas, and P. A. Monkewitz. The need for a pressure-term representation in empirical galerkin models of incompressible shear flows. *Journal of Fluid Mechanics*, 523(1):339–365, 2005. 159

[150] W. A. Olsen, O. A. Gutierrez, and R. G. Dorsch. The effect of nozzle inlet shape, lip thickness, and exit shape and size on subsonic jet noise. In *11th AIAA Aerospace Sciences Meeting*, 1973. 31

[151] J. Panda, R. G. Seasholtz, and K. A. Elam. Investigation of noise sources in high-speed jets via correlation measurements. *Journal of Fluid Mechanics*, 537:349–385, 2005. 30, 126, 130

[152] D. Papamoschou. Wavepacket modeling of the jet noise source. In *17th AIAA/CEAS Aeroacoustics Conference and Exhibit*, Portland, OR, USA, June 5-8 2011. 144

[153] L. Perret, E. Collin, and J. Delville. Polynomial identification of POD based low-order dynamical system. *Journal of Turbulence*, (7), 2006. 159

[154] R. A. Petersen and M. M. Samet. On the preferred mode of jet instability. *Journal of Fluid Mechanics*, 194(1):153–173, 1988. 12, 111, 124, 125, 135, 157

[155] O. M. Phillips. On the generation of sound by supersonic turbulent shear layers. *Journal of Fluid Mechanics*, 9(1):1–28, 1960. 22

[156] C. Picard and J. Delville. Pressure velocity coupling in a subsonic round jet. *International Journal of Heat and Fluid Flow*, 21(3):359–364, 2000. 8, 76, 125

[157] P. Plaschko. Helical instabilities of slowly divergent jets. *Journal of Fluid Mechanics*, 92(2):209–215, 1979. 12, 13

[158] D. C. Pridmore-Brown. Sound propagation in a fluid flowing through an attenuating duct. *Journal of Fluid Mechanics*, 4(pt 4):393–406, 1958. 23

[159] I. Proudman. The generation of noise by isotropic turbulence. *Proceedings of the Royal Society of London. Series A. Mathematical and Physical Sciences*, 214(1116):119–132, 1952. 18, 29

[160] Lord Rayleigh. On the question of the stability of the flow of fluids. *Philosophical Magazine*, 34:59–70, 1892. 9

[161] Lord Rayleigh. *The theory of sound*, volume 2. Dover Publications, 1945. 10

[162] R. Reba, S. Narayanan, and T. Colonius. Wave-packet models for large-scale mixing noise. *International Journal of Aeroacoustics*, 9(4):533–558, 2010. 76, 99, 114

[163] D. Rempfer. Investigations of boundary layer transition via galerkin projections on empirical eigenfunctions. *Physics of Fluids*, 8:175, 1996. 159

[164] O. Reynolds. An experimental investigation of the circumstances which determine whether the motion of water shall be direct or sinuous, and of the law of resistance in parallel channels. *Proceedings of the Royal Society of London*, 35(224-226):84–99, 1883. 9

[165] H. S. Ribner. Quadrupole correlations governing the pattern of jet noise. *Journal of Fluid Mechanics*, 38(01):1–24, 1969. 18

[166] D. Rodríguez, A. Sinha, G. Brès, and T. Colonius. Parabolized stability equation models in turbulent supersonic jets. In *18th AIAA/CEAS Aeroacoustics Conference and Exhibit*, Colorado Springs, CO, USA, June 4-6 2012. 133

[167] D. Ronneberger and U. Ackermann. Experiments on sound radiation due to non-linear interaction of instability waves in a turbulent jet. *Journal of Sound and Vibration*, 62(1):121–129, 1979. 13, 27, 36

[168] C. W. Rowley. Model reduction for fluids, using balanced proper orthogonal decomposition. *International Journal of Bifurcation Chaos in Applied Sciences and Engineering*, 15(3):997–1014, 2005. 159

[169] C. W. Rowley, T. Colonius, and R. M. Murray. Model reduction for compressible flows using POD and Galerkin projection. *Physica D: Nonlinear Phenomena*, 189(1-2):115–129, 2004. 159

[170] A. Samanta, J. B. Freund, M. Wei, and S. K. Lele. Robustness of acoustic analogies for predicting mixing-layer noise. *AIAA Journal*, 44(11):2780–2786, 2006. 33, 75, 77

[171] N. D. Sandham, C. L. Morfey, and Z. W. Hu. Nonlinear mechanisms of sound generation in a perturbed parallel jet flow. *Journal of Fluid Mechanics*, 565(1), 2006. 36

[172] N. D. Sandham, C. L. Morfey, and Z. W. Hu. Sound radiation from exponentially growing and decaying surface waves. *Journal of Sound and Vibration*, 294(1):355–361, 2006. 65, 77, 81, 85, 95

[173] N. D. Sandham and A. M. Salgado. Nonlinear interaction model of subsonic jet noise. *Philosophical Transactions of the Royal Society A*, 366(1876):2745–2760, 2008. 14, 134

[174] M. Schaffar. Direct measurements of the correlation between axial in-jet velocity fluctuations and far field noise near the axis of a cold jet. *Journal of Sound and Vibration*, 64(1):73–83, 1979. 30, 126, 130

[175] M. Schlegel, B. R. Noack, P. Jordan, A. Dillmann, E. Gröschel, W. Schröder, M. Wei, J. B. Freund, O. Lehmann, and G. Tadmor. On least-order flow representations for aerodynamics and aeroacoustics. *Journal of Fluid Mechanics*, 697:367–398, 2012. 155

[176] P. J. Schmid. Nonmodal stability theory. *Annual Review of Fluid Mechanics*, 39:129–162, 2007. 15, 148

[177] S. Sinayoko, A. Agarwal, and Z. Hu. Flow decomposition and aerodynamic sound generation. *Journal of Fluid Mechanics*, 668:335–350, 2011. 24, 75, 78

[178] P. R. Spalart. Application of full and simplified acoustic analogies to an elementary problem. *Journal of Fluid Mechanics*, 578:113, 2007. 156

[179] J. L. Stromberg, D. K. McLaughlin, and T. R. Troutt. Flow field and acoustic properties of a Mach number 0.9 jet at a low Reynolds number. *Journal of Sound and Vibration*, 72(2):159–176, 1980. 14, 32

[180] V. Suponitsky, N.D. Sandham, and C.L. Morfey. Linear and nonlinear mechanisms of sound radiation by instability waves in subsonic jets. *Journal of Fluid Mechanics*, 658:509–538, 2010. 36, 134, 144

[181] T. Suzuki and T. Colonius. Instability waves in a subsonic round jet detected using a near-field phased microphone array. *Journal of Fluid Mechanics*, 565:197–226, 2006. 12, 13, 17, 76, 86, 109, 125, 133

[182] G. Tadmor, D. Bissex, B. R. Noack, M. Morzynski, T. Colonius, and K. Taira. Temporal-harmonic specific POD mode extraction. In *AIAA Paper 2008-4190, 4th AIAA Flow Control Conference*, Seattle, Washington, June 23-26 2008. 66, 84

[183] C. K. W. Tam. Computational aeroacoustics examples showing the failure of the acoustic analogy theory to identify the correct noise sources. *Journal of Computational Acoustics*, 10(4):387–406, 2002. 156

[184] C. K. W. Tam and D. E. Burton. Sound generated by instability waves of supersonic flows. Part 1. Two-dimensional mixing layers. *Journal of Fluid Mechanics*, 138:249–272, 1984. 13

[185] C. K. W. Tam and D. E. Burton. Sound generated by instability waves of supersonic flows. Part 2. Axisymmetric jets. *Journal of Fluid Mechanics*, 138(-1):273–295, 1984. 13, 124

[186] C. K. W. Tam, M. Golebiowski, and J. M. Seiner. On the Two Components of Turbulent Mixing Noise from Supersonic Jets. In *2th AIAA/CEAS Aeroacoustics Conference and Exhibit*, State College, PA, May 6-8 1996. 25

[187] C. K. W. Tam and P. J. Morris. The radiation of sound by the instability waves of a compressible plane turbulent shear layer. *Journal of Fluid Mechanics*, 98(2):349–381, 1980. 13, 75

[188] H. K. Tanna. An experimental study of jet noise Part I: Turbulent mixing noise. *Journal of Sound and Vibration*, 50(3):405–428, 1977. 25, 31, 70, 84, 90, 107

[189] B. J. Tester and C. L. Morfey. Developments in jet noise modelling–theoretical predictions and comparisons with measured data. *Journal of Sound and Vibration*, 46(1):79–103, 1976. 24

[190] V. Theofilis. Advances in global linear instability analysis of nonparallel and three-dimensional flows. *Progress in aerospace sciences*, 39(4):249–316, 2003. 14

[191] K. W. Thompson. Time dependent boundary conditions for hyperbolic systems. *Journal of Computational Physics*, 68(1):1–24, 1987. 133

[192] C. E. Tinney, M. N. Glauser, and L. S. Ukeiley. Low-dimensional characteristics of a transonic jet. part 1. proper orthogonal decomposition. *Journal of Fluid Mechanics*, 612:107, 2008. 126

[193] C. E. Tinney and P. Jordan. The near pressure field of co-axial subsonic jets. *Journal of Fluid Mechanics*, 611:175–204, 2008. 9, 63, 76, 95, 106, 114, 125

[194] C. D. Tomkins and R. J. Adrian. Energetic spanwise modes in the logarithmic layer of a turbulent boundary layer. *Journal of Fluid Mechanics*, 545:141–162, 2005. 128

[195] C. Torrence and G. P. Compo. A practical guide to wavelet analysis. *Bulletin of the American Meteorological Society*, 79(1):61–78, 1998. 50

[196] M. Tutkun, W. K. George, J. M. Foucaut, S. Coudert, M. Stanislas, and J. Delville. In situ calibration of hot wire probes in turbulent flows. *Experiments in Fluids*, 46(4):617–629, 2009. 97, 126

[197] D. Violato and F. Scarano. Three-dimensional evolution of flow structures in transitional circular and chevron jets. *Physics of Fluids*, 23(12):124104–124104, 2011. 125

[198] K. Viswanathan. Aeroacoustics of hot jets. *Journal of Fluid Mechanics*, 516:39–82, 2004. 25, 31, 97, 107

[199] K. Viswanathan. Scaling laws and a method for identifying components of jet noise. *AIAA Journal*, 44(10):2274, 2006. 108

[200] K. Viswanathan and L. T. Clark. Effect of nozzle internal contour on jet aeroacoustics. *International Journal of Aeroacoustics*, 3(2):103–135, 2004. 31

[201] M. Wang, J. B. Freund, and S. K. Lele. Computational Prediction of Flow-Generated Sound. *Annual Review of Fluid Mechanics*, 38:483–512, 2006. 17, 40

[202] M. Wei. *Jet noise control by adjoint-based optimization*. PhD thesis, Ph. D. thesis, Department of Theoretical and Applied Mechanics, University of Illinois at Urbana-Champaign, Urbana, Illinois, 2004. 42

[203] M. Wei and J. B. Freund. A noise-controlled free shear flow. *Journal of Fluid Mechanics*, 546:123–152, 2006. xiii, xxi, 35, 39, 40, 41, 42, 44, 45, 49, 52, 57, 76, 77, 158

[204] M. Wei and C. W. Rowley. Low-dimensional models of a temporally evolving free shear layer. *Journal of Fluid Mechanics*, 618(1):113–134, 2009. 159

[205] AJ Yule. Large-scale structure in the mixing layer of a round jet. *Journal of Fluid Mechanics*, 89(3):413–432, 1978. 125

[206] K. B. M. Q. Zaman. Effect of nozzle exit conditions on subsonic jet noise. In *17th AIAA/CEAS Aeroacoustics Conference and Exhibit*, Portland, OR, USA, June 5-8 2011. 31

[207] K. B. M. Q. Zaman and A. K. M. F. Hussain. Vortex pairing in a circular jet under controlled excitation. Part 1. General jet response. *Journal of Fluid Mechanics*, 101(03):449–491, 1980. 7, 8

[208] K. B. M. Q. Zaman and J. C. Yu. Power spectral density of subsonic jet noise. *Journal of Sound and Vibration*, 98(4):519–537, 1985. 108

[209] X. Zhou and L. Sirovich. Coherence and chaos in a model of turbulent boundary layer. *Physics of Fluids A*, 4(12):2855–2874, 1992. 159

On considère les paquets d'ondes hydrodynamiques comme mécanismes de génération de bruit des jets subsoniques.
Cette approche résulte tout d'abord de l'analyse de données numériques - DNS d'une couche de mélange (Wei et Freund 2006) et LES d'un jet à Mach 0,9 (Daviller 2010) - permettant de déterminer les propriétés des sources en termes de compacité, d'intermittence et de structure azimutale. L'identification d'un rayonnement intermittent associé aux modifications des structures cohérentes des écoulements permet de proposer un modèle de paquet d'onde pour représenter ce phénomène dans l'analogie de Lighthill, dont l'enveloppe présente des variations temporelles d'amplitude et d'étendue spatiale. Celles-ci sont tirées de données de vitesse de simulations numériques de jets subsoniques, et un accord de l'ordre de 1,5dB entre le champ acoustique simulé et le modèle confirme sa pertinence.
L'exploration du concept proposé est ensuite poursuivie expérimentalement, avec des mesures de pression acoustique et de vitesse de jets turbulents subsoniques, permettant la décomposition des champs en modes de Fourier azimutaux. On observe l'accord des directivités des modes 0, 1 et 2 du champ acoustique avec le rayonnement d'un paquet d'onde. Les modes 0 et 1 du champ de vitesse correspondent également à des paquets d'onde, modélisés comme des ondes d'instabilité linéaires à partir des équations de stabilité parabolisées. Finalement, des corrélations de l'ordre de 10% entre les modes axisymétriques de vitesse dans le jet et de pression acoustique rayonnée montrent un lien clair entre les paquets d'onde et l'émission acoustique du jet.

Mots clés : aéroacoustique, jets – bruit, bruit aérodynamique, vélocimétrie par images de particules

Hydrodynamic wavepackets are studied as a sound-source mechanism in subsonic jets. We first analyse numerical simulations to discern properties of acoustic sources such as compactness, intermittency and azimuthal structure. The simulations include a DNS of a two-dimensional mixing layer (Wei and Freund 2006) and an LES of a Mach 0.9 jet (Daviller 2010). In both cases we identify intermittent radiation, which is associated with changes in coherent structures in the flows. A wave-packet model that includes temporal changes in amplitude and axial extension is proposed to represent the identified phenomena using Lighthill's analogy. These parameters are obtained from velocity data of two subsonic jet simulations, and an agreement to within 1.5dB between the model and the acoustic field of the simulations confirms its pertinence. The proposed mechanism is then investigated experimentally, with measurements of acoustic pressure and velocity of turbulent subsonic jets, allowing the decomposition of the fields into azimuthal Fourier modes. We find close agreement of the directivities of modes 0, 1 and 2 of the acoustic field with wave-packet radiation. Modes 0 and 1 of the velocity field correspond also to wavepackets, modelled as linear instability waves using parabolised stability equations. Finally, correlations of order of 10% between axisymmetric modes of velocity and far-field pressure show the relationship between wavepackets and sound radiated by the jet.

Keywords : aeroacoustics, jet noise, aerodynamic noise, particle image velocimetry